

Alma Mater Studiorum - Università di Bologna

**PARTIAL DISCHARGE PHENOMENA IN CONVERTER
AND TRACTION TRANSFORMERS: IDENTIFICATION
AND RELIABILITY**

PhD Thesis

by

Carlos Gustavo Azcárraga Ramos

Tutor: Prof. Eng. Andrea Cavallini

Coordinator: Prof. Eng. Domenico Casadei

Summary

After the development of power electronics converters, the number of transformers subjected to non-sinusoidal stresses (including DC) has increased in applications such as HVDC links and traction (electric train power cars). The effects of non-sinusoidal voltages on transformer insulation have been investigated by many researchers, but still now, there are some issues that must be understood.

Some of those issues are tackled in this Thesis, studying PD phenomena behavior in Kraft paper, pressboard and mineral oil at different voltage conditions like AC, DC, AC+DC, notched AC and square waveforms.

From the point of view of converter transformers, it was found that the combined effect of AC and DC voltages produces higher stresses in the pressboard than those that are present under pure DC voltages.

The electrical conductivity of the dielectric systems in DC and AC+DC conditions has demonstrated to be a critical parameter, so, its measurement and analysis was also taken into account during all the experiments.

Regarding notched voltages, the RMS reduction caused by notches (depending on firing and overlap angles) seems to increase the PDIV. However, the experimental results show that once PD activity has incepted, the notches increase PD repetition rate and magnitude, producing a higher degradation rate of paper.

On the other hand, the reduction of mineral oil stocks, their relatively low flash point as well as environmental issues, are factors that are pushing towards the use of esters as transformer insulating fluids. This PhD Thesis also covers the study of two different esters with the scope to validate their use in traction transformers. Mineral oil was used as benchmark.

The complete set of dielectric tests performed in the three fluids, show that esters behave better than mineral oil in practically all the investigated conditions, so, their application in traction transformers is possible and encouraged.

Acknowledgements

I would like to express my gratitude to my supervisor, Professor Andrea Cavallini for his support guidance and friendship during my PhD studies at the University of Bologna. His hard work and enlightening has made possible my PhD project.

I'm indebted to the Instituto de Investigaciones Eléctricas, Institution that has made growth as a professional and that allows me to enjoy electrical engineering. Its support has been very important during this study leaving.

I am also grateful to the financial sponsorship from the Mexican National Council of Science and Technology (CONACYT) which covers my tuition fees and living expenses.

I would like to thank the research team of the Laboratory of Technology Innovation: Prof. Davide Fabiani, Mr. Fabrizio Palmieri and specially Mr. Fabio Ciani. Their fellowship and advices helped me a lot during these three years.

I truly appreciate the support, help and friendship of our two voluntary technicians: Mr. Enzo Gervasi and Mr. Giancarlo Luppi. Their experience contributed always to improve my ideas and to manufacture better test cells. Unlike dielectrics, aging is not a problem for them!

I also want to thank all my mates of the laboratory: Luca, Marco, Victor, Oliviero, Paolo, Fabrizio Negri, Gaetano, Perla, Verdiana, Valentina and lots of friends that for space reasons, I'm not mentioning now. Your camaraderie makes me feel a real Italian! Grazie ragazzi!

Last but not least, I would like to take this opportunity to thank my wife Rossy, my son Diego and our families for their limitless love. Their support has encouraged me all the time!

Contents

1	Introduction.....	9
1.1	Research objectives.....	9
1.2	Thesis outline.....	10
2	Converter and traction transformer insulation materials.....	13
2.1	Mineral oil.....	14
2.2	Esters.....	14
2.3	Comparison between mineral oil and esters.....	15
2.3.1	Water solubility.....	16
2.3.2	Fire resistance.....	16
2.3.3	Environmental issues.....	16
2.4	Pressboard (transformerboard).....	18
3	Physical parameters that affect converter and traction transformer insulation.....	20
3.1	Water influence in oil-paper systems.....	20
3.2	Electrodes geometry.....	22
3.3	Temperature.....	24
3.4	Waveform influence on converter transformers insulation.....	24
3.5	Waveform influence on traction transformers insulation.....	31
4	Experimental setups, test procedures and data processing.....	33
4.1.1	Oil and pressboard conditioning cells.....	33
4.1.2	Karl Fischer titration.....	35
4.1.3	AC Breakdown test cells.....	36
4.1.4	Lightning impulse test cell.....	37
4.1.5	Sinusoidal and square waveform test cell.....	37
4.1.6	HVDC.....	38
4.1.7	Partial discharges.....	40
4.1.8	Conductivity test cell.....	46
4.1.9	Data processing - Weibull distribution.....	47
4.1.10	Data processing - Histograms.....	48
5	Results of insulating fluids comparison.....	49

5.1	Electrical breakdown (short gap, IEC 60156).....	49
5.2	Electrical breakdown (Long gap)	53
5.3	Electrical breakdown (Lightning impulse)	58
5.4	Partial discharges (point to plane geometry, oil)	63
5.5	Partial discharges (point to plane geometry, Pressboard barrier + oil)	69
5.6	Comsol® simulations for point to plane geometry with and without pressboard.....	75
6	Results of PD testing under HVDC and square waveform and under particular conditions.....	93
6.1	Partial discharges (point to plane geometry, influence of frequency and waveform)	94
6.2	Partial discharges under HVDC stresses	95
6.2.1	Behavior of PDIV in pressboard as a function of voltage distribution and space charge	95
6.2.2	Behavior of PD activity in pressboard as a function of overvoltage.....	99
6.2.3	Behavior of PD activity in insulating paper for notched voltage waveforms.....	101
6.3	Partial discharges dependence on oil flow speed	104
7	Discussion on dielectric fluid comparison results	109
7.1	Electrical breakdown (short gap, IEC 60156) and long gaps	109
7.2	Electrical breakdown (Lightning impulse)	111
7.3	Partial discharges (point to plane geometry, oil)	112
7.4	Partial discharges (point to plane geometry, Pressboard barrier + oil)	113
8	Discussion on results of PD testing under HVDC, square waveform and particular conditions	117
8.1	Partial discharges (point to plane geometry, influence of frequency and waveform)	117
8.1.1	Charge injection from electrodes	117
8.1.2	Ionization waves	119
8.2	Partial discharges under HVDC stresses	121
8.2.1	Behavior of PDIV in pressboard as a function of voltage distribution and space charge	121
8.2.2	Behavior of PD activity in insulating paper for notched voltage waveforms.....	131
8.3	Partial discharges dependence on oil flow speed	136
9	Conclusions and future work.....	138
9.1	Test cell for PDIV determination under divergent field	138
9.2	Traction transformers (comparison of dielectric fluid behavior)	138
9.3	Converter transformers.....	140
9.4	Oil flow speed influence	141
10	References.....	142

List of Figures

Fig. 2.1 Transformer insulation solid components.....	13
Fig. 2.2 Synthetic ester basic structure	15
Fig. 2.3 Typical synthetic ester structure	15
Fig. 2.4 Natural ester structure.....	15
Fig. 2.5 Cellulose structure.....	18
Fig. 2.6 Barrier effect on streamer behavior a)Oil without barriers shows higher BD probability. b) Ion guard effect due to streamer tip expansion, reducing local electric field. c) Bulkhead effect: reduction of electric field in oil channels (small arrows). Electric field vectors in pressboard are not displayed in this condition.	19
Fig. 3.1 Saturation curves for mineral oil and FR3.....	21
Fig. 3.2 Oomen equilibrium curve for oil and paper water exchange.....	22
Fig. 3.3 DC voltage distribution in the valve side of a HVDC transformer.....	25
Fig. 3.4 Valve bridges in ± 800 kV converter transformer.....	26
Fig. 3.5 Normalized frequency spectra of the u_a	26
Fig. 3.6 Normalized frequency spectra of the u_a'	27
Fig. 3.7 Potential and electric field distribution under AC, DC and polarity reversal voltages.....	28
Fig. 3.8 Electric field distribution in an oil-pressboard interface.....	30
Fig. 3.9 Typical locomotive power systems.....	32
Fig. 4.1 Conditioning system for oil and pressboard drying and impregnation	34
Fig. 4.2 Oil drying and degassing cell.....	34
Fig. 4.3 Thermodynamic states of water as a function of temperature and pressure.....	35
Fig. 4.4 Karl Fischer system for water determination	36
Fig. 4.5 Breakdown test cell (IEC 60156).....	37
Fig. 4.6 Lightning impulse test cell.....	37
Fig. 4.7 Square wave test cell.....	38
Fig. 4.8 HVDC test cell.....	39
Fig. 4.9 AC notched voltage at different firing and overlap angles	39
Fig. 4.10 Acoustic PD decoupling and biasing system.....	40
Fig. 4.11 PDIV test cell for insulating liquids.....	42
Fig. 4.12 Comparison of new and degraded needles	42
Fig. 4.13 Test cell for creeping discharges	43
Fig. 4.14 Test cell for PD measurement under HVDC voltages	43
Fig. 4.15 Voltage and electric field distribution under AC and DC voltages.....	45
Fig. 4.16 Conductivity test cell	46
Fig. 4.17 Polarization and depolarization currents measurement circuit	47
Fig. 5.1 Mean values of BDV at different moisture levels for the insulating liquids studied in this work	50
Fig. 5.2 Standard deviation of BDV at different moisture levels for the insulating liquids studied in this work	51
Fig. 5.3 BDV trends of mineral oil, FR3 and Ester X fluids	52
Fig. 5.4 Behavior of moisture during BDV tests	53
Fig. 5.5 Weibull shape parameter as a function of gap length (BDV).....	53
Fig. 5.6 Main statistical parameters for BDV (overall results)	54
Fig. 5.7 Statistical parameters for BDV.....	57
Fig. 5.8 Moisture behavior during impulse testing	58
Fig. 5.9 Main statistical parameters for lightning impulse testing (overall results)	59
Fig. 5.10 Weibull shape parameter as a function of gap length.....	59

Fig. 5.11 Statistical parameters for BDV.....	62
Fig. 5.12 Behavior of moisture during PDIV tests	63
Fig. 5.13 Main statistical parameters for PDIV in oil (overall results).....	64
Fig. 5.14 Statistical parameters for PDIV in oil	68
Fig. 5.15 Comparison of Weibull parameters for PDIV in oil for mineral oil and FR3	68
Fig. 5.16 Moisture behavior during PDIV testing in PB and oil geometries	69
Fig. 5.17 Comparison of moisture behavior with and without PB during PDIV testing	70
Fig. 5.18 Main statistical parameters for PDIV testing in pressboard and oil geometries (overall results).....	70
Fig. 5.19 Weibull shape parameter as a function of gap length.....	71
Fig. 5.20 Main statistical parameters for BDV (overall results).....	74
Fig. 5.21 Comparison of Weibull parameters for PDIV in pressboard and oil for mineral oil and FR3.....	75
Fig. 5.22 Geometry for creeping discharges modeling	76
Fig. 5.23 FEM 3D discretization for creeping discharges modeling	76
Fig. 5.24 Electric potential comparison at 5mm	77
Fig. 5.25 Electric field comparison at 5mm.....	77
Fig. 5.26 Electric field comparison at 5mm (over and inside PB sheet)	77
Fig. 5.27 Electric potential comparison at 40mm	78
Fig. 5.28 Electric field comparison at 40mm.....	78
Fig. 5.29 Electric field comparison at 40mm (over and inside PB sheet)	78
Fig. 5.30 Electric field comparison at 5mm gap with and without PB in mineral oil	79
Fig. 5.31 Electric field vectors comparison at 5mm gap with and without PB in mineral oil.....	79
Fig. 5.32 Electric field comparison at 40mm gap with and without PB in mineral oil	80
Fig. 5.33 Electric field vectors comparison at 40mm gap with and without PB in mineral oil.....	80
Fig. 5.34 Electric field comparison at 5mm gap with and without PB in FR3	81
Fig. 5.35 Electric field vectors comparison at 5mm gap with and without PB in FR3.....	81
Fig. 5.36 Electric field comparison at 40mm gap with and without PB in FR3	82
Fig. 5.37 Electric field comparison at 40mm gap with and without PB in FR3	82
Fig. 5.38 Electric field vectors comparison at 5 and 40mm gap in mineral oil.....	83
Fig. 5.39 Electric field vectors comparison at 5 and 40mm gap in mineral oil.....	83
Fig. 5.40 Comparison of minimum and maximum gaps in mineral oil (cross-section)	84
Fig. 5.41 Comparison of minimum and maximum gaps in FR3 (cross-section)	84
Fig. 5.42 Comparison of minimum and maximum gaps in mineral oil (over PB surface)	85
Fig. 5.43 Comparison of minimum and maximum gaps in mineral oil (over PB surface)	85
Fig. 5.44 Comparison of minimum and maximum gaps in mineral oil (mid plane)	86
Fig. 5.45 Comparison of minimum and maximum gaps in FR3 (mid plane)	86
Fig. 5.46 Comparison of electric field vectors in minimum and maximum gaps in mineral oil and FR3 (cross-section)...	87
Fig. 5.47 Geometry and mesh conditions for point to plane in oil.....	89
Fig. 5.48 Electric potential distribution in point to plane geometry at 5mm for mineral oil and FR3.....	89
Fig. 5.49 Electric field distribution in point to plane geometry at 5mm for mineral oil and FR3	89
Fig. 5.50 Electric field vectors distribution in point to plane geometry at 5mm for mineral oil and FR3.....	90
Fig. 5.51 Electric field as a function of gap= 5mm for mineral oil and FR3.....	90
Fig. 5.52 Electric potential distribution in point to plane geometry at 40mm for mineral oil and FR3.....	91
Fig. 5.53 Electric field distribution in point to plane geometry at 40mm for mineral oil and FR3	91
Fig. 5.54 Electric field vectors distribution in point to plane geometry at 40mm for mineral oil and FR3.....	91
Fig. 5.55 Electric field as a function of gap= 40mm for mineral oil and FR3.....	92
Fig. 6.1 PDIV Trend comparison as a function of frequency for sinusoidal and square waveforms for mineral oil and FR3 in a point to plane electrode configuration	94
Fig. 6.2 Rise time for a square waveform of 1 kHz.....	95
Fig. 6.3 Electrodes geometry for PDIV measurement during HVDC testing.....	95
Fig. 6.4 HVDC waveforms used during this work.....	96

Fig. 6.5 PDIV Weibull plots for oil-PB-oil geometry.....	97
Fig. 6.6 PDIV Weibull plots for oil-PB geometry.....	98
Fig. 6.7 PD patterns with AC and DC voltage.....	100
Fig. 6.8 PD amplitude, Q_{max} , repetition rate, N_w , and their product, $N_w \cdot Q_{max}$, under different test voltages	100
Fig. 6.9 Examples of phase to ground voltages and DC outputs in a transformer DC converter as a function of α and μ	101
Fig. 6.10 Weibull inception probabilities under voltage at different firing angles when $\mu=15^\circ$ (b, c, d) and under voltage at different overlap angles when $\alpha=15^\circ$ (e, f, g). The comparison between these plots is shown in h).....	103
Fig. 6.11 PD patterns at different voltage conditions.....	104
Fig. 6.12 Electrodes geometry for PDIV measurement as a function of oil speed	105
Fig. 6.13 Weibull alpha for PDIV and a function of oil speed.....	106
Fig. 6.14 PDIV trend for mineral oil at 50 and 70 °C.....	107
Fig. 6.15 PD patterns at different oil speeds.....	108
Fig. 6.16 Repetition rate, magnitude and polarity of PD pulses obtained at different frequencies.....	108
Fig. 7.1 Breakdown voltage for mineral oil and FR3 as a function of relative moisture	110
Fig. 7.2 Weibull parameters for AC BDV	111
Fig. 7.3 Statistics of impulse breakdown voltage (IBDV) for the two fluids at different gap lengths. Quasi-uniform field	112
Fig. 7.4 PD pattern and discharge behavior close to PDIV for 5 mm gap	114
Fig. 7.5 PDIV of mineral and ester oil without and with board.....	115
Fig. 7.6 Electric field at inception for mineral and ester oil without and with board (confidence intervals at 95% probability are also reported).....	116
Fig. 7.7 Oil humidity prior and after PDIV tests, (above) without and (below) with board	116
Fig. 8.1 Influence of space charge on the electric field distribution in a point to plane geometry	118
Fig. 8.2 Propagating electric field wave for positive needle electrode.....	120
Fig. 8.3 Propagating electric field wave for negative needle electrode.....	120
Fig. 8.4 PDIV peak values obtained from different electrodes condition.....	122
Fig. 8.5 Times for PD inception in AC above DC PDIV _{pk}	124
Fig. 8.6 Available time for PD inception due to AC overvoltages over DC PDIV.....	124
Fig. 8.7 Time to achieve steady state conditions under DC voltage for a) Oil-PB-oil and b) PB-Oil geometries	126
Fig. 8.8 Equivalent circuit for Oil-PB-oil geometry	127
Fig. 8.9 Polarization currents of dry and wet samples (PB-oil geometry).....	129
Fig. 8.10 Depolarization currents of dry and wet samples (PB-oil geometry).....	129
Fig. 8.11 Weibull chart for PDIV values obtained using different pre-charge times for Oil-PB geometry	130
Fig. 8.12 Box plots of the PDIV values obtained using different pre-charge times for Oil-PB geometry	131
Fig. 8.13 Normalized RMS values for notched waveforms as a function of α and μ	131
Fig. 8.14 Weibull scale parameter as a function of normalized RMS values.....	132
Fig. 8.15 PD amplitude at the notched edges under voltages at different firing and overlap angles.....	133
Fig. 8.16 PD amplitude at the rising front of notches as a function of ΔV	134
Fig. 8.17 ΔV of different AC with notches voltages: voltage 1: $\alpha=0^\circ$, $\mu=15^\circ$; voltage 2: $\alpha=15^\circ$, $\mu=15^\circ$; voltage 3: $\alpha=30^\circ$, $\mu=15^\circ$; voltage 4: $\alpha=15^\circ$, $\mu=5^\circ$; voltage 5: $\alpha=15^\circ$, $\mu=15^\circ$; voltage 6: $\alpha=15^\circ$, $\mu=25^\circ$	134
Fig. 8.18 Variation of N_w under voltages at different firing angles when the overlap angle $\mu=15^\circ$	135
Fig. 8.19 Variation of N_w under voltages at different overlap angles when the firing angle $\alpha=15^\circ$	135
Fig. 8.20 Repetition rate as a function of ΔV	135
Fig. 8.21 Fowler-Nordheim plot for a steel needle immersed in mineral oil	136

1 Introduction

Since the beginning of the commercial use of electricity, transformers have been one of the most important components in transmission and distribution systems and also in transport services (traction). For this historical reason, the world of transformers had been, up to some years ago, probably the most conservative one in the electrical industry. However, nowadays, paradigms in transformer design, construction and operation are changing due to the fact that power system operation and transport systems are undergoing radical transformations, mainly in control, safety, physical dimensions and environmental issues.

Power electronics is one of the technologies that have made possible the modern evolution of power systems, but it also has brought new challenges to power system elements design, especially regarding the insulation system. Transformers for example, are now exposed to electrical stresses that are no longer sinusoidal (including even DC).

This class of transformers include those used in HVDC links of conventional type (based on SCRs), those used in HVDC plus (based on MOSFETs, IGBTs) and traction transformers used in train power cars. The effects of non-sinusoidal voltages on transformer insulation have been investigated, but much remains to be said regarding recognition of partial discharge sources as well as endurance (in the presence or absence of partial discharges).

On the other side, some factors like the progressive reduction of naphthenic oil stocks, the relatively low flash point and environmental issues including biodegradability and toxicity, are pushing forward natural and synthetic ester oils.

1.1 Research objectives

The investigations reported in this PhD thesis are aimed to answer a number of questions related to the behavior of insulating systems of traction and converter transformers.

In traction transformers it is important to guaranty safety and good behavior of the insulations system under overload conditions. Logically, green policies regarding environmental issues should be also accomplished. In this way, it is important to compare the characteristics of the various insulating liquids available in the market that fulfill these requirements. A lot of work has been carried out to demonstrate the suitability of esters to replace mineral oil in power transformers, but there are some specific details that should be studied to cover all the operating conditions, mainly including non conventional stresses.

For converter transformers the situation is not different. A lot of research has been conducted to analyze the behavior of the transformer insulation system under DC stresses (including polarity reversal). However, the current knowledge is not complete yet due to the fact that there are a lot of particularities that have not been studied or fully understood.

According to the previous paragraphs, the objective of this PhD thesis is to provide additional insight in the way that insulating systems of traction and current transformers behaves under not full study operating conditions and particularities and the way to replicate those conditions for transformer or materials testing.

In order to cover the overall objective of this thesis, some particular objectives should be accomplished. These particular objectives are summarized below:

Regarding traction transformers:

The effect of partial discharges must be studied for mineral oil and esters. PD have proven to be the most important cause of failure in conventional transformers, so, the transformer design of traction transformers should take into account more effective ways to retard their inception or to withstand its effect once that they are present. In order to evaluate PD, it is important to determine accurately the partial discharge inception voltage (PDIV) under different conditions. PDIV assessment current practice stands on some standard electrode configurations and procedures that must be revised because they tend to underestimate the PDIV. So, once that an optimum procedure for PDIV assessments would be found, the following parameters will be studied:

- a. Behavior of esters in conventional dielectric tests.
- b. Corona in oil characteristics at different gaps and moisture levels.
- c. PD characteristics under creeping conditions.
- d. Mineral oil and ester response to square voltages in terms of PDIV.

Regarding converter transformers:

In this case, also PDIV is going to be used as the key parameter to analyze the behavior of paper-oil insulation systems. For this purpose, esters are not considered because their electrical conductivity is higher than that of the mineral oil, making higher the stress in the pressboard during DC steady state. The conditions to be studied to complete current knowledge and experience on the insulation system of converter transformers are:

- a. Combined effect of AC and DC on the behavior of the insulating system comparing it with the effects of pure AC and DC voltages.
- b. Effect of pre-charging the insulating system on the PDIV.
- c. Effect of fast transients (notched voltages) in the inter-turn insulation of converter transformers and in the insulation of the bushings of the converter side.
- d. Effect of space charge on the response of the oil to square voltage waveforms.

Along with the mentioned conditions for traction and converter transformers, the oil flow speed effect is going to be studied as well, because it is one of the conditions that takes place in both transformer types.

1.2 Thesis outline

The outline of this thesis is summarized as follows:

Chapter 1 Introduction

This chapter briefly introduces the research background of this thesis, the research objectives and the thesis outline.

Chapter 2 Converter and traction transformer insulation materials

It provides a general review of all the relevant materials used in modern transformer technology and considered in this work. Main characteristics of mineral oil, esters and pressboard are briefly described from the chemical and physical point of views. Explanation of insulation system design is also provided.

Chapter 3 Physical parameters that affect converter and traction transformer insulation

The influence of several parameters on the performance of transformers insulation system is described in this Chapter. Water dynamics and influence over the oil-paper system is addressed also. Due to the fact that laboratory testing requires the use of reliable transformer models that can replicate real transformer behavior, the effect of electrodes geometry is also described here.

One of the main differences of converter and traction transformers in comparison to normal AC transformers is the waveform influence. DC components in converter transformers and fast rise time square pulses in traction transformers stress the insulation system in a very different way. So, this Chapter presents the theoretical basis of those special stresses emphasizing the differences between them and the stresses that take place in conventional AC power transformer.

Chapter 4 Experimental setups, test procedures and data processing

Conditioning cells and processes for oil and pressboard samples are described. Moisture assessment was needed before and after the conditioning processes and during tests evolution. For that reason, Karl Fischer titration method is briefly analyzed, mainly from the point of view of the experiences with its use during this work. AC and impulse breakdown voltage cells are described including design details. Non conventional power supplies like HVDC and square wave supplies used during this work are also described. Partial discharges measurement setups for AC, square waveform, DC and AC+DC voltages are presented including specific details regarding test cells geometry and design.

Chapter 5 Results of insulating fluids comparison

In this Chapter are presented the obtained results for three different fluids: mineral oil, FR3 and a new, and a low viscosity natural ester, named Ester X. These results were obtained using standardized and non conventional tests described in Chapter 4: Breakdown voltages according IEC 60156, long gap breakdown, lightning impulse breakdown, point to plane partial discharge inception voltage (PDIV) in oil gaps and PDIV assessment of creeping discharges. Finite element modeling is also presented here to explain some behaviors that are not very clear from a glance, i.e. the effect of electrodes in creeping discharges at different gap distances and the effect of pressboard tangential barriers itself.

Chapter 6 Results of partial discharge testing under HVDC and square waveform and under particular conditions

This Chapter presents the results of non conventional tests like HVDC and square wave power supplies and the results of oil PDIV behavior as a function of flow speed and temperature in creeping conditions. From the point of view of HVDC testing, the main difference regarding standardized tests, is the fact that during this research work, pressboard samples are stressed not only using AC and DC separately, but in a simultaneous way (AC+DC at different conditions). For square waves, obtained results for PDIV as a function of frequency are also presented. The results of the impact of oil speed and temperature in creeping discharges PDIV are also included in this Chapter.

Chapter 7 Discussion on dielectric fluid comparison results

This chapter shows the analysis of the main results obtained during mineral oil and ester comparison. Among the most important results, it is possible to list the following: PD behavior is determined in

divergent fields using an improved method to assess PDIVs in both mineral oil and esters. B10 analysis proved to be the better approach for transformer design, because it provides most conservative results.

PDIV assessment in creep geometries was studied and a suitable test procedure for particular geometry is proposed. Gaps larger than 10 mm must be used because otherwise, the geometry of the test cell and the fluid properties can affect the reliability of the measurements, making difficult to identify the discharge source and type, mainly when “true” PDIV is measured and no patterns are still available. It has been shown that it is also convenient to analyze PD pulses for this purpose, despite the fact that this tool is not always available in the practice.

FR3 contributes to further drying of the pressboard as it can be noticed analyzing the moisture transfer between oil, FR3 and PB after PDIV measurements. This additional moisture in FR3 does not affect the dielectric behavior of this fluid according to the other results obtained during this work.

In general, it was found that FR3 offers a better or comparable performance in comparison with mineral oil in practically all the carried out tests, confirming the feasibility of the use of esters in practically all transformer operation types.

Chapter 8 Discussion on results of PD testing under HVDC, square waveform and particular conditions

In this Chapter are analyzed the results obtained from the comparison of square waveforms with conventional sinusoidal stresses from the point of view of PDIV at different frequencies. It was found that in this test conditions, homocharge and thermal effects play an important role in the behavior of the PDIV at low and high frequencies respectively for both mineral oil and FR3. Square voltages proved to be the waveform that stresses the fluids in a more important way in point to plane geometries (corona in oil).

It was also analyzed the effect of combined AC and DC stresses in PB barriers from the point of view of PDIV and PD magnitude. It was obtained that despite the fact that an equal electric field is necessary to incept PD in the PB in all conditions, once that PD are present, the discharges magnitude is always superior when only AC or combined AC+DC stresses are applied. So, the effect of combined AC+DC effect can impose additional stresses in barriers that should be considered in HVDC transformer testing.

Regarding notched voltage waveforms effect in interturn or bushings insulating paper, it was observed that RMS reduction of the notched waveforms contributes to increase the PDIV level. The drawback is that once that PD incept, the repetition rate and PD magnitude increases with the reduction of the RMS value (more wide and depth notches) contributing to accelerated aging of the insulating paper.

From the point of view of oil dynamics, it was also found that oil flow speed affects positively the behavior of DP in creeping geometries because the flow sweeps away ionized oil increasing PDIV.

Chapter 9 Conclusions and future work.

In this last Chapter, the main conclusions found during this PhD work are summarized. In addition, further activities to continue the study of the dielectric system endurance of converter transformers and the behavior of alternative insulating fluids in traction transformers are suggested.

2 Converter and traction transformer insulation materials

Internal components of power transformers require a blend of materials to be electrically isolated from each others. One can distinguish easily two main types of materials: oil (or other types of fluids) and cellulose. The synergy of those materials contributes to improve the behavior of the insulation system independently of the type of voltage that they can withstand in a separate way.

It is well known that when transformer materials are exposed to sinusoidal voltages the liquid insulation works at a higher stress level (it withstand a higher electric field) because of its lower dielectric constant. In case of direct current voltage, electrical conductivity becomes the dominant parameter for stress distribution. Hence, due to the fact that the impregnated pressboard has a lower conductivity in comparison with the oil, it is going to experience the higher electric field. A detailed description of this behavior, including other transient response in DC, is going to be presented in the HVDC section.

Besides the dielectric function of the insulating liquid, it also must dissipate heat from the active parts of the transformers. So, hydraulic and thermal parameters like viscosity are usually taken into account during the design process. Insulating paper and pressboard contribute in terms of dielectric behavior or as a mechanical element, covering energized metallic exposed parts (i.e. coils), dividing long oil channels in smaller volumes that enhances dielectric withstand (barriers) and mechanically support conductors and windings (separators). A cross section of a power transformer is showed in **Error! Reference source not found.** to graphically describe all relevant insulation components.

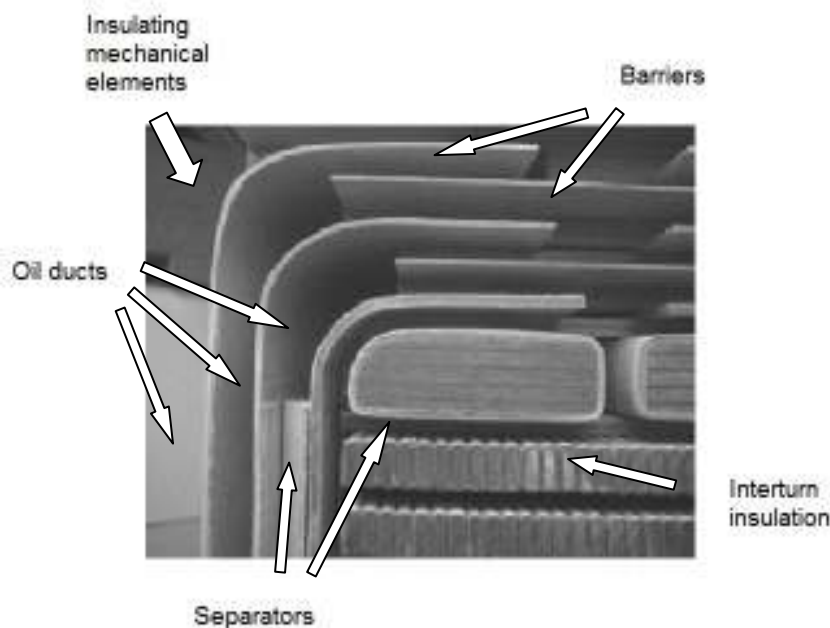


Fig. 2.1 Transformer insulation solid components

Inter-turn insulation: it's the insulation that is in direct contact with the conductors and it is normally composed by kraft paper. It constitutes around 20% of the total mass of solid insulation and operates at more or less the same temperature than the winding conductors.

Barriers: Under this definition one can find pressboard. The temperature of these elements is very close to the temperature of the oil, due to the fact that they are not in direct contact with conductors. There are two different options for these materials, high and low density. These two density levels have to be taken into account for during impregnation process and also during the electrical design. Barriers represent 20 or 30% of the total solid insulation mass inside the transformer.

Following, a brief description of transformer materials is presented.

2.1 Mineral oil

Mineral oil is the most commonly used insulating liquid for transformer applications. A lot of experience has been acquired with its use and process (the choice of a new mineral oil is guided by the IEC 60296 standard [1]). In service evaluation of mineral oils is defined by the standard IEC 60422 [2]). Nevertheless, due to modern environmental policies, the use of mineral oil is subject to additional requirements.

Mineral oil is a hydrocarbon mixture produced from the distillation of crude oil. Because of its wide availability, low cost and useful properties it is the insulating liquid most commonly used in transformer industry, mainly in medium and large power ranges.

Mineral oil is a transparent liquid composed mainly of various types of hydrocarbons, including straight chain alkanes, branched alkanes, cyclic paraffins and aromatic hydrocarbons.

There are two principal types of mineral oil used for transformers: paraffinic and naphthenic oils.

Paraffinic oil is derived from crude oil containing substantial quantities of natural paraffins. It has a relatively high pour point and may require the inclusion of additives to reduce it.

Naphthenic oil is derived from crude oil containing a very low level of paraffins. It provides better viscosity characteristics, longer life expectancy and low pour points. Naphthenic oil has more polar characteristics than paraffinic oil.

Mineral oils contain inhibitors that delay oxidation processes. If the inhibitors are natural, the oil is said to be uninhibited. If inhibitors are synthetic the oil is called inhibited.

2.2 Esters

Esters, synthetic or natural has been used up to now where fire safety and environmental protection are a concern. They are mainly used in power transformers and in transformers with demanding conditions, such as traction, trackside and wind farms. It is reported also that the use of esters enhances transformer insulating system from the point of view of moisture absorption in cellulose.

There are some standards and guides for the use of natural and synthetic esters in power transformers. New synthetic esters are specified according IEC 61099 and a maintenance guide is available as IEC 61203 [3]. There are not IEC documents for natural esters, but there is available an IEEE Guide (C57.147 – "IEEE Guide for Acceptance and Maintenance of Natural Ester Fluids in Transformers) and an ASTM Specification "ASTM D6871-03 (2008)".

Esters are substances that are synthesized from the reaction of alcohols and fatty acids. Fig. 2.2 shows a synthetic ester basic structure. O represents oxygen, C represents carbon, R and R' represent carbon chains. It is important to say that C=O double bonds behave differently from the C=C double bonds found in the chains of natural esters.

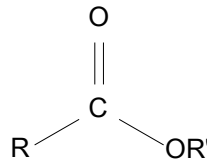


Fig. 2.2 Synthetic ester basic structure

It is important to say that the acids used in esters production are usually saturated (no C-C double bonds) in the chain, giving the synthetic esters a very stable chemical structure (good oxidation and thermal stability)

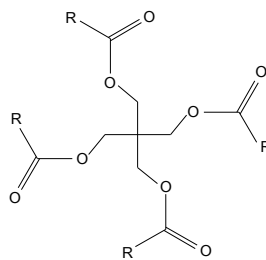


Fig. 2.3 Typical synthetic ester structure

Natural esters are produced from vegetable oils, which are themselves manufactured from renewable plant crops. Their structure is based on a alcohol chain, to which 3 naturally occurring fatty acid groups are bonded. Those acids may be the same or different. Plants produce these esters as part of their natural growth cycle.

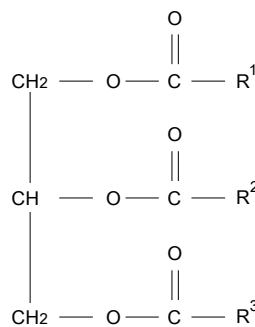


Fig. 2.4 Natural ester structure

Natural esters offer the advantage of high fire point as well as good biodegradability. The main drawback is the low oxidation stability in comparison with other insulating fluids.

The most popular natural esters are produced from soya, rapeseed and sunflower oil. This is due to factors such as availability, cost and having the desired performance characteristics.

2.3 Comparison between mineral oil and esters

Following, a brief description of main differences between mineral oil and esters is presented.

2.3.1 Water solubility

Water is a very polar molecule and polar molecules tend to be most strongly attracted to other polar molecules. In this context the term ‘polar’ refers to regions of a substance which have different attractions, like the poles of a magnet. Mineral oil is not polar. The ester linkages present in both natural and synthetic esters make these fluids ‘polar’, and like tiny magnets, these linkages are able to attract water molecules in a way that mineral and silicone oils cannot. Natural esters have 3 ester linkages per molecule, whilst synthetic esters may have 2-4 linkages per molecule. These differences become evident when we consider the amount of water that can dissolve in these fluids.

Table 1 shows the water solubility of transformer fluids at room temperature, i.e. the total amount of moisture content which the fluid can hold without free water being deposited.

Table 1 Water solubility of transformer fluids

Dielectric fluid	Ester linkages	Approx water saturation at 23°C (ppm)
Mineral oil	0	55
Natural ester	3	1100
Synthetic ester	4	2600

2.3.2 Fire resistance

Fire safety is a key concern of today’s users of insulating liquids, especially when considering their use in areas such as in subway tunnels or aboard ships. Equally this applies where they will be used in populated areas such as near offices, shops and in the workplace. Natural and synthetic esters can offer a high degree of fire safety, due to their low fire susceptibility.

Table 2 Flash and fire point for transformer fluids

Fluid type	Flash point °C	Fire point °C	Class
Mineral oil	160 -170	170 -180	O
Natural ester	>300	>350	K2
Synthetic ester	>250	>300	K3

2.3.3 Environmental issues

Environmental safety is determined with two basic criteria: biodegradability and low toxicity. In general fluids which possess a rapid biodegradation rate and can demonstrate low toxicity are classified as being ‘environmentally friendly’. These factors are important when considering the use of fluids in environmentally sensitive areas, such as water courses, to avoid contamination.

The term ‘biodegradability’ reflects the extent which the fluid is metabolized by naturally occurring microbes in soil or water courses, in the event of a spillage or leak. Clearly it is an advantage if spilt fluids can quickly disappear naturally without the need to instigate expensive clean up measures.

To be classified as readily biodegradable a substance must satisfy both of the following criteria:

- 60% biodegradation must occur within 10 days of exceeding 10% degradation
- At least 60% degradation must occur by day 28 of the test.

Both natural and synthetic esters are officially classified as being ‘readily biodegradable’ whilst mineral oils and silicone fluids are more resistant to biodegradation.

Following, in Table 3 are presented and summarized the key aspects of mineral oil and esters.

Table 3 Comparison between transformer fluids

Fluid	Advantages	Disadvantages
Mineral Oil	<ul style="list-style-type: none"> • Low Transformer Cost • Lower Viscosity at Low Temperatures • Liquid Dielectric Performance • Low Maintenance Cost • Biodegradable/Low Toxicity Fluid • Preventive Maintenance (DGA) • Load Break Operations • Long Service Life Expectancy • Typically Self-Healing Under Temporary Dielectric & Thermal Overstress • Easy to Reprocess/Dispose • Pour Point < -35°C • A Century of Application History 	<ul style="list-style-type: none"> • Higher Installation Cost • Relatively Low Fire Point • Not Favored by Insurance Companies • Containment with Absorption Bed may be Required • Deluge Extinguishing System may be Required • Longest Clearance Distances • Excessive Min. Clearance Distance & Fire Barriers may be Required (Outdoor) • Extensive Soil Spill Cleanup Likely • Not Classified as Edible Oil • Non-Renewable Resource • Growing Corrosive Sulfur Concerns
Natural esters	<ul style="list-style-type: none"> • Time to Kraft Paper End-of-Life Improvement 5-8 Times • Excellent Dielectric Properties • Excellent Clarity • Rapidly and Completely Biodegrades • Field Experience to 242 kV, 200 MVA • Excellent Lubricity • Non-Toxic per Standard Test Methods • Good Compatibility • Not Listed as Hazardous Waste • Low Maintenance Cost • Preventive Maintenance (DGA) • Food Grade Ingredients • Renewable Resource • Easy to Reprocess/Dispose • Long Service Life Expected • Typically Self-Healing under Temporary Thermal and Dielectric Stress • Complies with Edible Oil Act • Fully Miscible with Mineral Oil, HMWH & Most PCB Substitutes • Maintains > 300°C Fire Point up to 7% Mineral Oil Content 	<ul style="list-style-type: none"> • Higher Cost than Mineral Oil • Liquid Containment Required Per NEC 450-23 (Indoor) • Pour Point -21°C • Appropriate only for sealed Positive Pressure Dry Nitrogen Equipped Tanks
Synthetic esters	All the advantages of natural esters plus a very low pour point (-55°C)	<ul style="list-style-type: none"> • High cost • Compatibility problems (with PVC for example)

2.4 Pressboard (transformerboard)

Cellulose is the most important constituent of vegetables but it is never found pure in nature. Cotton fibre with a cellulose content of more than 95 % is probably the purest natural source. Most commonly, in wood, plant stalks, leaves and the like, cellulose is associated with other substances such as lignin and so-called hemicelluloses, both in considerable quantities. Thus, according to the species, wood contains on a dry weight basis 40 to 55 % cellulose, 15 to 35 % lignin, and 25 to 40 % hemicelluloses. The most common sources of cellulose for industrial use are wood pulp and cotton lint. In the paper industry, cotton fibres and cotton linters are only used for very specific applications. The bulk of the cellulose pulp is made from wood.

As raw material for the manufacturing of paper pulp, either soft wood (spruce, pine, fir, etc.) or hard woods (birch, beech, maple, eucalyptus, etc.) are being used. The advantage of soft wood is its longer fibers. The typical fiber length of spruce is 2.5 to 4.5 mm whereas the typical fiber length of beech is in the range of 0.7 to 1.7 mm. For paper and board with a high mechanical strength, softwoods that grow in regions with low average temperatures are optimum.

For the manufacturing of paper and pressboard for electrical insulation, mainly unbleached softwood kraft pulp is used. The cellulose is refined from the tree by the so-called "sulphate" or "kraft" process.

The trees are supplied to the pulp factory as 1 to 4 m long logs. The logs are debarked and cut into chips with a side length of 20 to 40 mm and a thickness of 5 to 10 mm, which can be stored up to 6 months. The chips are cooked in a mixture of sodium hydroxide, sodium carbonate, sodium sulphide and sodium sulphate. Today this cooking process is continuous.

The wood chips are impregnated with these substances either at ambient pressure and a temperature of 60 to 70 °C or with elevated pressure at 110 °C for 10 to 20 minutes. The chips are then cooked at 160 to 180 °C and 8 to 9 bar for 0.5 to 2 hours. After the cooking process, the solid and the liquid phase are separated. The fibers are then neutralized with an acidic solution and subsequently washed with water. For the manufacturing of electrical grade pulp, this washing process is of utmost importance, since at this process step, any ionic impurities are removed from the pulp.

Electrical grade cellulose is normally not bleached; therefore the pulp is dried right after the washing process. The pulp is dewatered in a process that is similar to the paper making process. The dewatering machine consists of a screen-, press- and drying part. The drying part can either be heated rolls or a so called "flash drying" equipment, where the wet fibers are fluffed and blown into a heated chamber where they are dried at a temperature of about 260 °C.

Cellulose is a linear condensation polymer consisting of anhydroglucose joined together by glycosidic bonds.

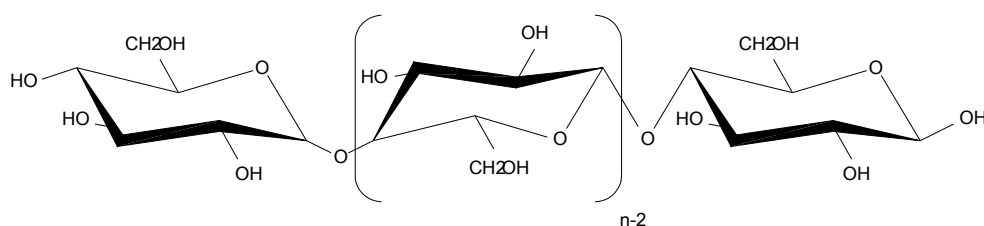


Fig. 2.5 Cellulose structure

The degree of polymerization (average number of glycosidic rings in a cellulose macromolecule could be very high at the beginning of the process, but it is usually reduced at around 1200. When the molecule is fully extended it takes the form of a flat ribbon with highly hydrophilic hydroxyl groups protruding laterally and capable of forming inter and intra-molecular hydrogen bonds. The surface of the ribbon consists mainly of hydrogen atoms linked directly to carbon and is therefore hydrophobic. These two features of the molecular structure of cellulose are responsible for its supramolecular structure and this in turn determines many of its chemical and physical properties.

Pressboard is used in transformer main insulation system because several reasons: Pressboard barriers limit field distortion at the streamer head after impact on barrier, working as an ion guard, expanding the tip geometry (Fig. 2.6b). Barriers also limit field stress in the unaffected insulation, if subdivisions are provided (bulkhead effect, Fig. 2.6c).

Pressboard can take over field from conductive oil gaps (DC, nonlinearity of oil conductivity).

Regarding geometric aspects (size), pressboard barriers obstruct particle drift to the electrodes and limit propagation of streamers and instabilities of conductivity, temperature and current density (streamer effect, distance effect).

Pressboard barriers affect propagating streamers because they limit accumulation of charge (which is critical for a barrier) along streamer's path and they increase surface discharge inception voltage, if properly located and formed.

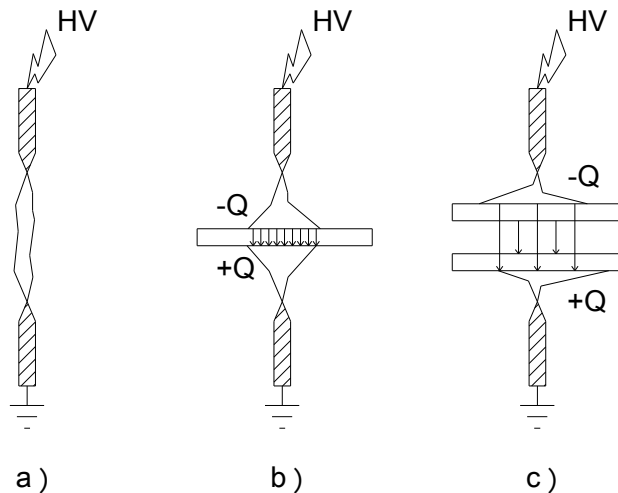


Fig. 2.6 Barrier effect on streamer behavior a) Oil without barriers shows higher BD probability. b) Ion guard effect due to streamer tip expansion, reducing local electric field. c) Bulkhead effect: reduction of electric field in oil channels (small arrows). Electric field vectors in pressboard are not displayed in this condition.

Despite the name, barriers are not design to block discharges but to prevent their inception controlling electric field.

3 Physical parameters that affect converter and traction transformer insulation

3.1 Water influence in oil-paper systems

Different authors report the negative effect of water in life expectancy of cellulose insulation [4][5] [6] [7] [8]. Moisture degrades pressboard and insulating paper in such a way that the mechanical strength of cellulose reduces one half when water content increases twice.

There are three different sources of water inside a transformer: residual water, water as a byproduct of normal aging and water ingress from the outside of the transformers

Cellulose degradation in presence of water is caused by three processes: oxidation, pyrolysis and hydrolysis. Taking into account the activation energy of each chemical reaction and considering transformer work conditions (low oxygen contain and normal work temperature), hydrolysis is the dominating process. Cellulose molecules chains scission depends on carboxylic acids dissociated in water and hence both carboxylic acids and water are produced during cellulose aging. Besides reduce aging reactions, water also reduce overall insulation strength and partial discharge inception voltage, increasing the risk of catastrophic failures because the increment of bubbling risk at high operating temperatures or during the dynamic water exchange during transformer thermal cycles.

Oil and cellulose behavior in presence of water is very different. Cellulose is a hydrophilic material and oil is hydrophobic. So, in a power transformer water is stored mainly inside solid insulation and only a very small part is dissolved in oil. Nevertheless, water exchange is a dynamic process that strongly depends on operation conditions.

Cellulose structure is a lattice of fibers and pores [9][10]. Water adsorption starts in cellulose surface and in micro-capillary structures of fibers. When water molecules in vapor phase join those structures, they move in a limited way thanks to electromagnetic attraction of polar portions of cellulose. This process takes places until other water molecules occupy all the available exposed fiber structures, forming a molecular layer of water, known as monolayer.

If water molecules concentration on the cellulose surface exceeds the available capillary structures, the excess molecules pressure the monolayer to the inner part of the insulation, forcing them to be adsorbed by inner cellulose molecules. The excess molecules in this way form a new monolayer that replaces the former one. This part of the process is called multilayer. If there is available an enough quantity of water molecules, the process is repeated until reaching equilibrium condition.

A similar process takes place during water desorption from cellulose. However, in order to initiate the process and in a different way in comparison with adsorption, it is require an activation energy, that is commonly provided by a temperature increment. For this reason, when temperature increases, the quantity of water that the cellulose can admit is reduced.

Insulating liquids show low water affinity and only admit few parts per million of water. Over that value, known as saturation limit, water cannot be dissolved in oil and it becomes free water.

Saturation limit depends on the temperature of the oil. This dependency could be modeled using Arrhenius law, like:

$$W_{s-oil} = 10^{(A-B)/T_k} \quad \text{Eq. 1}$$

W_{s-oil} = Oil saturation limit (ppm)

T_k = Oil temperature (°K)

A, B = Experimental coefficients

It is possible to find in the literature some common values for the experimental coefficients of different dielectric fluids [5][11]. In Fig. 3.1 the saturation curves for mineral oil and FR3 ester based on soy seeds are displayed at a temperature of 20°C.

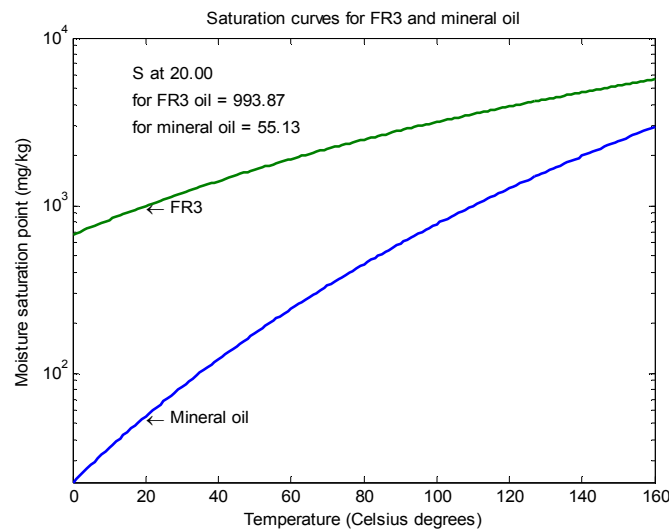


Fig. 3.1 Saturation curves for mineral oil and FR3

Besides the temperature dependency, during oil aging processes, some polar byproducts that show water affinity are produced. Those byproducts modify also the saturation limit during the complete aging of the oil. Due to the fact that during this work, only new oil was used, no details regarding this dependency are described.

Until now, a simplified explanation of the physics of water in cellulose and oil has been described. Next, the dynamic water exchange inside these transformer materials is explained.

As already has been explained, temperature influences the behavior of water in cellulose and oil. So, a dynamic equilibrium takes place at different temperatures, moving the moisture from one to other material. In order to assess moisture distribution inside the transformer insulation system considering the existence of thermodynamic equilibrium between cellulose and its neighborhood, it is clear that it must be an equilibrium between the water vapor partial pressures and hence between different relative concentrations. In this way, relative moisture saturation in each material could be defined as:

$$R_S = \frac{P}{P_{sat}} = \frac{W_c}{W_{s-c}} = \frac{W_{oil}}{W_{s-oil}} \quad \text{Eq. 2}$$

Where

R_s = Relative saturation

P_{sat} = Saturation pressure of water vapor

P = Partial pressure of water vapor

W_c = Water content in cellulose

W_{s-c} = Water saturation value in cellulose

W_{oil} = Dissolved water in oil

W_{s-oil} = Water saturation value in oil

Different authors have proposed equilibrium curves to determine water content in cellulose as a function of dissolved moisture in oil or as a function of air relative moisture, depending on the material surrounding the cellulose or on the water vapor partial pressure. Those curves are usually obtained in an experimental way but are based on isothermal sorption. The most famous equilibrium curve was plotted by Oomen [12].

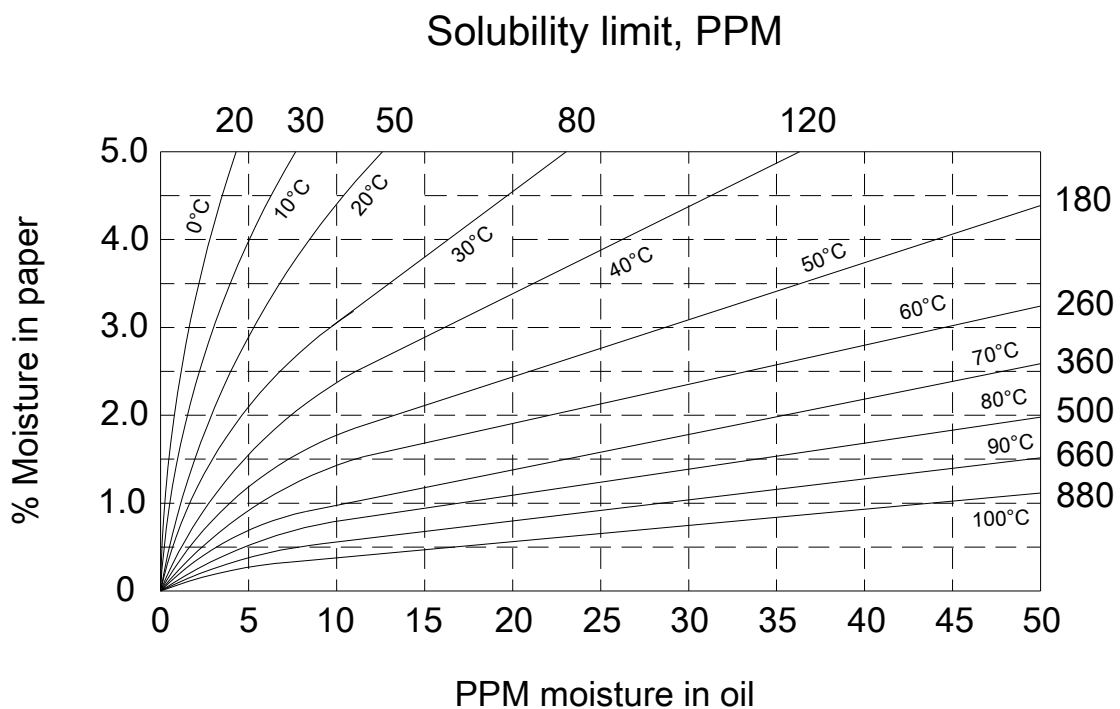


Fig. 3.2 Oomen equilibrium curve for oil and paper water exchange

Although these curves have proven their usefulness to determine the content of water in the cellulose by means of assessing oil moisture, one must consider that they are not 100% accurate, due to diverse factors (thermodynamic equilibrium is not guaranteed during sampling. Karl Fischer errors can occur, etc.).

3.2 Electrodes geometry

The influence of electrodes on the breakdown strengths of insulating liquids depends on both electrode material and electrode dimensions, including electrode area and gap distance. A generally accepted fact is

that the breakdown strength is decreased as electrode dimensions increases, due to the increased probability of initiating a breakdown via localized field enhancement.

It has been reported that breakdown strength of a dry, clean and degassed oils depends on the electrode material used in the breakdown tests [13][14]. Further investigation using DC voltage confirmed that the liquid strength depended on the material of the cathode electrode, rather than the anode electrode [15]. A possible explanation is that the breakdown process of clean oils is triggered by the electrons emitted from the electrode.

The natural oxide film that usually covers cathode electrode surface constitutes an effective layer which may hinder the neutralization and electron emission, thus affecting the dielectric strength of the liquid [15].

For contaminated oil, the influence of electrode material on the breakdown strength is not as significant as in clean oil[16]. Breakdowns in contaminated liquids usually occur at much lower voltages due to contaminants that work as weak links, rather than due to the emitted electrons from the cathode.

The influence of electrode dimension includes two effects: the influence of electrode area and the influence of gap distance. The dielectric strength of insulating liquids decrease with the increase of electrode area (electrode area effect) and gap distance [17][18][19]. Usually the increase of the electrode area and the effect of the gap length, are included in only one term: the volume effect [20][21].

The volume effect is usually attributed to weak-links in both the liquid and on the electrode surface, such as the gas bubbles and micro-protrusions [22]. With the enlargement of the stressed zone, more weak-links are involved in the liquid breakdown, leading to a lower dielectric strength.

Under divergent fields, for breakdown and also for PDIV detection, the streamer initiation is affected by the local electric field surrounding the point electrode, while the streamer propagation is governed by the local field surrounding the streamer tip. Therefore, the electrode configuration affects the streamer properties mainly through its influence on the field distribution between electrodes and it is assumed that particles are less important.

Despite a variety of factors that influence liquid breakdown, the mechanisms in uniform fields and in divergent fields are similar in the sense that they are both triggered by the occurrence of a streamer, and a breakdown will occur when the streamer bridges the liquid gap.

However, there are also differences between the breakdown mechanisms in uniform fields and in divergent fields. In uniform fields, almost every streamer will propagate to breakdown due to a high average field. Therefore, the liquid breakdown is determined by streamer inception, and the breakdown voltage is approximately the same as the streamer inception voltage [23]. On the other hand, the liquid breakdown under divergent field is determined by streamer propagation due to a low average field. Thus, the breakdown voltage is much higher than the streamer inception voltage and PDIV can be assessed in a better way.

Under AC voltage, the relationship between streamer inception field is slightly different. In uniform fields ($>10^{-1} \text{ cm}^2$), the streamer inception field of filtered oil (equal to breakdown field) under AC voltage is lower than that under impulse voltage. This is attributed to longer voltage application duration, and thus a higher chance of streamer initiation at lower voltage [24]. For contaminated oil, the streamer inception voltage is further decreased due to contaminants. In highly divergent fields ($<10^{-3} \text{ cm}^2$), the AC streamer inception field becomes higher than impulse streamer inception field. This effect can be explained as follows: under

AC voltage, there is more available time to accumulate space charge in the electrodes neighborhood. This space charge reduces the local field on the point electrode, making necessary higher voltages to produce the inception field. Under impulse voltages the effect of space charge is negligible, due to the fact that voltage duration is not so long to allow its build up[25].

3.3 Temperature

As temperature increases, the dielectric strength of most of the solid insulations reduces. Due to increase in dielectric loss (and power factor), insulation temperature goes up further. The insulation ohmic resistance reduces with the increase of temperature, which results in flow of more current in the insulation. It may finally lead to the current run-away condition and eventual breakdown. The deterioration of the solid insulation strength with increase of temperature is opposite to the effect usually observed for the transformer oil.

The oil dielectric strength usually increases with temperature in the operating range. A marked improvement in the strength with the temperature increase is observed for the oil containing high moisture content. The temperature effects are dynamic in the sense that a considerable amount of time is required for establishing equilibrium between moisture in the oil and that in the solid insulation made of cellulose material. During different thermal loading conditions, there is a continuous interchange of moisture affecting the strength to some extent. For a reasonable temperature rise, the amount of moisture in the oil reduces, and thus this helps to keep the transformer insulation system in a healthy condition. It is known that an increase of temperature usually increases the mobility of carriers and conductivity. Hence, the breakdown voltage of oil should decrease with the increase in temperature; experiments conducted by many researchers show the opposite trend for BDV and for PDIV [26]. The variation of carriers and mobility, therefore, may not possibly be used to explain the results of experiments. There is some amount of gas bubbles present in the oil and their solubility increases with temperature; this explains the increase of strength with the temperature.

Hence, it is generally not preferable to keep a transformer idle for a long time. Even a spare transformer should be kept in no-load condition for a reasonable amount of time periodically. The strength increases with temperature from -5°C to about 80 to 100°C; above which it reduces. Below -5°C, the strength increases rapidly as moisture particles in suspension get frozen. No testing as a function of temperature was carried up during this research work.

3.4 Waveform influence on converter transformers insulation

Transmission and distribution of electrical energy started with direct current. In Germany in 1882, a 50 km long 2 kV DC transmission line was commissioned. At that time, the only available way to convert the relative DC high voltages to final user levels was the use of rotating DC machines. Soon, it was observed that in AC systems, the voltage conversion is simpler because the possibility of use two important equipments: the power transformer and the synchronous generator. Power transformer allows high power transmission with very low losses. It can deal with voltage regulation and it contributes to control short-circuit currents. Transformers require less maintenance operation than DC rotative machines. AC synchronous generators offer lots of advantages in comparison with DC generators: real and reactive power control, dynamic voltage regulation, etc. For these reasons AC transmission systems were accepted as the better option and still now they continue to be the power system core.

Despite the AC systems advantages, some operation problems are evident, especially regarding modern requirements [27]:

- Reactive nature of power lines limits transmission capacitive, especially in long links. This effect is more evident if the link is constructed with high voltages cables.
- Power connection between different countries is very common. Due to the fact that power systems in those different countries can operate at different frequencies and they might not be synchronized, AC transmission systems between those geographical areas is impossible.
- New connections to meshed grids could be a problem because the increase of short-circuit levels and non defined power flow scenarios.
- Dynamic control of instabilities is impossible.

Due to those disadvantages and to new power electronics devices which can now be use in power system voltage levels, DC voltage is gaining again popularity, especially in long distance transmission and in off-shore applications.

There are two main types of HVDC systems, those that use line current sourced commutated converters (LCC) and those with self commutated voltage sourced converters (VSC). Line commutated current sourced converters are the older technology. At the beginning, those systems employed mercury arc rectifiers that then were substituted by power thyristors. Current line commutated systems use air insulated water cooled thyristors, with a minimum number of valves parallel connection.

Self commutated voltage sources converters require semiconductors devices with controlled turn on and turn off capacities. IGBT technology has made possible compact converters with four quadrant operation for the lower power range of power systems (less than 250 MW). ABB call these converter technology HVDC light [28] and Siemens calls it HVDC Plus [29]. Multilevel converters using this technology offer low harmonics contain at a higher loss level.

In order to reduce harmonics in LCC (high power applications), 12 pulse converters have become popular. This topology needs the series connection of two six pulses converters. This is possible by means of two converters fed by two power transformers connected in the vector groups Yy0 and Yd5 (30° phase shift).

Converter side windings of both transformers are exposed to DC voltages, stressing in a combined way the insulating system. Normally the DC voltages in the valve side are distributed as shown in Fig. 3.3[30].

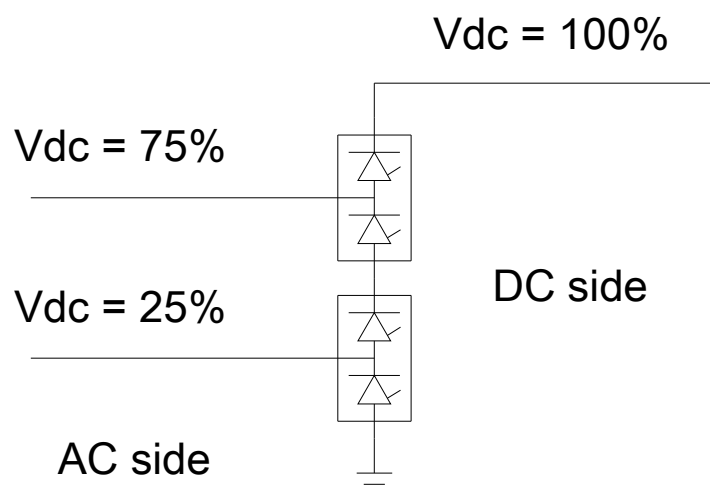


Fig. 3.3 DC voltage distribution in the valve side of a HVDC transformer

In order to verify this theoretical distribution for a typical 12-pulse converter system consisting of two six-pulse rectifiers [8] (Fig. 3.4), the output voltages of the converter transformer were calculated using a commercial software. The results (displaced by 30 electrical degrees) of one of those simulations are shown in Fig. 3.5 and Fig. 3.6.

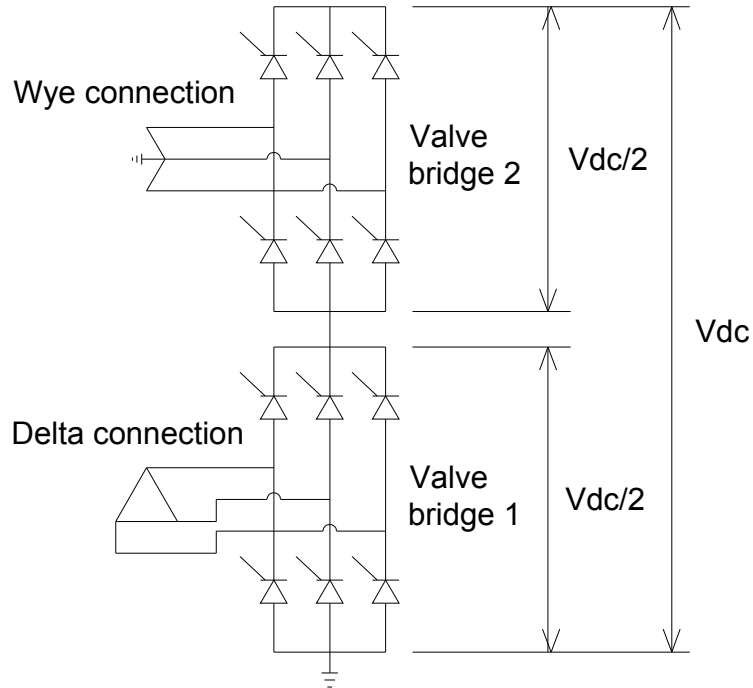


Fig. 3.4 Valve bridges in ± 800 kV converter transformer

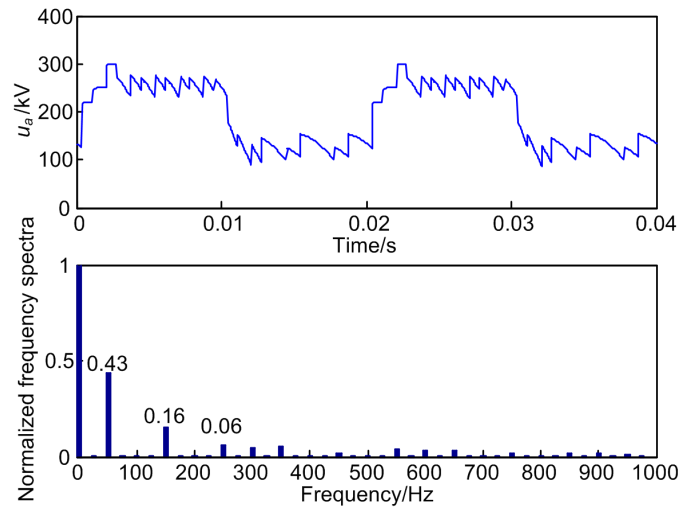


Fig. 3.5 Normalized frequency spectra of the u_a

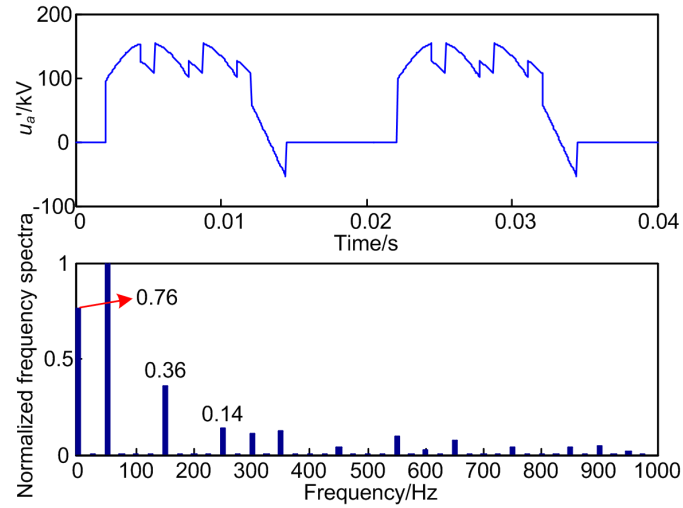


Fig. 3.6 Normalized frequency spectra of the u_a'

Now, once that DC voltage bias was intuitively explained, mathematical description of AC and DC phenomena in transformer insulation systems can be presented:

The electric field can be defined as the gradient of voltage in a particular region (Eq. 3)

$$\vec{E} = -\nabla V \quad \text{Eq. 3}$$

The Ampere law establishes two different current types, conduction and displacement current. Conduction current is mainly governed by the electrical conductivity (electron mobility) whereas displacement current is mainly influenced by dielectric permittivity. In order to make possible displacement current, it is necessary a time dependent electric field.

$$\vec{\delta} = \varepsilon \frac{d\vec{E}}{dt} + \sigma \vec{E} \quad \text{Eq. 4}$$

Substituting total current, in continuity equation, one can obtain

$$\nabla \cdot \left(\varepsilon \frac{\partial \vec{E}}{\partial t} + \sigma \vec{E} \right) = 0 \quad \text{Eq. 5}$$

Putting Eq.5 in terms of electric potential and then regrouping the terms, Eq. 6 and then Eq. 7 can be obtained.

$$\nabla \cdot \left(\varepsilon \frac{\partial \nabla V}{\partial t} + \sigma \nabla V \right) = 0 \quad \text{Eq. 6}$$

$$\left(\varepsilon \frac{\partial}{\partial t} + \sigma \right) (\nabla^2 V) = 0 \quad \text{Eq. 7}$$

Eq. 7 is the well known Laplace equation, in which conduction and displacement effect are taken into account. It is evident from this equation that when direct current is applied, time dependence becomes zero, so, conductivity is the important parameter to be considered. On the other hand, when time

dependent voltage is applied, displacement effect is dominant because the conductive term becomes negligible.

The worst case occurs during polarity reversal of DC voltage. In this case both terms become important and the complete insulating systems are stressed at the maximum level. Fig. 3.7 shows voltage distribution in a transformer cross-section when it is fed with AC, DC and during DC polarity reversal [31].

As it could be observed, in AC voltage, electric field is distributed in an inverse proportion to the permittivity of the materials. This can be explained using the definition of perfect and isotropic dielectric and applying border conditions between two materials with dielectric permittivities ϵ_1 and ϵ_2 .

Applying Gauss theorem in a cylinder with dl height and dS base, located in the interface between the two dielectrics, we have:

$$\oiint \vec{D} \times \hat{n} dS = Q_{free} \quad \text{Eq. 8}$$

If there are not free charges at the dielectrics interface at the beginning of the process, Gauss equation can be written for this region as:

$$\oiint \vec{D} \times \hat{n} dS = 0 = D_1^n = D_2^n \quad \text{Eq. 9}$$

Applying constitutive relationships, we obtain finally:

$$\epsilon_1 E_1^n = \epsilon_2 E_2^n \quad \text{Eq. 10}$$

$$\frac{\epsilon_{oil}}{\epsilon_{PB}} = \frac{E_{PB}^n}{E_{oil}^n} \quad \text{Eq. 11}$$

This equation describes the inverse proportion of the electric field and the materials permittivity.

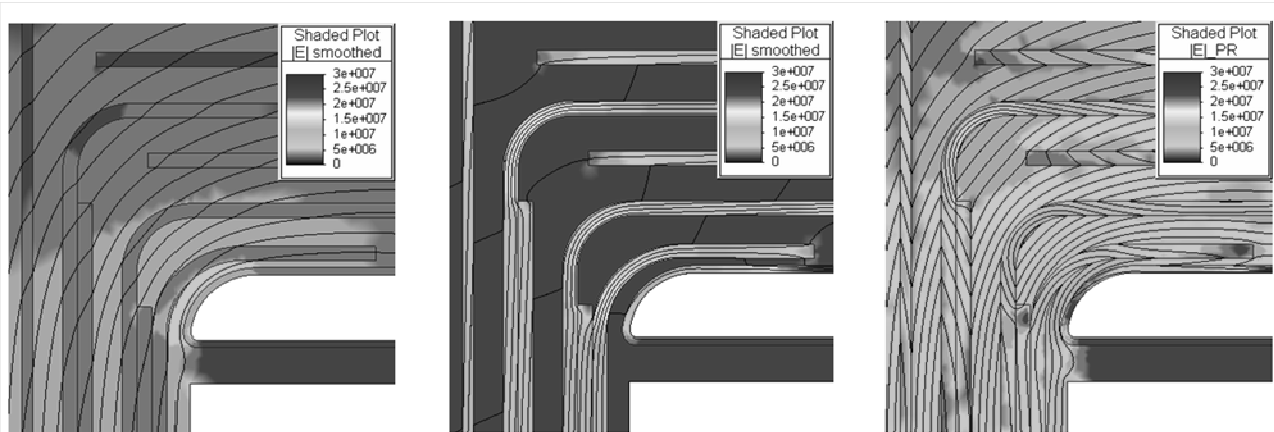


Fig. 3.7 Potential and electric field distribution under AC, DC and polarity reversal voltages

In DC voltage, during the initial transient (step response), the electric field also shows a capacitive distribution like in AC, due to voltage time dependency. During this transient, current density decrement is

also noticeable. The cause of this decrement is the charge carriers movement. These carriers are pushed in the electric field direction and accumulated in the oil and pressboard interface, causing a reduction of the density of free charge carriers.

The complete transient phenomena could be modeled by means of a theoretical capacitance, called Maxwell capacitor [32]. This capacitor has one or more layers of dielectrics, that can be reduced to only two layers with thickness a and b . Using Maxwell and Ohm laws (Eq. 12 and Eq. 13), continuity equation (Eq. 14) can be written in terms of the electric field.

$$\rho = \nabla \cdot D = \nabla \cdot \varepsilon E \quad \text{Eq. 12}$$

$$J = \sigma E \quad \text{Eq. 13}$$

$$\nabla \cdot J + \frac{\partial \rho}{\partial t} = 0 \quad \text{Eq. 14}$$

$$\nabla \cdot \sigma E + \frac{\partial}{\partial t} (\nabla \cdot \varepsilon E) = 0 \quad \text{Eq. 15}$$

$$(\sigma_a E_a - \sigma_b E_b) + \frac{\partial}{\partial t} (\varepsilon_a E_a - \varepsilon_b E_b) = 0 \quad \text{Eq. 16}$$

Total applied voltage V is:

$$V = aE_a + bE_b \quad \text{Eq. 17}$$

Writing Eq. 17 in terms for example of E_a , we obtain:

$$\dot{E}_a (\varepsilon_a b + \varepsilon_b a) + (\sigma_a b + \sigma_b a) E_a = \sigma_b V + \varepsilon_b \dot{V} \quad \text{Eq. 18}$$

Using a step function with amplitude $V = \begin{cases} V(0) = V_0 \\ \dot{V} = 0 \end{cases}$ one can obtain:

$$E_a = \frac{\sigma_b}{(\sigma_a b + \sigma_b a)} V_0 \left(1 - e^{-t/\tau}\right) + \frac{\varepsilon_b}{(\varepsilon_a b + \varepsilon_b a)} V_0 e^{-t/\tau} \quad \text{Eq. 19}$$

The second term of this equation represents the transient response, dominated by permittivity magnitudes whilst the first term represents the steady state condition, where conductivity is the predominant parameter.

Transient duration depends on the constant time of the system, which depends on the magnitude of the applied electric field, temperature, electronic mobility, moisture, oil dynamics and space charge.

During steady state (DC condition), the ratio between pressboard and oil conductivities (τ) goes from 10 to 500. τ is strongly influenced by oil quality mainly, and can change remarkably even for the same oil batch depending for example on local temperature differences.

Common permittivity values for mineral oil and pressboard are $\epsilon_{oil} = 2.2$ and $\epsilon_{pb} = 4.4$, so, oil must withstand two times the relative electric field of the pressboard in AC. For DC, we can make a similar assumption, but in terms of electric conductivity. As it has been quoted previously, oil conductivity depends on many factors. So, in order to illustrate electric field distribution in oil and pressboard in DC, one must take for example a ratio of 100 (it means that oil is 100 times more conductive than pressboard). Thus, the field in the board is about 100 times the field in the oil if $a=b$, where a and b are the thickness of the oil and pressboard layers. Fig. 3.8 shows graphically the electric field distribution in an oil-pressboard interface.

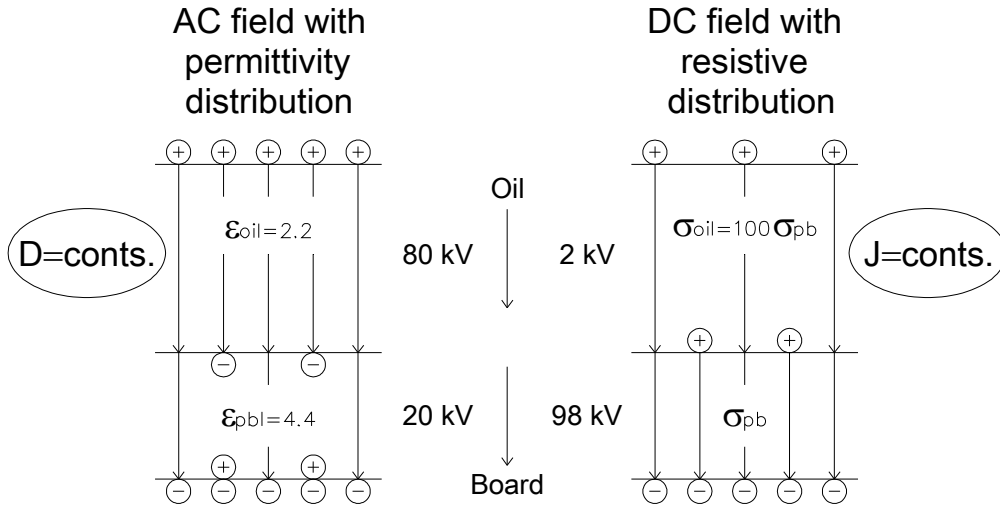


Fig. 3.8 Electric field distribution in an oil-pressboard interface

Until now, the effect of space charge in the oil-pressboard interface has been neglected to understand in an easier way the voltage distribution in the materials. In the following, the deduction of the equation that governs space charge accumulation at the interfaces is derived. For quasi-electrostatic field, Maxwell and continuity equations can be written as:

$$\nabla \times E = 0 \quad \text{Eq. 20}$$

$$\nabla \cdot D = \nabla \cdot \epsilon E = \rho \quad \text{Eq. 21}$$

$$\nabla \cdot J + \frac{\partial \rho}{\partial t} = 0 \quad \text{Eq. 22}$$

Using Ohm law, Eq. 21 and Eq. 22 become:

$$J \cdot \nabla \frac{\epsilon}{\sigma} + \frac{\epsilon}{\sigma} \nabla \cdot J = \rho \quad \text{Eq. 23}$$

The elimination of $\nabla \cdot J$ leads to:

$$\frac{\partial \rho}{\partial t} + \frac{\sigma}{\epsilon} \rho = \frac{\sigma}{\epsilon} J \cdot \nabla \frac{\epsilon}{\sigma} \quad \text{Eq. 24}$$

In pure DC state, the accumulated space charge remains constant, so that, Eq. 24 becomes:

$$\rho = J \cdot \nabla \frac{\varepsilon}{\sigma} \quad \text{Eq. 25}$$

Using Eq. 13, Eq. 25 becomes:

$$\rho = \sigma E \cdot \nabla \frac{\varepsilon}{\sigma} \quad \text{Eq. 26}$$

According to this equation, external factors that can produce changes (gradient) of ε and σ must be taken into account to assess charge accumulation. Transformer losses and external changes of ambient or local temperatures can lead to the enhancement of electric conductivity and hence of space charge accumulation at interfaces. Even in the case of DC voltages in a single material, charge accumulation can occur. The polarity of the space charge depends on conduction mechanisms through the electrodes and the bulk dielectric material. One can observe two different kinds of charge accumulation: homocharge and heterocharge [33].

Homocharge has the same polarity of the nearest electrode. In this case, the charge transport between the electrode and the dielectric is superior to the charge transport capacity of the bulk dielectric. Homocharge tends to reduce dielectric gaps, contributing to breakdown.

Heterocharge has opposite polarity with respect to the nearest electrode. It occurs when the contact between the electrode and the dielectric blocks the extraction of mobile charges. In this case, charge transport in the bulk dielectric is superior to the limited current in the contact of the electrode and the dielectric. The accumulation of heterocharge produces local degradation of the dielectric system.

Both types of charge accumulation affects the behavior of the dielectric system under DC conditions, enhancing electric field in the interfaces and complicating even more the DC influence on oil-pressboard insulating systems.

3.5 Waveform influence on traction transformers insulation

Massive transportation systems with lower environmental impact are a most in modern cities. Electrical transportation systems accomplish this requirement easily, offering a high reliability. Inside the core of these systems, the traction transformer is one of the most important elements. Traction transformers are not ordinary power or distribution transformers. They have to face several special requirements, like voltage regulation, impedance, commutation, short-circuit withstand and harmonic losses.

Several aspects of traction transformers are covered by IEEE Standard C57.18.10 “Standard Practices and Requirements for Semiconductor Power Rectifier Transformers”. but, it was found that there are some specific issues of traction transformers which were not adequately covered therein.

Electric locomotives generally have four asynchronous three-phase motors, but the traction circuit could be different, depending on the type of locomotive: The first option has two three-phase inverters and two choppers (one per bogie) which can feed the motors with a variable voltage ranging from 0 to 4200 V, depending on catenary voltage (from a minimum of 1200 to 4000 V). The second option uses a rectifier when the locomotive is fed with 25 kV AC or choppers when it is fed with 3 and 1.5 kV DC.

In Fig. 3.9 two schematics of a locomotive power system are displayed. In both cases, the transformers are mounted on the train, but it is also possible to mount the transformers in the traction substation. From the point of view of dielectric stresses, in these two cases, transient over voltages are caused by harmonic

currents circulation inside transformer windings. When IGBT converter is used in railway technology, transformer winding faces fast switching pulses, which produce the same stress that transient over-voltages caused by harmonics.

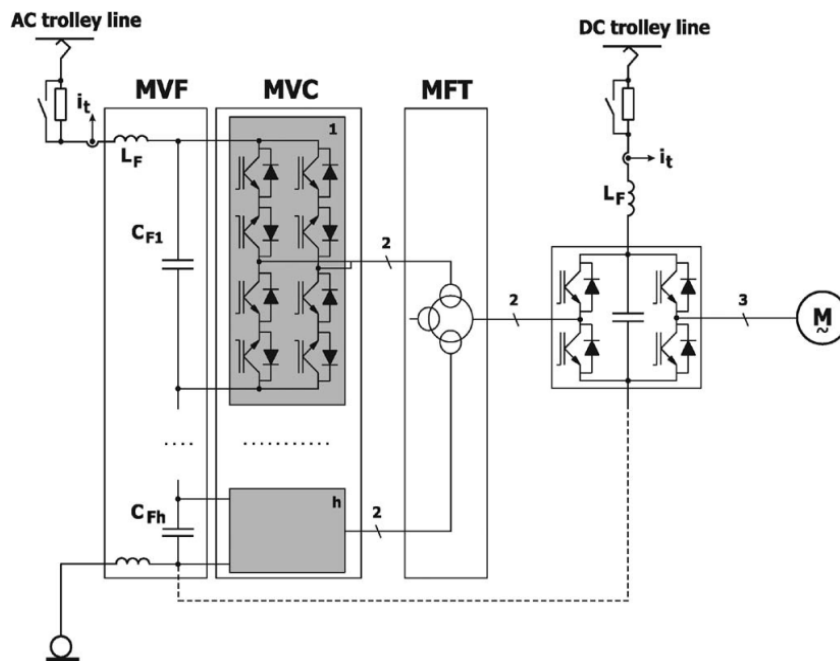
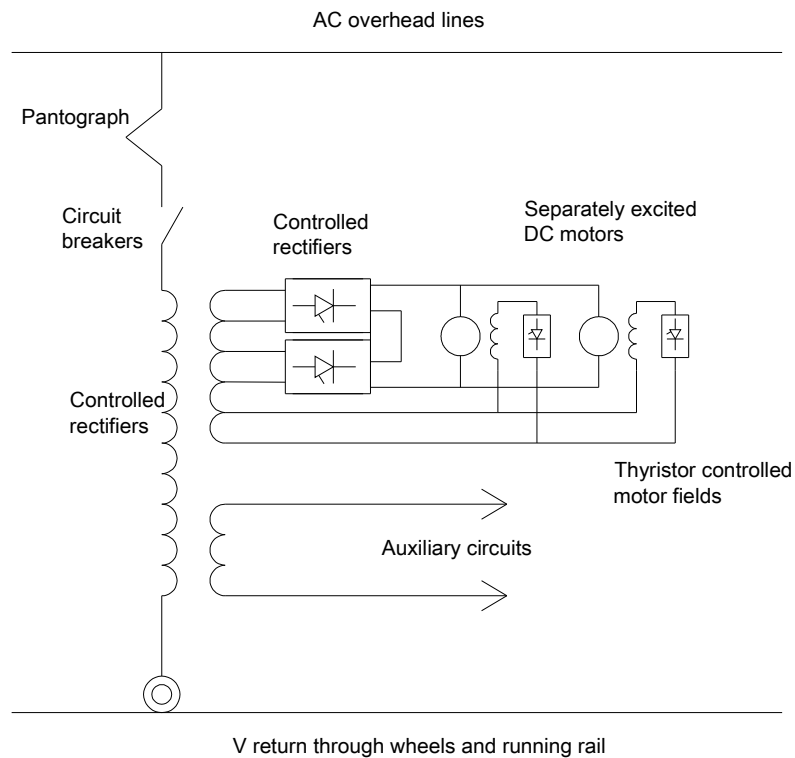


Fig. 3.9 Typical locomotive power systems

4 Experimental setups, test procedures and data processing

4.1.1 Oil and pressboard conditioning cells

In order to condition oil and pressboard to match the requirements of relevant standards (ASTM D2413 – 99[34]), different procedures were followed.

The pressboard is heated and vacuum-dried whilst the dielectric liquids are vacuum-degassed and dried. For this research work, the pressboard was dried in small individual samples, but for other applications the process could be applied when PB is assembled between electrodes. For impregnation purposes, the dielectric liquid is dried and degassed prior to introducing it into the chamber containing the dried pressboard. The same procedure is followed for preparation of oil samples.

The drying, degassing and impregnation chambers should be designed in such a way that they could be heated when it is required. The chambers could be autoclaves with pressure and temperature control, or containers that could be used in an oven equipped with a thermal control unit capable of maintaining selected temperatures as high as 250°C. The chambers should have a connection to a vacuum pump capable of maintaining absolute pressures as low as 75 Pa as measured by a suitable vacuum gauge. Conditioning chambers are constructed with Pyrex glass or stainless steel to avoid contamination.

To dry the oil, a sealed vacuum container is required. Once this container is filled with the oil, it is connected to the vacuum pump at 75 Pa during 24 h. In order to extract moisture and gasses trapped in the bottom levels of the oil volume, a magnetic stirrer is used to produce oil flow. Sometimes, it is also convenient to increase a little the temperature of the oil to increase the degassing efficiency.

In order to dry the pressboard before impregnation, specimens are piled loosely in the impregnating chamber at 115 °C and an absolute pressure of 75 Pa or less for at least 24 h.

For pressboard impregnation it is important to arrange a pressboard pieces in such a way that the liquid impregnates the paper from the bottom. After the liquid has completely covered the paper, vacuum process is interrupted with desiccated air. A 8 h period at atmospheric pressure is required for the pressboard to become completely impregnated. The time required for impregnation is dependent on the rate of liquid penetration of the pressboard, which in turn is an inverse function of its density, its thickness, and the liquid viscosity.

Loose pieces of PB impregnate more quickly. Once impregnated, samples should not be removed from immersion in the dielectric liquid, because moisture absorption will occur into them.

The most complete conditioning system developed for this research work to dry oil, pressboard and perform impregnation, is shown in Fig. 4.1.

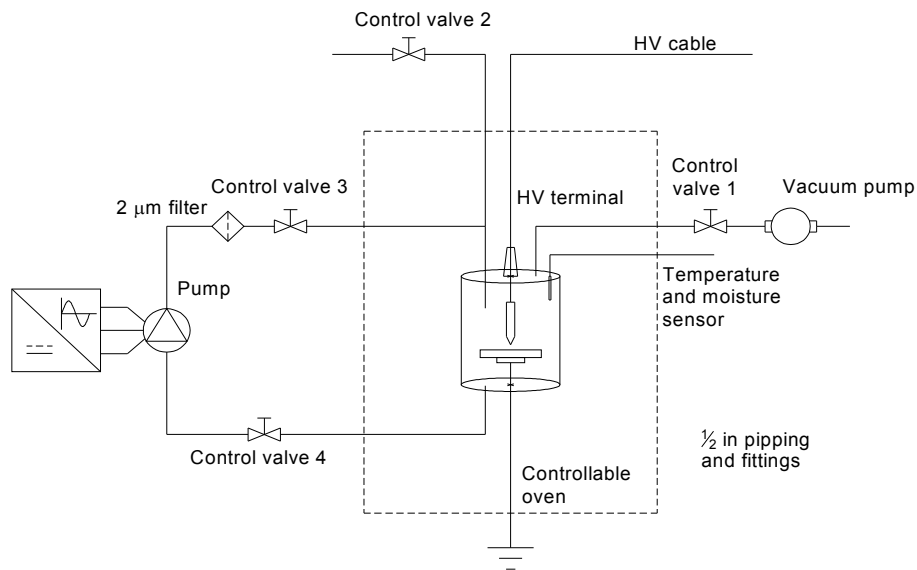


Fig. 4.1 Conditioning system for oil and pressboard drying and impregnation

Control valves 2, 3 and 4 are used for oil filtering and to empty the conditioning cell. This recirculation system is fed with a variable speed pump that it is use for test purposes, when the conditioning cell is used also as test chamber. Control valve 1 is provided to connect or disconnect the vacuum pump from the cell. A Vaisala MMT330 moisture and temperature sensor could be connected to the cell to assess physical parameters of the oil during the process. This cell can be used for electrical testing.

A simpler oil drying and degassing setup, which cannot be used for testing is depicted in Fig. 4.2

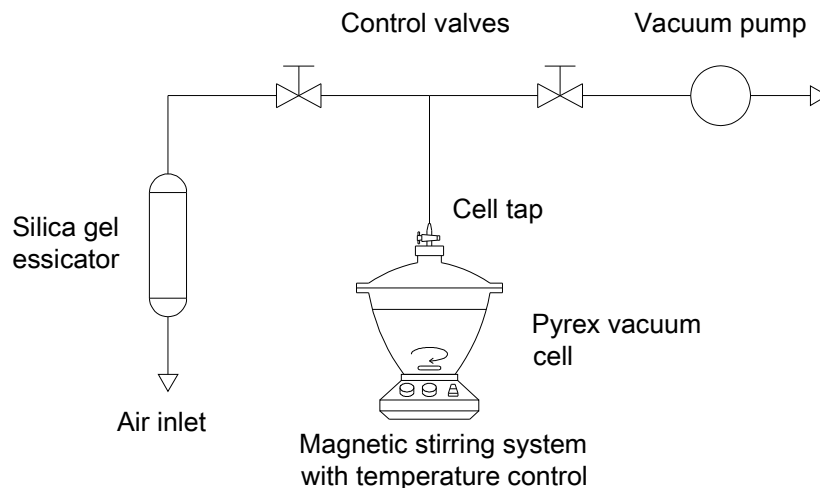


Fig. 4.2 Oil drying and degassing cell

Vacuum drying process is based in the diagram depicted in Fig. 4.3. As it can be noticed, water boiling temperature depends on cell pressure. If pressure decreases, for example to 50 Pa, water vaporizes at around -30°C, making easy its extraction from pressboard and oil. Vacuum process also extracts gasses trapped in pressboard fibers. Those gasses produce positive local pressure inside pressboard, avoiding impregnation.

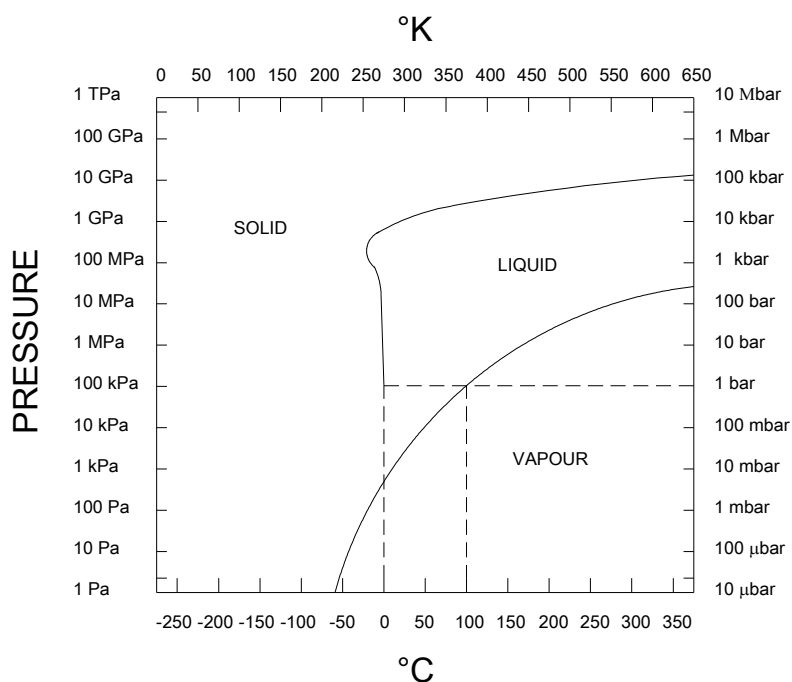


Fig. 4.3 Thermodynamic states of water as a function of temperature and pressure

4.1.2 Karl Fischer titration

Karl Fischer titration is maybe the most used method for water determination in solid, liquids and gases. Water assessment using this method could be coulometric or volumetric. During this work, the coulometric method was used for all the analyzed samples. Coulometric titration is based in the determination of the consumed electric charge during the reaction of the moisture dissolved in the test sample with the titration reagent [35].

In the case of oil samples, a small oil volume is directly injected in the reaction vessel that already contains the titration reagent. For pressboard and other solid materials, a sample is heated in an oven to vaporize water and other gasses. This gas phase is transferred to the titration vessel and is then processed in the same way as oil samples. The titration vessel for coulometric assessment of water contains an electrolysis cell that is usually constructed using two chambers, connected between them by a porous diaphragm.

Karl Fischer method has two main advantages: it offers a high selectivity for water assessment, due to the fact that the titration can be only produced in presence of water and it is very suitable for small samples.

Regarding disadvantages of the Karl Fischer method, it could be say that a wrong sampling process can affect the reliability of the final water determination. Main aspects to control during sampling are:

1. Bubbles have to be avoided during the sampling process, so, the tip of the needle should be inserted in the liquid completely to reduce air aspiration.
2. The sampling syringe should be oven dried before use and store in a dry place. It is important to use different syringes for different fluids to avoid sample contamination.
3. During sample injection in the to the titration vessel, the needle must be inserted deeply, in order to prevent the fluid to touch the vessel walls, reducing in this way the effective oil volume that has been previously weighted.

In addition, the titration reagent must be chosen carefully, because with some samples it can produce additional water, biasing the measurements.

The Karl Fischer titration system used in this research work is shown in Fig. 4.4.



Fig. 4.4 Karl Fischer system for water determination

The reagent used to carry up the tests was the Sigma Aldrich Coulomat E, which offers the better behavior for both mineral oil and natural esters.

4.1.3 AC Breakdown test cells

The dielectric breakdown voltage of an insulating liquid is of importance as a measure of the liquid's ability to withstand electric stress without failure. The dielectric breakdown voltage serves to indicate the presence of contaminating agents such as water, dirt, cellulosic fibers, or conducting particles in the liquid, one or more of which may be present in significant concentrations when low breakdown voltages are obtained. However, a high dielectric breakdown voltage does not necessarily indicate the absence of all contaminants; it may merely indicate that the concentrations of contaminants that are present in the liquid between the electrodes are not large enough to affect the average breakdown voltage of the liquid when tested by this test method.

The dielectric breakdown voltage test cells were designed or use to study the effect of uniformity of the electric field, the area and volume effects, the speed of the voltage rise, stirring effect after each shot and resting time between shots. For each type of study, different parameters were controlled, i.e. water content of the oil, presence of particles in the oil and oil temperature.

Two test cells were used, one commercial BAUR oil tester DPA test set and a 100 kV test set for gaps longer than 3 mm. For the later test set, a variable gap with two Rogowski profiles with 45 mm flat zone was designed and developed. The control of the voltage magnitude and increase rate of this test cell was carried up by a regulator that is connected to the low voltage windings of a Phenix Technologies AC test transformer. The measurement of the test voltage was made by means of a capacitive voltage divider. Breakdown current was limited using a series resistance and a fuse element.

The Baur systems is a commercial oil tester that fulfills IEC 60156[36] requirements (with semi-spherical electrodes).The test vessel is displayed in Fig. 4.5.

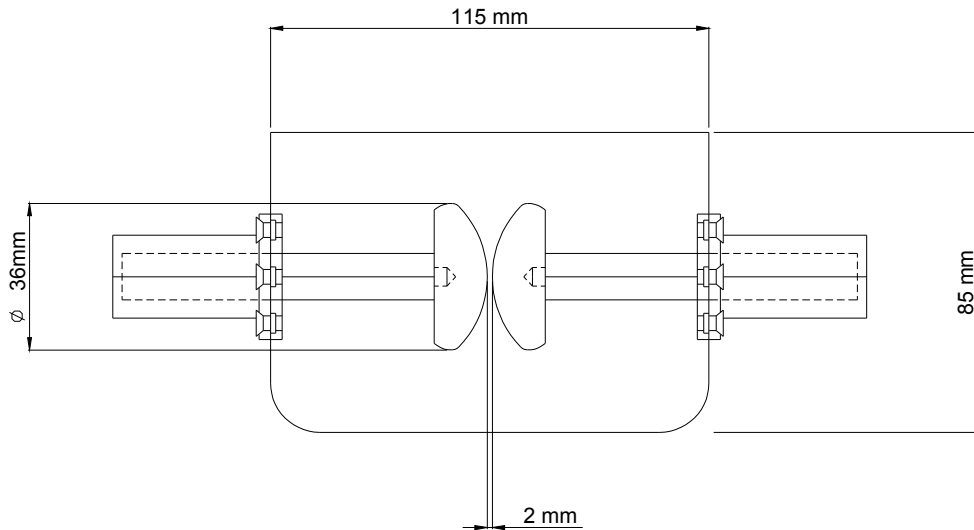


Fig. 4.5 Breakdown test cell (IEC 60156)

4.1.4 Lightning impulse test cell

An impulse test cell to evaluate oil performance was constructed. This cell offers the possibility of change electrode geometries, adjust the gap between them and remove bubbles and carbon byproducts after a discharge by means of a magnetic stirrer. Outer sheds prevent air flashover during testing operations. Internal sheds minimize the flashover probability at the interface between oil and the container. A schematic view of the developed test cell is depicted in Fig. 4.6. The electrodes consist of polished brass Rogowski profiles with a 25 mm flat zone.

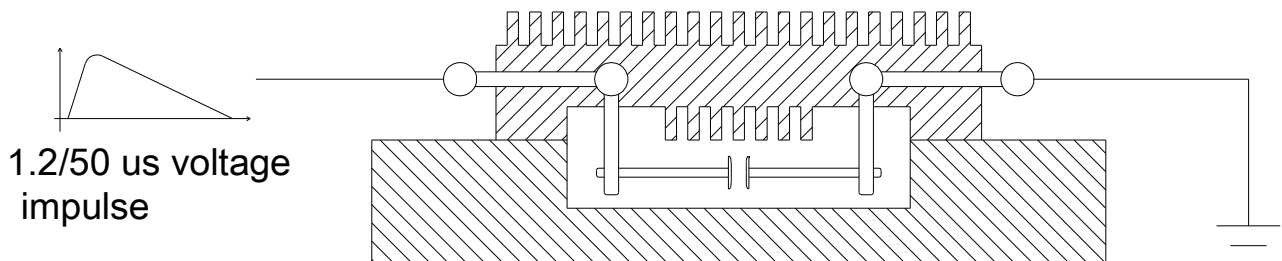


Fig. 4.6 Lightning impulse test cell

A 600 kV peak Marx type Impulse generator with 6 stages, with mechanically controlled spinterometers, equipped with a capacitive voltage divider was used for the tests. Applied impulses were standard 1.2, 50- μ s positive polarity voltage waveforms.

4.1.5 Sinusoidal and square waveform test cell

For PDIV testing under sinusoidal voltage, two options were used: a 100 kV PD free test transformer, controlled by an AC regulator or a Trek 30/20 electronic amplifier driven by a signal generator. The Trek amplifier can supply ± 30 kV peak with 1 kHz bandwidth. The Trek system besides AC sinusoidal voltage was used as well to provide square waveforms with different frequencies and complex voltages waveforms to replicate HVDC converter behavior.

The signal generator used to drive the electronic amplifier is a HP 33120A, which can be fully controlled by means of a RS232 serial port or a GPIB 488 connection [37]. This signal generator offers also the possibility of upload pre-defined user waveforms that then can be used as a function library during automatic and manual mode.

For applied voltage measurement, capacitive or resistive dividers were used depending if AC or DC voltages are assessed.

Partial discharge activity was coupled using a 50 Ω impedance, a high frequency current transformer and a coupling capacitor, depending the required interference discrimination and measurement purposes. Those PD sensors were connected to a Techimp PDBase system[®] to obtain convenient N-Q- ϕ PD patterns and smart noise filtering using t-f maps.

Typical test setup configuration is depicted in Fig. 4.7.

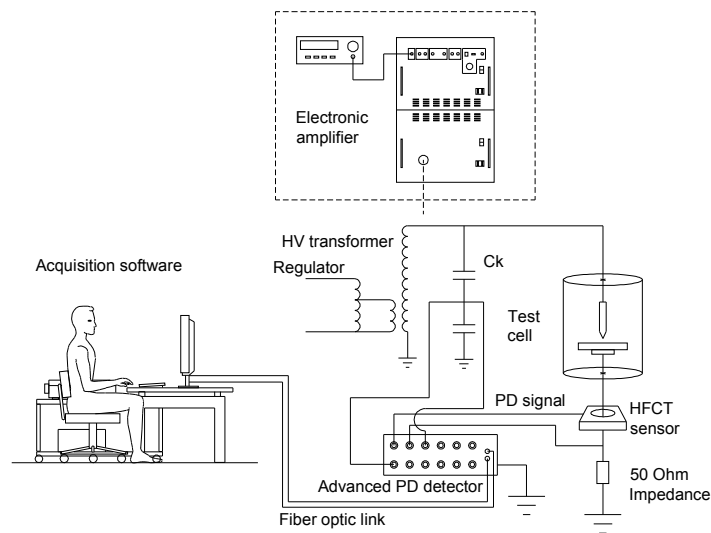


Fig. 4.7 Square wave test cell

4.1.6 HVDC

HVDC test setup is shown in Fig. 4.8. Basically, the power supply is composed by two high voltage elements, a direct power supply and a potential transformer. The DC power supply is an electronic audio amplifier, connected to a high frequency transformer that feeds a diode/capacitor voltage multiplier. After this stage, a capacitor is connected as low pass filter to condition the output. The amplifier input signal must be a variable amplitude sinusoidal 15 kHz voltage in order to reduce AC ripple, to bias the amplifier and to control the voltage output level. The maximum DC output is 40 kV whilst the maximum AC peak voltage is 100 kV. This test setup replicates in a simplified way the waveforms showed in Fig. 3.5 and Fig. 3.6.

In order to evaluate the effect of voltage notches that are present in the bushings of the valve side of HVDC transformers, the same setup that is used for square waveform testing, but in this case, sinusoidal waveforms with notches at different fire angles were loaded in the signal generator. Examples of this waveforms are shown in Fig. 4.9. The firing and overlap angles (α and μ , respectively) are considered here to be independent parameters (in a real converter this is not the case) to account for all possible situations. Realistic ranges for the values of α and μ were derived from [38], where it is reported that the boundaries

of the firing and overlap angles are from 0 to about 37 degrees and 0 to 25 degrees, respectively. Notched voltages at different firing and overlap angles are plotted in the Figure.

A resistive divider is used for AC, DC and Combined ACDC voltage measurement and for synchronization of PD measurement. The phase reference can be taken also from the potential transformer low voltage winding.

An acoustic PD detection system was also used during measurement with the aim of PD source discrimination (in general, is expected that oil PDs show large signals compared to discharges occurring in pressboard cavities, making easier their detection). The acoustic detection system is composed by a Physical Acoustic R15I-AST sensor, a portable 4262 PicoScope and a decoupling circuit (Fig. 4.10) that bias the sensor and allows signal acquisition.

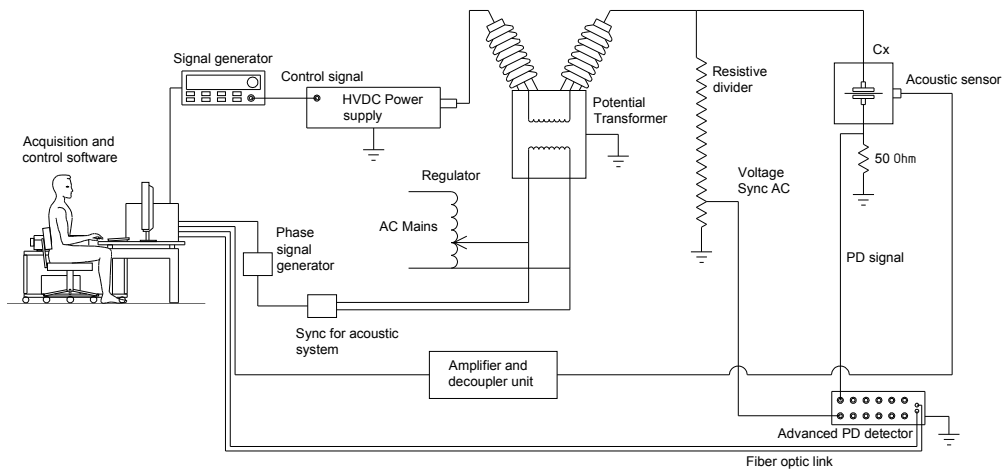


Fig. 4.8 HVDC test cell

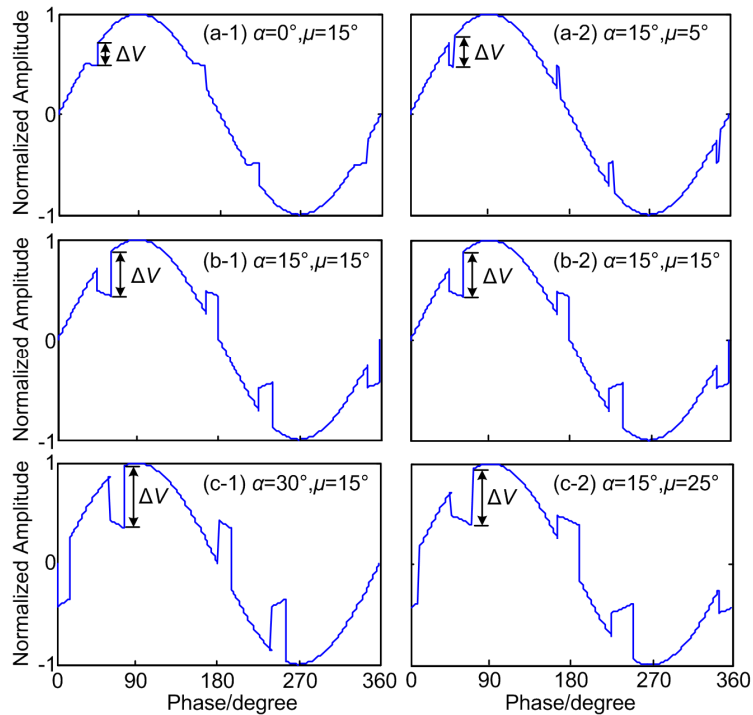


Fig. 4.9 AC notched voltage at different firing and overlap angles

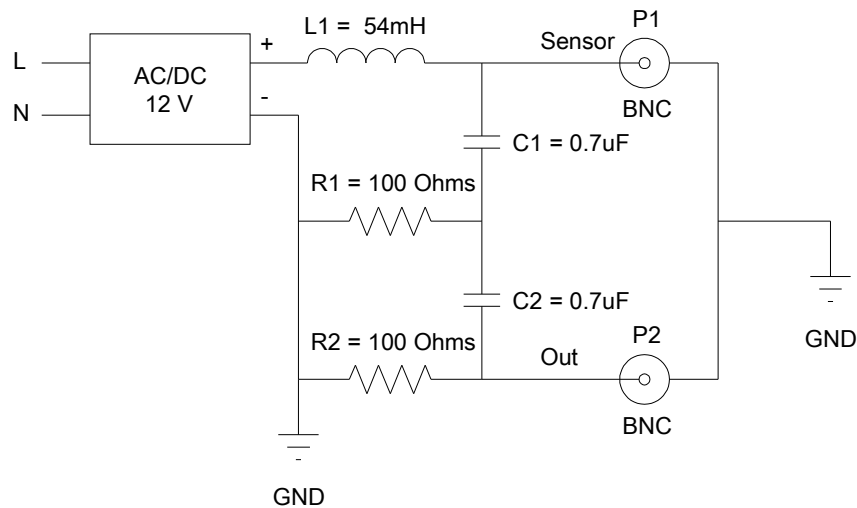


Fig. 4.10 Acoustic PD decoupling and biasing system

4.1.7 Partial discharges

There are three possible sources of partial discharges in power transformers: discharges in oil gaps, discharges along oil-cellulose interfaces and discharges inside stressed cellulose in HVDC transformers [39]. PD are usually attributed to inappropriate design or construction, but they can occur because of in use contamination and aging as well [40][41] [42]. Over a limited amount of time, partial discharge process is not a problem, but they can lead to full complete insulation breakdown over sufficiently long times. For that reason, insulating liquids in power transformers are required to withstand high electrical stresses without the inception of partial discharges [43].

The partial discharge inception voltage (PDIV) is one of the most important parameters to be controlled in high voltage insulation [44]. For this reason there is a lot of experience in its measurement under well established conditions, as those listed in IEC 61294 Insulating Liquids – Determination of the Partial Discharge Inception Voltage (PDIV) – Test Procedure [45] and in [46]. The final aim is to overstress dielectric liquids in such a way that design rules could be inferred.

PD have random characteristics that make accurate and precise measurement of the PDIV a very difficult task. The determination of PD inception is more or less arbitrary, depending on the definition of the PDIV [47][48].

The definitions of PDIV have been published in IEC 60270[49] and IEC 61294. In IEC 60270, the PDIV is defined as the applied voltage at which repetitive partial discharges are first observed in the test object. The problem of this definition is that the test operator must determine at what repetition rate the partial discharge can be regarded as repetitive. Therefore in practice, the inception voltage is usually regarded as the lowest applied voltage at which the magnitude of a PD pulse becomes equal to or exceeds a specified level. In this type of definition, only partial discharges with an apparent charge higher than the threshold value are regarded as the actual partial discharges in the test object. Thus, the PDIV measurement results depend on the choice of the threshold value.

The PDIV definition in IEC 61294 avoids the use of the term "repetitive". In IEC 61294, the noise level is required to be less than 50 pC. Thus, the threshold is chosen as twice that of the noise level, and the PDIV of an insulating liquid is defined as the lowest voltage at which a partial discharge occurs of an apparent charge equal to or exceeding 100 pC when the sample is tested under the specified condition. Since the

threshold of PDIV is twice of the maximum allowed background PD noise, separation of the actual PDs in the test cell from the background noises can be easily achieved. This definition is applicable when testing complete devices.

Note that, due to the randomness of the PD process and the self-recovery ability of the liquid dielectrics, partial discharges usually appear in the form of PD pulse bursts that consist of a series of discrete current pulses occurring over a finite time interval of a few μs [50][51]. The reported PD charge is the apparent charge measured by commercially available PD detectors, being proportional to the integration of all the charges contained in a PD pulse burst.

In a lab, more accurate PDIV measurements can be achieved. In fact, lower background noise levels are usually achieved. Furthermore, alternative means to detect the first PD events can be deployed. In this research work, 2pC sensitivity was achieved as noise level. To avoid the use of the repetitive discharge concept, PDIV is obtained as soon as the very first PD pulse appears during the measurements. The full test setup to perform the PD detection has been displayed previously in Fig. 4.7.

In order to produce a high stress in the oil, IEC 61294 utilizes a highly divergent electric field provided by a needle to sphere electrode configuration. It requires the use of a needle electrode with 3 μm tip curvature as the high potential electrode, and a sphere electrode with 12.5 mm or 13 mm diameter as the opposite ground electrode.

For PDIV measurements performed during this work, a slightly different test cell was used. The electrodes geometry is produced by a Fine Science Tools needle with a tip diameter of 1 micrometer and a Rogowski electrode with 40 mm diameter in the flat zone. The use of such configuration should make the test relatively independent of moisture and particle contaminations. A hermetic Teflon test cell equipped with a micrometric adjustment device was used to perform PDIV testing at four different test gaps in a point to plane geometry immersed in mineral oil or FR3. The selected gap lengths were 5, 10, 20 and 40 mm. The high voltage electrode of the test cell is a 5 mm length, 0.5 mm diameter needle, with a 1 μm tip radius. (Fig. 4.11)

The dielectric fluid samples used during the tests, were previously dried and degassed under vacuum condition (<0.5 mBar) and continuous stirring during 24 hours. The final moisture level after the sample conditioning was quantified using Karl Fischer titration.

The initial test voltage (V_i) was roughly determined for each fluid using [52]:

$$E_{MAX} = \frac{2 \cdot V}{r \cdot \ln(1 + 4d/r)} \quad \text{Eq. 27}$$

where r = tip radius and d = test gap

Starting from V_i , voltage steps of 200 V were applied during 3 minutes until a streamer pulse or a PD burst took place. When this happened, the voltage level was recorded and defined as the PDIV value, stopping consequently the acquisition process. The voltage was then decreased to the initial value and the procedure restarted again. This test cycle was repeated until 10 PDIV values were obtained.

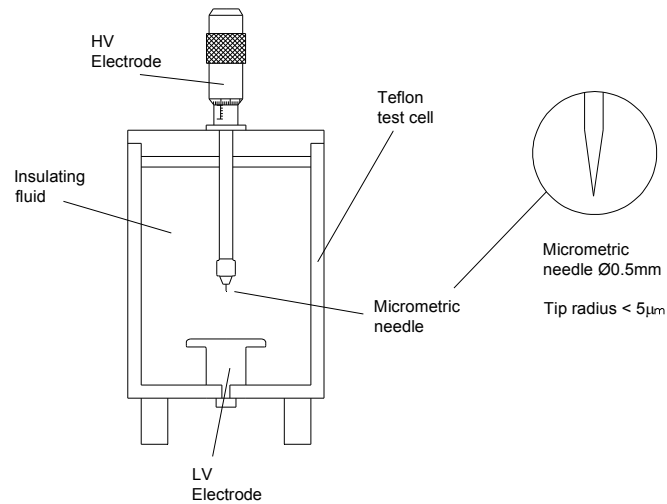


Fig. 4.11 PDIV test cell for insulating liquids

During the process, special care was taken regarding the needles tip mechanical integrity. Once that the trend of the measurements started to show an incremental behavior, the needles were replaced and the last two PDIV values were discarded and obtained again with the new needle. Fig. 4.12 shows the comparison between new and degraded needles.

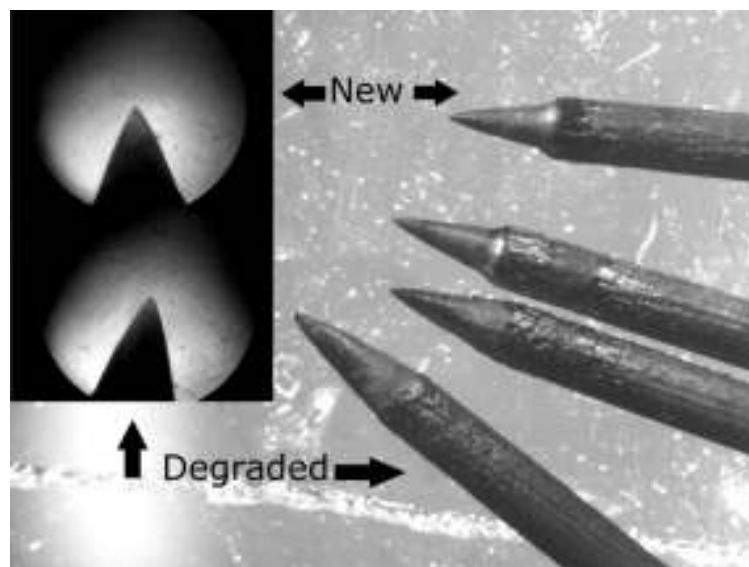


Fig. 4.12 Comparison of new and degraded needles

The use of the previously described procedure is the only way to achieve an accurate comparison between PDIV values of different transformer liquids.

Surface discharges behavior in oil-cellulose interfaces was studied in a different way. Pressboard sheets were conditioned and impregnated according ASTM D2413–99 in mineral oil and FR3. A sample holder as shown in Fig. 4.13 was used to assess the PDIV level in a pressboard sheet immersed in both fluids. The adjustable arm of the HV electrode was set in such a way that the needle forms a 30° angle respect to the horizontal plane (pressboard sheet). In order to obtain similar contact forces between the needle and the pressboard, the complete body of the HV electrode runs freely by gravity. In this way, the weight of the electrode becomes the contact force and it was uniform for all the tested pressboard samples. The LV electrode can be moved to obtain the test gaps (5, 10, 20 and 40 mm) and it also works as sample fastener.

The initial test voltage was obtained empirically, rising the voltage using a sacrifice needle until surface PDs appeared. Once obtained these voltage values (Vs) for each gap and dielectric fluid, the sacrifice needle was substituted for a new needle and the test procedure started from a voltage level 3 kV lower than Vs. The test procedure described for the point to plane geometry in oil was carried out in this setup as well in order to assess the PDIV level.

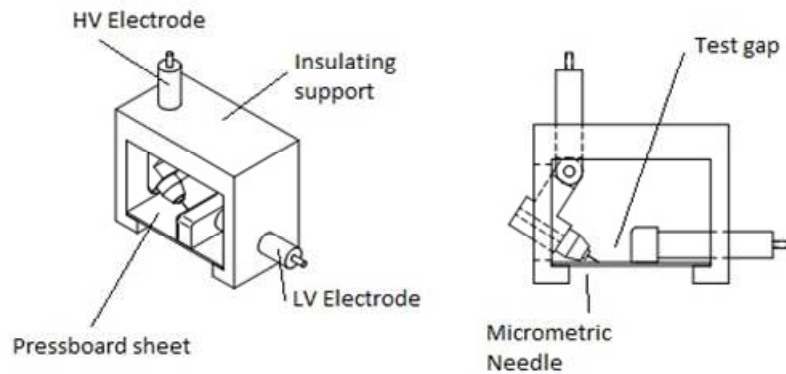


Fig. 4.13 Test cell for creeping discharges

For PDIV determination in HVDC, a test cell with the elements displayed in Fig. 4.14 was designed and manufactured. The mechanical support offers three advantages: the pressboard thickness can be varied from 1 to 2 mm, the oil gaps can be controlled by means of a threaded axis and it is compatible with testing materials. In all test configurations during this work, 1 mm was selected as oil or pressboard thickness. The horizontal layout of the electrodes prevents the allocation of bubbles between the Rogowski electrodes and the pressboard layer.

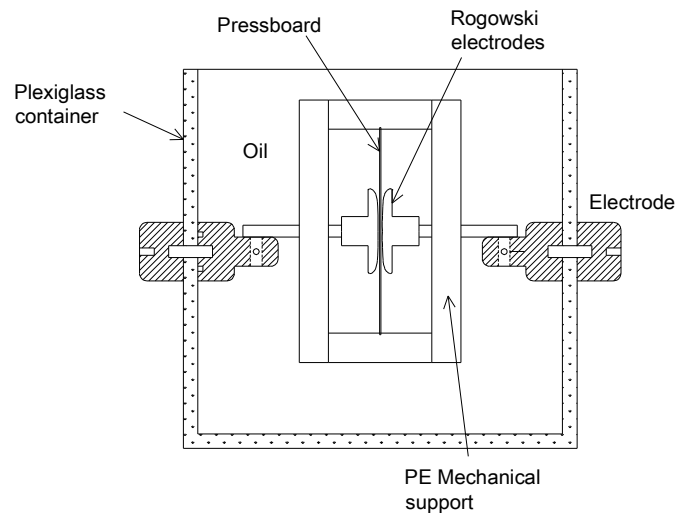


Fig. 4.14 Test cell for PD measurement under HVDC voltages

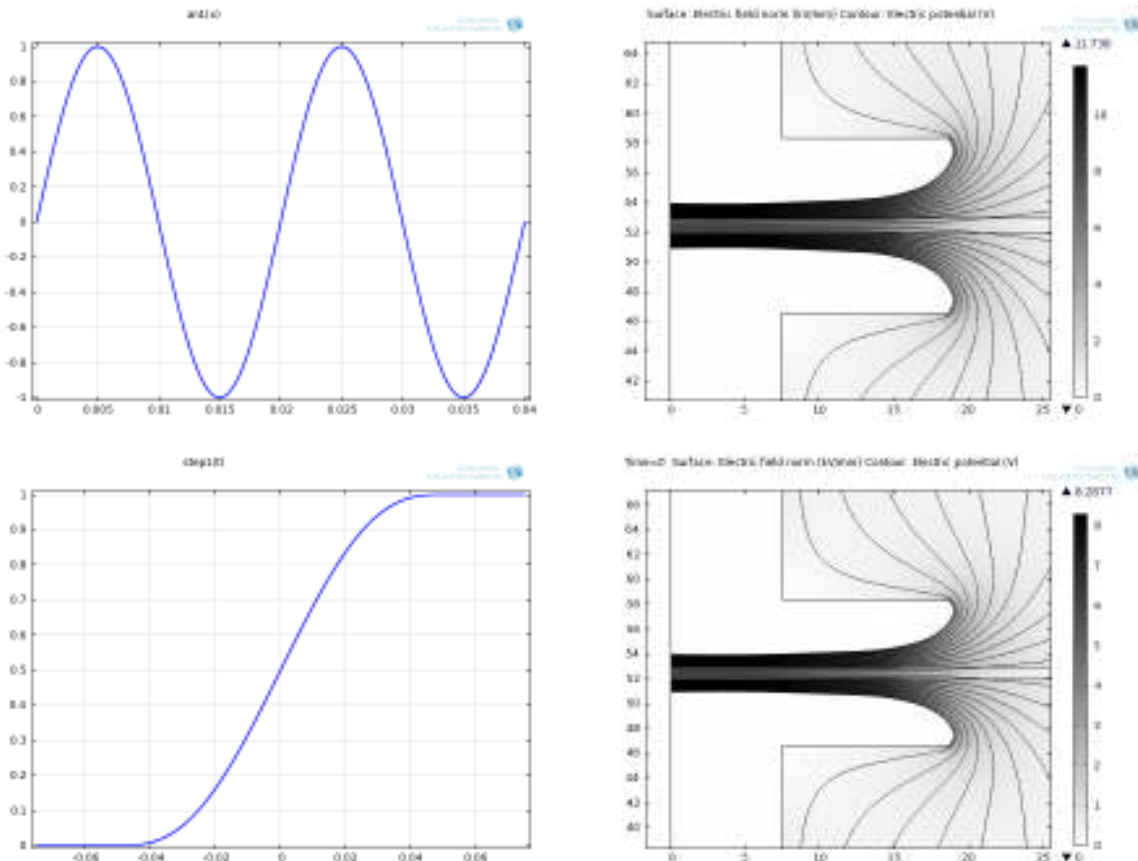
When HVDC testing is carried up, four different procedures are followed:

- AC testing
- DC testing
- AC+DC testing
- AC notched voltage testing (for insulating paper)

In AC testing, the test procedure is similar to that followed during PDIV assessment in point to plane geometry. In DC testing, prior to PDIV measurements, stabilization time should be allowed for the sample to arrive to steady state. This time varies depending on the time constant of the sample and for the evaluated specimens, it ranged from 15 minutes to 1 hour, depending on oil electrical conductivity. This stabilization time was observed each time that the DC voltage was increased, when some PD occur during the transient and then disappear.

For AC+DC testing, the peak value of the AC waveform was set at each voltage step, as 40% of the DC amplitude. In this case, due to the AC component, no stabilization time is required. In Fig. 4.15, the simulation of the behavior of the test cell at the three first different conditions is shown.

Considering linear response for both AC and DC power supplies, the AC+DC response should be the addition of independent AC and DC field distributions. Modeling this effect is complicated due to the fact that integration time steps are very different for the two voltage regimes. To calculate AC response, at least a time step of 0.002 s is required in order to divide the AC cycle in 10 segments. On the other hand, as can be seen also in Fig. 4.15, integration times for DC are in the seconds or minutes range. Thus, simple superposition of AC and DC responses cannot model in detail the physics of this problem.



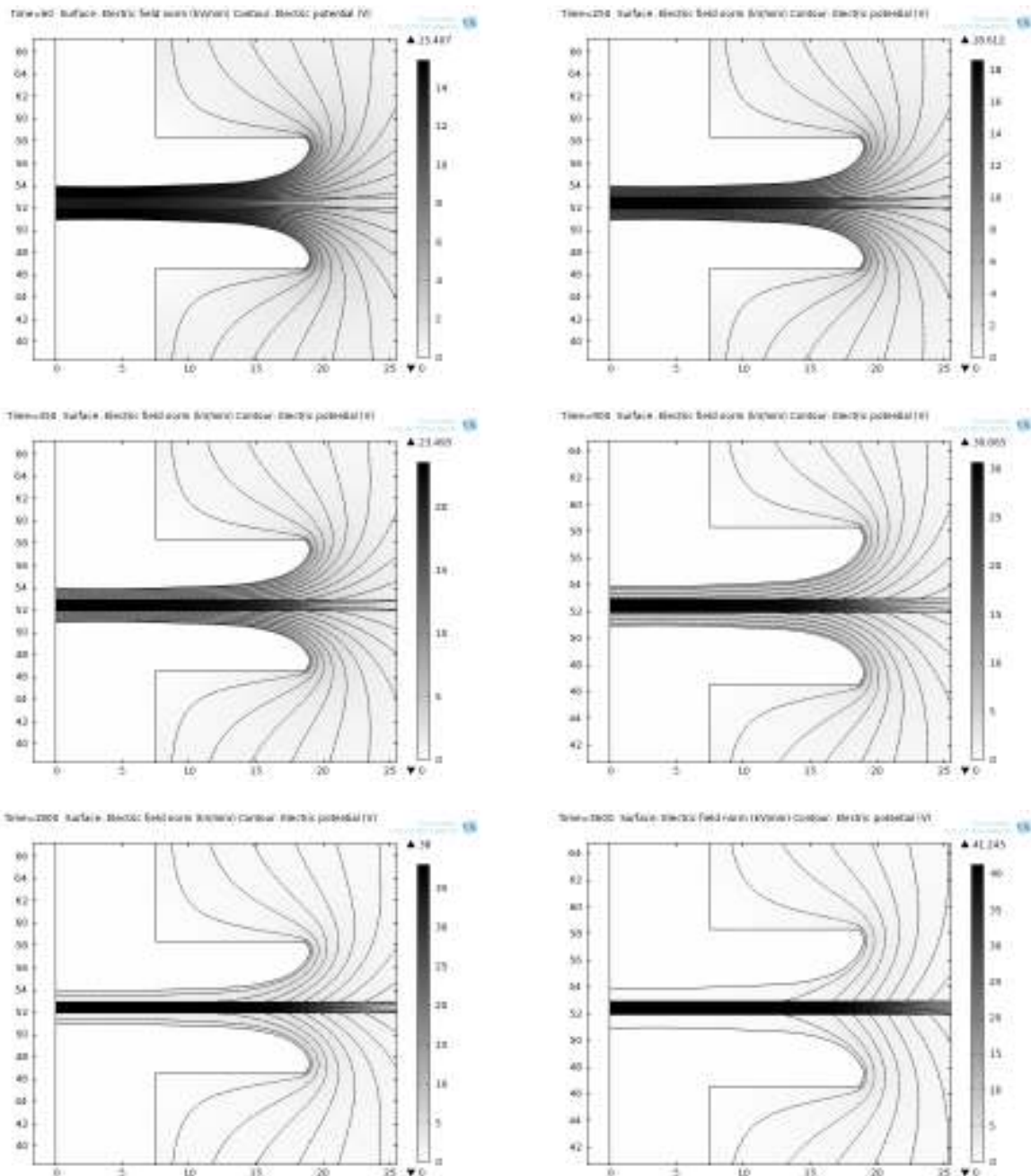


Fig. 4.15 Voltage and electric field distribution under AC and DC voltages

For AC notched voltages (HVDC), specimens were made out of not-fully impregnated kraft paper discs (thickness 0.1 mm, diameter 94 mm). These were embedded in pseudo-Rogowski electrodes and immersed in mineral oil to avoid surface discharges and flashover. In the experiments, the PD current taking place in the cavity was coupled by a high frequency ferrite core current transformer (with bandwidth of 40 MHz) connected to the ground line. The coupled signal was then processed and recorded by the PD measurement instrument.

The PDIV, PD repetition rate, amplitude and pattern were recorded in the experiments. For PDIV detection, the voltage was raised in steps of about 15 V/s. Between tests, the sample was discharged about 5 minutes to remove charges produced by the previous PD events. Since, after some time, PD activity change due to conditioning, the PDIV under sinusoidal voltage with and without notches were measured during each test

condition. Then, the detected PDIV under notched voltage was reported in relative values as explained by Eq. 28:

$$PDIV^* = PDIV(\alpha, \mu) / PDIV(AC) \quad \text{Eq. 28}$$

4.1.8 Conductivity test cell

The measurement of polarization and depolarization currents following a DC voltage step is one way in the time domain to investigate the slow polarization processes [53]. The dielectric memory of the test object must be cleared before the measurement. The voltage source should be free of any ripple and noise in order to record the small polarization and depolarization currents with sufficient accuracy. The procedure consists in applying a DC charging voltage of known magnitude to the test object for a long time, until steady state is observed. During this time, the polarization current $I_{pol}(t)$ through the test object is measured, arising from the activation of the polarization process with different time constants corresponding to different insulation materials and to the conductivity of the object, which has been previously carefully discharged.

After the polarization characterization, the DC voltage is removed and the depolarization current ($I_d(t)$) is also measured until steady state. The complete trend allow time constant assessment and the final value of the depolarization current can be used in order to calculate the sample conductivity. Fig. 4.16 shows a schematic draw of the test cell designed and constructed for polarization and depolarization currents assessment.

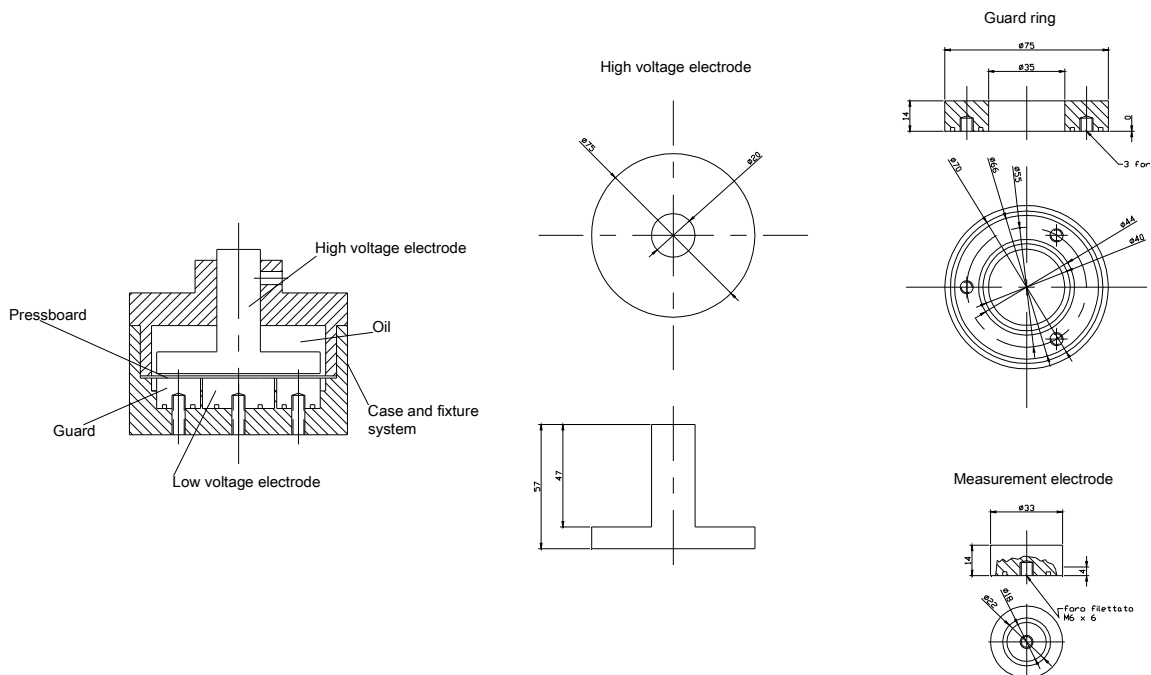


Fig. 4.16 Conductivity test cell

The test cell is connected to a Keithley 248 high voltage DC source and to a Keithley 617 programmable electrometer in order to carry out the tests. The complete circuit is shown in Fig. 4.17. It can be noticed that the DC power supply includes charge and discharge resistances and a switch that allows the commutation from the charge to the discharge process. Both the DC power supply and the electrometer are controlled by means of Labview® software that uses a GPIB 488 interface for data exchange.

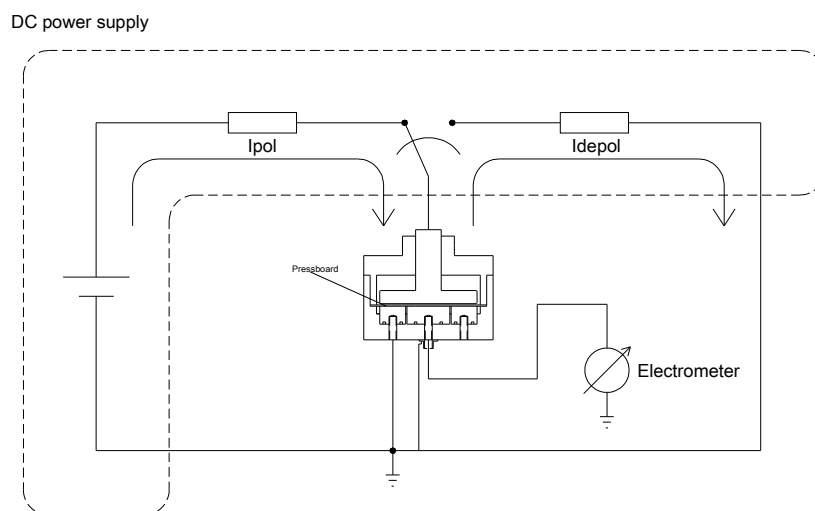


Fig. 4.17 Polarization and depolarization currents measurement circuit

4.1.9 Data processing - Weibull distribution

Failure data, such as that described in degradation of electrical insulation, may be represented in a histogram form as numbers of specimens failed in consecutive periods or under specific circumstances. The mean and standard deviation of this data set is easily found using even a scientific calculator. Whilst the Normal is probably the best known and its parameters (the mean and standard deviation) are easily calculated; it is not usually appropriate to dielectric failure analysis. In particular the Normal distribution has a finite probability of failure at (physically impossible) negative times. An important step in analyzing breakdown data is the selection of an appropriate distribution.

Distributions for electrical breakdown include the Weibull, Gumbel, and lognormal. The most common for insulation systems is the Weibull and for that reason is used extensively in this work. The expression for the cumulative density function for the two-parameter Weibull distribution is shown in Eq. 29.

$$F(X) = 1 - \exp\left[-(X/\eta)^\beta\right] \quad \text{Eq. 29}$$

where:

X is the measured variable,

F(X) is the probability of failure at a voltage or time less than or equal to X. For tests with large numbers of specimens, this is approximately the proportion of specimens that breakdown or fail.

η is the scale parameter and is positive

β is the shape parameter and is positive.

The scale parameter η represents the time, voltage, electric field, etc. for which the failure probability is 0.632 (that is $1 - 1/e$) where e is the exponential constant). It is analogous to the mean of the Normal distribution. The units of η are the same as X, that is, voltage, electric stress, time, number of cycles to failure etc.

The shape parameter β is a measure of the range of the failure times or voltages. The larger β is, the smaller is the range of breakdown voltages or times. It is analogous to the inverse of the standard deviation of the Normal distribution.

The two-parameter Weibull distribution of Eq. 29 is a special case of the three-parameter Weibull distribution that has the cumulative distribution function shown in Eq. 30.

$$F(X) = 1 - \exp\left[-(X - \gamma/\eta)^\beta\right] \quad \text{Eq. 30}$$

The additional term γ is called the location parameter. $F(X) = 0$ for $t = \gamma$, that is, the probability of failure for $X < \gamma$ is zero.

Data distributed according to the two-parameter Weibull function should form a reasonably straight line when plotted on Weibull probability paper. In this kind of paper, the measured data are plotted on the horizontal axis, which is scaled logarithmically. The probability of breakdown is plotted on the vertical axis, which is also highly non-linear.

Various computational techniques are available for estimating the Weibull parameters. The 1987 version of [54] recommended the use of the maximum likelihood technique but this has been found to give biased estimates of the parameters, especially for small data sets. The technique used here was developed by has been found to be the optimum technique for complete, singly censored and progressively censored data, Montanari et al [55], [56], [57]. However, for large data sets least-squares linear regression and maximum likelihood techniques are adequate.

It is often useful to estimate the time, voltage or stress for which there is a given probability of failure $p\%$; this is known as the p_{th} percentile. In constant stress life tests, these percentiles are sometimes referred to as “B lives.” For example, the “B10 life” is the age at which 10% of the components will fail at a given voltage stress. The p_{th} percentile, t_p , may be estimated by using Eq. 31.

$$\hat{t}_p = \alpha \left[-\ln(1 - p/100) \right]^{\frac{\gamma}{\beta}} \quad \text{Eq. 31}$$

Where p is expressed as a percentage.

If the same experiment involving the testing of many specimens is performed a number of times, the values of the parameter and percentile estimates from each experiment differ. This variation in estimates results from the statistical nature of insulation failure. Therefore, any parameter estimate differs from the true parameter value that is obtained from an experiment involving an infinitely large number of specimens. Hence, it is common to give with each parameter estimate a confidence interval that encloses the true parameter value with high probability. In general, the more specimens tested, the narrower the confidence interval. For this work 10 or 5 specimens were taken to calculate Weibull parameters.

4.1.10 Data processing - Histograms

During this work, histograms are mainly used for trend detection during for example, PDIV assessment. A positive trend in the histogram could be correlated for instance, to needle tip degradation (rounded tips produce local lower electric fields). A negative trend could be correlated to degradation of the sample due to moisture ingress.

5 Results of insulating fluids comparison

As it was said before, for most transformer designs, mineral oil has proven to be a cost-effective insulating fluid. This seemed to continue in the future, but now, in applications where fire safety, protection of the environment and high temperature are important considerations, transformers based on alternative fluids are demonstrating to be a more viable option. Despite the fact that esters are in use from some years ago, it is important to compare the behavior of mineral oil and natural esters in some particular conditions that are considered to be important during transformer design and operation and until now not fully studied. In this Chapter, the results of some benchmark dielectric tests are presented in order to have elements that allow us to make such comparison. The benchmark tests selected for this work are:

1. AC electrical breakdown at short and long gaps
2. Impulse breakdown
3. Partial discharge in at high divergent fields
4. Creeping partial discharges in oil-pressboard interfaces

For the AC breakdown, it is important to assess the influence of moisture and volume effect, so, samples with different water concentration was evaluated at different gap lengths. Since most of those alternative fluids are more viscous than mineral oil, the standing time before carrying out the tests and the stirring time between two consecutive tests must be longer to allow gas bubbles and byproducts to disperse. This fact was taken into account during testing of FR3.

Partial discharge behavior has been studied in alternative fluids by a number of different institutions and work is still ongoing to characterize these fluids. We present the results obtained from the point of view of a laboratory PDIV. This is, the voltage at which we observed the very first discharge and not when a complete pattern is produced.

It is common to find in the literature, results regarding the behavior of AC and impulse breakdown during creeping. No results are available for PDIV in this geometry condition, despite the fact that this parameter can be also used for transformer design. For this reason, in addition to PD measurements in oil, we propose in this work the characterization of creeping discharges in oil-PB interfaces, analyzing the influence of fluids parameters, their matching with pressboard parameters and the effect of electrode and gap geometries. The results of this contribution are also reported in this Chapter.

In all cases, the statistical results are depicted along with bar plots that are useful to detect artificial trending due to instrumentation or test setup defects. FEM modeling using Comsol® is used to clarify experimental results when necessary. In the following sections the main results of the selected bench mark tests with their simulation are reported.

5.1 Electrical breakdown (short gap, IEC 60156)

Tests were performed in strict accordance with IEC 60156, which states that 6 breakdown tests should be carried out to measure the average breakdown voltage.

Tests were performed using a Baur DPA 75 C oil tester, with semi-spherical electrodes. The distance between the electrodes was held constant in all tests, equal to 2.5 mm.

The oils were tested from the driest possible conditions (except for mineral oil, as the BDV was too high to be evaluated with the Baur DPA 75 C oil tester)

As mineral and ester oils are characterized by different viscosities the test procedure was set up as follows:

1. Voltage ramp of 2 kV/s
2. Testing times as specified in Table 4.

Table 4 Testing times for breakdown test

	Rest time prior testing (min)	Stirring time between shots (min)	Rest time between shots (min)
Mineral oil	2	1	1
Ester oils	10	1	1

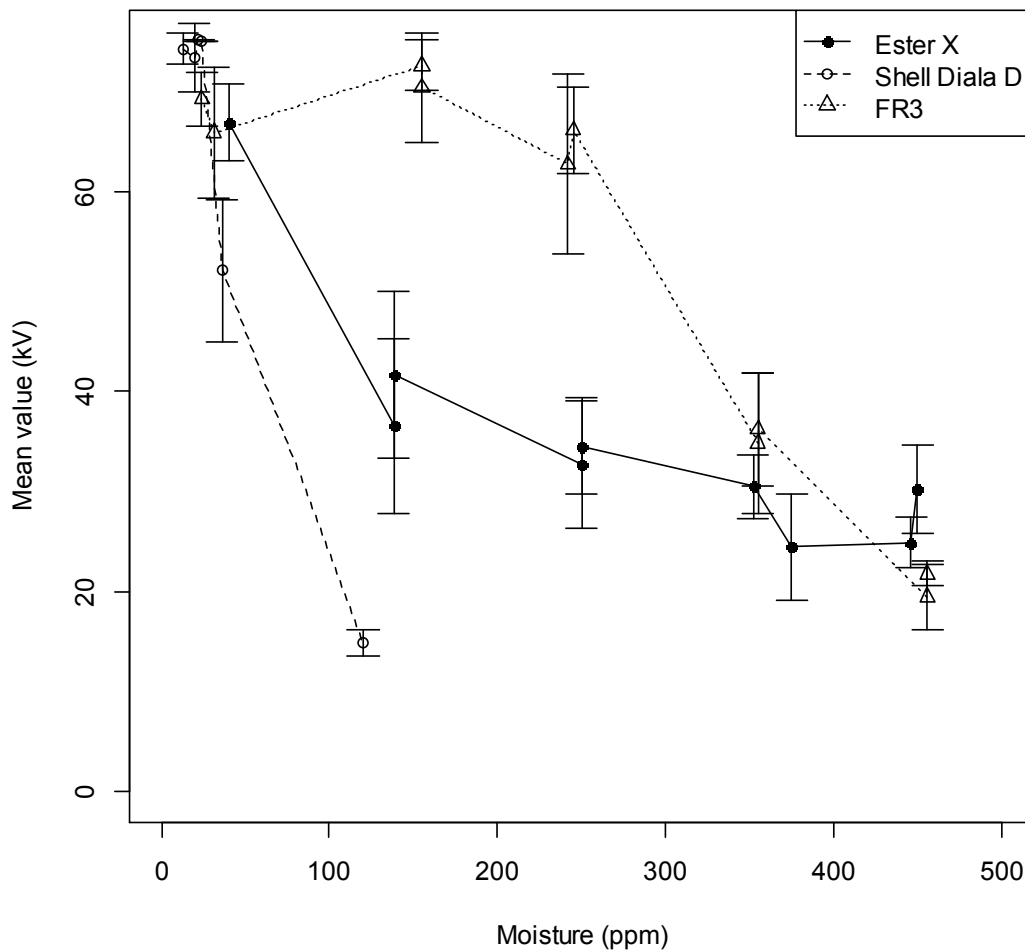


Fig. 5.1 Mean values of BDV at different moisture levels for the insulating liquids studied in this work

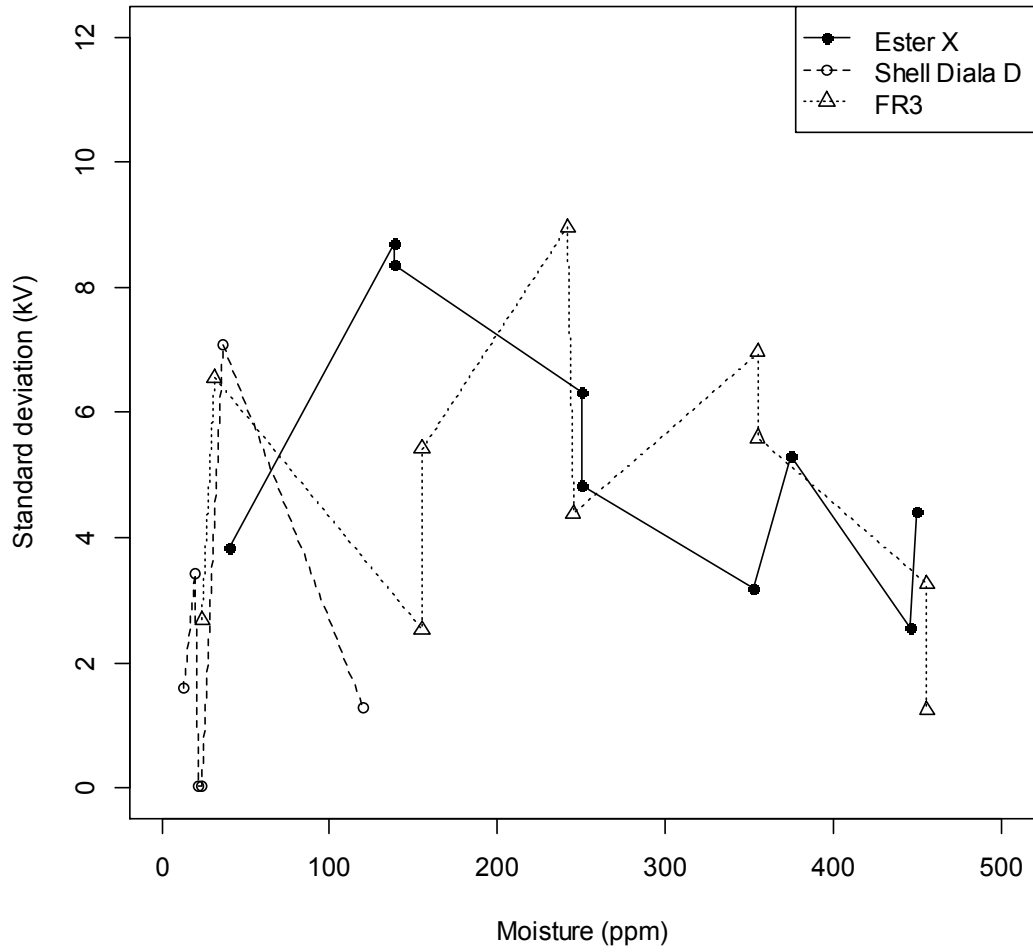
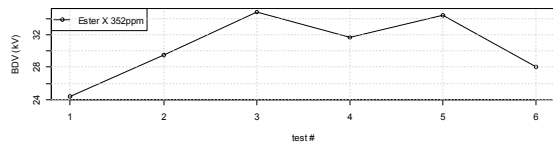
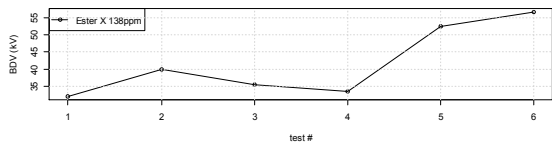
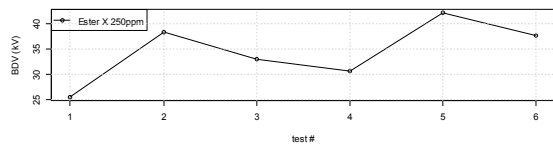
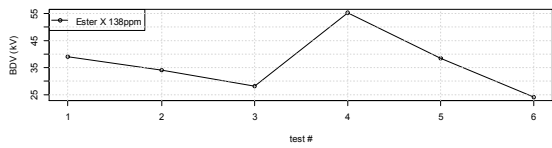
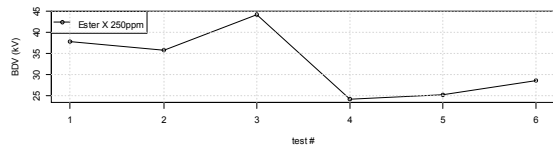
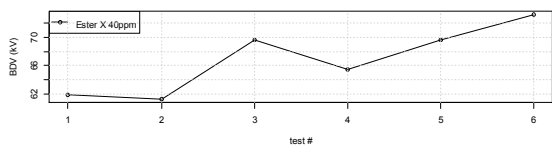


Fig. 5.2 Standard deviation of BDV at different moisture levels for the insulating liquids studied in this work



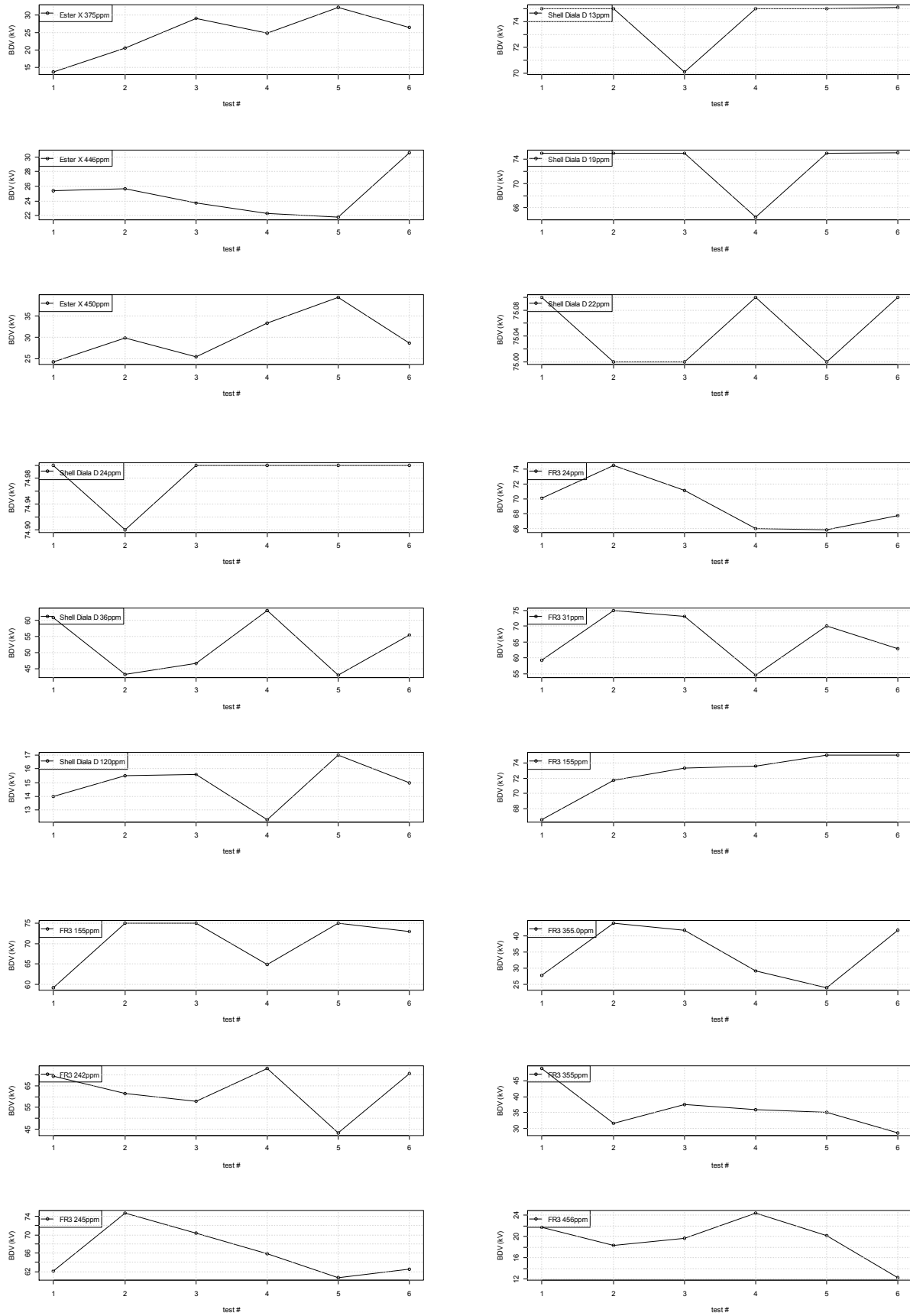


Fig. 5.3 BDV trends of mineral oil, FR3 and Ester X fluids

5.2 Electrical breakdown (Long gap)

The electrodes used for these tests were of the pseudo-Rogowski type, with a diameter of 40 mm (in the flat area). The electrode gaps were 1, 2 and 5 mm. For gaps of 1 and 2 mm, the Baur DPA 75 C oil tester was used. Above, given the limited maximum test voltage achieved by this system (75 kV), the electrodes were connected to a 100 kV transformer. For these latter tests, given the limited arc interruption capabilities of the system (realized through a semiconductive fuse on the high voltage connection and a protection circuit on the low voltage side) the oil sample was changed at each test.

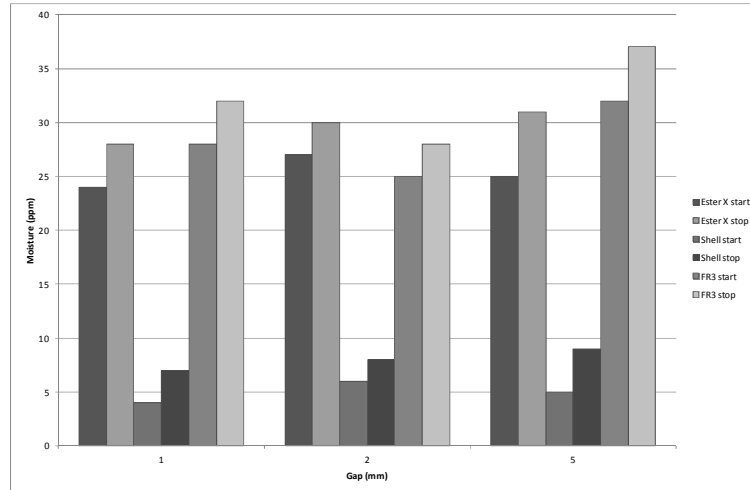


Fig. 5.4 Behavior of moisture during BDV tests

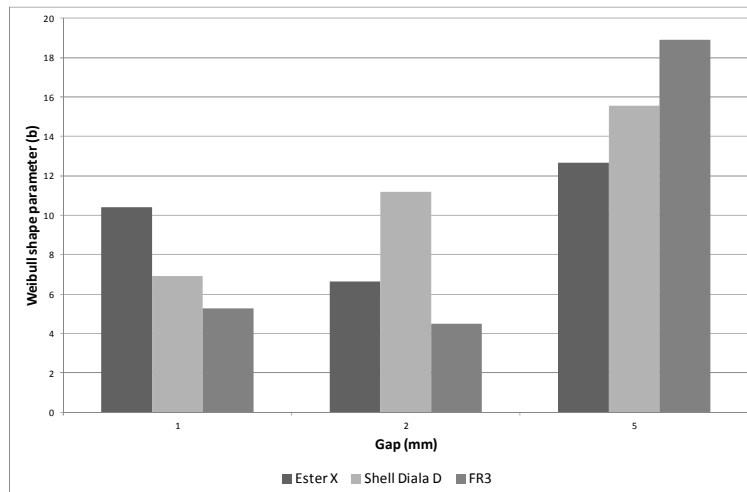


Fig. 5.5 Weibull shape parameter as a function of gap length (BDV)

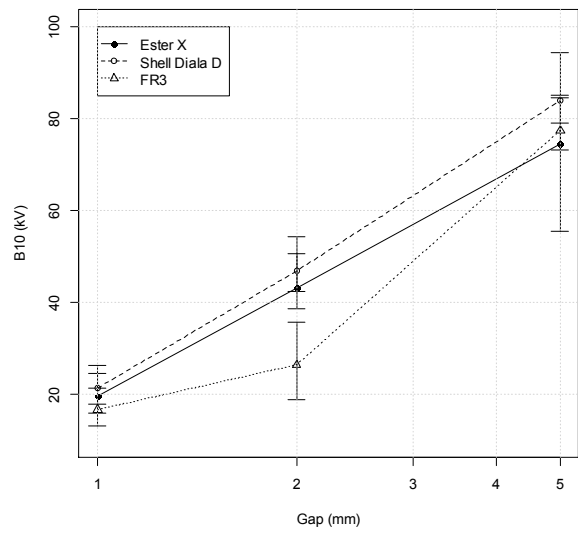
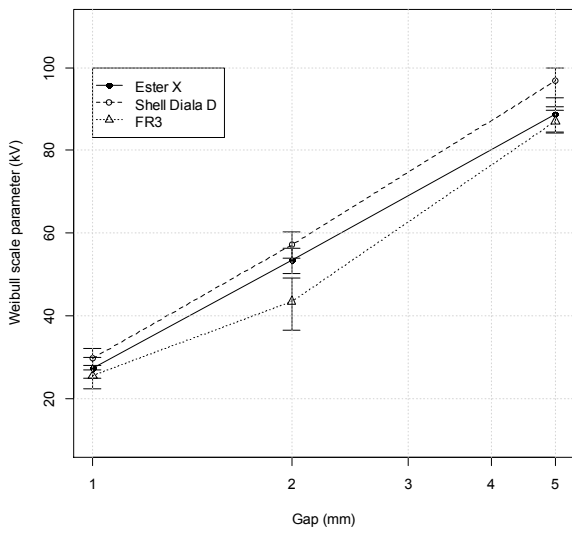
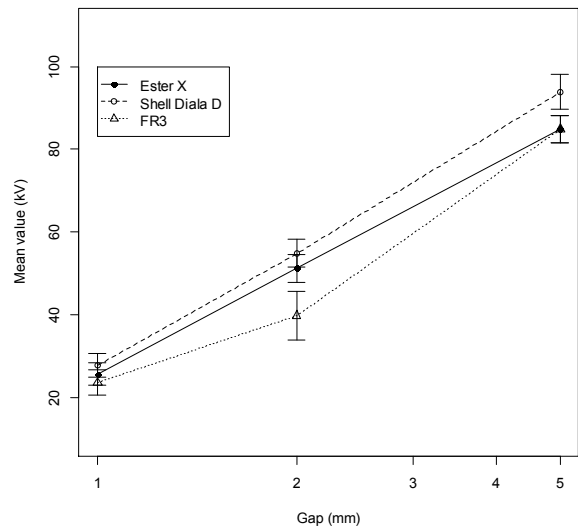
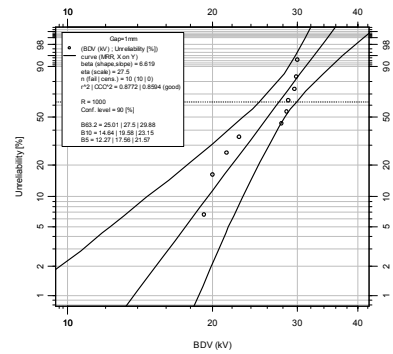
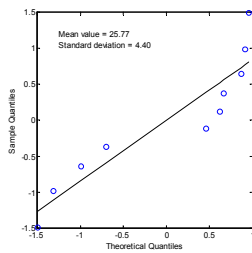
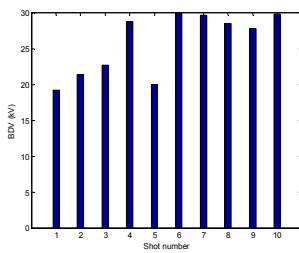


Fig. 5.6 Main statistical parameters for BDV (overall results)

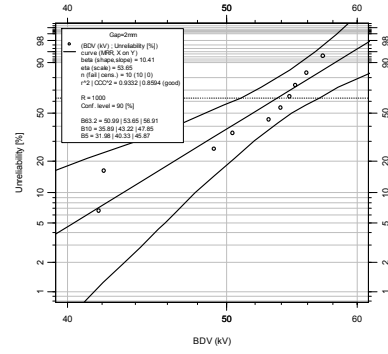
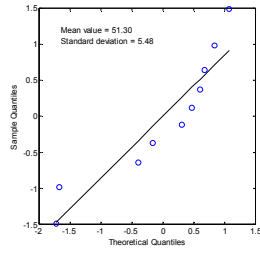
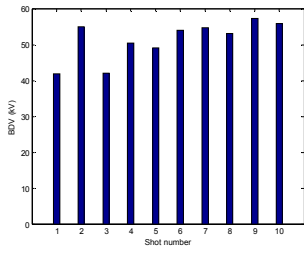


Ester X

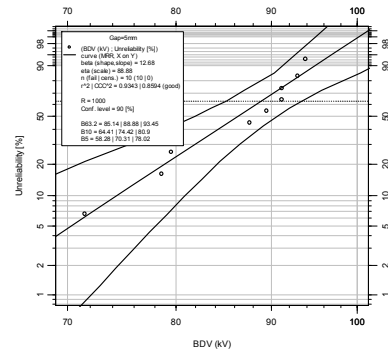
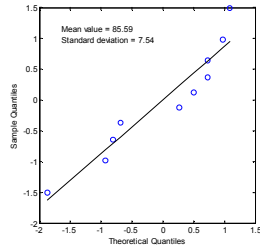
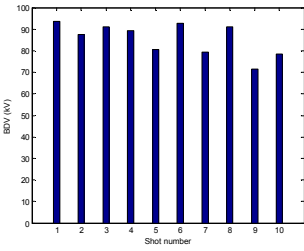
Gap: 1 mm
 H0=24ppm,
 (HR=2.3%),
 H1=28ppm
 (HR=2.7%),
 22°C



Gap: 2 mm,
H0=27ppm,
(HR=2.6%),
H1=30ppm
(HR=2.9%),
22°C

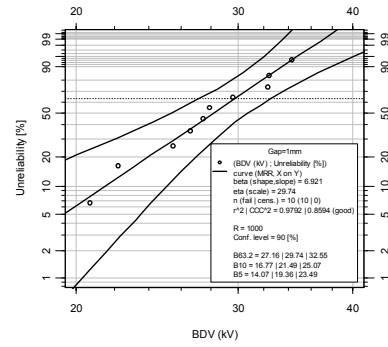
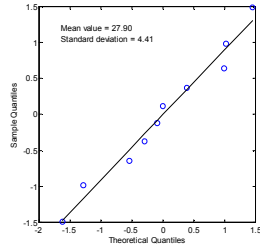
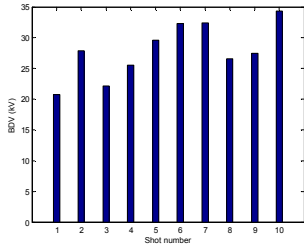


Gap: 5 mm,
H0=25ppm,
(HR=2.4%),
H1=31ppm
(HR=3.0%),
22°C

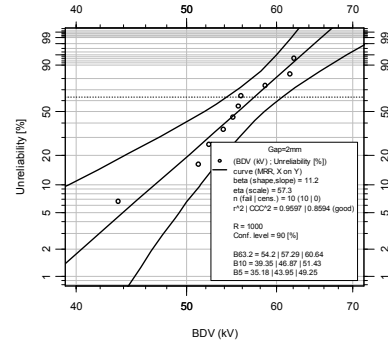
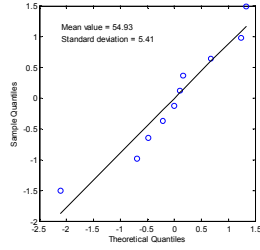
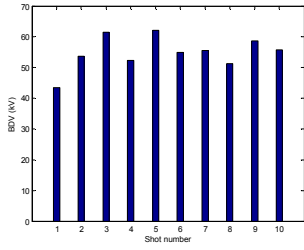


SHELL DIALA D

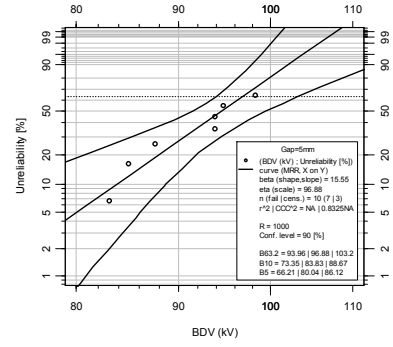
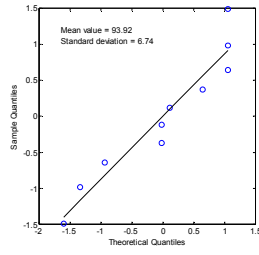
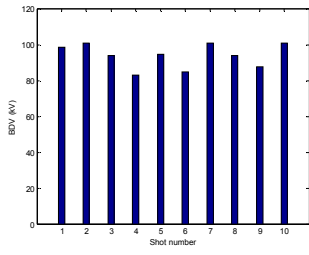
Gap: 1 mm,
H0=4ppm,
(HR=6.7%),
H1=7ppm
(HR=11.7%),
22°C



Gap: 2 mm,
H0=6ppm,
(HR=10.0%),
H1=8ppm
(HR=13.3%),
22°C

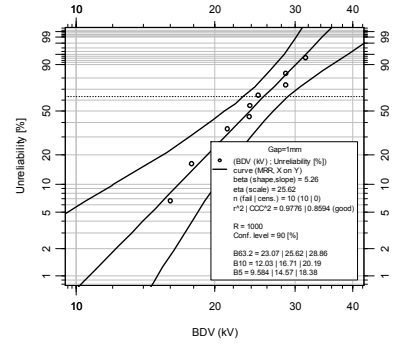
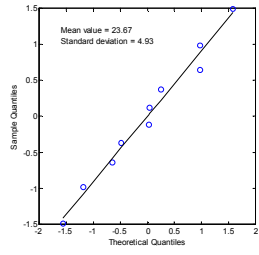
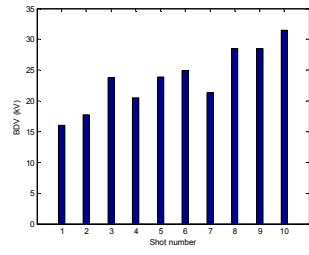


Gap: 5 mm,
H0=5ppm,
(HR=8.3%),
H1=9ppm
(HR=15%),
22°C

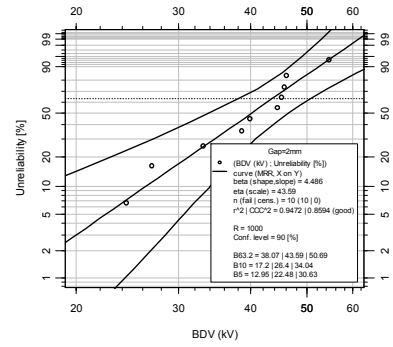
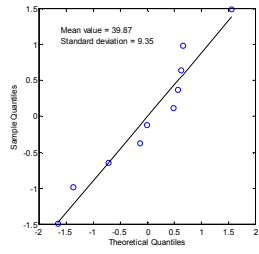
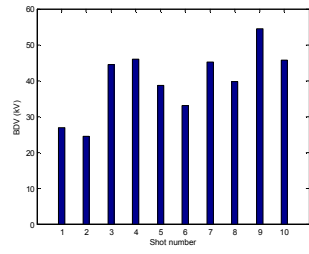


FR3

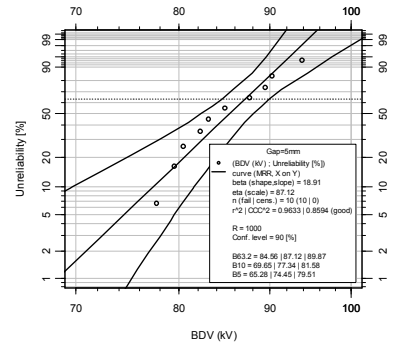
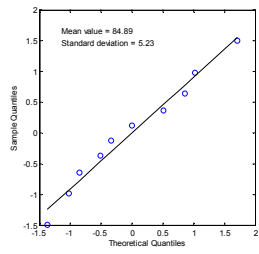
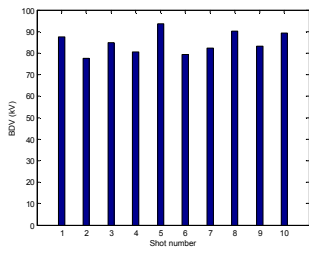
Gap: 1 mm,
H0=28ppm,
(HR=2.7%),
H1=32ppm
(HR=3.1%),
22°C



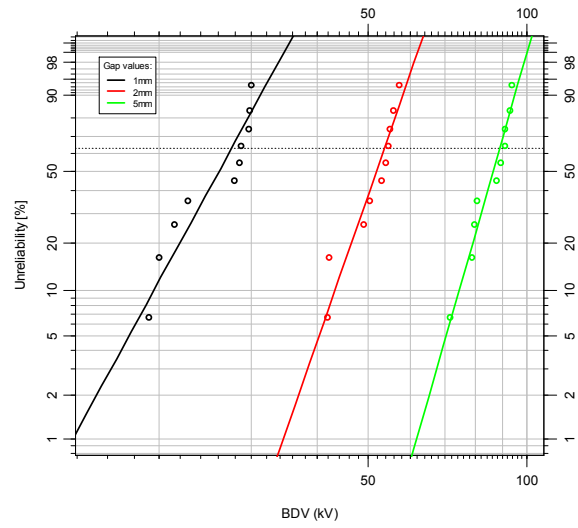
Gap: 2 mm,
H0=25ppm,
(HR=2.4%),
H1=28ppm
(HR=2.7%),
22°C



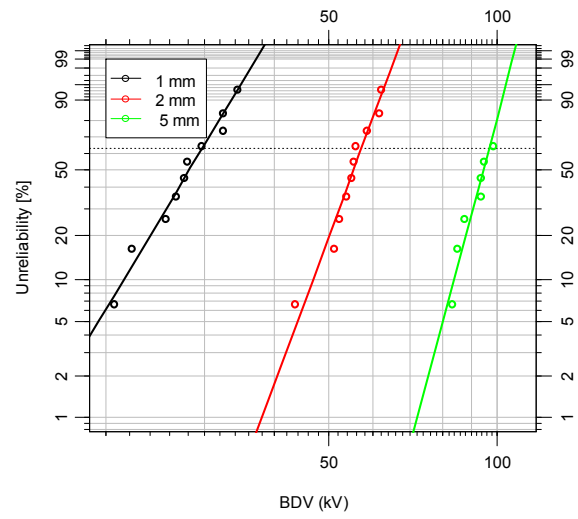
Gap 5 mm,
H0=32ppm,
(HR=3.1%),
H1=37ppm
(HR=3.6%),
22°C



Ester X



Shell Diala D



FR3

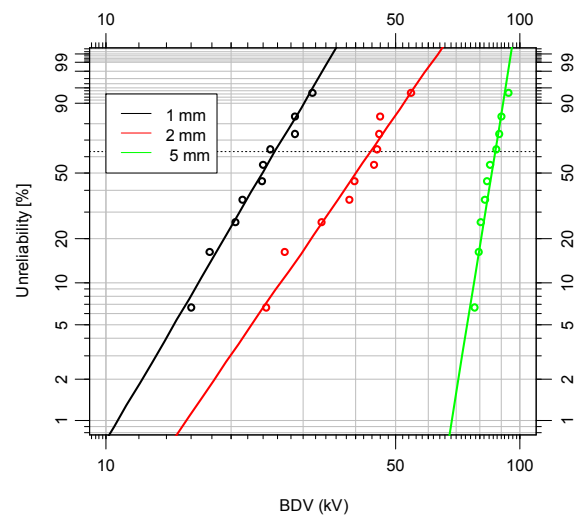


Fig. 5.7 Statistical parameters for BDV

5.3 Electrical breakdown (Lightning impulse)

The test cell used for this investigation had plane/plane electrodes, with a variable gap. A standard lightning impulse voltage (1.2/50 μ s) was used to stress the oil gap.

The test was raised in steps of 2 kV for gaps 1 and 2 mm long and 3 kV for 5 mm gap.

Three shots were made at each voltage level before increase it to the next step. If breakdown took place during one of these shots, the voltage level was reported as the BD voltage, the electrodes were cleaned and the oil was left at rest for at least 10 minutes. If BD voltage trend showed a decreasing behavior after three BD events, despite the rest period between them, the insulating liquid under test was changed as it was assumed that discharge by-products could have reduced the dielectric strength of the fluid.

Two data were censored when testing FR3, as it was suspected that breakdown did not occur in the region between the electrodes.

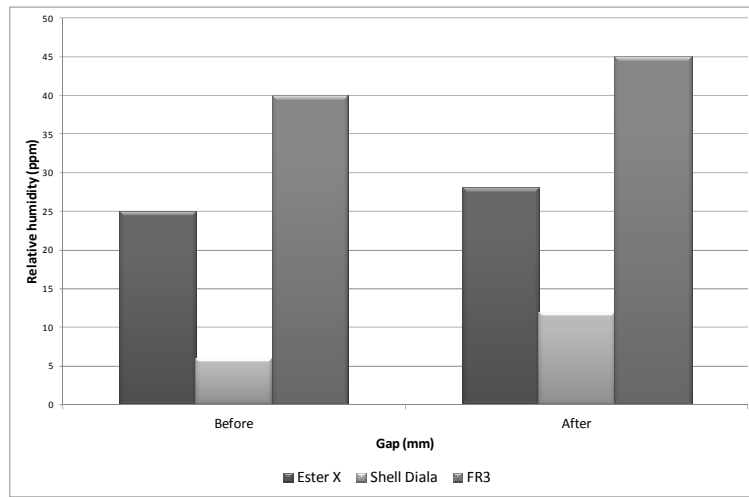


Fig. 5.8 Moisture behavior during impulse testing

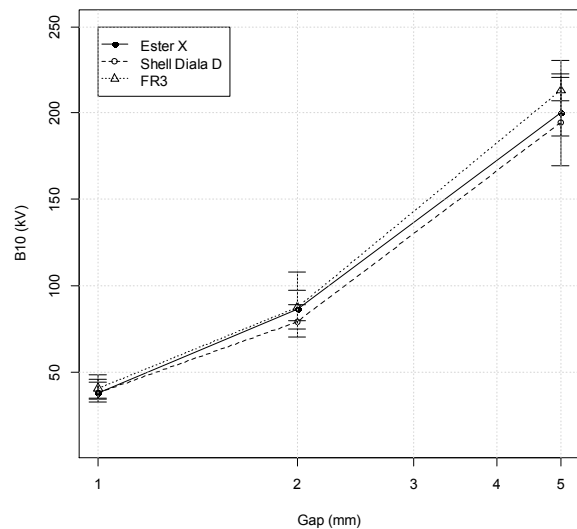
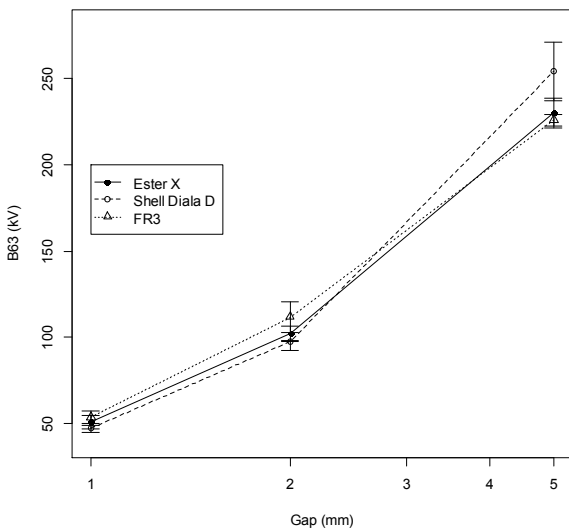


Fig. 5.9 Main statistical parameters for lightning impulse testing (overall results)

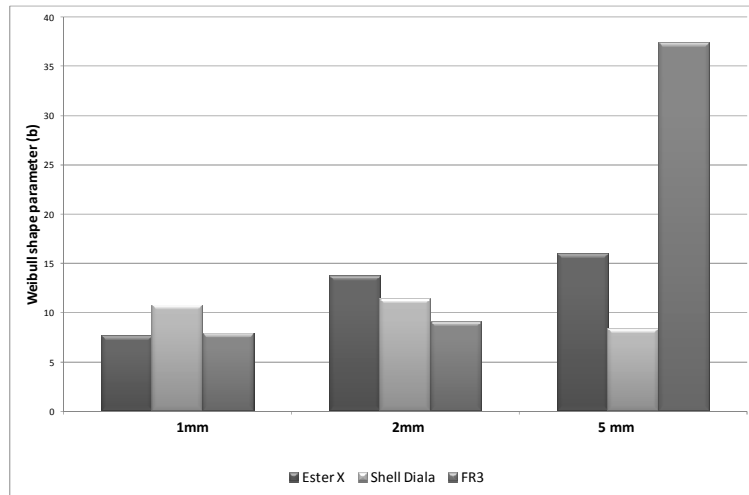
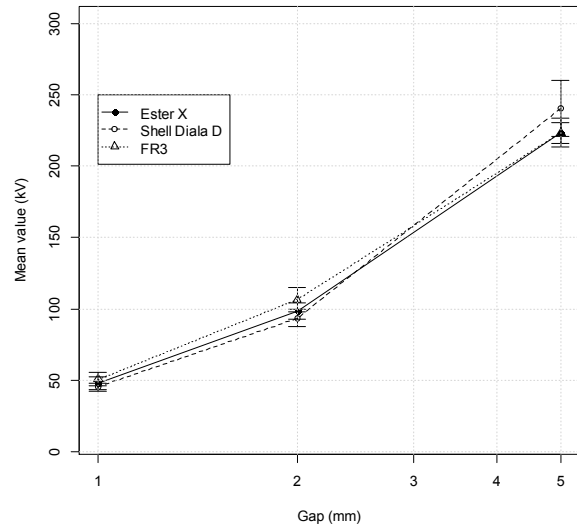
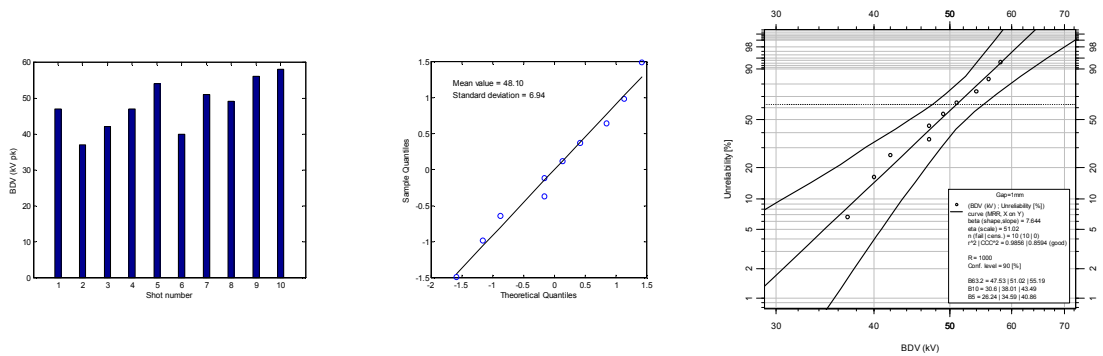


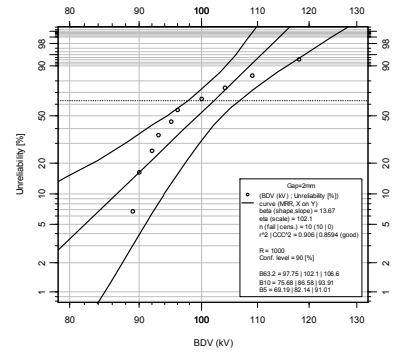
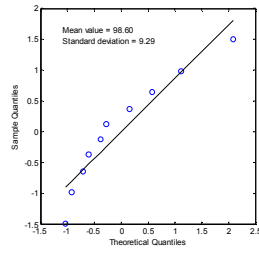
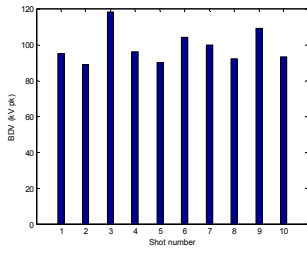
Fig. 5.10 Weibull shape parameter as a function of gap length

Ester X

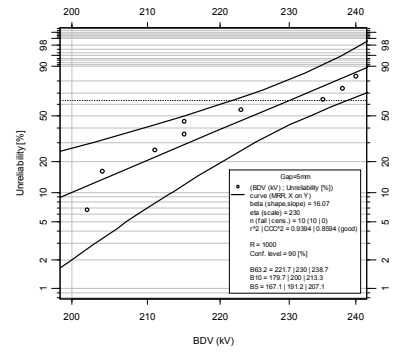
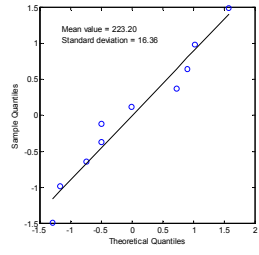
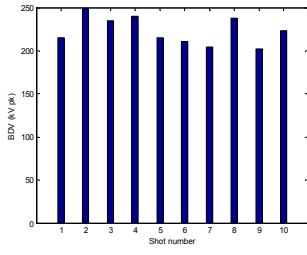
Gap: 1 mm



Gap: 2 mm

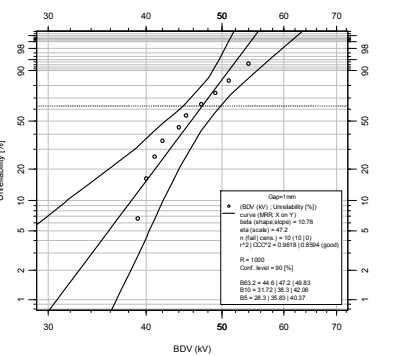
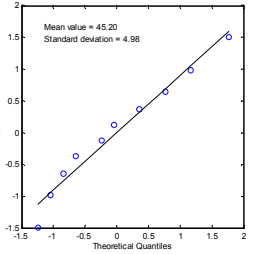
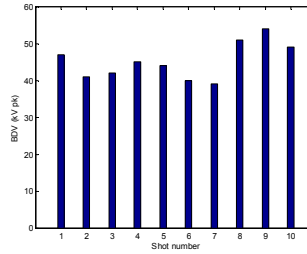


Gap: 5 mm

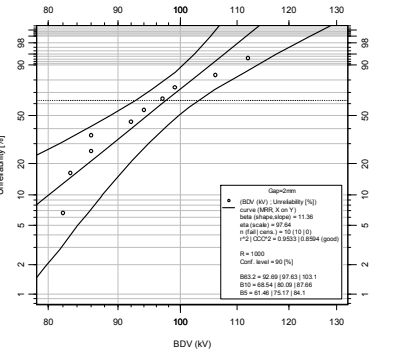
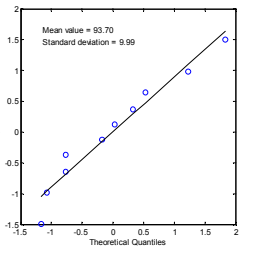
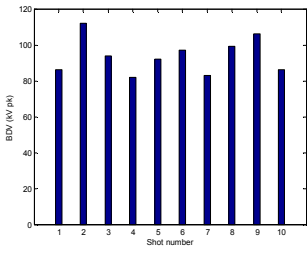


SHELL DIALA D

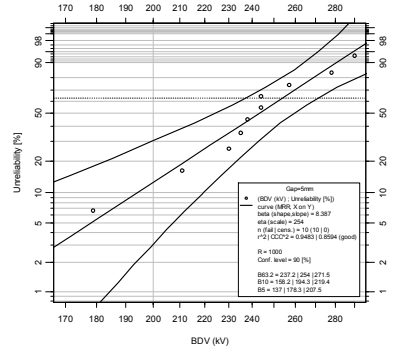
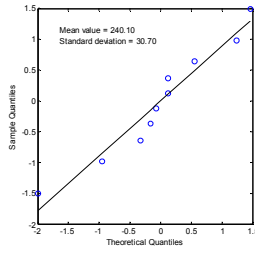
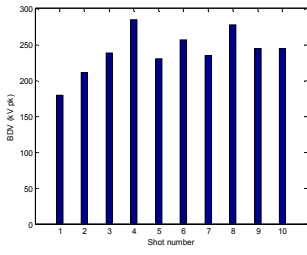
Gap: 1 mm



Gap: 2 mm

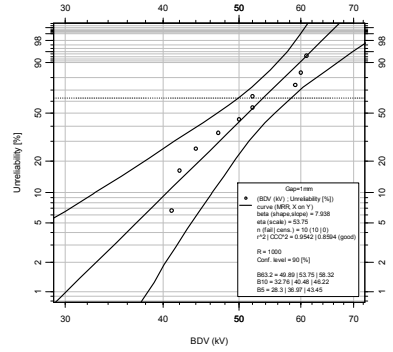
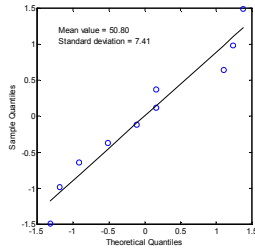
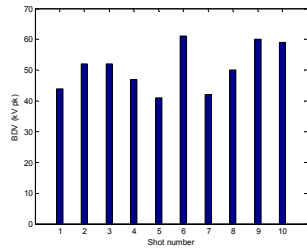


Gap: 5 mm

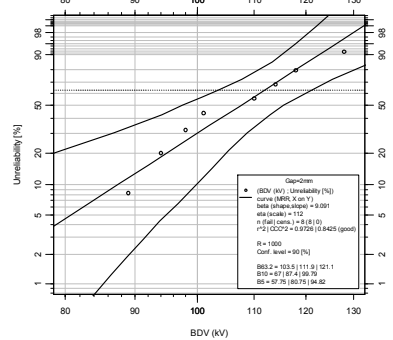
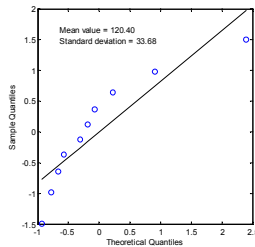
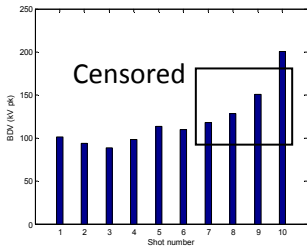


FR3

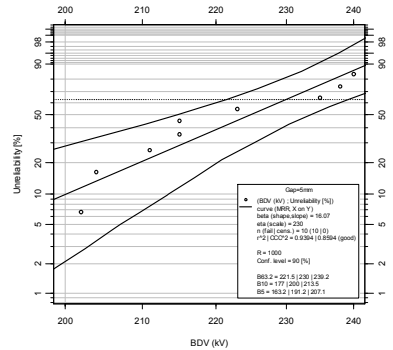
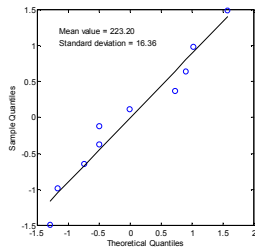
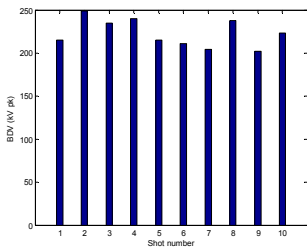
Gap: 1 mm



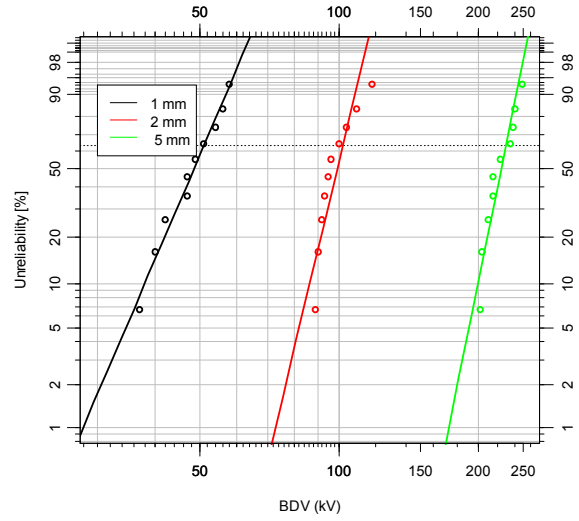
Gap: 2 mm



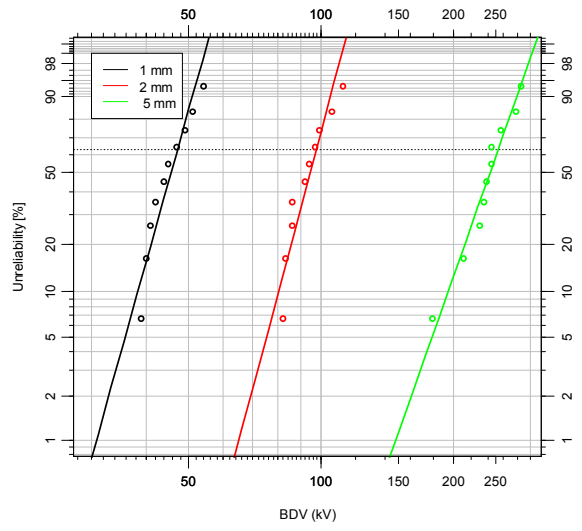
Gap 5 mm



Ester X



Shell Diala D



FR3

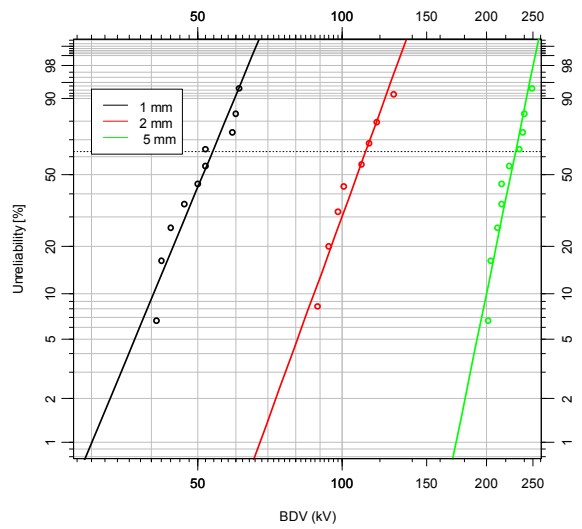


Fig. 5.11 Statistical parameters for BDV

5.4 Partial discharges (point to plane geometry, oil)

The test cell consists of a standard point/plane electrode configuration. High voltage electrodes were realized using Fine Science Tools tungsten needles having tip radius of $1\mu\text{s}$ and body diameter of 2.5mm. The sharpness of the needle tip was checked at regular times, and replaced whenever the point appeared to be deteriorated (lower sharpness). The vessel containing the electrodes is open to the external atmosphere. The test cell was realized as sketched in Fig. 4.11.

Inception of PD was evaluated in post-processing, by searching PD pulses having the typical streamer shape, or the formation of voltage-correlated structures in the PD pattern.

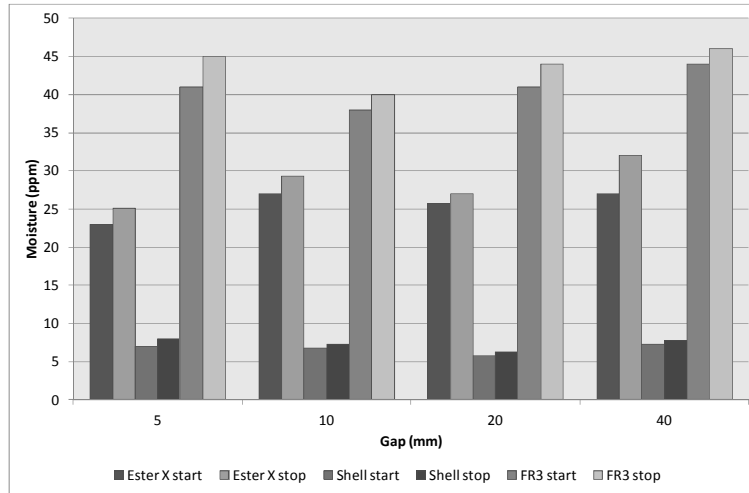


Fig. 5.12 Behavior of moisture during PDIV tests

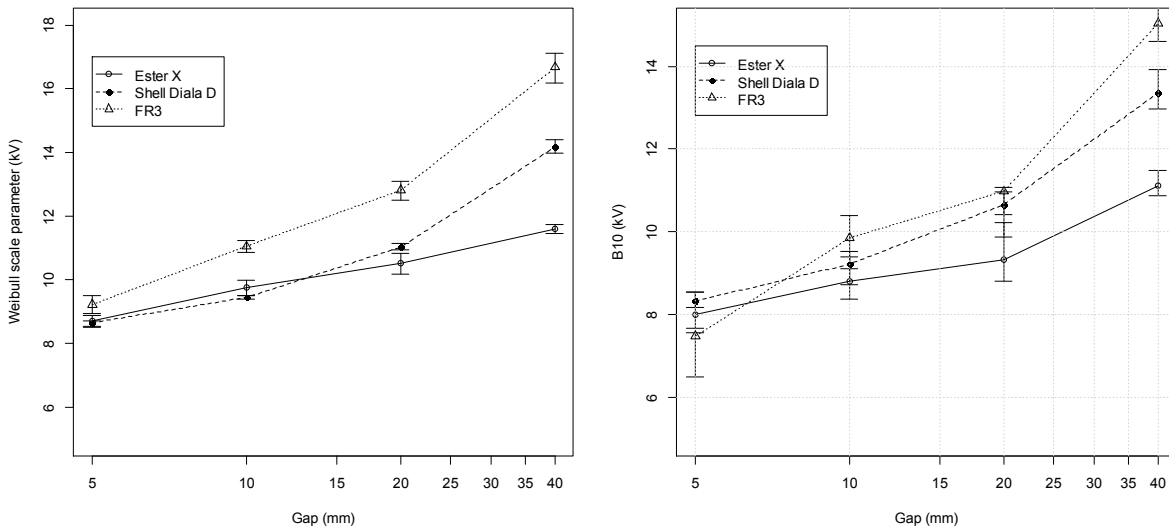
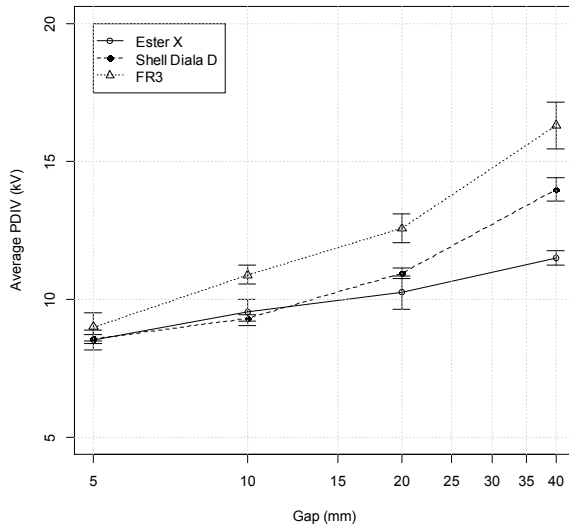
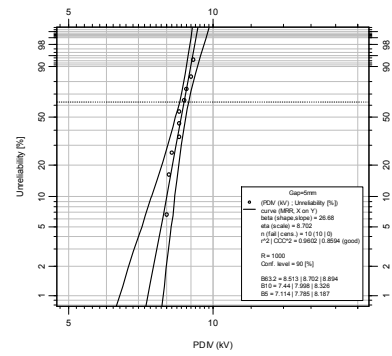
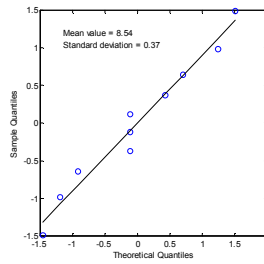
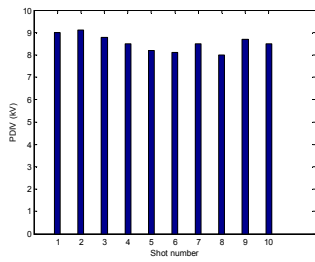


Fig. 5.13 Main statistical parameters for PDIV in oil (overall results)

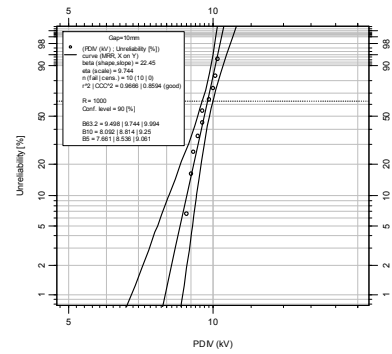
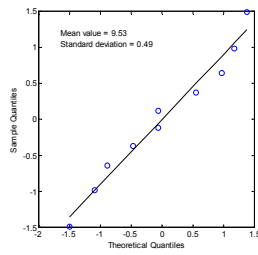
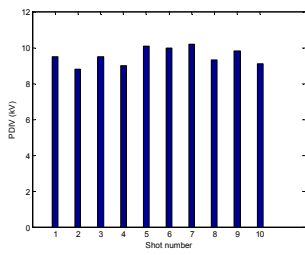


Ester X

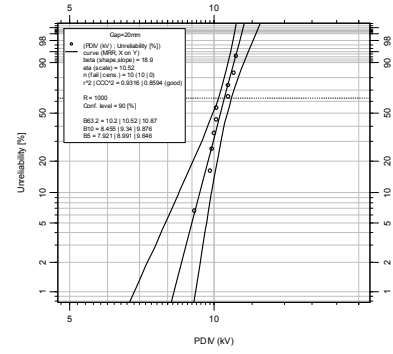
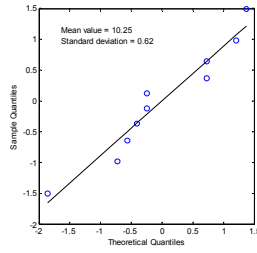
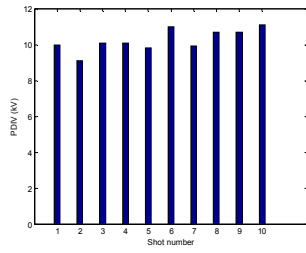
Gap:5mm,
H0=23ppm,
(HR=2.2%),
H1=25.1ppm
(HR=2.4%)
23°C



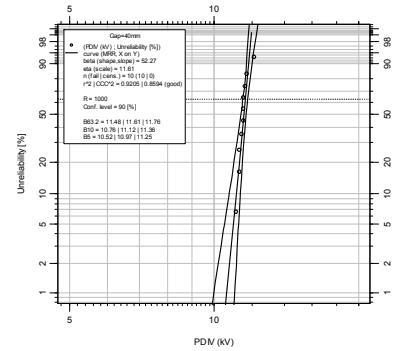
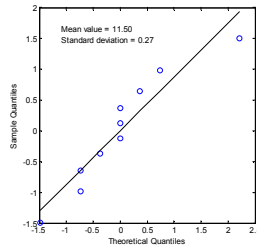
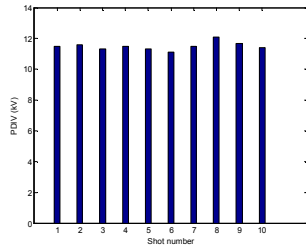
Gap:10mm,
H0=27ppm,
(HR=2.6%),
H1=29.3ppm
(HR=2.8%)
23°C



Gap:20mm,
H0=25.7ppm,
(HR=2.4%),
H1=27ppm
(HR=2.6%)
23°C

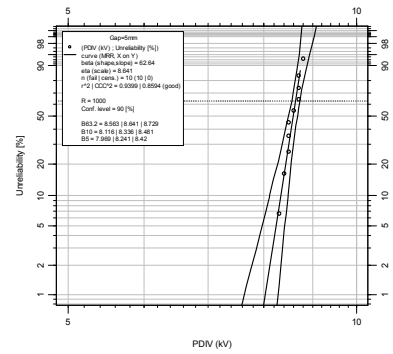
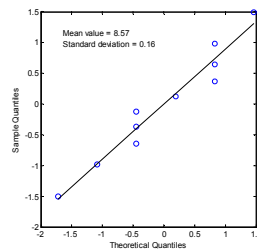
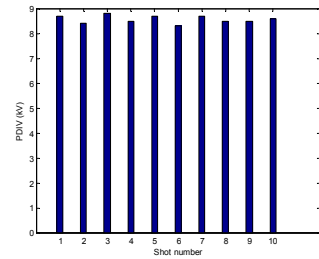


Gap:40mm,
H0=27ppm,
(HR=2.6%),
H1=32ppm
(HR=3%)
23°C

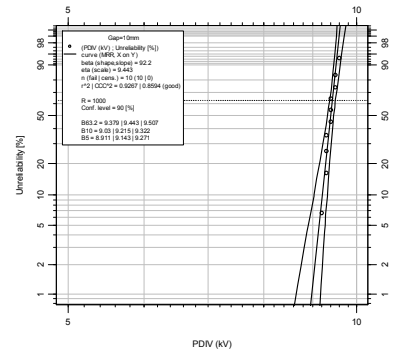
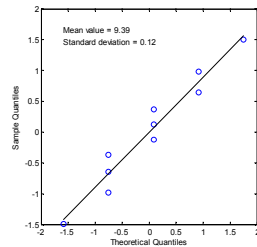
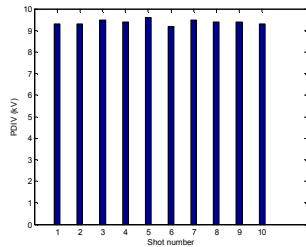


Mineral oil

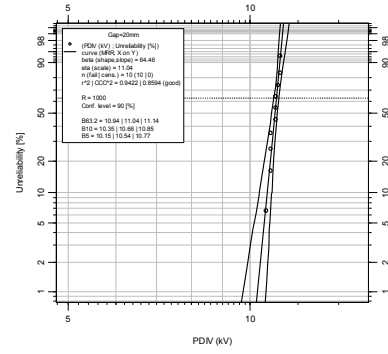
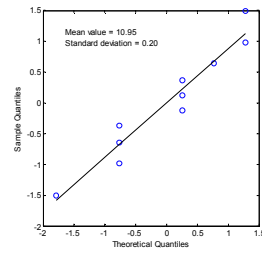
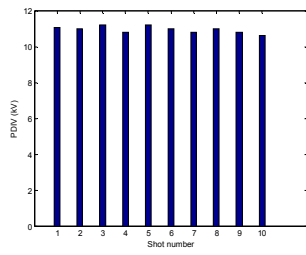
Gap:5mm,
H0=7ppm,
(HR=11.2%)
H1=8ppm
(HR=12.8%)
23°C



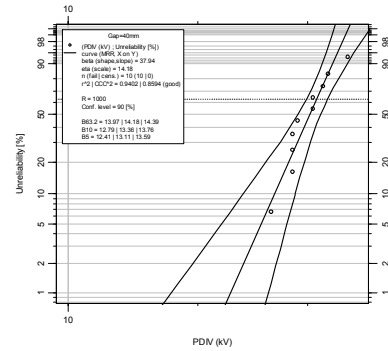
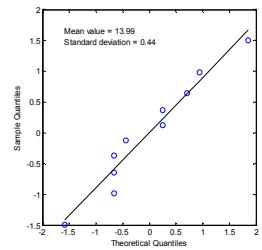
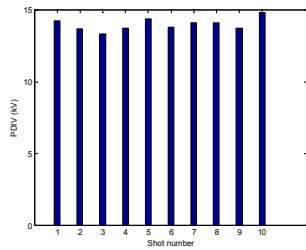
Gap:10mm
H0=6.8ppm
(HR=10.9%)
H1=7.3ppm
(HR=11.7%)
23°C



Gap:20mm,
H0=5.8ppm
(HR=9.3%)
H1=6.3ppm
(HR=10.0%)
23°C

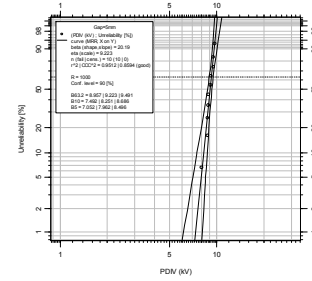
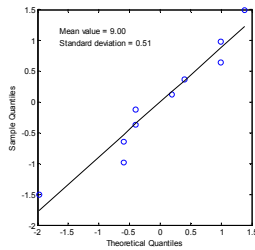
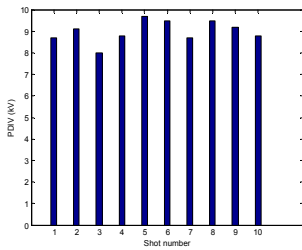


Gap:40mm
H0=7.3ppm
(HR=11.7%)
H1=7.8ppm
(HR=12.5%)
23°C

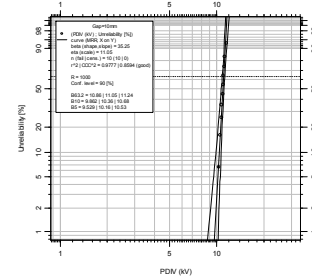
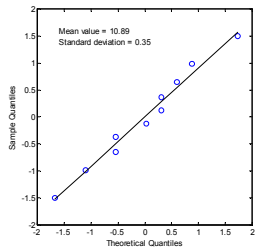
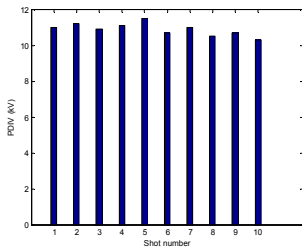


FR3

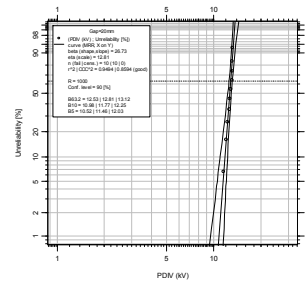
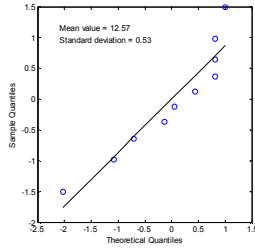
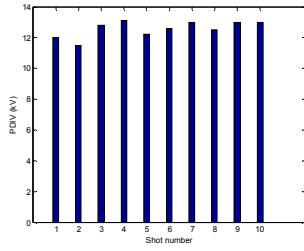
Gap:5mm,
H0=41ppm
(HR=3.9%),
H1=45ppm
(HR=4.4%),
23°C



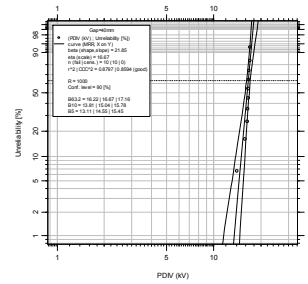
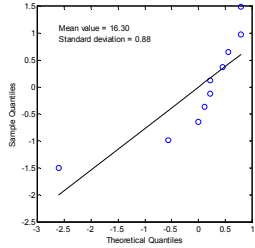
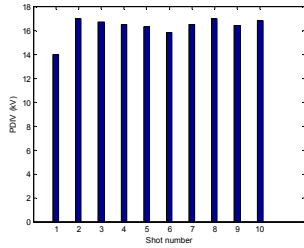
Gap:10mm,
H0=38ppm
(HR=3.7%),
H1=40ppm
(HR=3.9%),
23°C



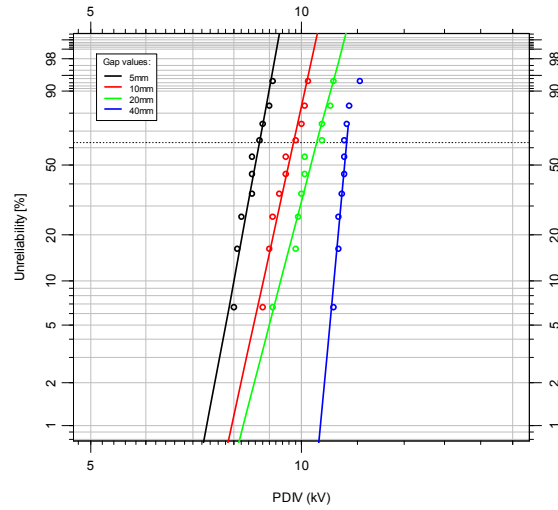
Gap:20mm,
H0=41ppm,
(HR=3.9%),
H1=44ppm
(HR=4.3%),
23°C



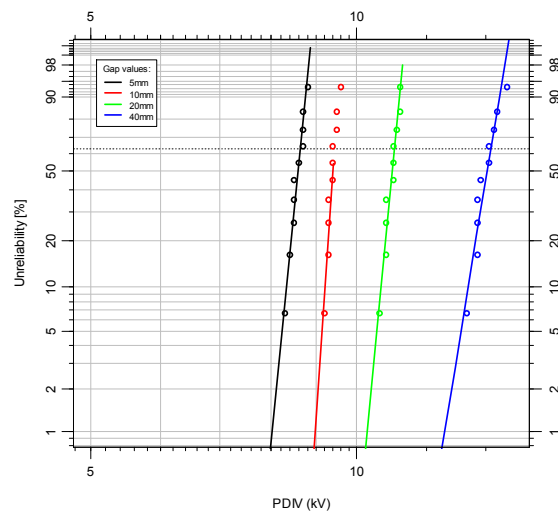
Gap:40mm,
H0=41ppm,
(HR=3.9%),
H1=46ppm
(HR=4.5%),
23°C



Ester X



Shell Diala D



FR3

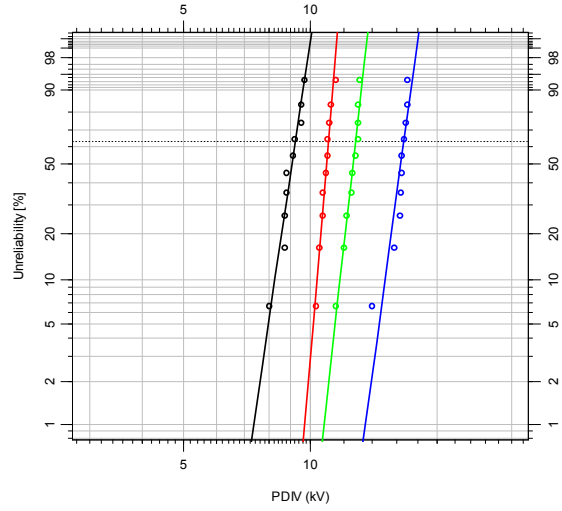


Fig. 5.14 Statistical parameters for PDIV in oil

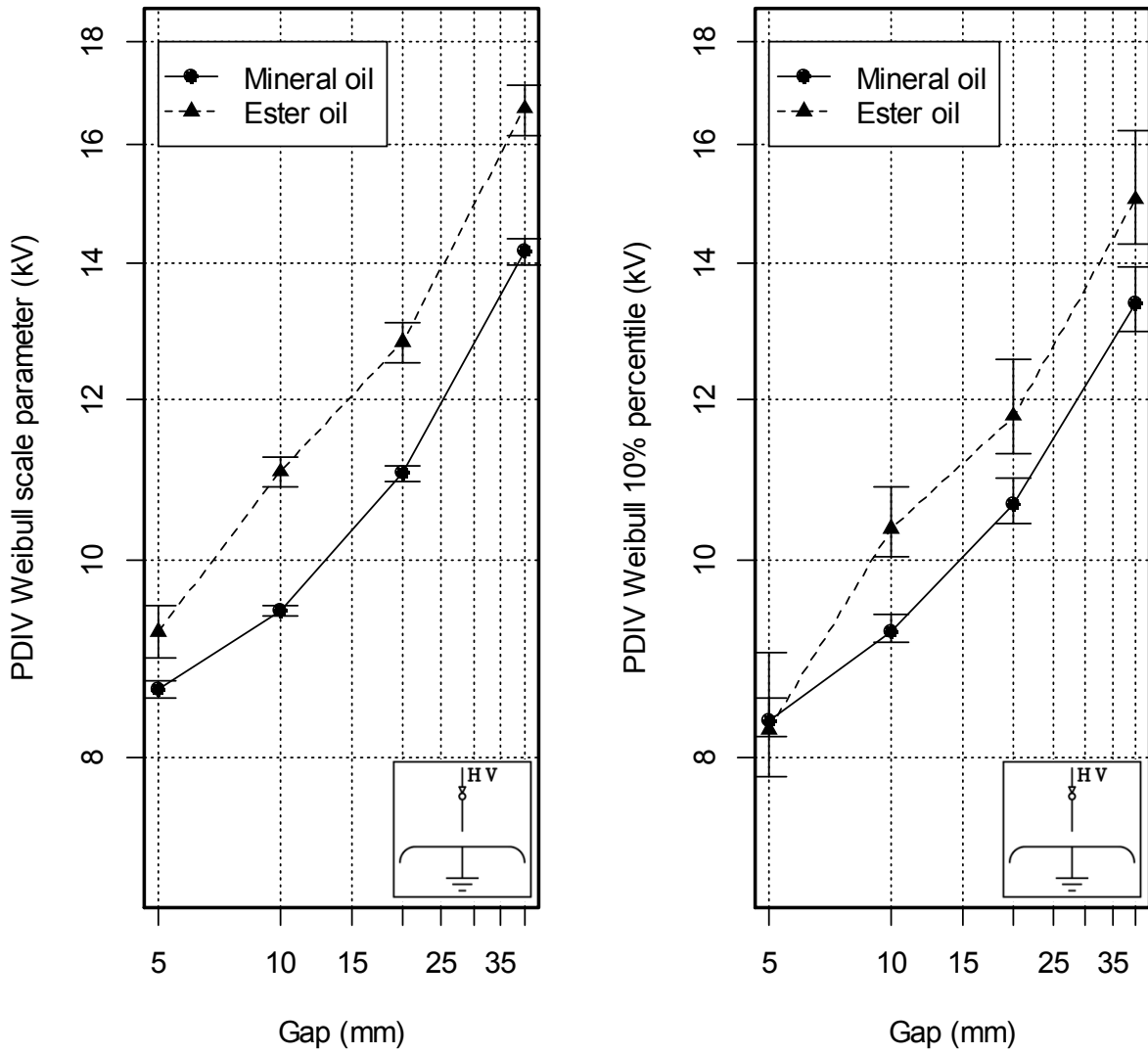


Fig. 5.15 Comparison of Weibull parameters for PDIV in oil for mineral oil and FR3

5.5 Partial discharges (point to plane geometry, Pressboard barrier + oil)

The test cell consists of a standard point/plane electrode configuration. High voltage electrodes were realized using Fine Science Tools tungsten needles having tip radius of $1\mu\text{s}$ and body diameter of 2.5mm. The sharpness of the needle tip was checked at regular times, and replaced whenever the point appeared to be deteriorated (lower sharpness). The vessel containing the electrodes is open to the external atmosphere.

The test cell was realized as sketched in Fig. 4.13. The tungsten needle was fixed to a mobile support, and kept in contact with the pressboard through gravity. In this way, the force holding in contact the pressboard and the needle was constant in all tests. To modify the distance between the needle and the ground electrode, the support was lifted first from the pressboard, slid as required and eventually laid down again. In this way, damage of the needle tip was avoided.

The measurement circuit consisted of a Hipotronics 30kV transformer, and 1nF coupling capacitor. The PD signal was coupled through a $50\ \Omega$ resistor in series with the test object under test. During the tests, the level of noise was below 5 pC.

The following the protocol agreed PDIV was tested using:

1. All oils was dry as much as possible.
2. Pressboard dried 24 hours at $100\ ^\circ\text{C}$, and then immersed in dry oil for 24 hours, under vacuum.
3. Voltage ramps consisting of steps of 250 V, each lasting 300 s.

Inception of PD was evaluated in post-processing, by searching PD pulses having the typical streamer shape, or the formation of voltage-correlated structures in the PD pattern.

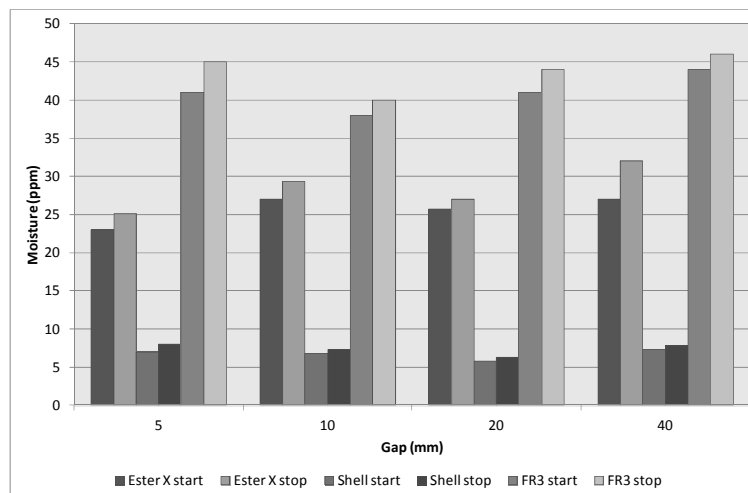


Fig. 5.16 Moisture behavior during PDIV testing in PB and oil geometries

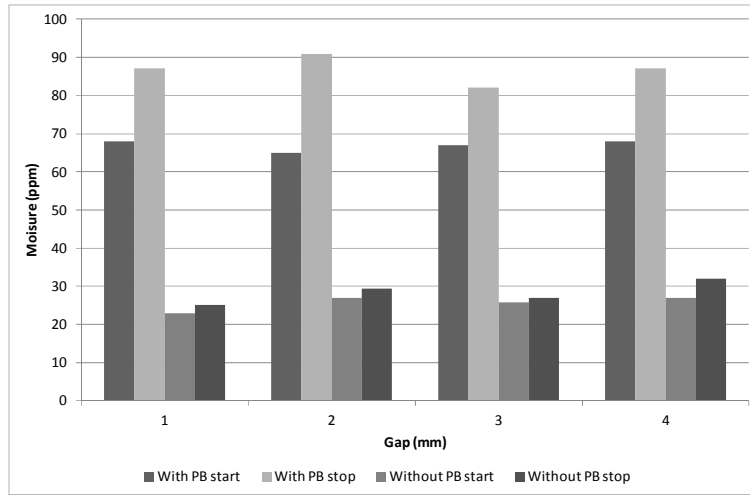


Fig. 5.17 Comparison of moisture behavior with and without PB during PDIV testing

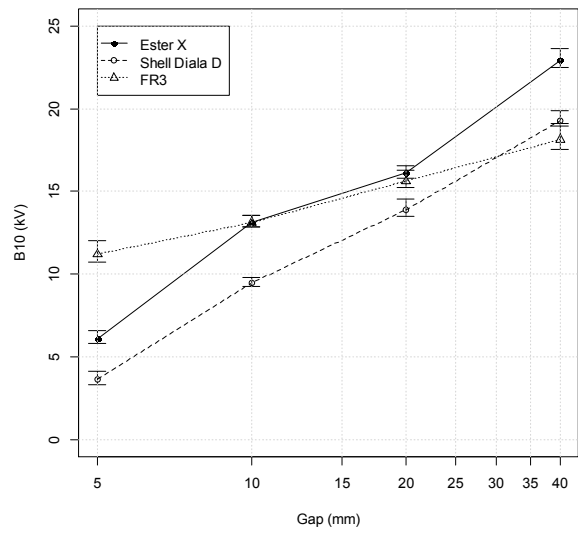
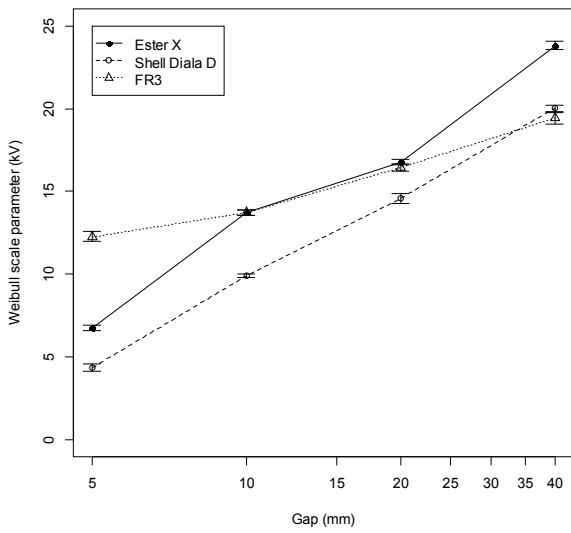
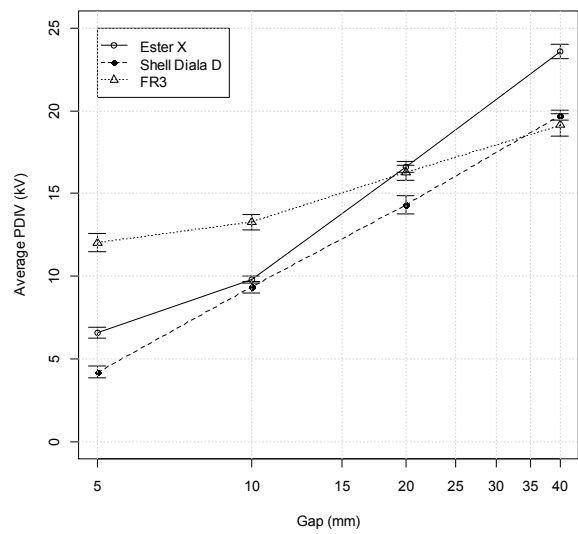


Fig. 5.18 Main statistical parameters for PDIV testing in pressboard and oil geometries (overall results)



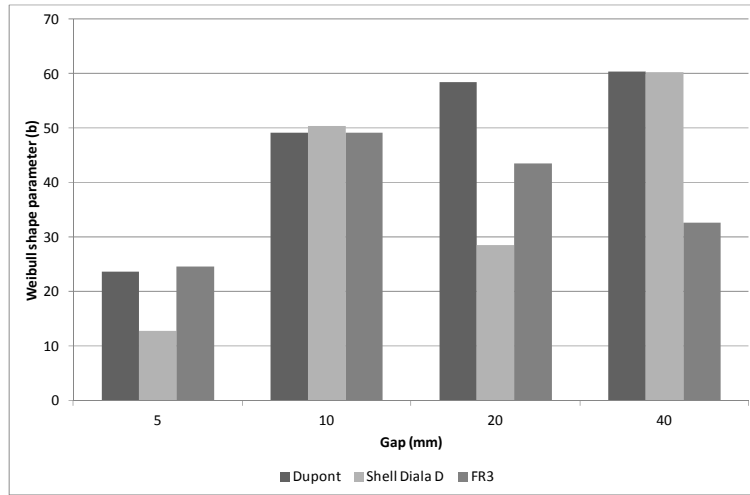
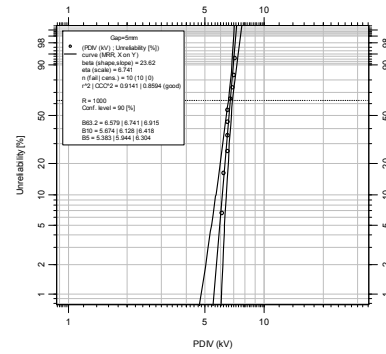
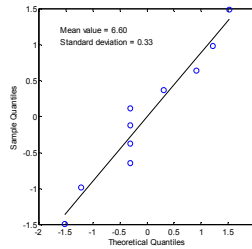
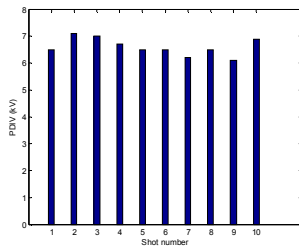


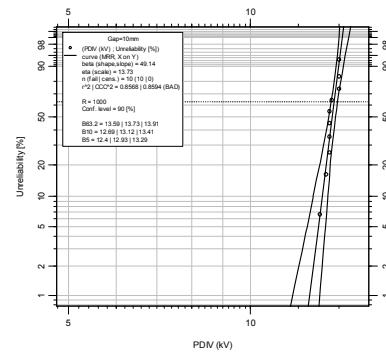
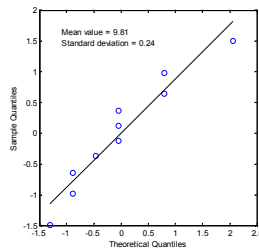
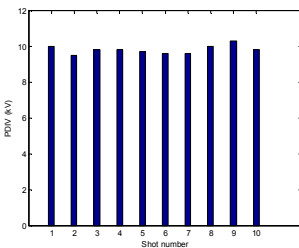
Fig. 5.19 Weibull shape parameter as a function of gap length

Ester X

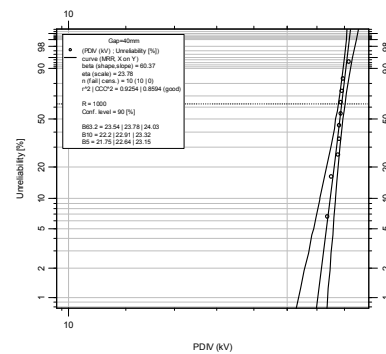
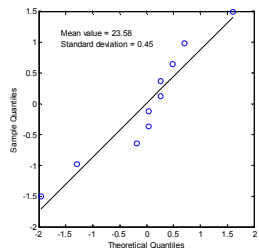
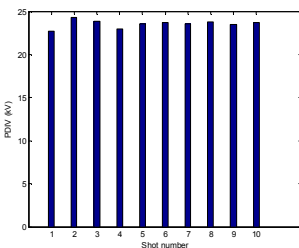
Gap: 5mm
H0=68ppm,
(HR=6.6%),
H1=87ppm
(HR=8.4%),
22°C



Gap: 10mm,
H0=65ppm,
(HR=6.3%),
H1=91ppm
(HR=8.8%),
22°C

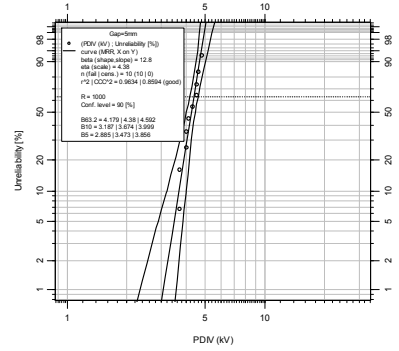
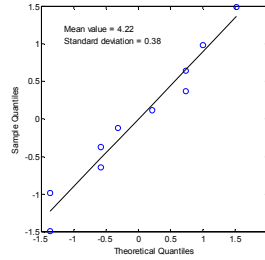
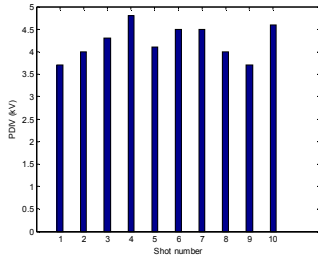


Gap: 40 mm
H0=68ppm,
(HR=6.6%),
H1=87ppm
(HR=8.4%),
22°C

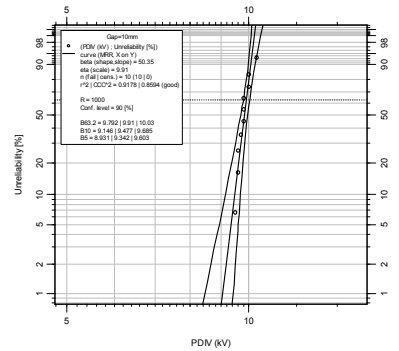
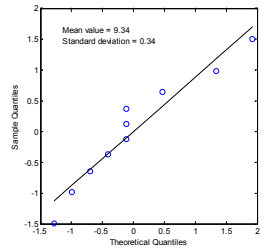
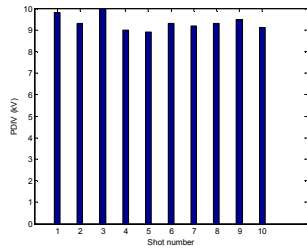


Mineral oil

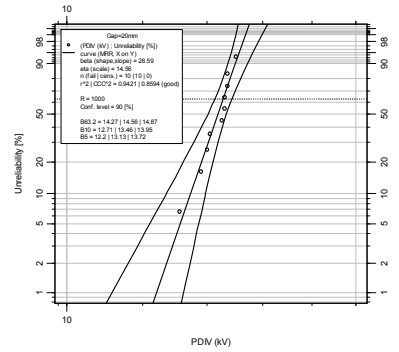
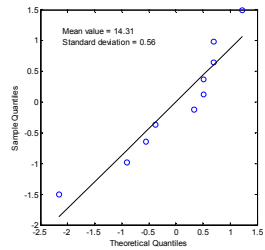
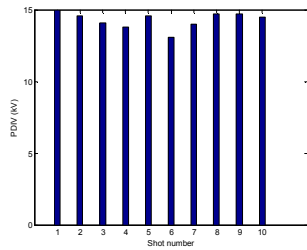
Gap:5mm,
H0=8ppm,
(HR=13.3%)
H1=12ppm
(HR=20.0%)
22°C



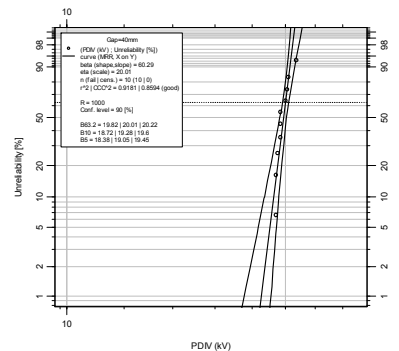
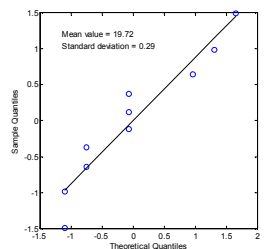
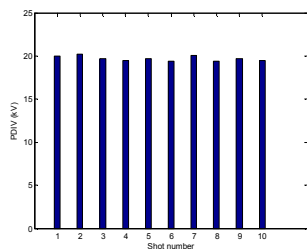
Gap:10mm,
H0=7ppm,
(HR=11.7%)
H1=11ppm
(HR=18.3%)
22°C



Gap:20mm,
H0=10ppm,
(HR=16.7%)
H1=13ppm
(HR=21.7%)
22°C

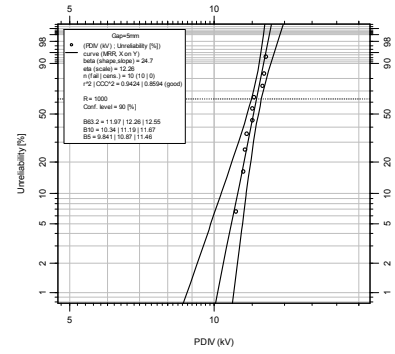
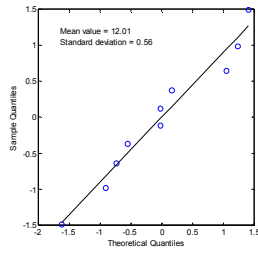
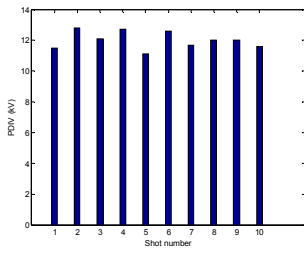


Gap:40mm,
H0=8ppm,
(HR=13.3%)
H1=11ppm
(HR=18.3%)
22°C

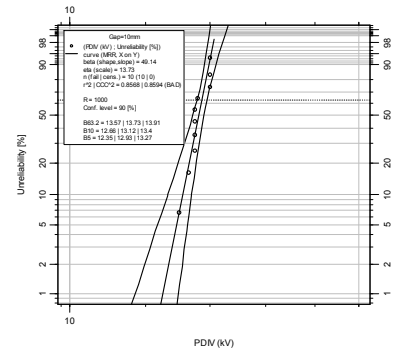
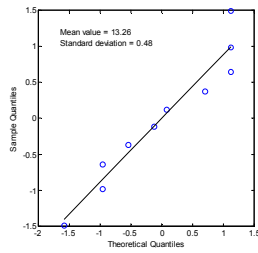
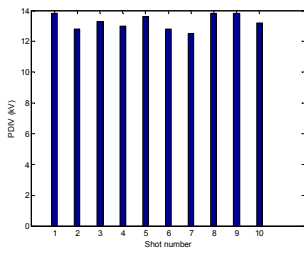


FR3

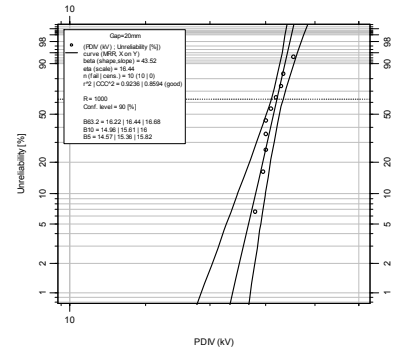
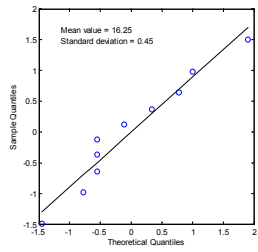
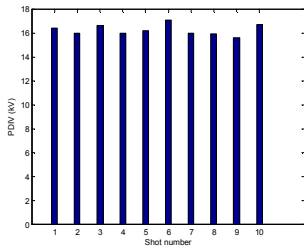
5 mm gap,
 H0=49ppm,
 (HR=4.7%),
 H1=72ppm
 (HR=6.9%),
 22°C



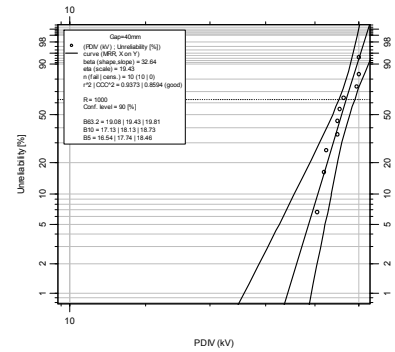
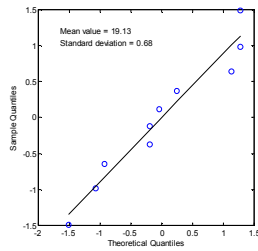
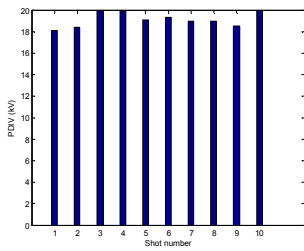
10 mm gap,
 H0=50ppm,
 (HR=4.9%),
 H1=81ppm
 (HR=7.9%),
 22°C



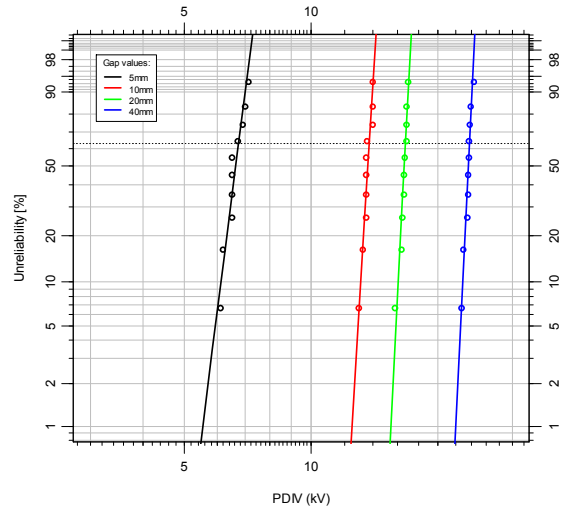
20 mm gap,
 H0=43ppm,
 (HR=4.2%),
 H1=65ppm
 (HR=6.3%),
 22°C



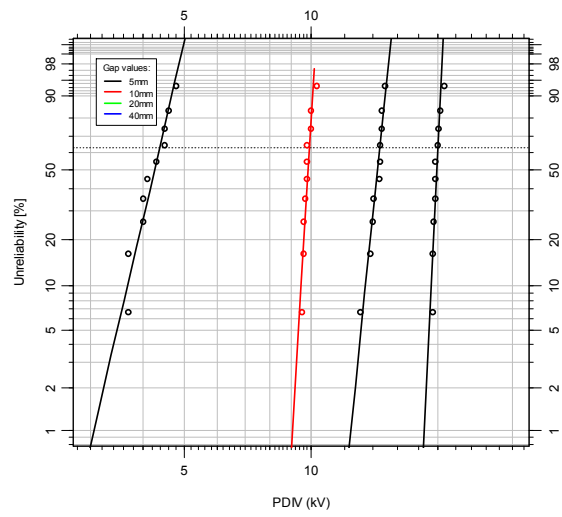
40 mm gap,
 H0=40ppm,
 (HR=3.9%),
 H1=55ppm
 (HR=5.3%),
 22°C



Ester X



Shell Diala D



FR3

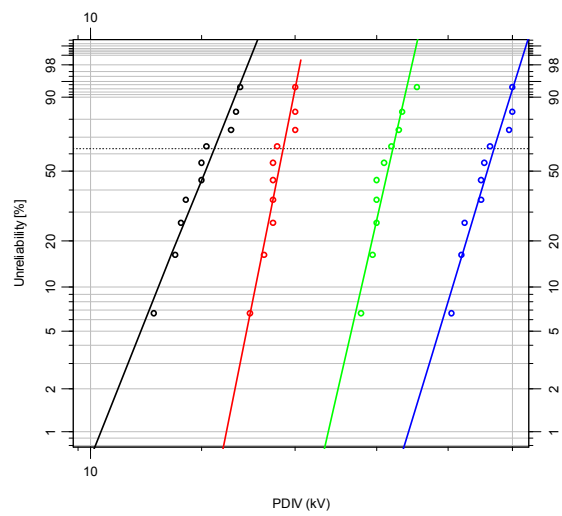


Fig. 5.20 Main statistical parameters for BDV (overall results)

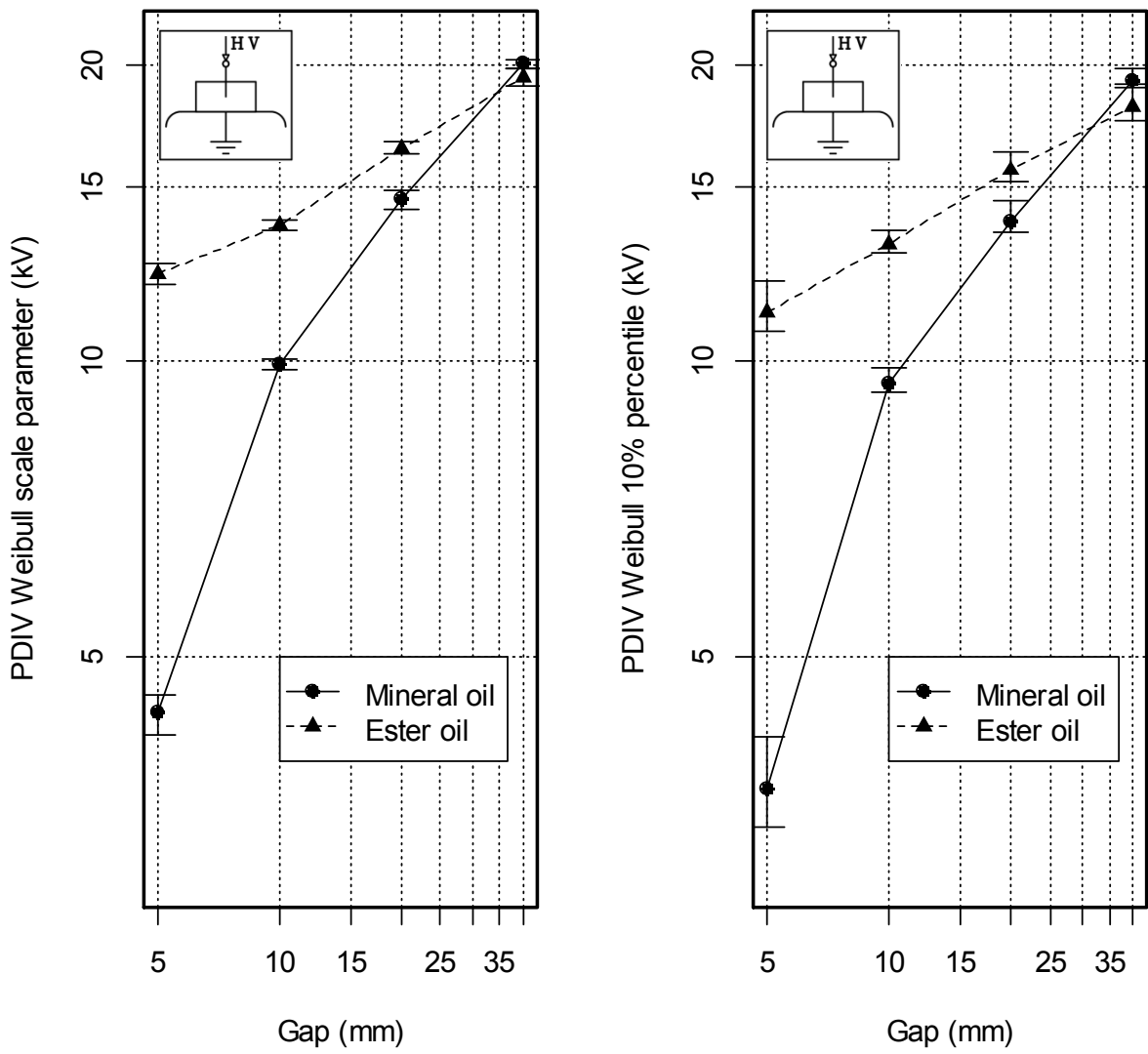


Fig. 5.21 Comparison of Weibull parameters for PDIV in pressboard and oil for mineral oil and FR3

5.6 Comsol® simulations for point to plane geometry with and without pressboard

Electrodes configurations were modeled in Comsol Multiphysics®. Each geometry was discretized prior to the solving process and the ground electrodes were set for each gap changing material and boundary conditions (i.e. from to electrical insulation to ground condition in the Electric Currents physics). In this way, the same mesh is used for all the possible gap distances. In order to evaluate electrical parameters, some probes and paths were defined depending on the parameter and on the results display.

The geometry of the needle has a 5 μ m radius tip and a body diameter of 0.5mm. The following parameters were used for FEM modeling:

Table 5 Parameter for FEM modeling

Material	Relative permittivity	Electrical conductivity (S/m)
Mineral oil	2.2	3.75E-15
Ester	3.2	33E-15
Mineral oil impregnated board	3.5	12.37E-15
Ester impregnated board	4.1	17.1E-15

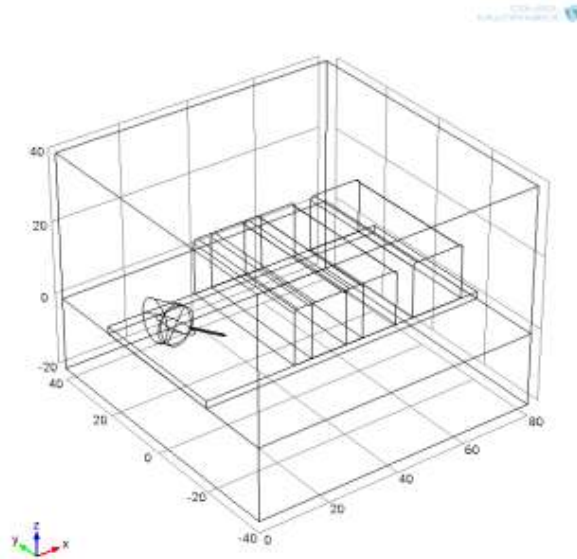


Fig. 5.22 Geometry for creeping discharges modeling

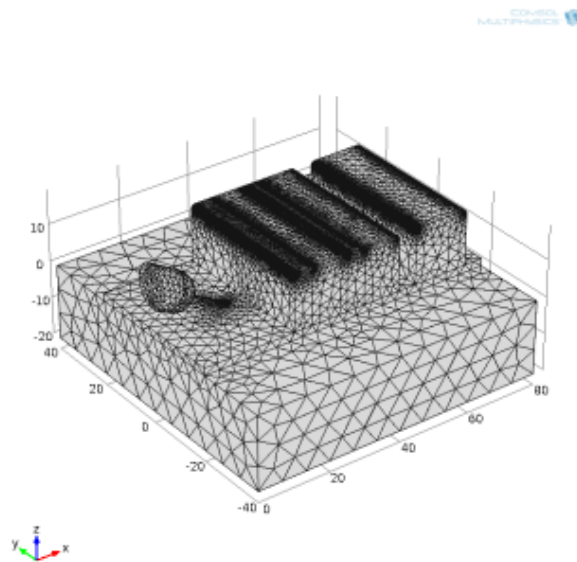


Fig. 5.23 FEM 3D discretization for creeping discharges modeling

Following, a collection of simulation results for the more extreme gaps is presented for mineral oil and FR3 with pressboard bridged gap and for oil gap using the same test cell.

Mineral oil, 5mm gap with PB

FR3, 5mm gap with PB

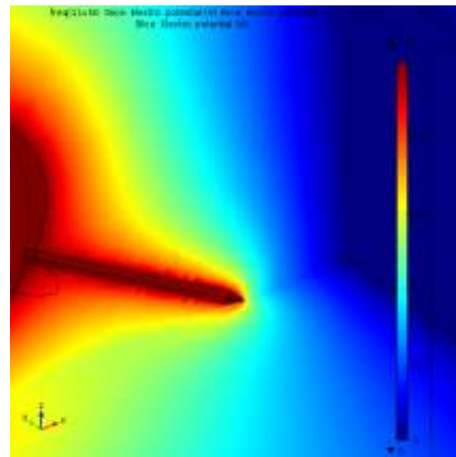
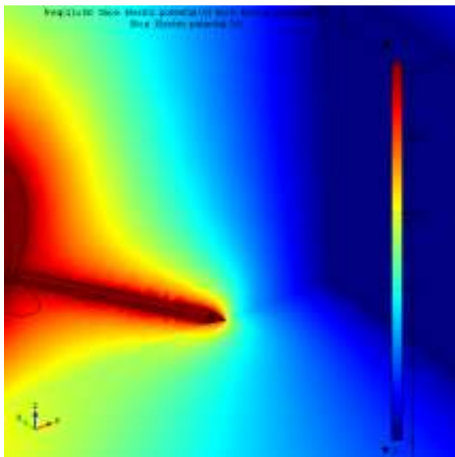


Fig. 5.24 Electric potential comparison at 5mm

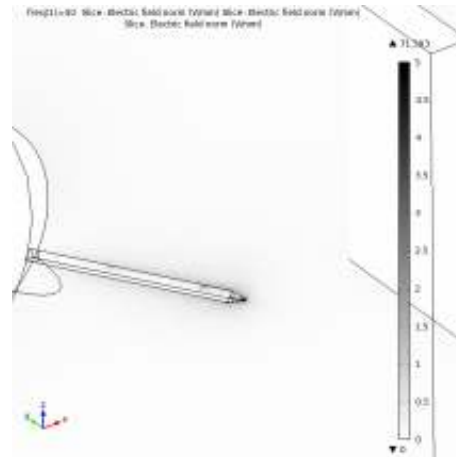
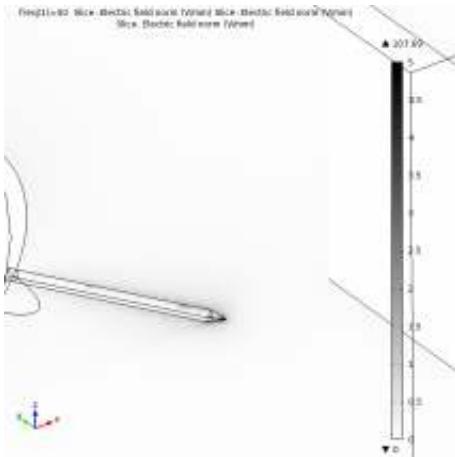


Fig. 5.25 Electric field comparison at 5mm

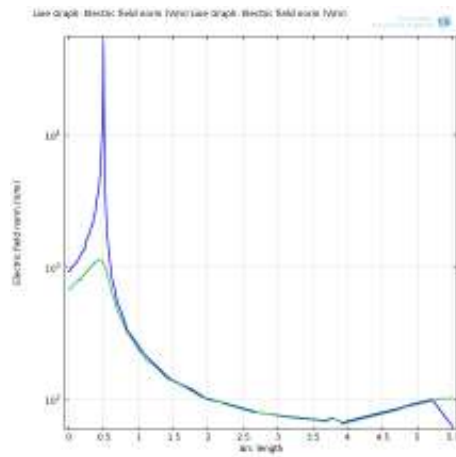
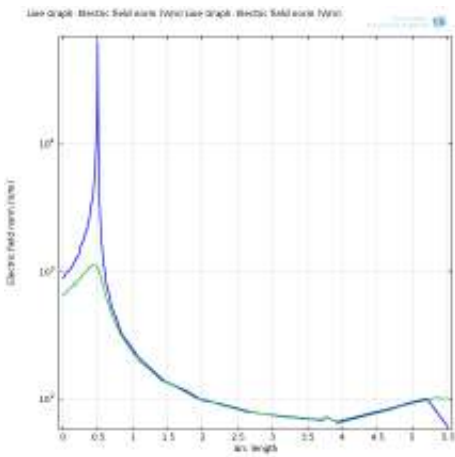


Fig. 5.26 Electric field comparison at 5mm (over and inside PB sheet)

Mineral oil, 40mm gap with PB

FR3, 40mm gap with PB

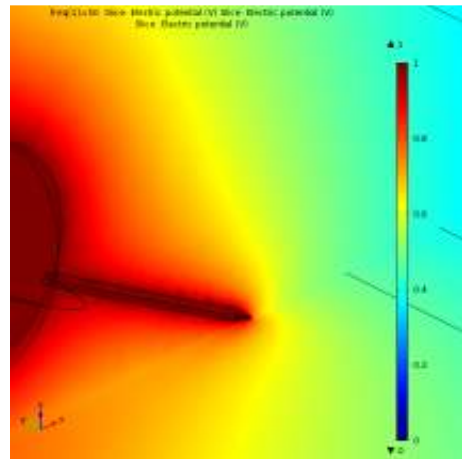
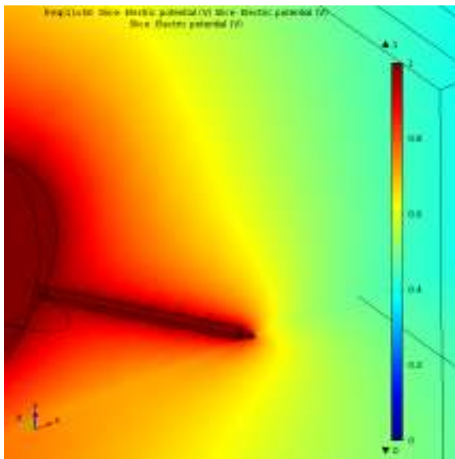


Fig. 5.27 Electric potential comparison at 40mm

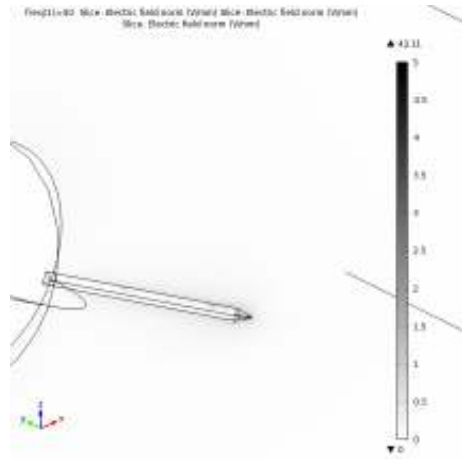
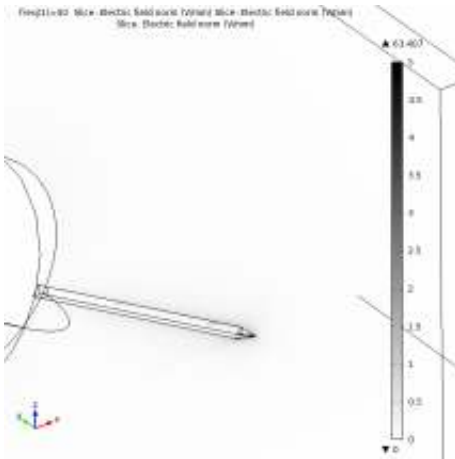


Fig. 5.28 Electric field comparison at 40mm

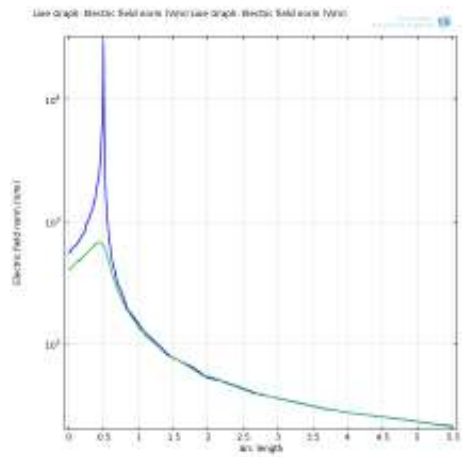
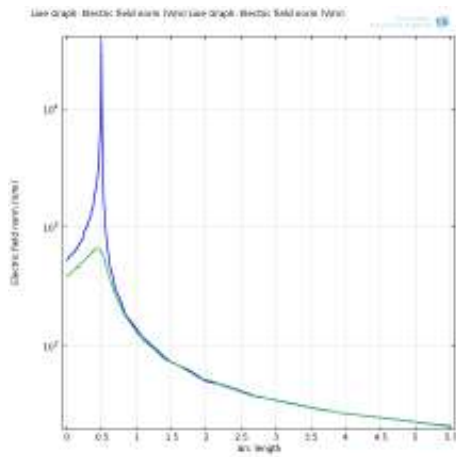
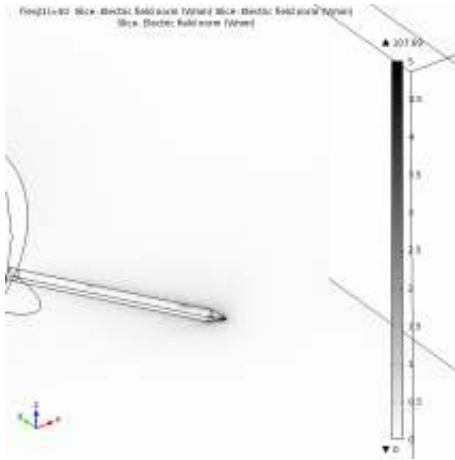


Fig. 5.29 Electric field comparison at 40mm (over and inside PB sheet)

Minerale oil, 5mm gap

With PB



Without PB

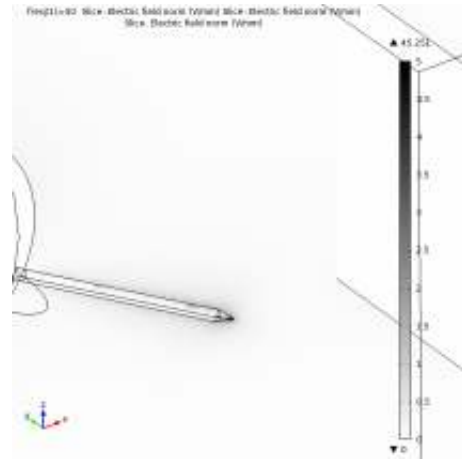


Fig. 5.30 Electric field comparison at 5mm gap with and without PB in mineral oil

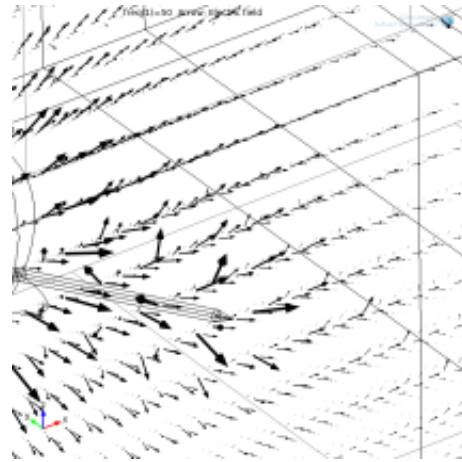
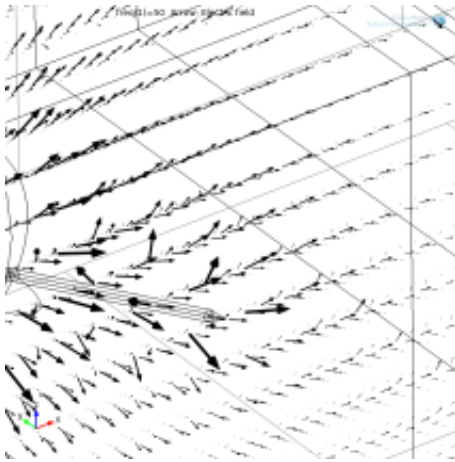


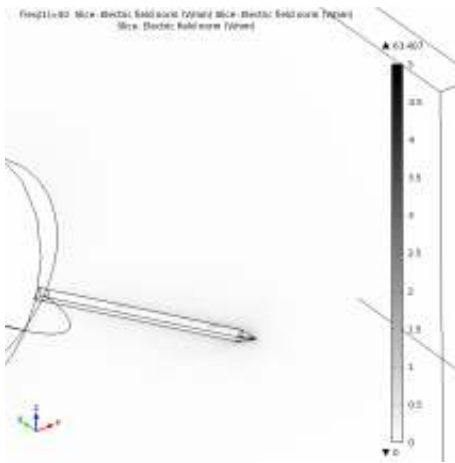
Fig. 5.31 Electric field vectors comparison at 5mm gap with and without PB in mineral oil

Freq	50
Electric field norm, PB surf	88.3161
Electric field norm, Upper oil	154.3711
Electric field norm, PB	0.0119

Freq	50
Electric field norm, PB surf	44.5726
Electric field norm, Upper oil	82.4382
Electric field norm, PB	0.014

Minerale oil, 40mm gap

With PB



Without PB

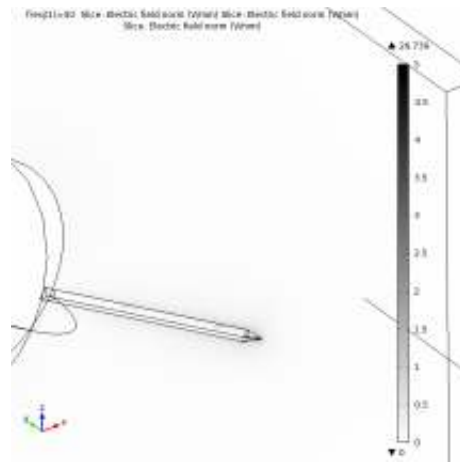


Fig. 5.32 Electric field comparison at 40mm gap with and without PB in mineral oil

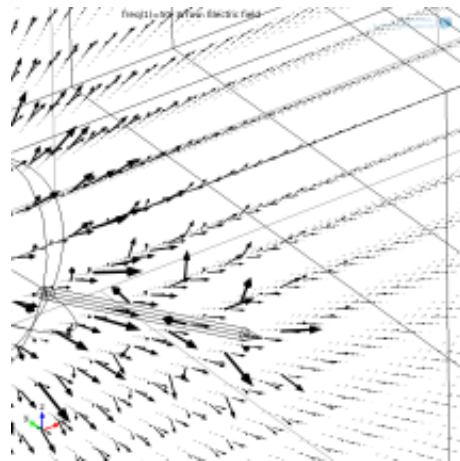
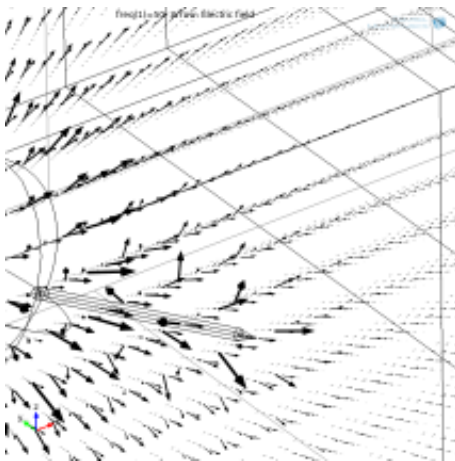


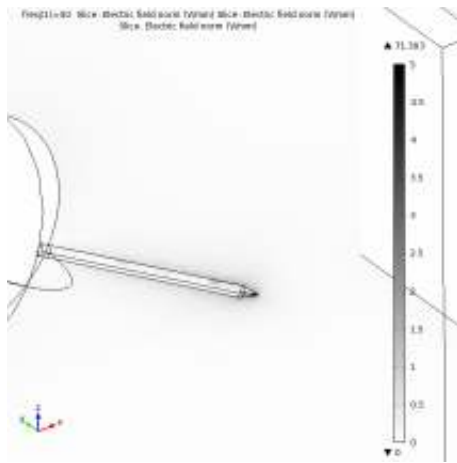
Fig. 5.33 Electric field vectors comparison at 40mm gap with and without PB in mineral oil

Freq	50
Electric field norm, PB surf	52.0019
Electric field norm, Upper oil	90.8856
Electric field norm, PB	0.0124

Freq	50
Electric field norm, PB surf	26.3375
Electric field norm, Upper oil	48.6681
Electric field norm, PB	0.0141

FR3, 5mm gap

With PB



Without PB

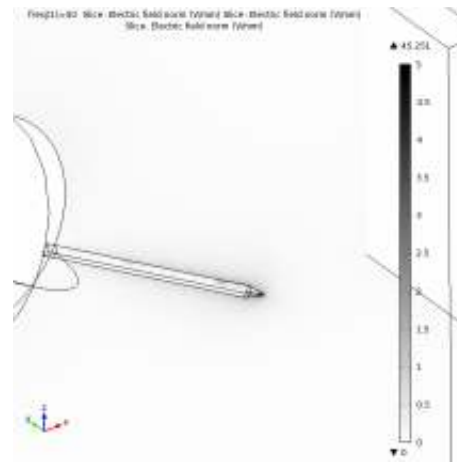


Fig. 5.34 Electric field comparison at 5mm gap with and without PB in FR3

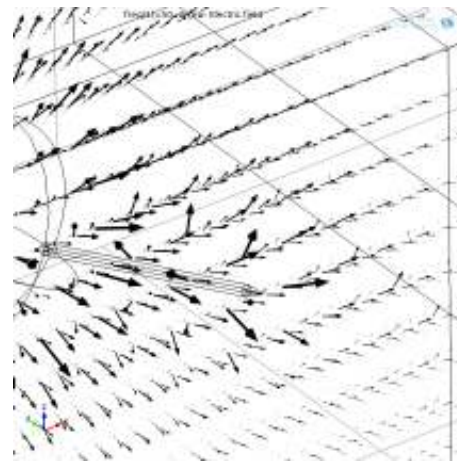
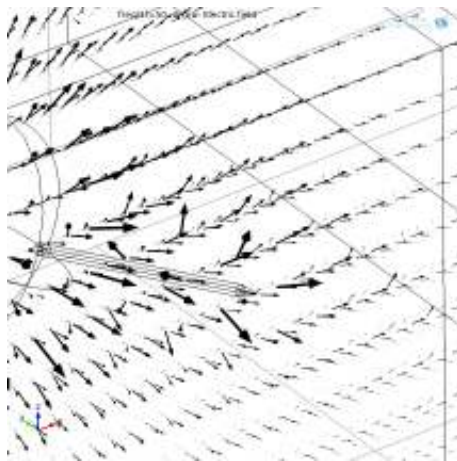
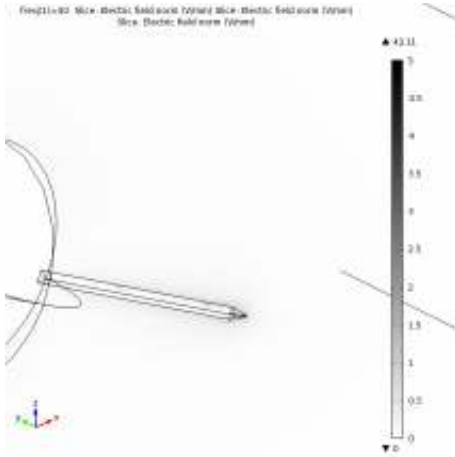


Fig. 5.35 Electric field vectors comparison at 5mm gap with and without PB in FR3

Freq	50	Freq	50
Electric field norm, PB surf	63.338	Electric field norm, PB surf	44.5726
Electric field norm, Upper oil	109.1686	Electric field norm, Upper oil	82.4382
Electric field norm, PB	0.0128	Electric field norm, PB	0.014

FR3, 40mm gap

With PB



Without PB

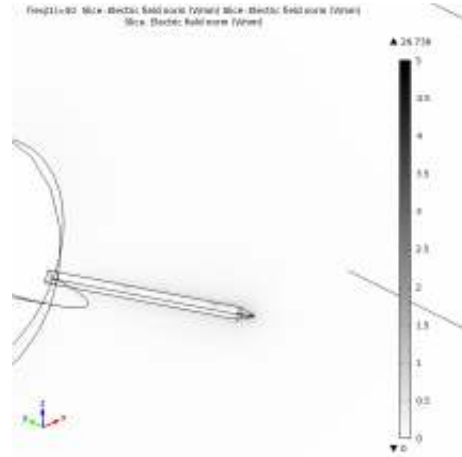


Fig. 5.36 Electric field comparison at 40mm gap with and without PB in FR3

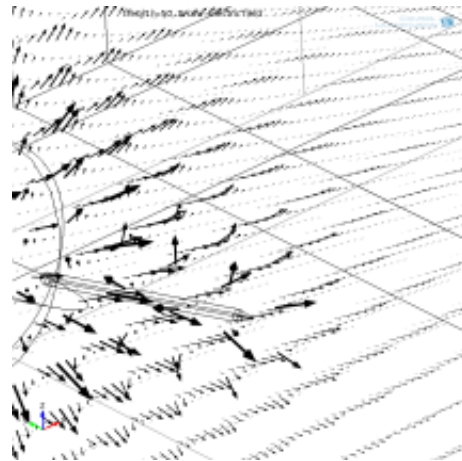
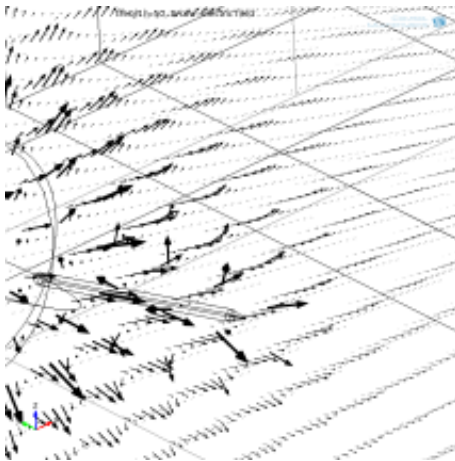


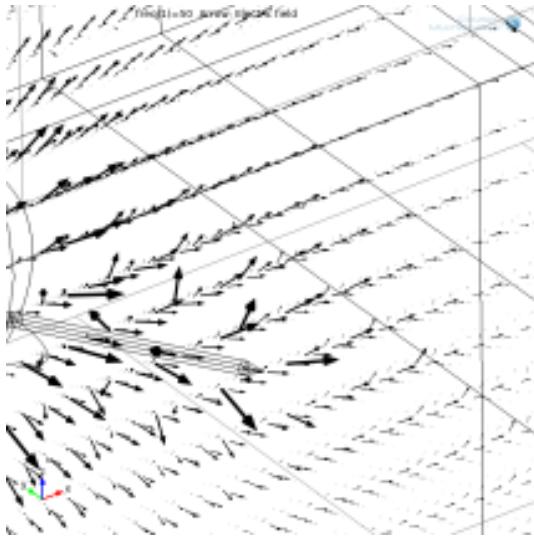
Fig. 5.37 Electric field comparison at 40mm gap with and without PB in FR3

Freq	50
Electric field norm, PB surf	37.3591
Electric field norm, Upper oil	64.3829
Electric field norm, PB	0.0131

Freq	50
Electric field norm, PB surf	26.3375
Electric field norm, Upper oil	48.6681
Electric field norm, PB	0.0141

Differences between electric field vectors for 5 and 40 mm in mineral oil and FR3

Mineral oil 5 mm



Mineral oil 40 mm

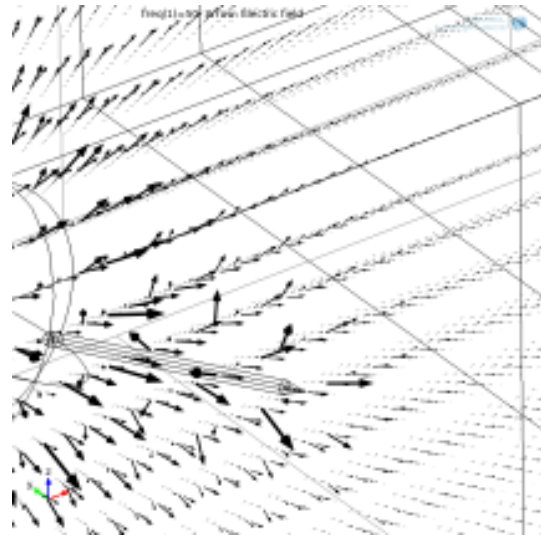
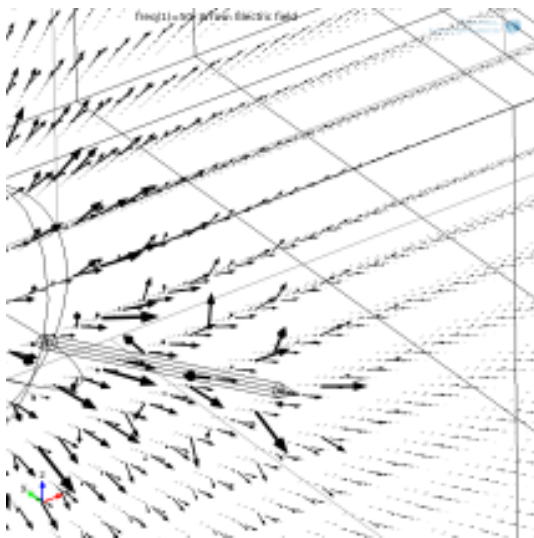


Fig. 5.38 Electric field vectors comparison at 5 and 40mm gap in mineral oil

FR3 5 mm



FR3 40 mm

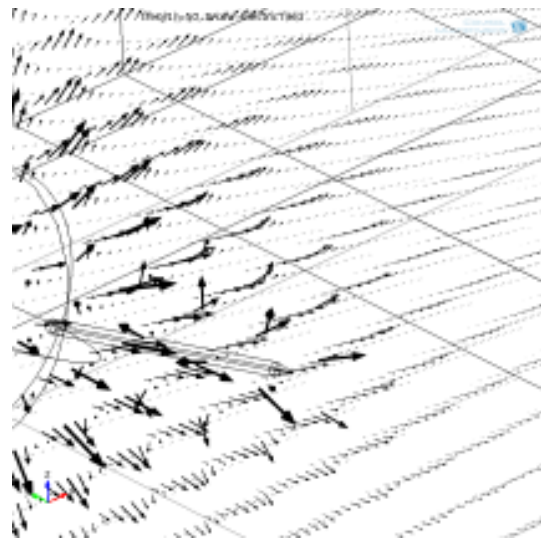
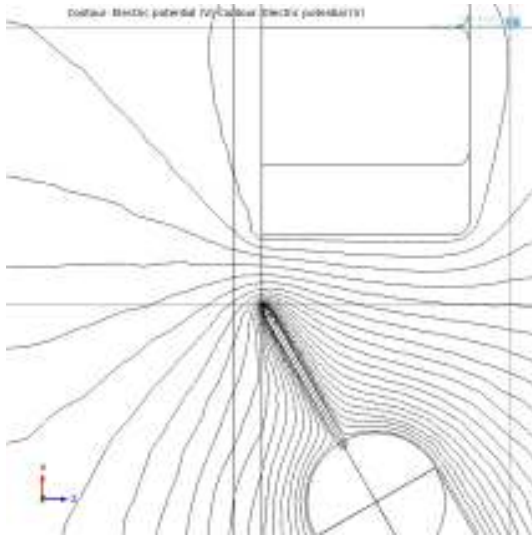


Fig. 5.39 Electric field vectors comparison at 5 and 40mm gap in mineral oil

Differences between potential distribution for 5 and 40 mm in mineral oil and FR3

Mineral oil 5 mm cross-section



Mineral oil 40 mm cross-section

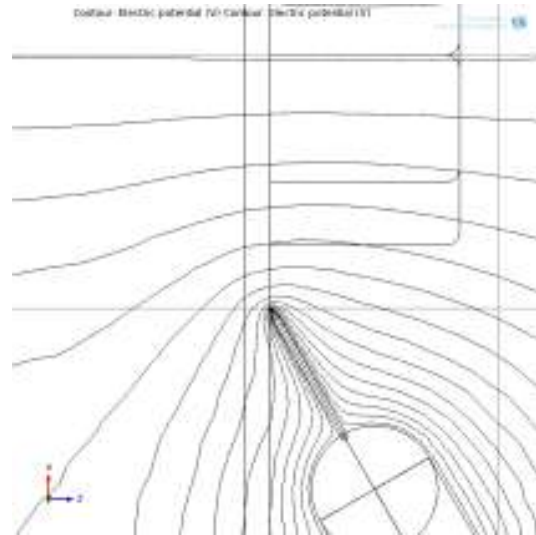
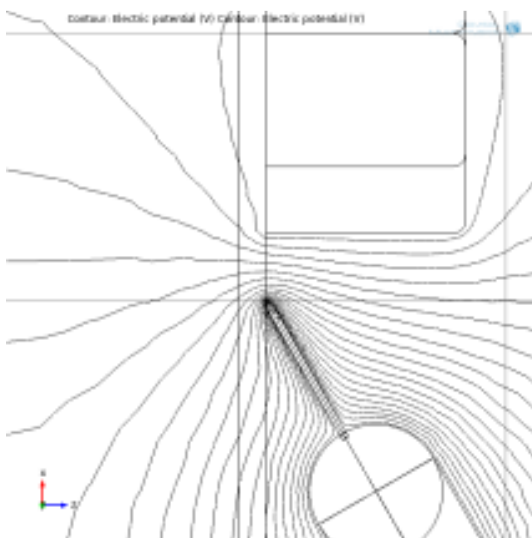


Fig. 5.40 Comparison of minimum and maximum gaps in mineral oil (cross-section)

FR3 5 mm cross-section



FR3 40 mm cross-section

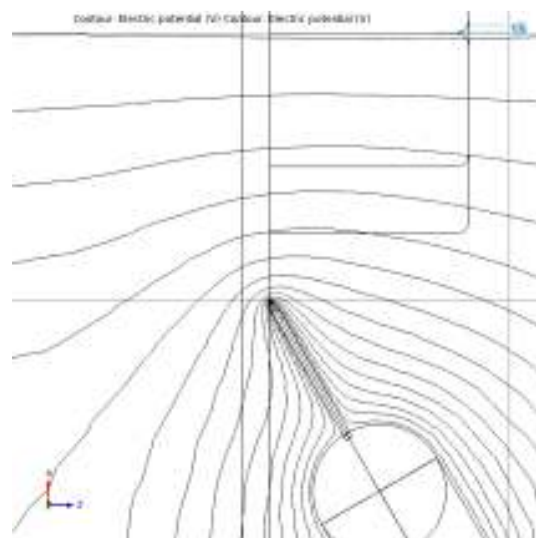


Fig. 5.41 Comparison of minimum and maximum gaps in FR3 (cross-section)

Differences between potential distribution for 5 and 40 mm in mineral oil and FR3

Mineral oil 5 mm over PB surface

Mineral oil 40 mm over PB surface

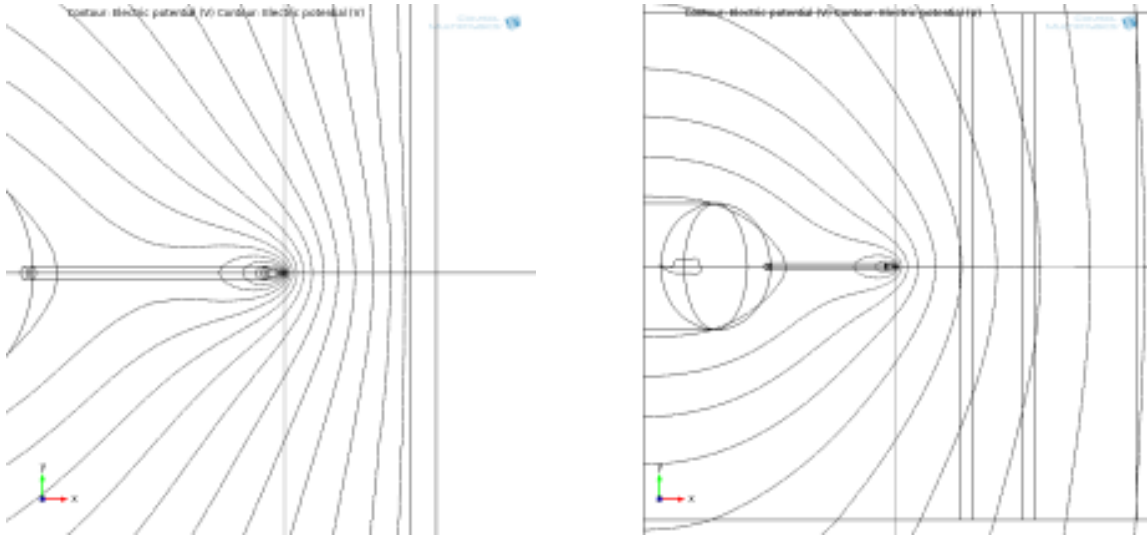


Fig. 5.42 Comparison of minimum and maximum gaps in mineral oil (over PB surface)

FR3 5 mm over PB surface

FR3 40 mm over PB surface

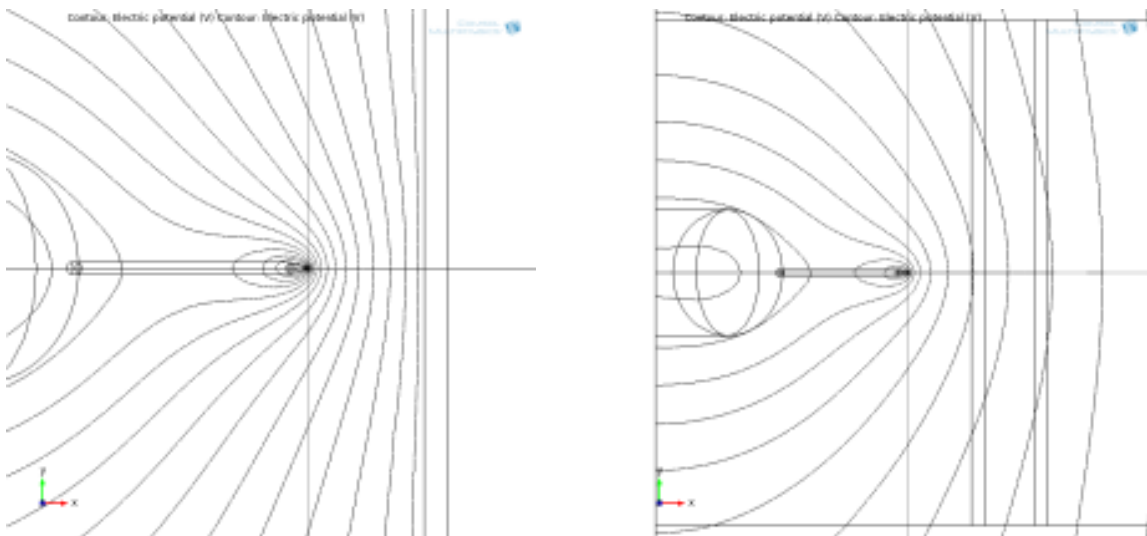


Fig. 5.43 Comparison of minimum and maximum gaps in mineral oil (over PB surface)

Differences between electric field vectors for 5 and 40 mm in mineral oil and FR3 in the half of the needle

Mineral oil 5 mm cross-section

Mineral oil 40 mm cross-section

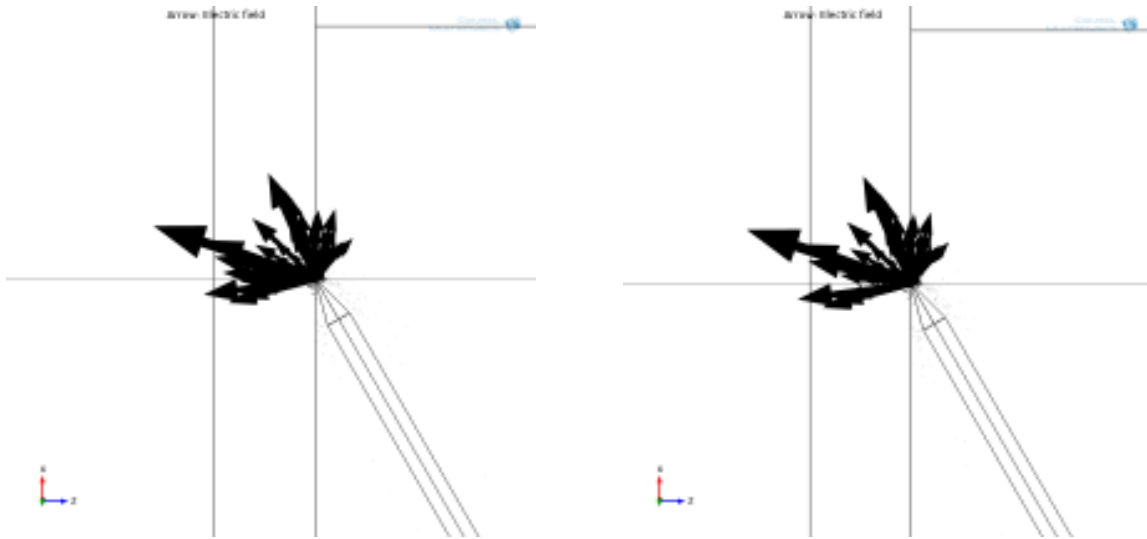


Fig. 5.44 Comparison of minimum and maximum gaps in mineral oil (mid plane)

FR3 5 mm cross-section

FR3 40 mm cross-section

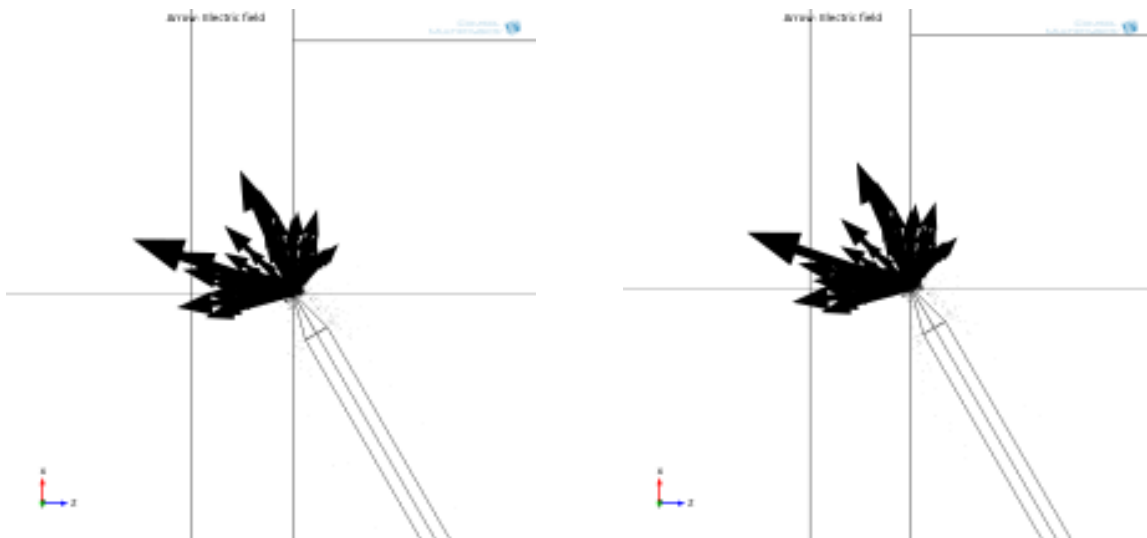
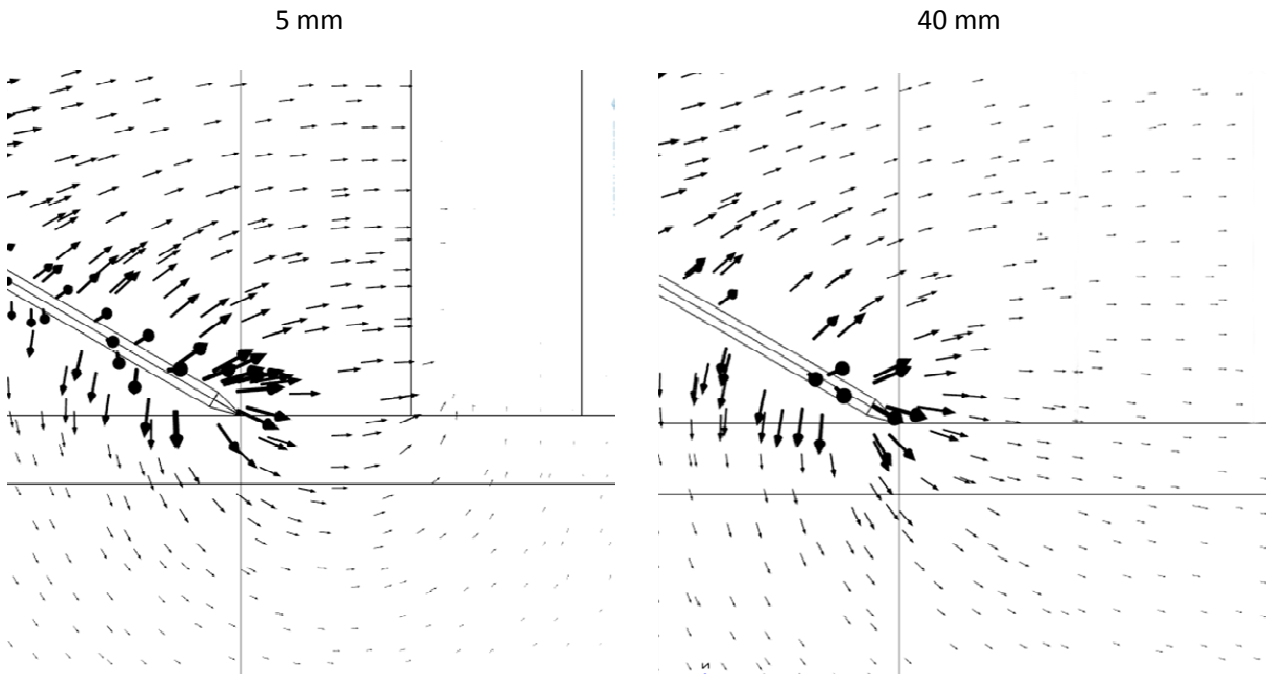


Fig. 5.45 Comparison of minimum and maximum gaps in FR3 (mid plane)

Differences between electric field vectors for 5 and 40 mm in mineral oil and FR3 (parallel plane from needle cross-section = 0.1mm)

Electric field vectors in mineral oil (cross-section)



Electric field vectors in FR3 (cross-section)

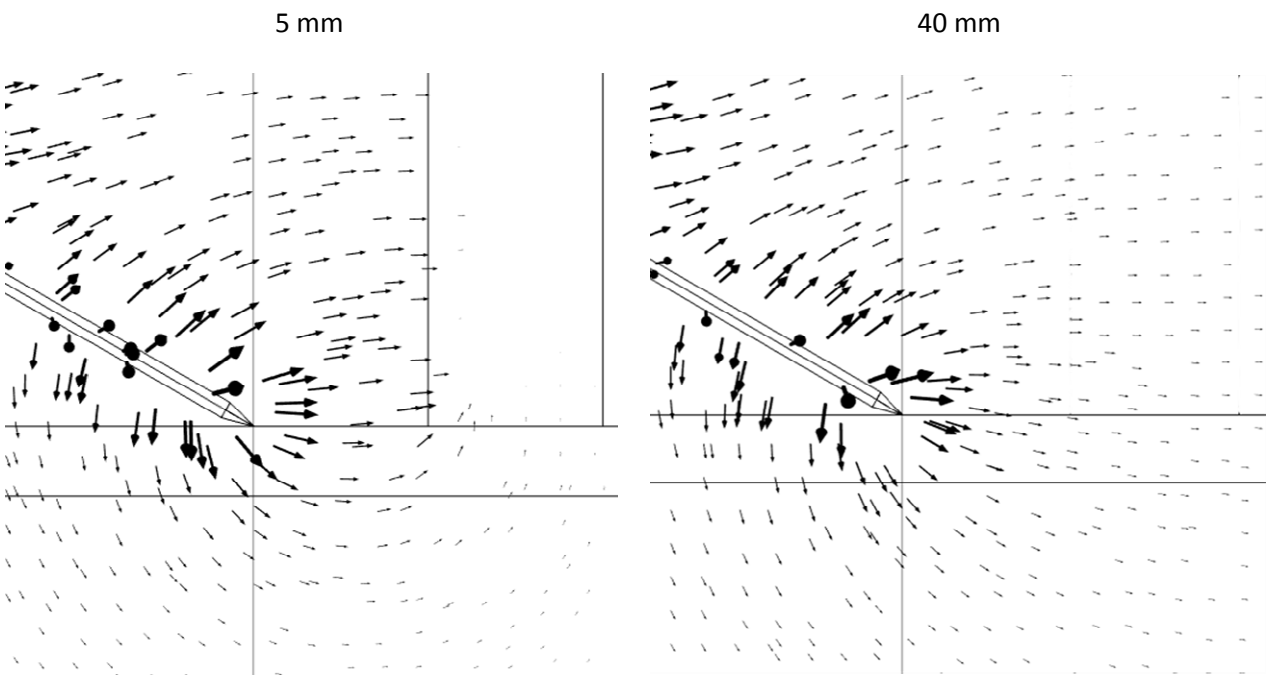


Fig. 5.46 Comparison of electric field vectors in minimum and maximum gaps in mineral oil and FR3 (cross-section)

Electric field maximum values for point to plane geometry, with or without PB barrier.

Table 6 Emax for point to plane geometry

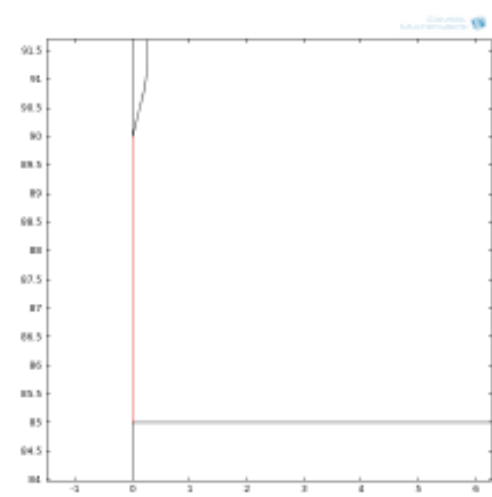
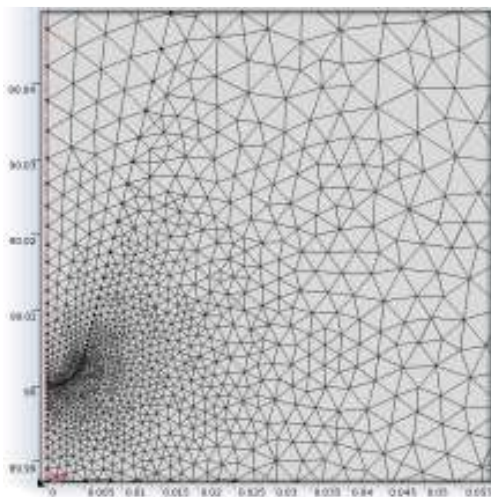
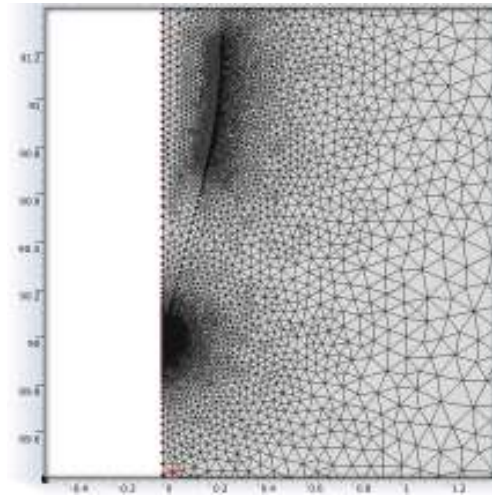
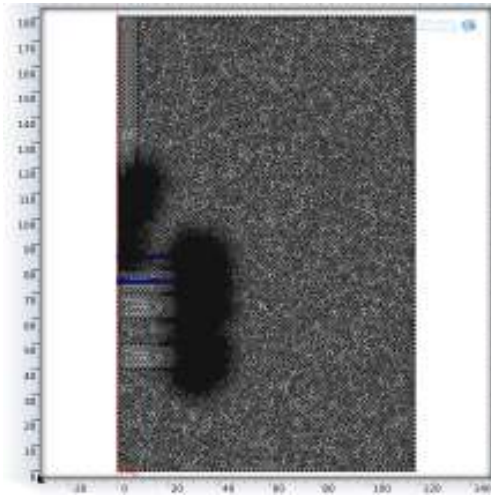
Gap (mm)	Surface discharges test cell											
	E with PB (V/mm)						E without PB (V/mm)					
	Mineral oil			FR3			Mineral oil			FR3		
	PB surf	Upper oil	Inside PB	PB surf	Upper oil	Inside PB	PB surf	Upper oil	Inside PB	PB surf	Upper oil	Inside PB
5	88.31	154.37	0.0119	63.34	109.17	0.0128	44.57	82.44	0.014	44.57	82.44	0.014
10	76.68	134.02	0.0123	54.96	94.73	0.0132	38.65	71.45	0.0144	38.65	71.45	0.144
20	64.78	113.22	0.0126	46.47	80.09	0.0134	32.71	60.45	0.0146	32.71	60.45	0.0146
40	52.00	90.89	0.0124	37.36	64.38	0.0131	26.34	48.67	0.0141	26.34	48.67	0.0141

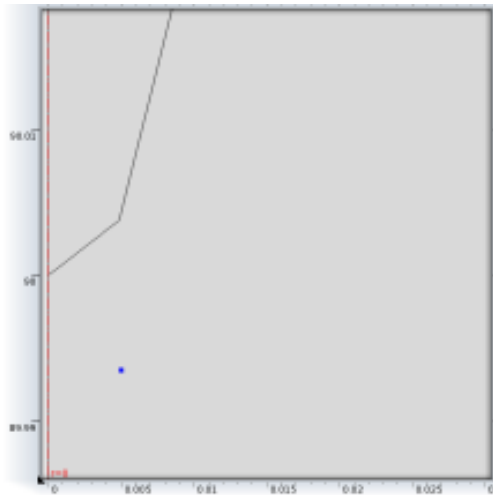
Geometry conditions

Needle tip radius = 5µm

Needle tip chamfer = 1 mm

Needle body diameter = 0.5mm





Analysis line length = 5 mm

Probe point coordinates (minimum distance from the tip allowed by resolution= $p(0.005,89.9935)$)

Fig. 5.47 Geometry and mesh conditions for point to plane in oil

Point to plane geometry with mineral oil and FR3 and gap=5mm

Mineral oil 5mm gap

FR3 5mm gap

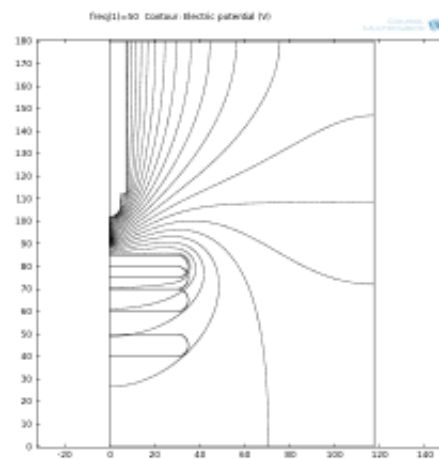
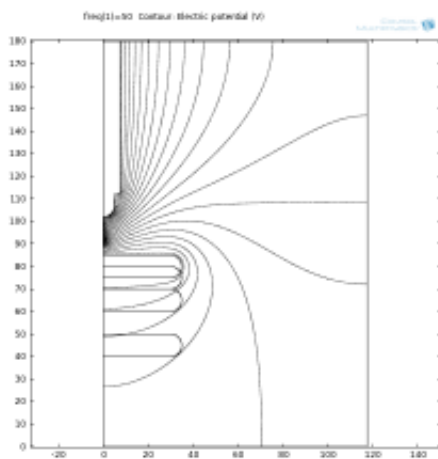


Fig. 5.48 Electric potential distribution in point to plane geometry at 5mm for mineral oil and FR3

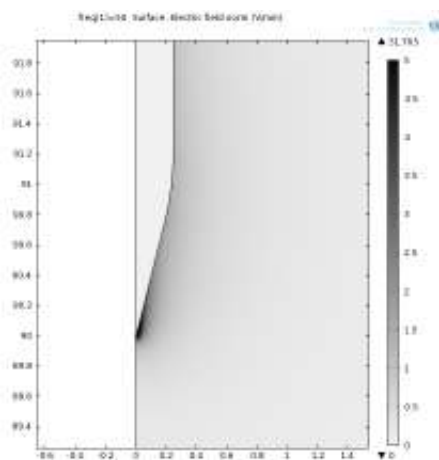
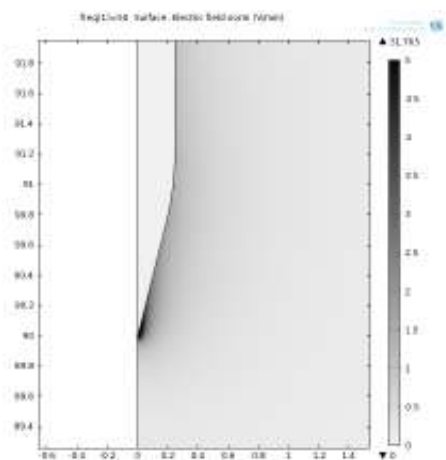


Fig. 5.49 Electric field distribution in point to plane geometry at 5mm for mineral oil and FR3

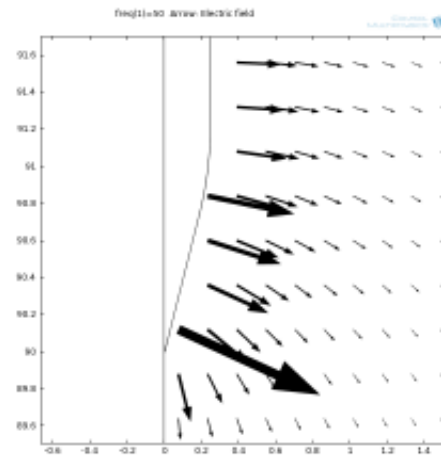
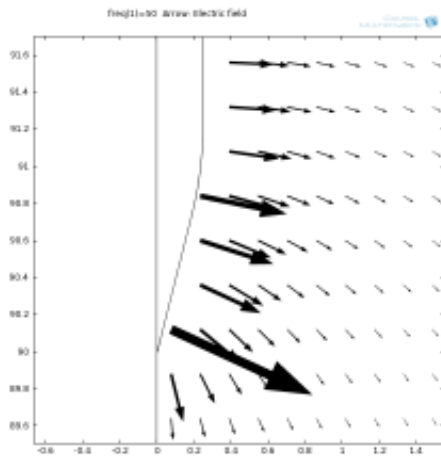


Fig. 5.50 Electric field vectors distribution in point to plane geometry at 5mm for mineral oil and FR3

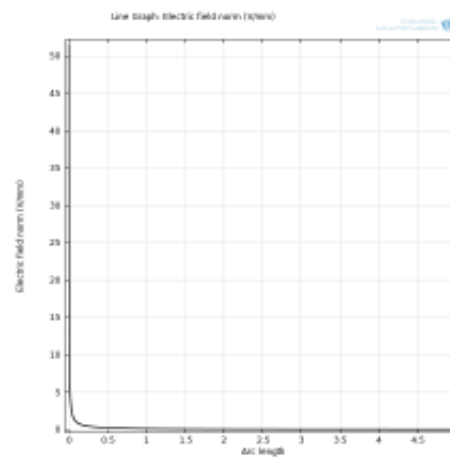
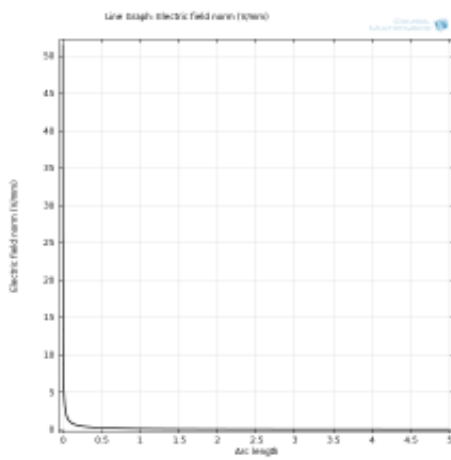


Fig. 5.51 Electric field as a function of gap= 5mm for mineral oil and FR3

freq	50	freq	50
Electric field norm, Domain Probe 1	51.9138	Electric field norm, Domain Probe 1	51.9138
Electric field, r component	3.0603	Electric field, r component	3.0603
Electric field, z component	-9.9917	Electric field, z component	-9.9917
Boundary Probe 1	25.9569	Boundary Probe 1	25.9569

Point to plane geometry with mineral oil and FR3 and gap=40mm

Mineral oil 40mm gap

FR3 40mm gap

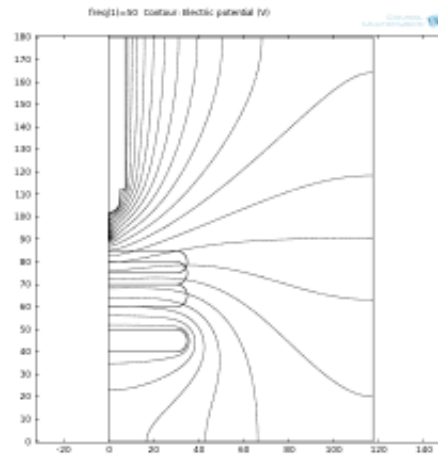
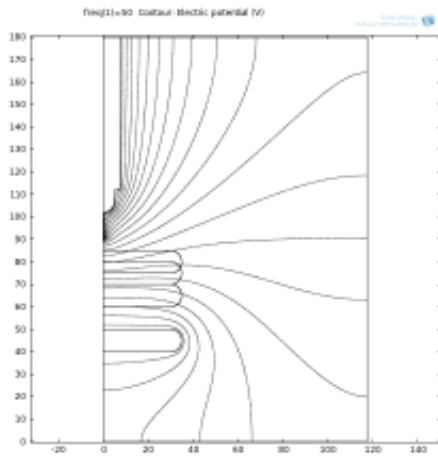


Fig. 5.52 Electric potential distribution in point to plane geometry at 40mm for mineral oil and FR3

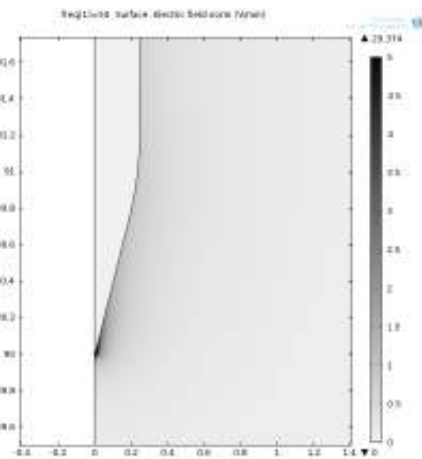
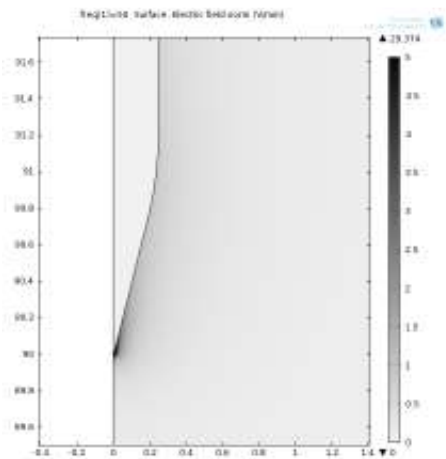


Fig. 5.53 Electric field distribution in point to plane geometry at 40mm for mineral oil and FR3

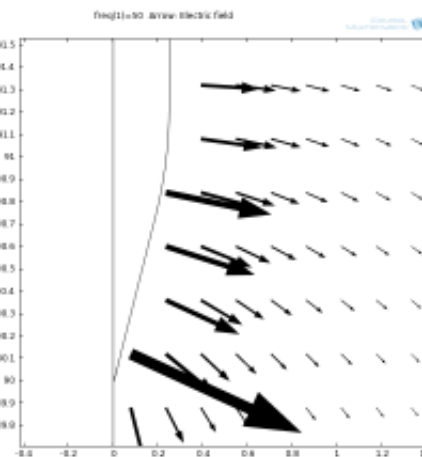
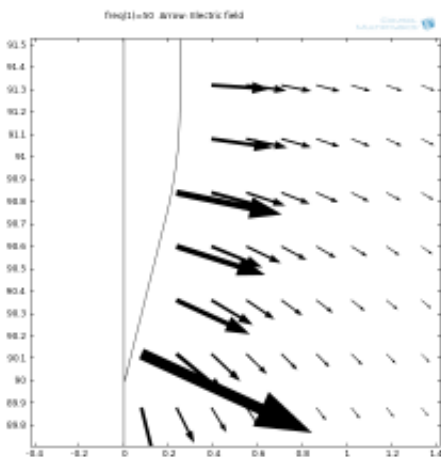


Fig. 5.54 Electric field vectors distribution in point to plane geometry at 40mm for mineral oil and FR3

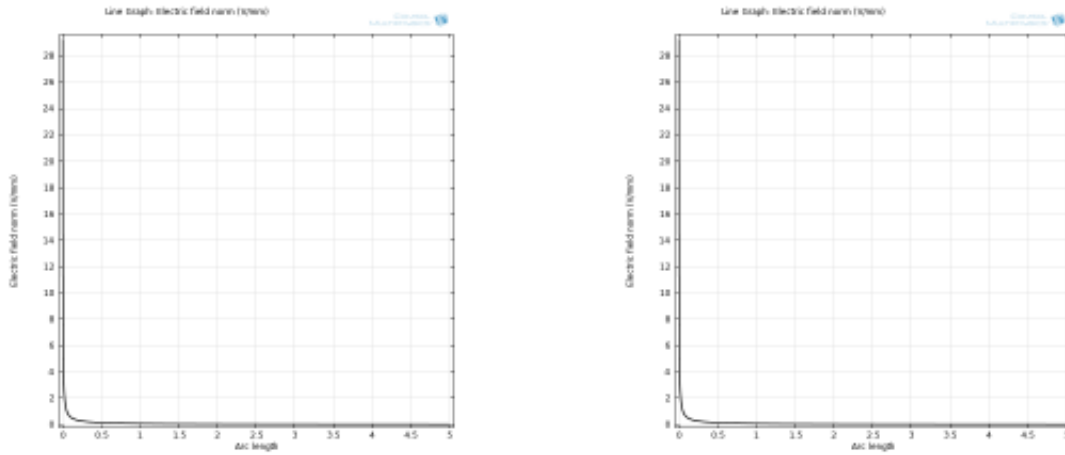


Fig. 5.55 Electric field as a function of gap= 40mm for mineral oil and FR3

freq		50	freq		50
Electric field norm, Domain Probe 1		29.4583	Electric field norm, Domain Probe 1		29.4583
Electric field, r component	r	1.7367	Electric field, r component	r	1.7367
Electric field, z component	z	-5.6692	Electric field, z component	z	-5.6692
Boundary Probe 1		14.7292	Boundary Probe 1		14.7292

Electric field maximum values for 1 V in point to plane configuration.

Table 7 Emax for point to plane configuration

Oil gap (mm)	E (V/mm)	
	Mineral oil	FR3
5	51.9138	51.9138
10	44.4931	44.4931
20	36.9372	36.9372
40	29.4583	29.4583

6 Results of PD testing under HVDC and square waveform and under particular conditions

This Chapter reports the results obtained for different operating modes that take place in HVDC and traction transformers. These results were obtained from different test setups that simulate some conditions that takes place inside HVDC transformer insulation system. The studied conditions were:

1. Effect of frequency and waveform in oil PDIV behavior
2. Effect of composite HVDC stresses in pressboard main barriers considering over-voltage stresses
3. Effect of cunmutation transients in inter-turn paper insulation
4. Impact of oil flow speed and the temperature of the flowing oil in PD behavior

The execution of the experimental tests had the aim to clarify how those conditions influence transformer insulating system behavior as is explained below:

Traction and HDCV light and HVDC plus transformers experience voltage square waveforms during their operation. For this reason it is important to analyse the effect of this kind of voltages at different frequencies, making a comparison with the results obtained from conventional sinusoidal stresses. Such comparison should help to understand if those stresses can degrade in an accelerated way the dielectric fluids or not. Despite the fact that from the point of view of HVDC, the use of esters is not feasible, the understanding of esters behavior in squared waveform conditions is important, because those fluids are used commonly in traction transformers.

From the point of view of HVDC testing, separated AC and DC tests are carried out in transformers at the factory and in the field. Those test conditions are unrealistic, because the ACDC combined effect can impose additional stresses in barriers. In this Chapter the results of the combined effects are reported and described for ulterior analysis.

Another important results for PDIV behavior under HVDC conditions are those reported in this Chapter for notched voltage waveforms. These stresses are present in interturn insulation and in fase to ground insulation of bushings due to conmutation at the firing and overlap angles. Despite the fact that those stresses are mentioned like a possible cause of transformer failure, no information of their impact on PD physics is available in literature, so, the results reported here are also an important contribution of this research work.

It is claim that the oil flow speed can affect the PDIV in two different ways: the oil flow sweeps away ionized oil increasing the PDIV contributing to a PDIV increase or the PDIV can decrease due to tribological effect of the flow. Experimental work was carried out and the results obtained in a creeping geometry at different oil speeds for two different temperatures are reported in order to improve the understanding of this parameter, mainly from the point of view of PDIV increment.

6.1 Partial discharges (point to plane geometry, influence of frequency and waveform)

Fig. 6.1 shows the comparison of the behavior of PDIV for mineral oil and FR3 at 0.1, 50, 150 and 1000 Hz in sinusoidal and square voltage waveforms. The experiments were randomized from the point of view of frequency in order to avoid trends. This is, the frequency was changed to different test values after complete a PDIV detection, for example, after PDIV detection at 50 Hz, the frequency was set to 1 kHz for the next PDIV detection. Once that the PDIV at 1 kHz was determined, the frequency was changed to 150 Hz repeating the operation for PDIV assessment. The procedure was repeated for 0.1 Hz and then for all the other frequencies until 10 PDIV values were recorded for each frequency.

Each point in the plot represents the Weibull scale parameter obtained from 10 measurements. Once that positive or negative trends were observed during the measurements, the insulating fluids were changed for a new and dry sample and the needle was replaced.

The tests were first performed for mineral oil. When it was necessary to change the type of fluid, this is, to evaluate FR3 behavior, a needle previously characterized in mineral oil in all the test frequencies was used as a reference for the first set of measurements.

The front of the applied square waveforms is shown in Fig. 6.2. It's important to notice that for all the tested frequencies, the rise time was around 0.1 ms for square waves.

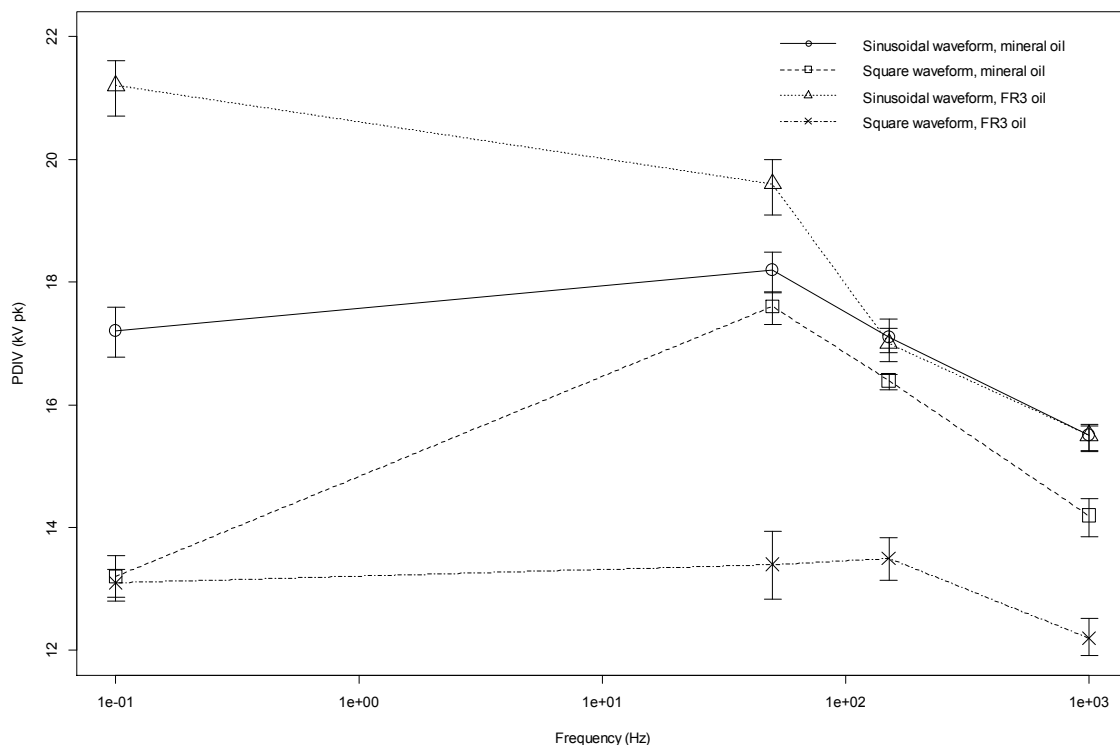


Fig. 6.1 PDIV Trend comparison as a function of frequency for sinusoidal and square waveforms for mineral oil and FR3 in a point to plane electrode configuration

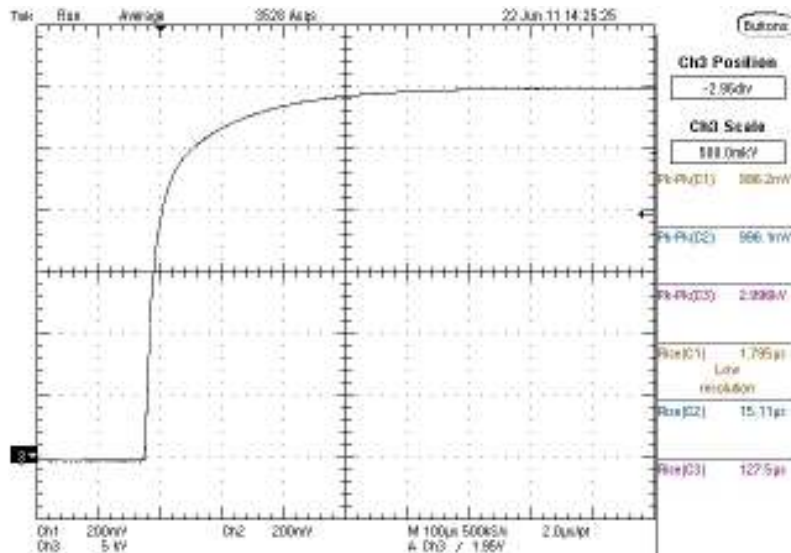


Fig. 6.2 Rise time for a square waveform of 1 kHz.

6.2 Partial discharges under HVDC stresses

6.2.1 Behavior of PDIV in pressboard as a function of voltage distribution and space charge

Two different configurations of pressboard barriers can be found in power transformers: barriers in contact with electrodes and barriers that separate oil volume. To replicate those conditions, two different geometries were used for HVDC testing: a) HV electrode-oil-pressboard-oil-LV electrode and b) HV electrode-oil-pressboard-LV electrode (Fig. 6.3). These two configurations are named PB-Oil-pb and PB-Oil respectively. In both cases, layers of 1mm for each material were evaluated under AC, DC and AC+DC stresses between Rogowski electrodes. In the particular case of AC voltage, only an impregnated pressboard sheet of 1mm thickness was stressed without oil gap.

As described first, for PDIV detection, voltage steps of 250 V were used to raise the potential till PDIV. The difference between the test procedures for AC, DC and AC+DC is the fact that for all the configurations stressed with DC, the time steps last 20 minutes. This larger time is needed in order to allow the system to approach steady state. For AC, the time steps were 3 minutes.

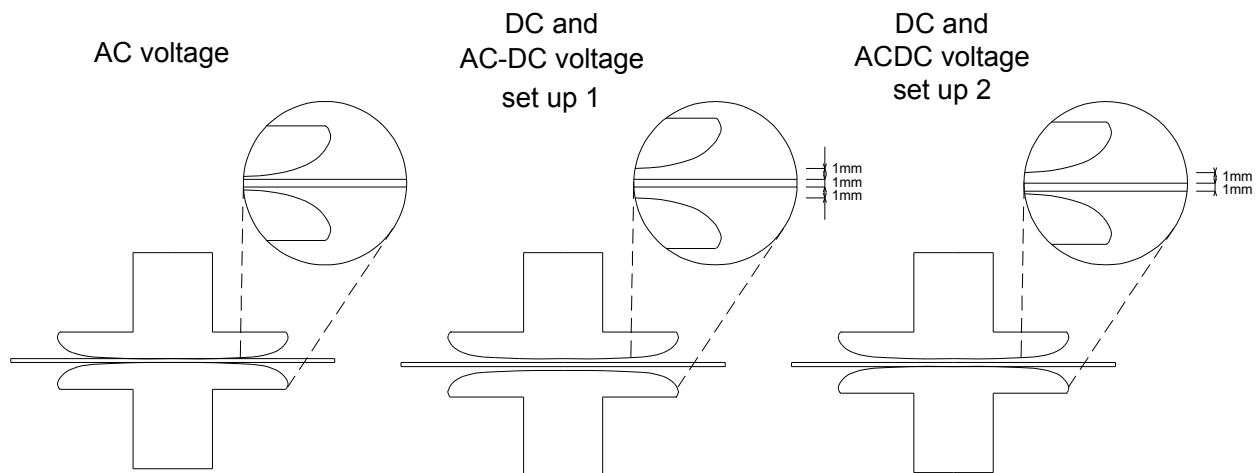


Fig. 6.3 Electrodes geometry for PDIV measurement during HVDC testing

For AC+DC combined stress, the AC peak value component was set as 40% of the DC amplitude as shown in Fig. 6.4, trying to replicate the voltages observed in converter transformers.

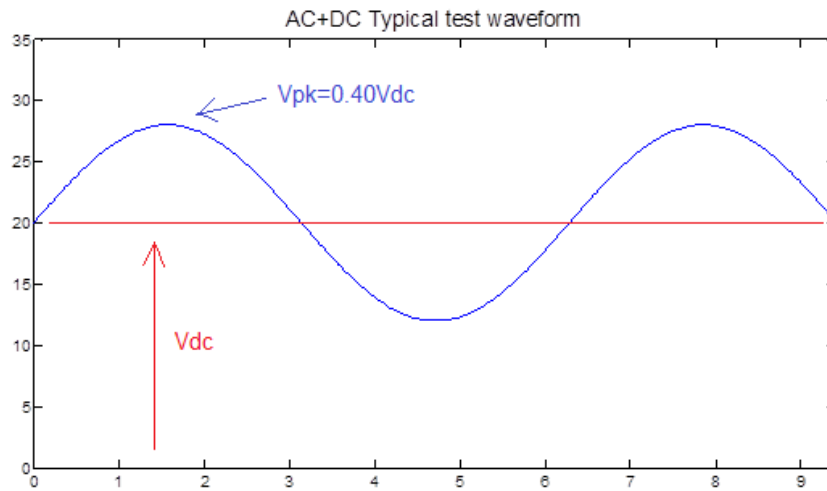


Fig. 6.4 HVDC waveforms used during this work

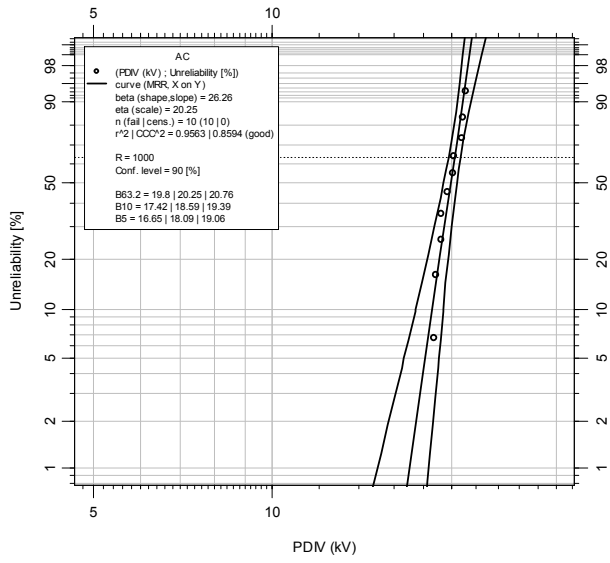
The electric parameters of the materials used for these tests are shown in Table 8

Table 8 Electric parameters used to calculate electric field distribution

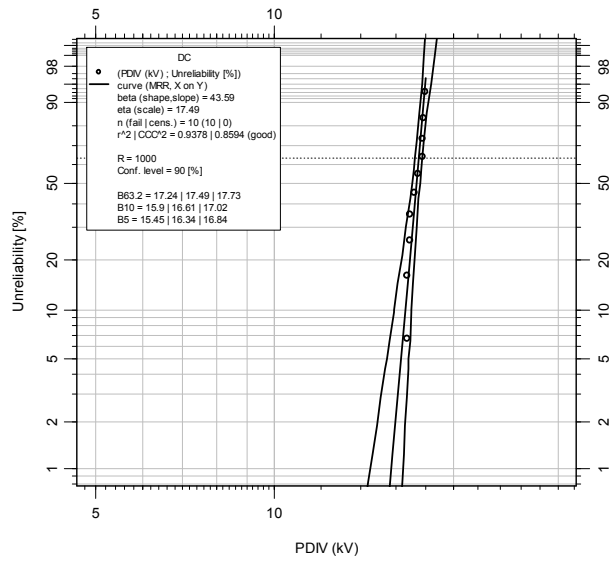
Material	Relative permittivity	Electrical conductivity (S/m)
Mineral oil	2.2	3.75E-15
Impregnated pressboard	4.4	12.37E-15

The results obtained for both geometries are shown. It is important to remark that an acoustic system for PD detection was employed in order to discriminate discharges occurring in the oil during the transient induced by step changes of the voltage. This system can detect PD activity in oil with high sensitivity whereas internal and surface PDs are better picked up by electrical methods. The equivalent sensitivity in the circuit conditions for the acoustic system was <2 pC.

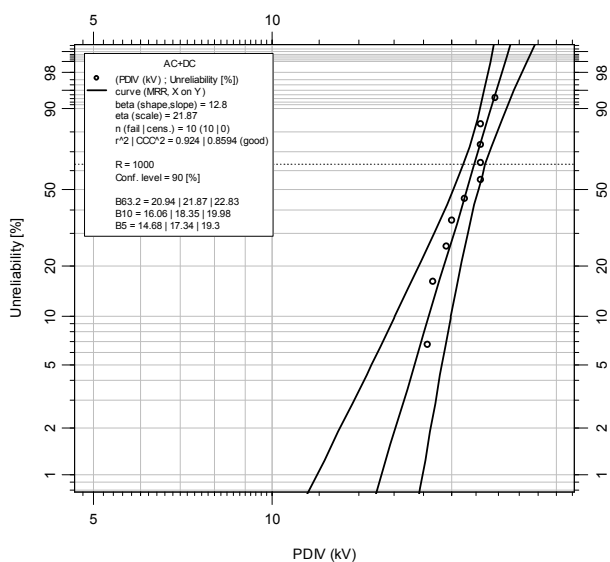
PDIVs for oil-PB-oil geometry are shown in Fig. 6.5. In the other hand, Fig. 6.6 displays the PDIVs for oil-PB configuration. It could be noticed from these plots that PDIV is lower for Oil-PB geometry in comparison to Oil-PB-oil geometry as intuitively was supposed due to the fact that this geometry has the smaller total gap (2mm).



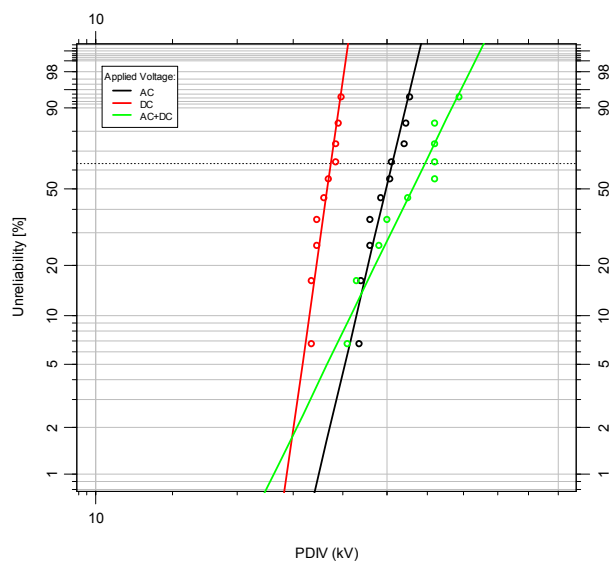
AC



DC

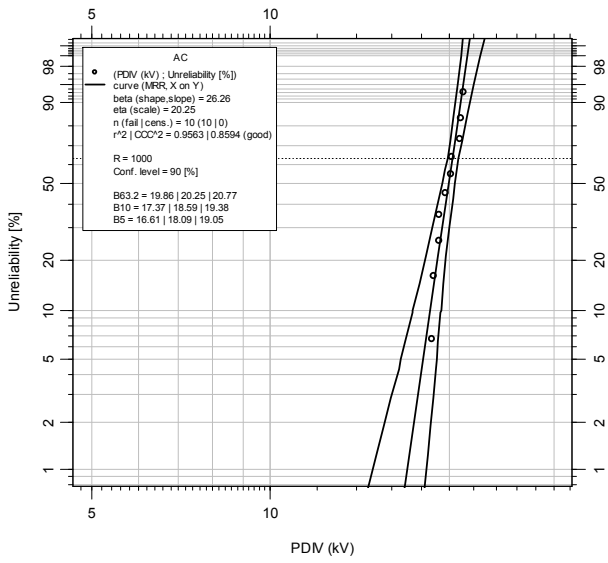


AC+DC

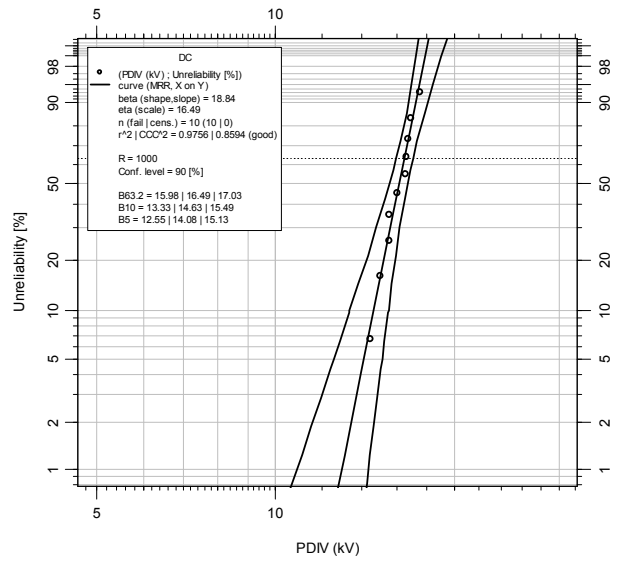


Combined plots

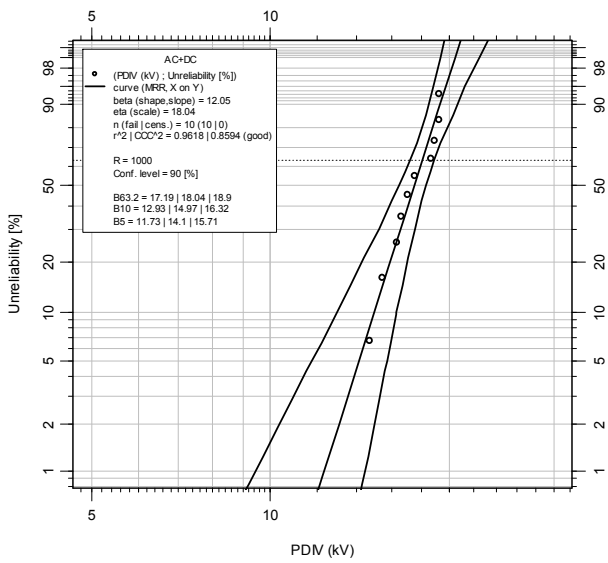
Fig. 6.5 PDIV Weibull plots for oil-PB-oil geometry



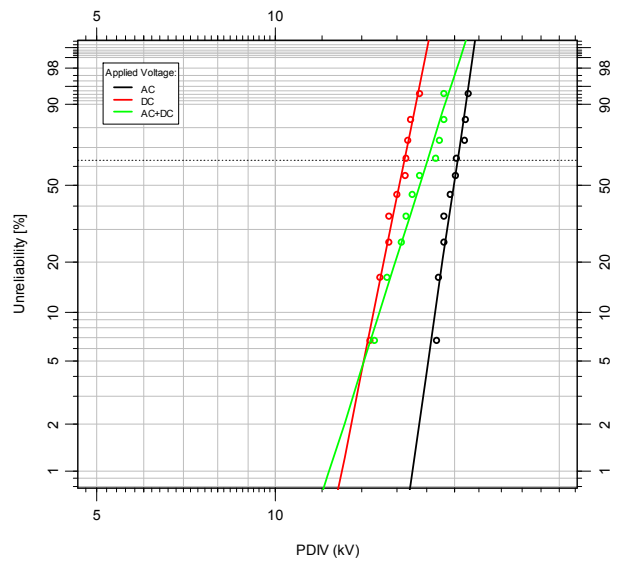
AC



DC



AC+DC



Combined plots

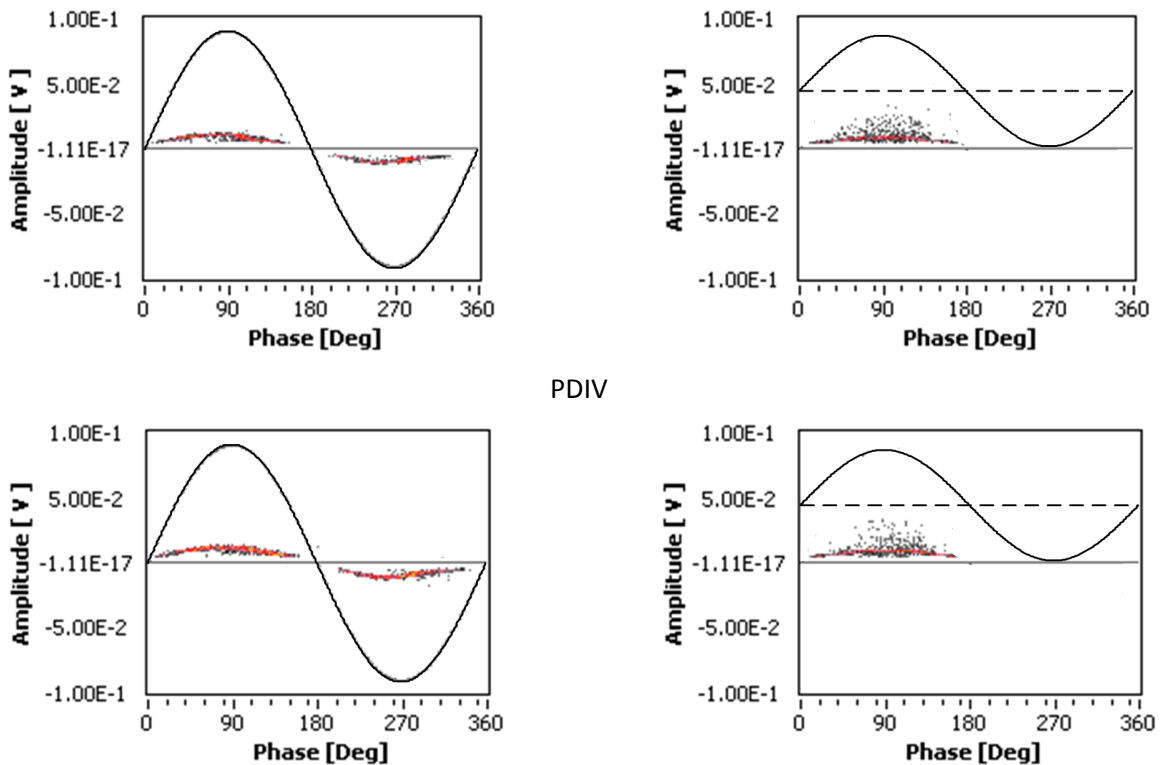
Fig. 6.6 PDI Weibull plots for oil-PB geometry

6.2.2 Behavior of PD activity in pressboard as a function of overvoltage

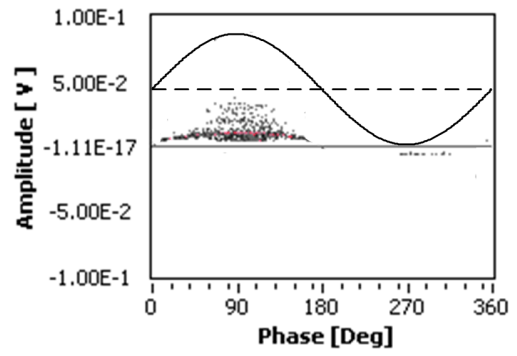
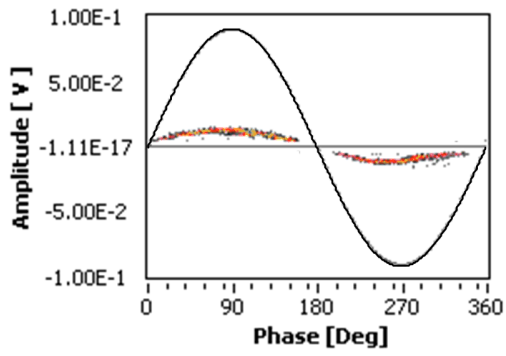
Besides the PDIV behavior, it is also useful to know the behavior of pressboard-oil interfaces as a function of overvoltages. Overvoltage is defined for this particular case, as an increment of the applied voltage over the PDIV value. Also, in this case, it is better to consider PDIV as the needed voltage to obtain a given PD pattern. Fig. 6.7 reports the PD patterns under AC and AC+DC voltages at different voltage amplitudes. Experimental results show that the PD patterns under AC+DC voltages are different from those under AC voltage. In fact, the electrical field is capacitive graded under AC voltages, therefore the electric field in the oil, the weakest part of the system for AC, is stronger than that in the pressboard. Therefore, PD mostly occur in the oil. The PD patterns between the positive and negative power frequency phases of the oil-gap discharge are symmetrical in this case.

With DC voltage, the field in pressboard is stronger, which could point to some PD in the pressboard. This makes larger PD distribute in the positive frequency cycle. In addition, some PD also occur in the oil, which cross the oil gap and form a space charge on the pressboard. This charge can discharge back when the voltage is equal to zero influencing the PD pattern behavior.

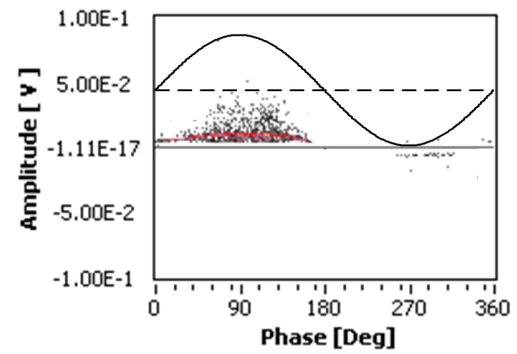
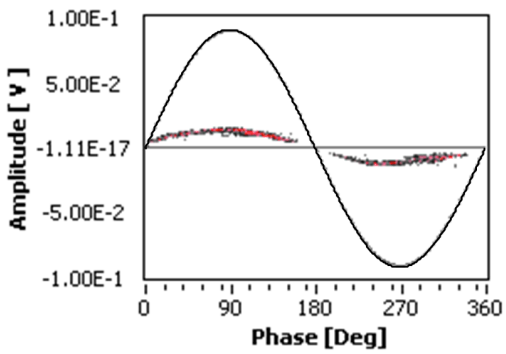
Fig. 6.8 shows PD amplitude, Q_{max} , repetition rate, N_w , and their product, $N_w \cdot Q_{max}$, under different test voltages. The results show that Q_{max} and $N_w \cdot Q_{max}$ under AC+DC voltage are both larger than those under AC voltage, while repetition rates are lower. The fitting curves and equations are labeled in the corresponding figures. The test statistics for the hypothesis H_0 that the correlation coefficient is equal to 0 are: 28.09, 10.03, 16.41, 15.94, 18.28, and 12.23, respectively. They are all larger than the critical value of t -distribution: 2.13 ($\alpha=0.05, n=4$), which shows that the fittings are all meaningful.



1.1 PDIV



1.2 PDIV

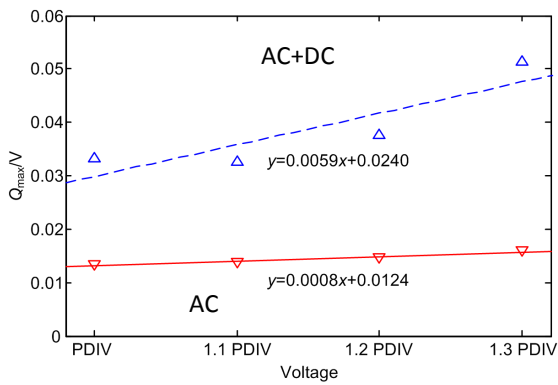


1.3 PDIV

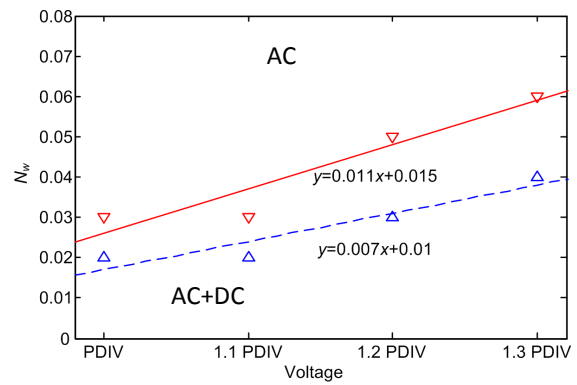
AC

AC+DC

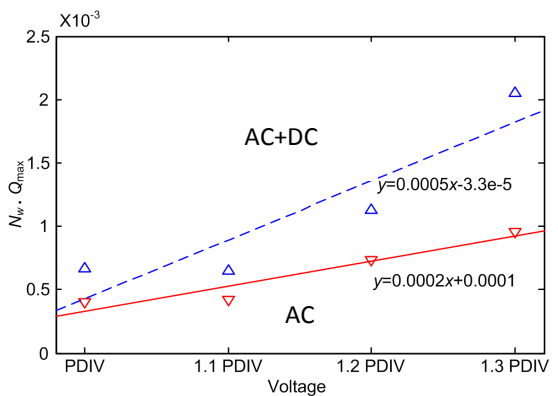
Fig. 6.7 PD patterns with AC and DC voltage



Behavior of Q_{max} as a function of voltage amplitude



Behavior of N_w as a function of voltage amplitude



Behavior of $N_w \cdot Q_{max}$ as a function of voltage amplitude

Fig. 6.8 PD amplitude, Q_{max} , repetition rate, N_w , and their product, $N_w \cdot Q_{max}$, under different test voltages

6.2.3 Behavior of PD activity in insulating paper for notched voltage waveforms

During converter operation, valve commutations cause notches in the sinusoidal waveform applied to HV bushing and turn/turn insulation in proximity of converter-side terminals. The material subjected to electrical stresses in this case is oil impregnated Kraft paper. Line-to-ground voltage waveforms at transformer terminals were derived from the simplified analysis reported in [58] (where the DC smoothing inductance is assumed to be infinite). The firing and overlap angles (α and μ , respectively) are considered here to be independent parameters (in a real converter this is not the case) to account for all possible situations. Realistic ranges for the values of α and μ were derived from [38], where it is reported that the boundaries of the firing and overlap angles are from 0 to about 37 degrees and 0 to 25 degrees, respectively. Fig. 6.9 shows an example the different voltages that are reproduced for testing. In this Figure besides the AC phase to ground voltages (including the notched one) it is possible to see in yellow the DC output.

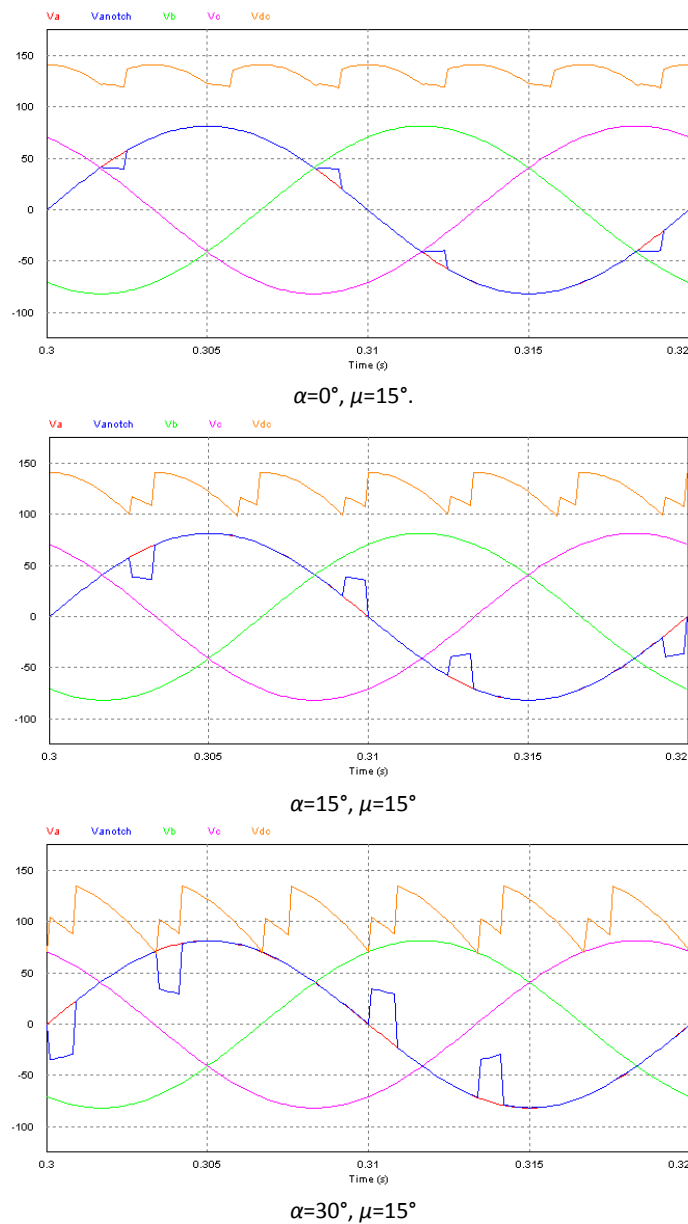


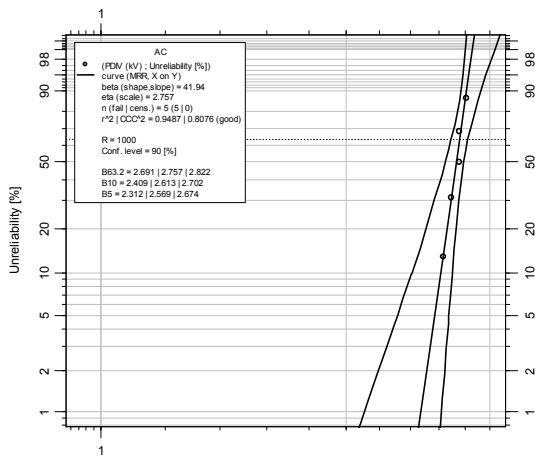
Fig. 6.9 Examples of phase to ground voltages and DC outputs in a transformer DC converter as a function of α and μ

For AC notched voltage waveforms, PDIV values at different test conditions are displayed in Table 9. It is important to notice that the PDIV values were normalized using Eq. 28 ($PDIV^* = PDIV(\alpha, \mu) / PDIV(AC)$)

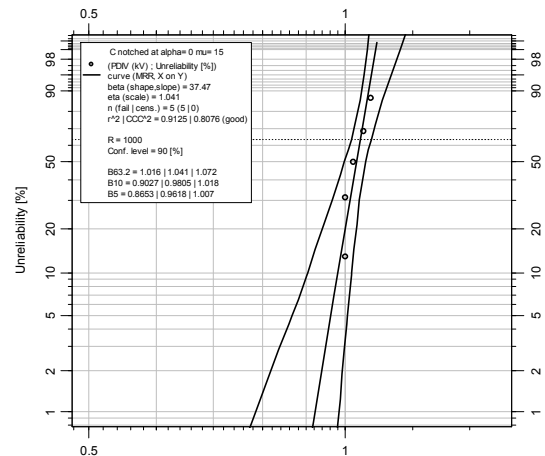
Table 9 PD Data and Testing Conditions for different firing and overlap angles

Voltage type	PDIV	1	2	3	4	5
AC sinusoid $\alpha=0^\circ$, $\mu=15^\circ$	PDIV(AC)	2.75	2.69	2.81	2.63	2.75
	PDIV(α,μ)/ PDIV(AC)	2.75/ 2.75	2.69/ 2.63	2.88/ 2.75	2.69/ 2.69	2.81/ 2.63
	PDIV*	1.00	1.02	1.05	1.00	1.07
$\alpha=15^\circ$, $\mu=15^\circ$	PDIV(α,μ)/ PDIV(AC)	3.06/ 2.88	3.00/ 2.88	2.88/ 2.56	3.06/ 2.94	3.13/ 2.94
	PDIV*	1.06	1.04	1.13	1.04	1.06
	PDIV(α,μ)/ PDIV(AC)	2.75/ 2.50	2.81/ 2.75	3.44/ 3.00	2.81/ 2.56	3.31/ 2.94
$\alpha=30^\circ$, $\mu=15^\circ$	PDIV(α,μ)/ PDIV(AC)	2.75/ 2.50	2.81/ 2.75	3.44/ 3.00	2.81/ 2.56	3.31/ 2.94
	PDIV*	1.10	1.02	1.15	1.10	1.13
	PDIV(α,μ)/ PDIV(AC)	2.88/ 2.75	2.94/ 2.94	2.94/ 2.88	3.31/ 3.19	3.31/ 3.31
$\alpha=15^\circ$, $\mu=5^\circ$	PDIV(α,μ)/ PDIV(AC)	2.88/ 2.75	2.94/ 2.94	2.94/ 2.88	3.31/ 3.19	3.31/ 3.31
	PDIV*	1.05	1.00	1.02	1.04	1.00
	PDIV(α,μ)/ PDIV(AC)	3.31/ 2.94	3.25/ 3.00	3.19/ 2.88	3.38/ 3.06	3.31/ 2.94
$\alpha=15^\circ$, $\mu=25^\circ$	PDIV(α,μ)/ PDIV(AC)	3.31/ 2.94	3.25/ 3.00	3.19/ 2.88	3.38/ 3.06	3.31/ 2.94
	PDIV*	1.13	1.08	1.11	1.10	1.13

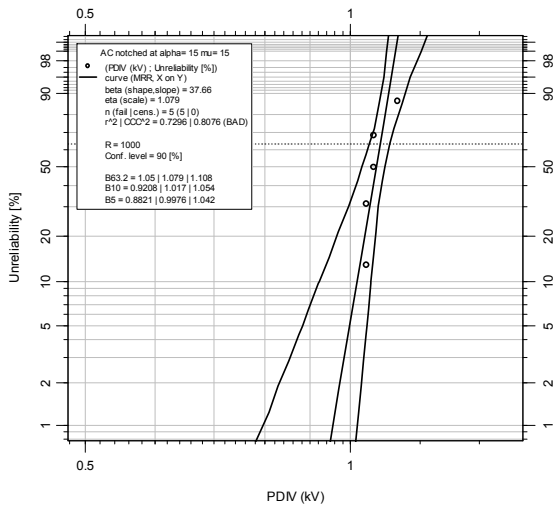
The related Weibull plots for these results are shown in Fig. 6.10. In addition to PDIV values, PD pulses were recorded for establishing statistical PD patterns under different waveform and peak voltages, i.e. 5 kV, 6 kV and 7 kV. Fig. 6.11 reports the PD patterns under different waveforms when the peak voltage is 7 kV.



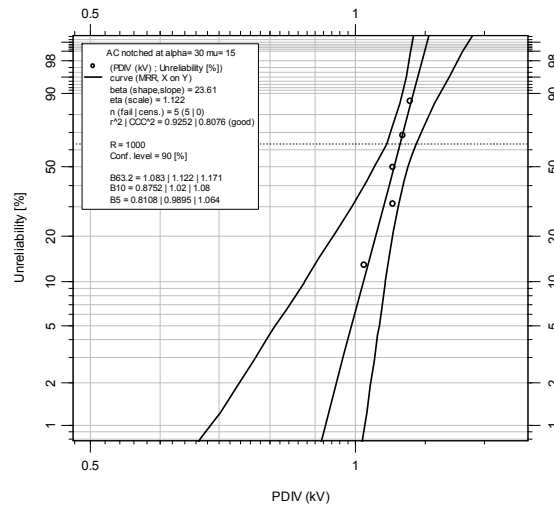
a)



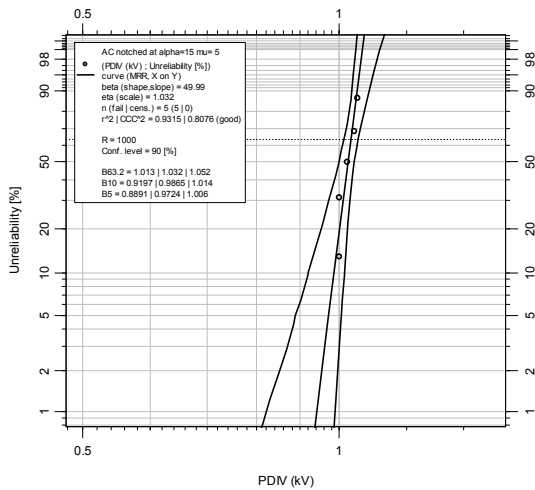
b)



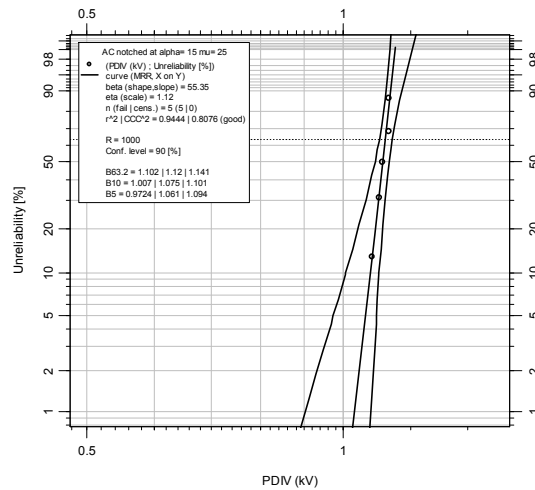
c)



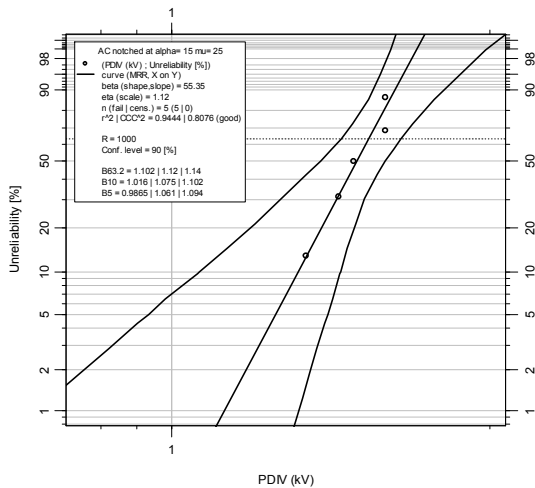
d)



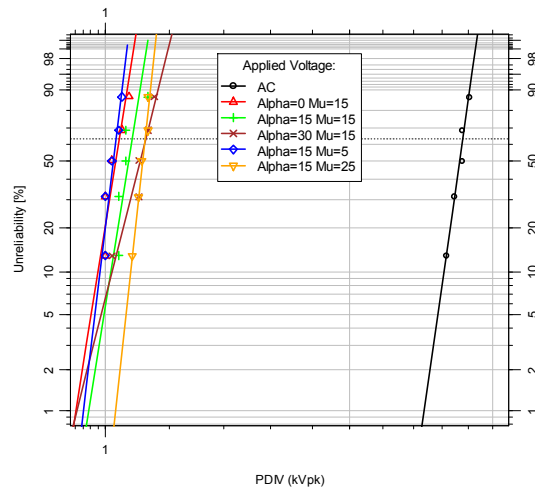
e)



f)

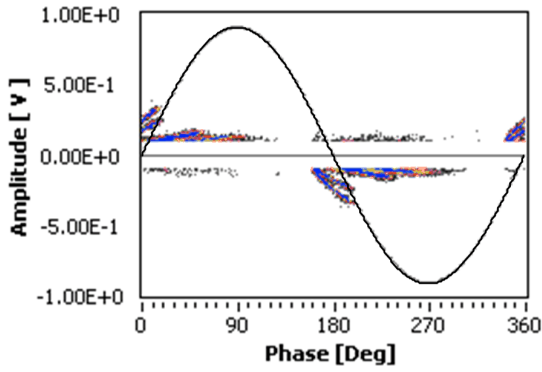


g)

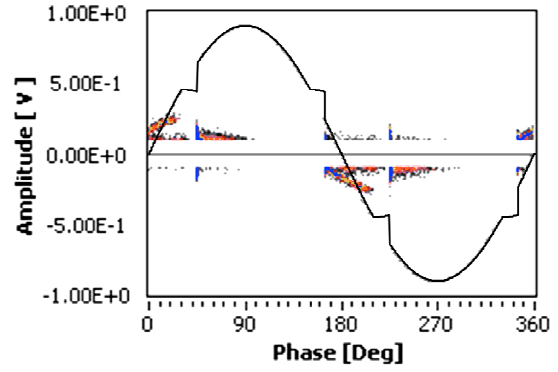


h)

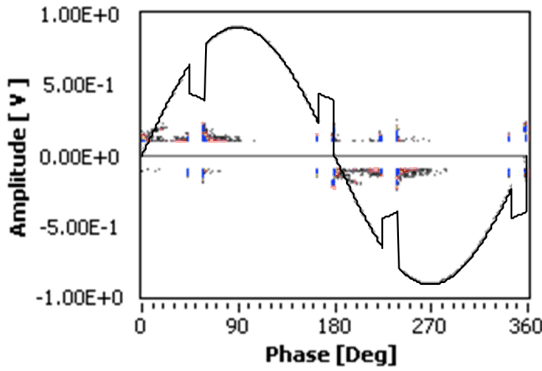
Fig. 6.10 Weibull inception probabilities under voltage at different firing angles when $\mu=15^\circ$ (b, c, d) and under voltage at different overlap angles when $\alpha=15^\circ$ (e, f, g). The comparison between these plots is shown in h).



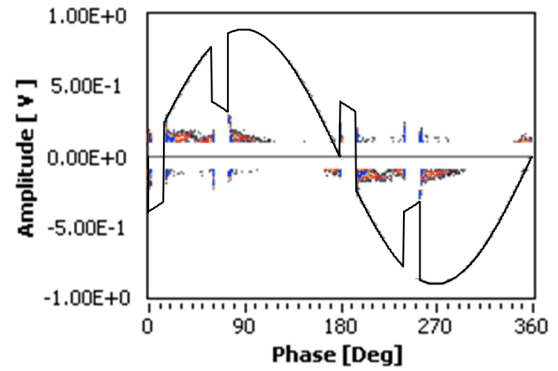
PD pattern under AC sinusoidal voltage with amplitude of 7 kV



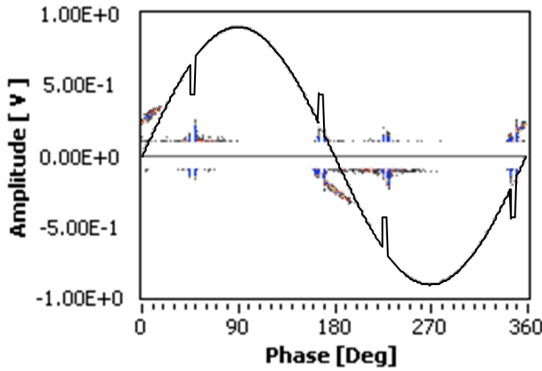
PD patterns under AC notched voltage at $\alpha=0^\circ$, $\mu=15^\circ$ with amplitude of 7 kV



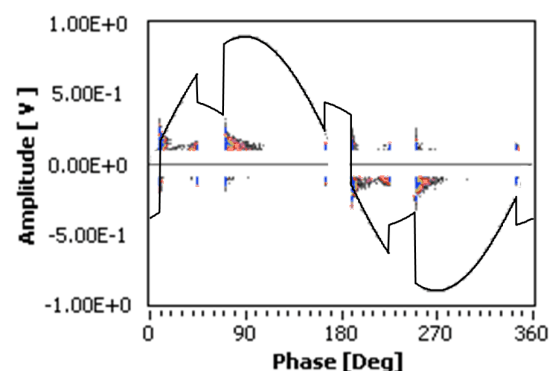
PD patterns under AC notched voltage at $\alpha=15^\circ$, $\mu=15^\circ$ with amplitude of 7 kV



PD patterns under AC notched voltage at $\alpha=30^\circ$, $\mu=15^\circ$ with amplitude of 7 kV



PD patterns under AC notched voltage at $\alpha=15^\circ$, $\mu=5^\circ$ with amplitude of 7 kV



PD patterns under AC notched voltage at $\alpha=15^\circ$, $\mu=25^\circ$ with amplitude of 7 kV

Fig. 6.11 PD patterns at different voltage conditions

6.3 Partial discharges dependence on oil flow speed

In order to assess the influence of the oil speed over partial discharge inception voltage (PDIV) and PD patterns of paper-oil systems, several measurements were carried out using a point to plane geometry, similar to the one reported in literature[59]. The gap (30 mm long) of this geometry is bridged by means of a pressboard layer, which provides the surface discharge path. The high voltage point electrode diameter is 1 mm, with a tip radius of 400 μm . The low voltage electrode is covered with oil impregnated paper in order to prevent direct flashover and serves also as a mechanical fastener. A scheme of the electrodes and test sample geometry is shown in detail in Fig. 6.12. In this figure it is also sketched the nozzle used to

direct the oil flow towards the discharge area. The nozzle is located at a distance of 200 mm from the tip, and the oil flows from the needle tip to the ground electrode.

The pressboard samples are square layers of 100 mm length and 1 mm thickness and were dried in an oven during 48 h at 105°C. After the drying, they were impregnated during 24 h under vacuum.

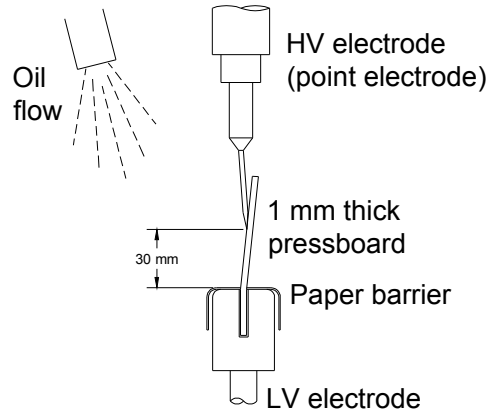


Fig. 6.12 Electrodes geometry for PDIV measurement as a function of oil speed

To analyze the effect of oil speed over PDIV, the frequency of the power inverter was adjusted at 25, 35, 45 and 50 Hz. In order to obtain oil speed values, the oil flow, Q , was calculated by measuring the oil volume displaced during a fixed amount of time. Then, using the pipe section, S , of the circulation system, and the continuity equation.

$$v = Q / S \quad \text{Eq. 32}$$

an estimate of the oil speed (in the pipes) was achieved. Using this approach, hydraulic losses calculation at accessories and filter is not necessary. However, due to the fact that hydraulic losses are generally a nonlinear function of speed, the complete procedure was repeated for each frequency value selected for the power supply of the pump. The procedure was repeated for 50 and 70°C without observing significant changes, due to the fact that the set of conditions used match laminar flow regime. A summary of the obtained Q and v values at each frequency is listed in Table 10.

Table 10 Q and v values obtained during the tests

Temperature °C	50		70	
Pump frequency (Hz)	Q (m ³ /s)	V (mm/s)	Q (m ³ /s)	V (mm/s)
Off	0	0	0	0
25	$1.9 \cdot 10^{-5}$	150	$2.1 \cdot 10^{-5}$	167
35	$15.2 \cdot 10^{-5}$	1200	$17.4 \cdot 10^{-5}$	1370
45	$45.6 \cdot 10^{-5}$	3590	$48.5 \cdot 10^{-5}$	3820
50	$51.6 \cdot 10^{-5}$	4070	$55.6 \cdot 10^{-5}$	4390

In practice, transformer oil speed is generally below 500-600 mm/s [60].

Table 10 shows that the experiments were carried out with oil speeds at the nozzle output much higher than those observed in a transformer. Indeed, the nozzle is located 200 mm far from the gap and the oil speed at the gap is supposed to be lower than that at the nozzle due to oil viscosity and oil counter flow, so that the results reported here should be considered in qualitative terms only.

Ten measurements were carried out for each temperature and oil speed condition in order to assess their effect on PD parameters. Each time carbonized spots could be detected visually in proximity of the needle top, the sample was replaced using another one, cut out from the same pressboard sheet and processed in an identical way. This procedure is very important to achieve stationary test conditions, due to the fact that carbonized spots modify the electric field at the needle tip, thus affecting PDIV measurements and PD patterns.

Weibull analysis was applied to each data set with the goal to verify trends. The Weibull parameters for the complete set of experiments are displayed in Table 11. Fig. 6.13 shows, as an example, the Weibull distributions obtained with the oil temperature equal to 50°C.

Reported data in Table 11 for the scale parameter α are summarized in Fig. 6.14, where the α values are reported along with their 90% confidence intervals (evaluated through Montecarlo simulation). The figure emphasizes that PDIV tends to increase with oil speed, being this effect more marked with higher temperatures. It is worthwhile also to notice that the shape parameter β is in general very large, and tends to increase with oil speed, showing minimum values (i.e., larger statistical dispersion of the measured data) for still oil. Eventually, Fig. 6.15 and Fig. 6.16 show PD patterns and repetition rates measured for a temperature of 50 °C, varying the pump speed.

Table 11 Weibull parameters obtained during the tests

Temperature (°C)	50			70		
Pump Frequency Hz	α (kV)	β	Rep.Rate 1/cycle	α (kV)	β	Rep.Rate 1/cycle
Off	25.8	31.2	0.20	26.0	32.5	0.01
25	26.2	63.1	0.01	27.5	61.8	0.01
35	26.6	52.2	0.25	28.7	48.2	0.01
45	28.3	53.8	0.11	29.0	121.0	0.04
50	28.8	36.3	0.02	30.0	67.0	0.01

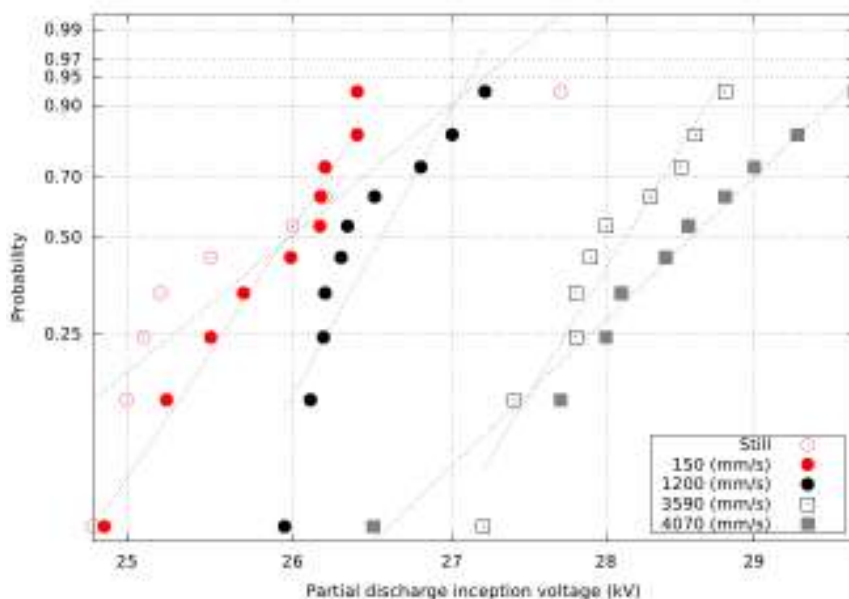


Fig. 6.13 Weibull alpha for PDIV and a function of oil speed

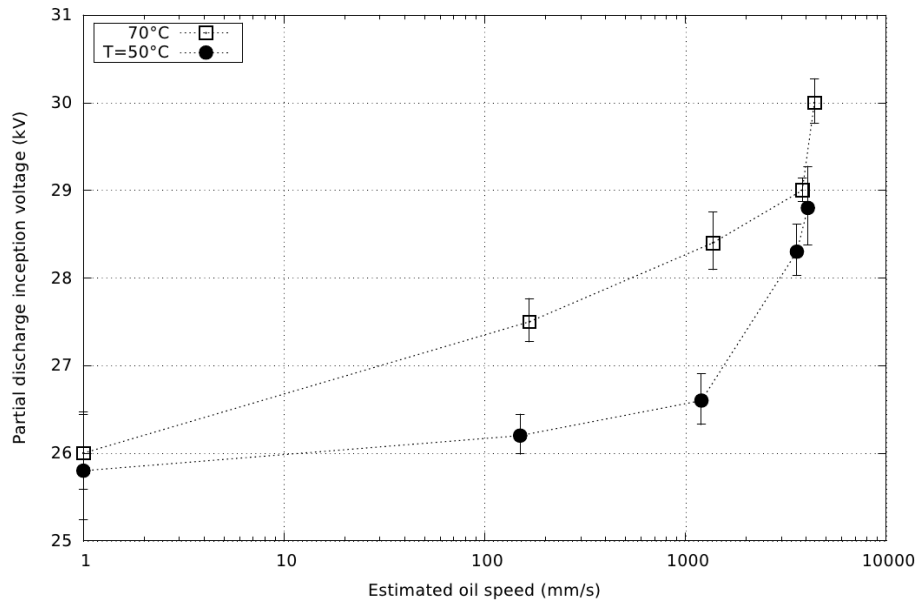
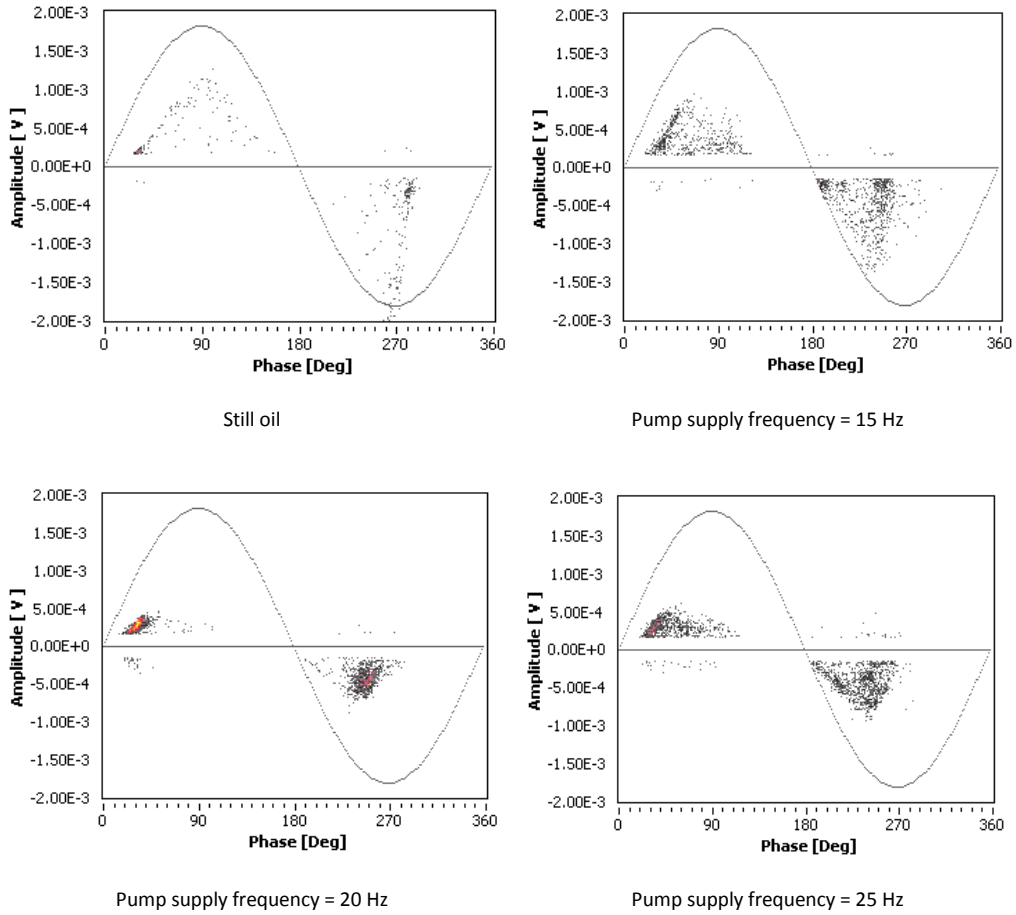


Fig. 6.14 PDIV trend for mineral oil at 50 and 70°C



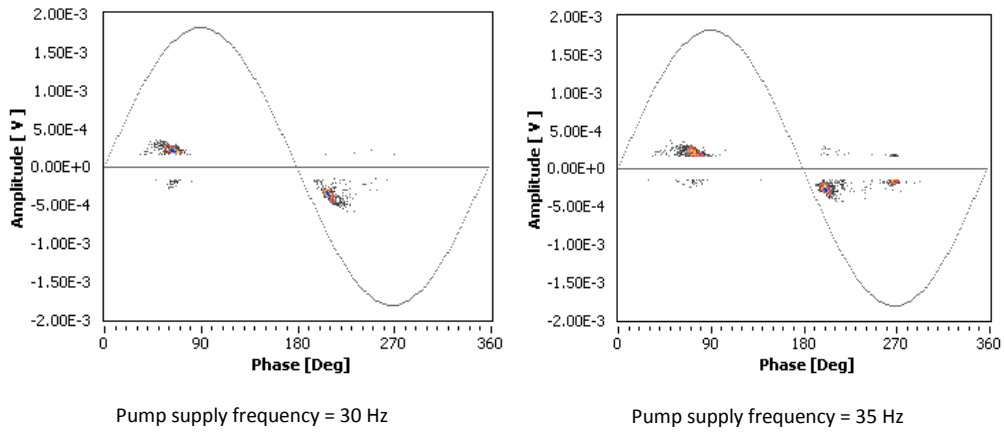


Fig. 6.15 PD patterns at different oil speeds

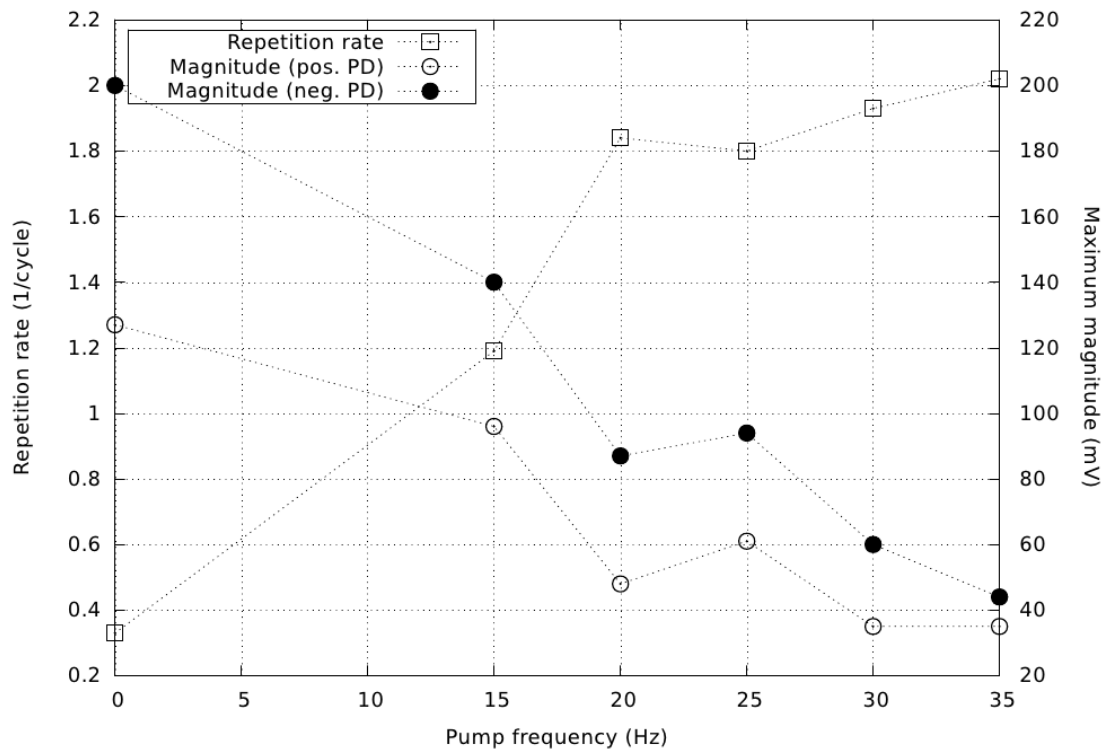


Fig. 6.16 Repetition rate, magnitude and polarity of PD pulses obtained at different frequencies

7 Discussion on dielectric fluid comparison results

7.1 Electrical breakdown (short gap, IEC 60156) and long gaps

These tests were performed in accordance with IEC 60156. Results of similar tests have been described already in literature: it has been found that ester and mineral oils behave in comparable ways whenever relative humidity levels are comparable [61]. Results of these tests are reported in Fig.95 as a function of relative humidity (RH). Humidity saturation levels S (in ppm) were calculated as a function of temperature T (in °K) using:

$$S(T) = 10^{\left(A - \frac{B}{T}\right)} \quad \text{Eq. 33}$$

The constants $A=5.3318$ and $B=684$, derived from [62] were used for FR3 and Ester X, the Shell constants $A=7.3$ and $B=1630.0$ were used for mineral oil [5]. The saturation levels thus provided are 68 ppm and 1088 ppm for mineral oil and FR3 and Ester X, respectively. It is important to say at this point that the Ester X properties are in general less satisfactory than FR3 and mineral oil, and for that reason all the analysis here are related to the comparison of these two fluids.

The results confirm that ester and mineral oils show a similar behavior: BDV is almost constant up to a specific RH level, and then it drops abruptly. From the results reported in Fig. 7.1, ester oil seems to drop at lower RH levels, if compared with mineral oil.

It can be noticed here that for new, dried and filtered oils, 2.5 mm are a too large gap to achieve breakdown at each shot due to the voltage limitation of commercial testers (75 kV in this case). Consequently, for the lowest humidity levels, accurate data could not be obtained, as many tests were censored. Probably, a gap 2.5 mm is a reasonable choice for used oils, containing particles coming from e.g. cellulose thermal degradation and oil circulation pump wearing. However, for comparing new, highly-purified fluids, a shorter gap should be considered in the standards.

The complete results of these tests are summarized in Fig. 5.1 and Fig. 5.2. Fig. 5.3 shows the results achieved in each test sequence. Since test results appear in sequences with alternatively increasing or decreasing trend, or without trend at all, it can be speculated that no systematic errors were made during the tests. It is also worthwhile observing that, in some measurements, especially for mineral oil, Baur DPA 75 C reported the value “>75 kV” at the end of the test. It was ascertained that breakdown did indeed occur, but not exactly the mechanism (the manual does not mention this).

From Fig. 5.1, which reports the average BDV values together with confidence ($P=0,95$) intervals, it can be observed that Ester X fluid shows a behavior that is intermediate between mineral oil and FR3. Fig. 5.2 shows the standard deviation of the tests values. It can be observed that the oils tend to behave in similar way.

Dry mineral oil shows, on average, the largest BDV values.

For long gaps, due to the fact that our test setup does not provide an effective current limitation, all the tested insulating liquids were replaced after each breakdown. Fluids replacement was decided after some preliminary breakdown testing. During this preliminary testing, it was observed that, as it was said before, BDV is always higher for mineral oil. But despite this advantage, once that the first BD event in mineral oil took place, the following BD events, using the same sample, showed a decremental trend that exhibited a higher negative derivative in comparison with esters. This suggests that esters have a better behavior after a high energy BD. This behavior could be related to the improved thermal properties of those fluids (higher flash point).

In all cases, during preliminary tests, fluids were replaced after 5 BDV events because of the higher concentration of combustion byproducts that was observed easily during visual inspection.

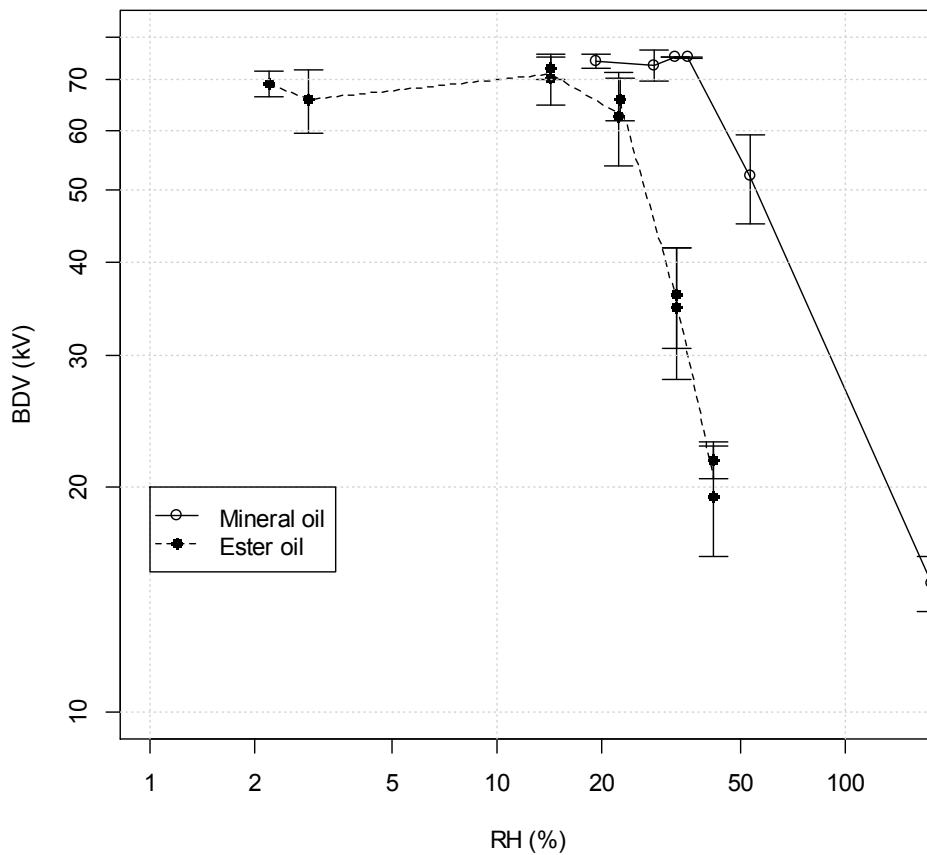


Fig. 7.1 Breakdown voltage for mineral oil and FR3 as a function of relative moisture

Fig. 7.2 shows the scale parameter and B10 of mineral oil and FR3 comparison. Both results show that the behavior of FR3 and mineral oil is very similar. In general, mineral oil shows a more linear behavior as a function of gap length for both statistic parameters. For 2 mm gaps, it was found that B10 is lower for FR3, so, it represents the fact that 10% of the evaluated samples is going to breakdown at a value (≈ 25 kV) that could be comparable to the BDV for 1 mm for mineral oil and FR3 when confidence intervals are taken into account.

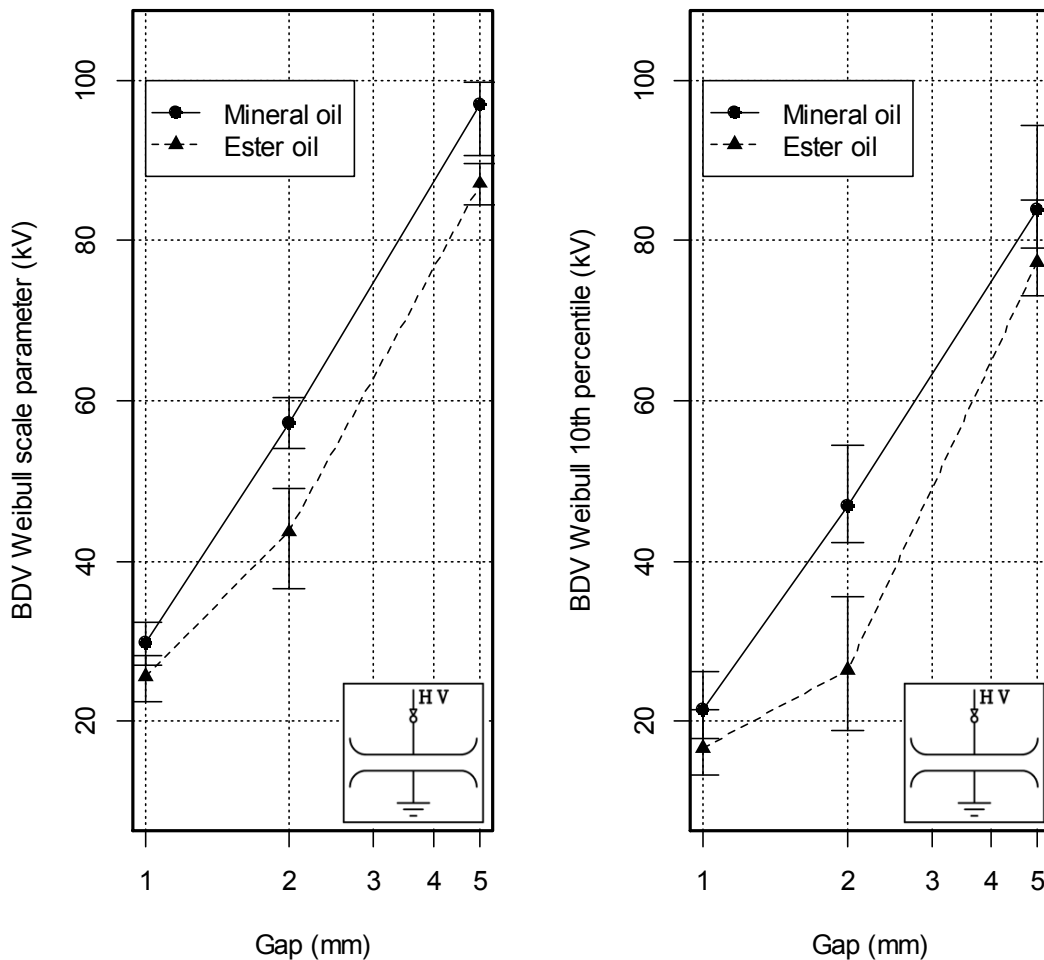


Fig. 7.2 Weibull parameters for AC BDV

7.2 Electrical breakdown (Lightning impulse)

There are two standards available regarding this kind of tests, ASTM D3300 and IEC60897. Both standards suggest the use of high divergent fields in order to make that the moisture content do not influence the dielectric characteristics of the fluids. In order to evaluate the lightning impulse behavior from a more realistic point of view, positive impulses in a plane to plane geometry were used (Quasi-uniform fields obtained through pseudo-Rogowski electrodes having a diameter of 40mm). A 600 kV/20 kJ Passoni-Villa impulse generator was used to carry out these tests. The 1.2/50 μ s impulse voltages were applied in steps of 5 kV and the oil was replaced after each breakdown event.

Despite the different test setup, the obtained results matches those ones previously reported in literature for divergent fields. In general, mineral oil seems to perform better in all oil gaps from the Weibull B63 point of view.

In terms of Weibull B10, this is, for a reliability of 90%, the trends change. In this case, FR3 shows the better behavior and the mineral oil the worst one, but obviously at lower breakdown values. For transformer design, these conservative values should be taken into account to guarantee a safe project.

Because the voltage for fast streamer transition is lower for ester fluids, so, these fluids are able to propagate at larger distances at moderate voltages

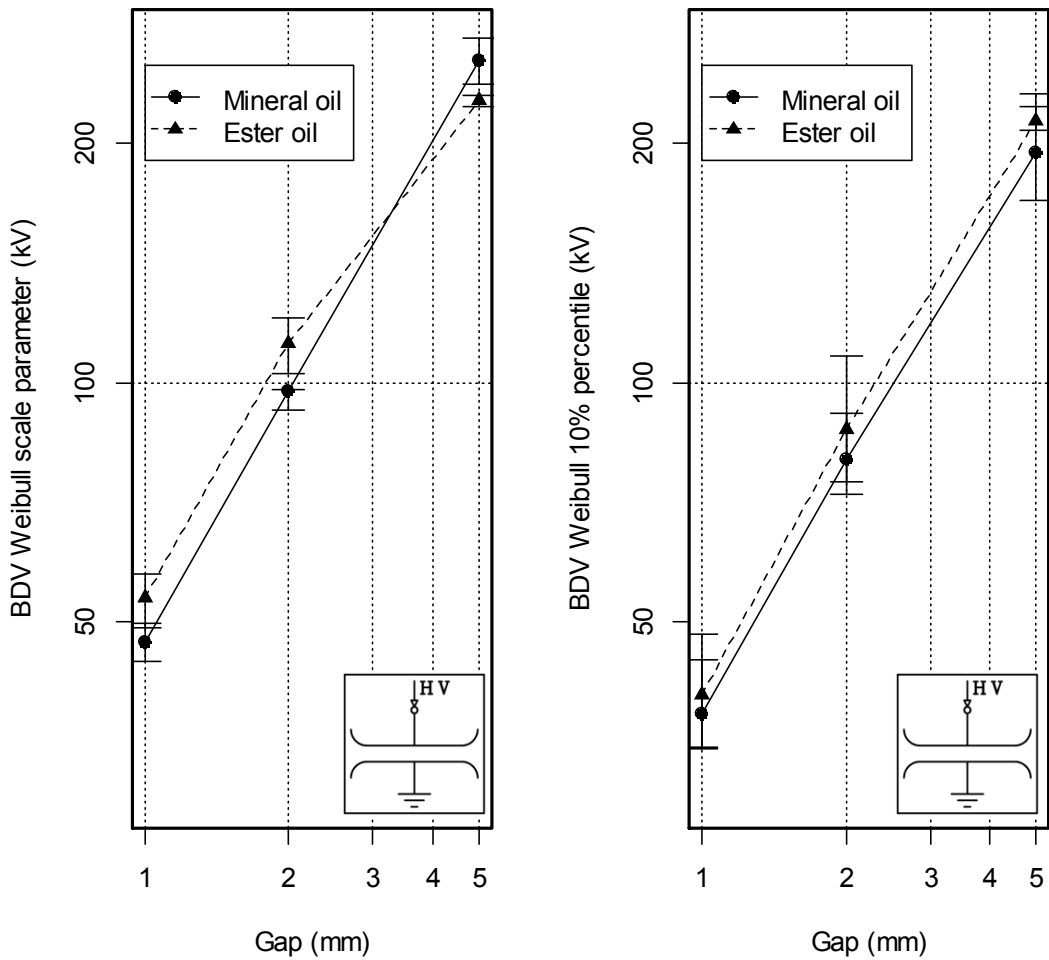


Fig. 7.3 Statistics of impulse breakdown voltage (IBDV) for the two fluids at different gap lengths. Quasi-uniform field

7.3 Partial discharges (point to plane geometry, oil)

Fig. 5.12 shows moisture in oil (absolute values) at the beginning and end of each test. Fig. 5.13 shows a direct comparison between the results achieved by the three fluids, including the Weibull shape parameter for the three oils and the 10% percentile (B10) of PDIV.

Corona in oil test proved that natural ester oils can have larger PDIV if compared to mineral oils, as proved by Fig. 5.15, which reports the Weibull shape parameter and the 10th percentile (indicated as B10) of PDIV values recorded at each gap length. The figure also shows the corresponding confidence intervals (confidence=95%), which highlight that ester fluids data are characterized by a larger variance of experimental data. For design purposes it is more appropriate to investigate lower probability percentiles of the Weibull distribution. Therefore, if the fluids are compared on the basis of B10, mineral and ester oils behave in similar ways, and design fields could be similar.

In order to understand these results, it is interesting to focus on inception fields, rather than voltages. Comparing the partial discharge inception field would, in fact, provide more insight on the inherent insulating properties of the fluids or board/fluid interfaces. Simulation results, shown in Section 5.6, help to make possible this analysis. Table 12 shows the results of FEM modeling and analytic results for inception field as a function of unitary voltage. In this table, the inception fields are also displayed. Since the permittivity of the fluids does not alter the solution of the problem, the unit fields (i.e., fields obtained applying 1 V) are the same for mineral and FR3. Therefore, the relationship existing between PDIV obtained

from these two fluids is preserved when PD inception fields are dealt with. Thus, FR3 performs better than mineral oil at all gap lengths. Provided that sufficient data are available, this could be explained considering the distribution of ionization energies for the two fluids. Another factor that should be accounted for is the larger conductivity of FR3 with respect to mineral oil. Since an important role in PD inception is played by the space charge injected by the tip during the negative half-cycle of the supply voltage, it is possible that a more conductive fluid prevents the buildup of space charge, thus reducing the field at the needle tip when the tip voltage becomes positive.

Table 12 Estimated PD inception fields for point to plane geometry

Gap (mm)	E. Field @ 1V (V/mm)		PDIV (kV)		Inception field (MV/mm)	
	FEM	Eq.27	MO	EO	MO	EO
5	51.9	48.2	8.6	9.2	0.45	0.48
10	44.5	44.5	9.4	11.0	0.42	0.49
20	36.9	41.3	11.0	12.8	0.40	0.47
40	29.4	38.5	14.2	16.7	0.42	0.49

7.4 Partial discharges (point to plane geometry, Pressboard barrier + oil)

Fig. 5.18 shows the behavior of the three dielectric fluids in terms of Weibull scale parameter α (63.2% percentile) and the Weibull shape parameter. For the Shape parameter, the test performed on Shell Diala D at 20mm was censored removing the least PDIV value (13.1kV).

PDIV Weibull shape parameter and 10% percentile (B10) along with their confidence intervals (confidence = 95%) are reported in Fig. 5.21. In this case, it is interesting to observe that ester fluids behave better than mineral oil, particularly for short gaps. As shown by the short length of the confidence intervals, the variance of measured data is fairly limited.

Simulations results for unitary voltage (see section 5.6), considering the presence of pressboard are reported in Table 3. In this table, the inception field is calculated again taking the product of electric field at unitary voltage and the measured PDIV, neglecting the effect of the permittivity changes due to the interface oil-pressboard.

Table 13 Estimated PD inception fields for point to plane geometry with pressboard

Gap (mm)	E. Field @ 1V (V/mm)		PDIV (kV)		Inception field (MV/mm)	
	MO	EO	MO	EO	MO	EO
5	154.4	82.4	4.4	12.3	0.68	1.01
10	134.0	71.4	9.9	13.7	1.33	0.98
20	113.2	60.4	14.6	16.4	1.65	0.99
40	90.9	48.7	20.0	19.4	1.82	0.95

The first evidence coming from Table 13 is that unit electric fields (electric fields at 1 kV) are larger than those obtained without board. Furthermore, mineral oil per-unit electric fields are about twice if compared to those of FR3, which partly explains why this ester tends to have higher PDIV values. This latter result can be explained considering that FR3 and board have similar permittivity. When inception fields are evaluated, the comparison with values obtained in the absence of oil highlight that the board increases the withstand

of both fluids. However, the results are somehow contradictory, as the inception field for mineral oil increases by a factor of about 3 going from short to long gaps, while FR3 inception field is almost constant. It is interesting to compare the behavior of PDIV and inception field for the two fluids, also considering the confidence intervals in order to highlight how much the changes observed in Table 12 can be ascribed to random fluctuations. This comparison is reported in Fig. 7.5 and Fig. 7.6, which highlights that inception fields can be considered constant, except in one case, i.e., for mineral oil in the presence of the board.

The evidence that inception fields in free oil are generally lower than those measured when the needle is placed in contact with pressboard could be explained resorting to the structure of the pressboard/oil interface proposed in [63]. It is assumed that the transition zone between bulk oil and bulk pressboard is made by a mixture of pressboard fibers projecting into the oil, and oil. Mitchinson et alia [59] also provided a microscope image of the pressboard/oil interface, confirming the presence of the board fibers protruding into the oil. According to this, the interface could be strengthened by Van Der Waals forces, which would prevent oil molecules directly in contact with PB to drift freely, forming a no-slip layer or, in other words, a zone with a gradual transition from bounded to free oil molecules.

In order to explain the different behavior of mineral oil and FR3 inception field as a function of gap length for creepage discharges it is useful to inspect the electric vector field in proximity of the needle tip. Fig. 5.46 shows that in the neighborhood of the needle tip region, exist significant differences between the two fluids at short gaps, whereas the behavior is similar at long gaps. In particular, it can be observed that, for a gap of 5 mm, the electric field in FR3 tends to be parallel to or directed into the board sheet. On the contrary, for mineral oil, a large number of field lines are directed from the needle into the oil. For a 40 mm gap, the electric field tends to be parallel to or directed into the board sheet for both fluids. This would support a different mechanism in PD inception at short gaps: PD are incepted in the weak points of the interface for FR3, in the oil for mineral oil. For long gaps, PD are incepted in the interface for both fluids. This speculation is confirmed by observing the PD pattern and PD pulse sequences at short gaps reported in Fig. 7.4: mineral oil displays the typical pattern of bubble discharges (with PD pulse bursts, as described by Pompili [64][65]), whereas FR3 that of surface discharges.

It is worthwhile observing that speculations on the board/oil interface would support less electric field in the liquid for FR3, given the lower permittivity mismatch between the board fibers and the fluid. This, together with the better performance of FR3 in corona inception tests, would indicate larger inception fields for this fluid, whereas, at long gaps, mineral oil performs better. A possible explanation is that the Van Der Waals forces in the no-slip layer are stronger for the oil/board interface. However, this remains to be proved.

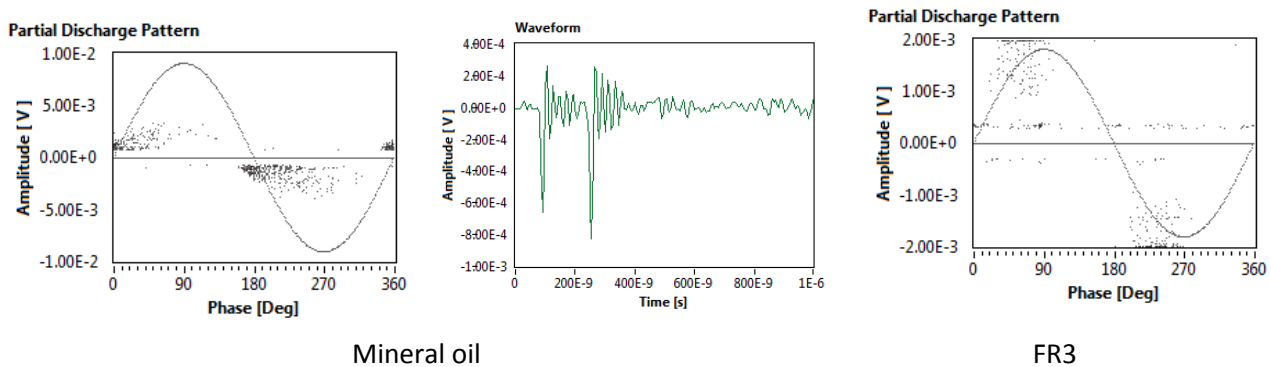


Fig. 7.4 PD pattern and discharge behavior close to PDIV for 5 mm gap

The picture provided till now is still incomplete. Both Mitchinson [59] and Dai[66] underline that incepting creeping PD on a fully dried pressboard surface is very difficult. On the contrary, wet pressboard sheet usually display lower PDIV values. As an example, Dai found a reduction of PDIV from 38 kV to 28 kV for a gap of 40 mm, when raising the relative humidity of the pressboard from <0.5% to 2.5%. In [67], it is speculated that the leakage current flowing in the pressboard can (a) heat the oil in the pores, causing gassing and, eventually, inception of PD in the pores, (b) when PD within the pores are energetic enough to further dry the pressboard and release gases, phenomena similar to dry band arcing are incepted. Since ester oils are highly hygroscopic they could contribute to a further drying of the pressboard during the impregnation phase and beyond, a process that would prevent excessive current density levels in the board. This was confirmed experimentally by evaluating the oil moisture content at the beginning and end of the tests (about 1 day to complete measurements at one gap for a single fluid). These data are reported in Fig. 7.7, which shows that the humidity content of the oil does not increase appreciably for tests performed without pressboard sheets (the increase is associated with diffusion from the atmosphere into the oil). On the contrary, for tests performed using a pressboard sheet, the increase is much more marked for FR3. This evidence proves that moisture extraction continues even after drying and impregnation and can help to ensure long-term behavior of the insulation.

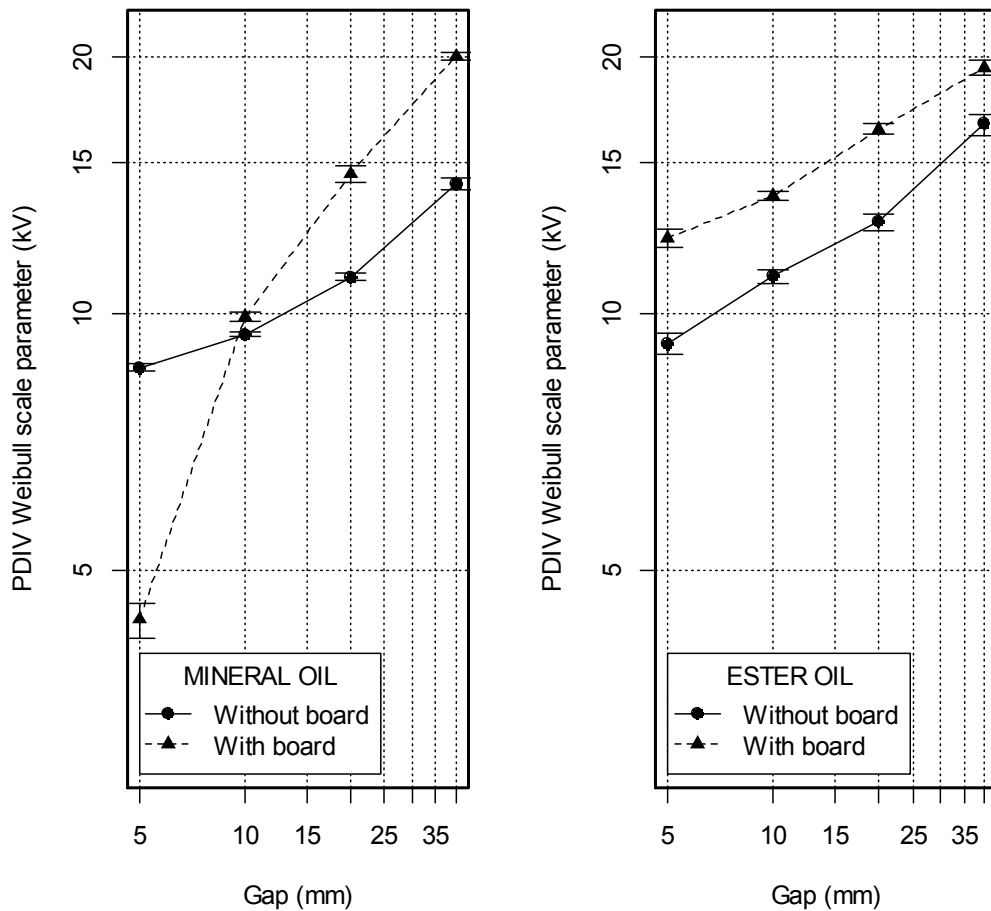


Fig. 7.5 PDIV of mineral and ester oil without and with board

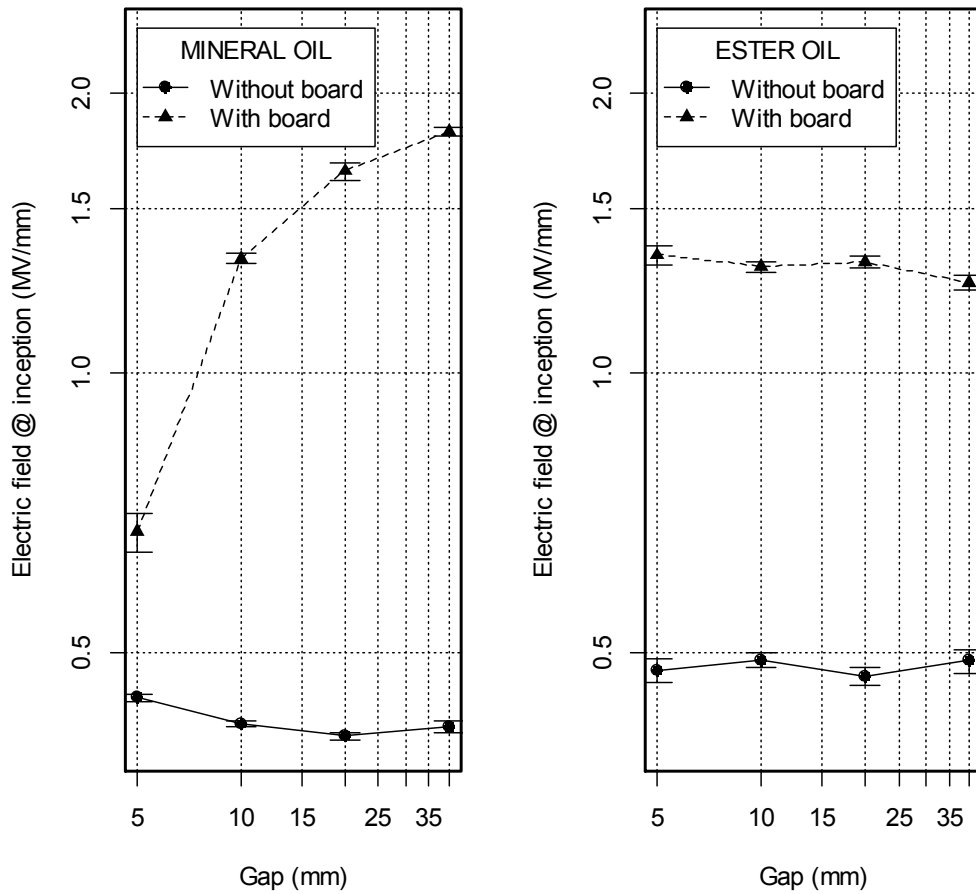


Fig. 7.6 Electric field at inception for mineral and ester oil without and with board (confidence intervals at 95% probability are also reported)

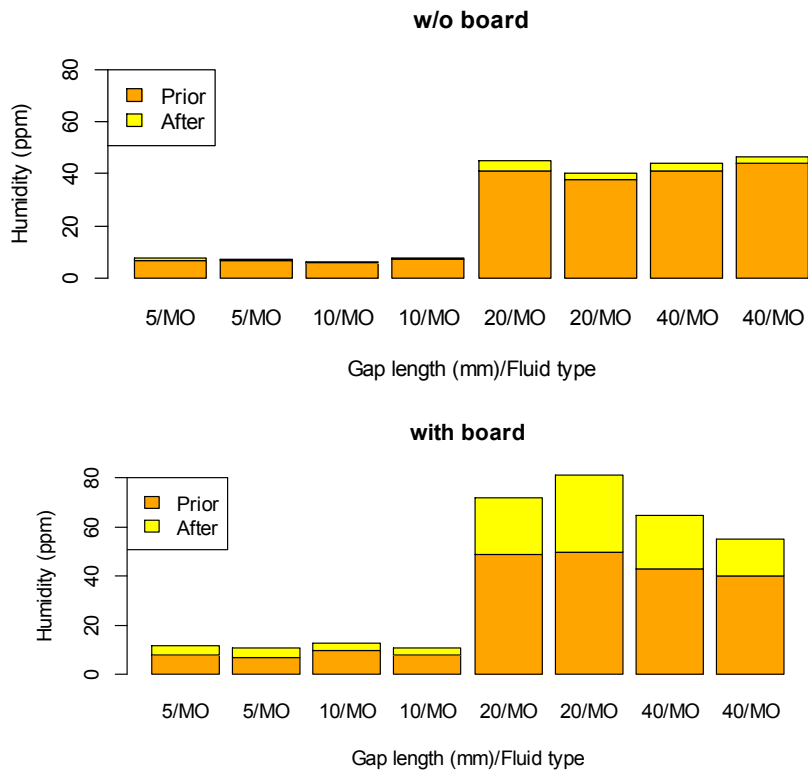


Fig. 7.7 Oil humidity prior and after PDIV tests, (above) without and (below) with board

8 Discussion on results of PD testing under HVDC, square waveform and particular conditions

8.1 Partial discharges (point to plane geometry, influence of frequency and waveform)

When voltage is applied to the test cell, a high electric field is produced at the needle tip. In this region, the dielectric behavior under this high electric field might be influenced by impurities, oil additives, dissolved water, and gases, etc. causing streamers to take place. However, these influences are probably negligible in comparison with the role played by space charge. Indeed, space charge plays an important role in streamer inception as is explained in the following two different points of view: charge injection from the electrodes and transient distribution of ionizing wave (after [68] [69]).

8.1.1 Charge injection from electrodes

Considering charge injection, it is possible to recall thermo-ionic and Fowler-Nordheim emission to explain how charge injection from the metallic electrode is possible. Fowler and Nordheim work has shown to be valid for metal/vacuum interfaces. For metal/liquid interfaces the equation must be corrected with liquid permittivity and true ions masses in liquid [68]. Up to now, this formulation has not been derived in a definitive way. Despite this fact, the equation of Fowler-Nordheim can be used intuitively to describe an electric field dependent current density in the liquids due to electrons tunneling from the metal/liquid interface. The level of electron tunneling increases exponentially with the electric field level. This happens because, as the electric field increases, the potential barrier at the interfaces becomes narrower leading to an exponential increase of the probability of electrons tunneling through the barrier. The basic equation for Fowler-Nordheim emission is:

$$J = \frac{e^3 |\vec{E}|^2}{8\pi h \phi t^2 \left(\frac{\Delta\phi}{\phi}\right)} \exp\left(-\frac{8\pi \sqrt{2m} \phi^{\frac{3}{2}}}{3he |\vec{E}|} v \left(\frac{\Delta\phi}{\phi}\right)\right) \quad \text{Eq. 34}$$

Where J is the emitted current, e is the electron charge, E is the electric field, h is the Planck's constant value, ϕ is the metal's work function, m is the effective mass of the electron and $t^2 \left(\frac{\Delta\phi}{\phi}\right)$ and $v \left(\frac{\Delta\phi}{\phi}\right)$ are parameters that can be estimated to take into account barrier reduction during field emission.

When charge is injected in the liquid close to the needle electrode (high voltage electrode), it affects the field distribution and hence the streamer inception voltage in the following way:

For alternating voltage applied to the test cell, independently of its nature (sinusoidal or square), when the point electrode has a negative polarity, negative space charge will build up in the neighborhood of the electrode (homocharge). This homocharge will reduce the local field around the electrode as shown in Fig. 8.1 A) increasing the streamer inception voltage.

Following a similar reasoning, the space charge with opposite polarity to that of the needle electrode (heterocharge) will reduce the streamer inception voltage. Heterocharge will build up when the mobility of carriers is relative low, so that the voltage applied by the generator might change polarity faster than the amount of time necessary to remove the space charge itself. It is important to remember that electrons will attach to oil molecules forming negative ions (having lower mobility, $10^{-9} \text{ m}^2/\text{Vs}$ than electrons $10^{-4} \text{ m}^2/\text{Vs}$) following a relaxation process with a time constant $\tau = 200 \text{ ns}$ [70] i.e. almost immediately. Therefore, when the voltage applied to the point electrode changes polarity due to voltage sign change, it is possible that the region surrounding the HV electrode contains negative charges remaining from the previous negative half cycle because negative ion drift is limited by the low ion mobility.

During the positive cycle, when there is a large amount of previously injected space charge, it is possible that only a fraction of the negative ions reaches the positive needle tip and gets neutralized, whereas some ions further away from the point electrode will remain in the liquid gap. This heterocharge will enhance the local field around the electrode tip as shown in Fig. 8.1 B) increasing ionization probability of "healthy oil".

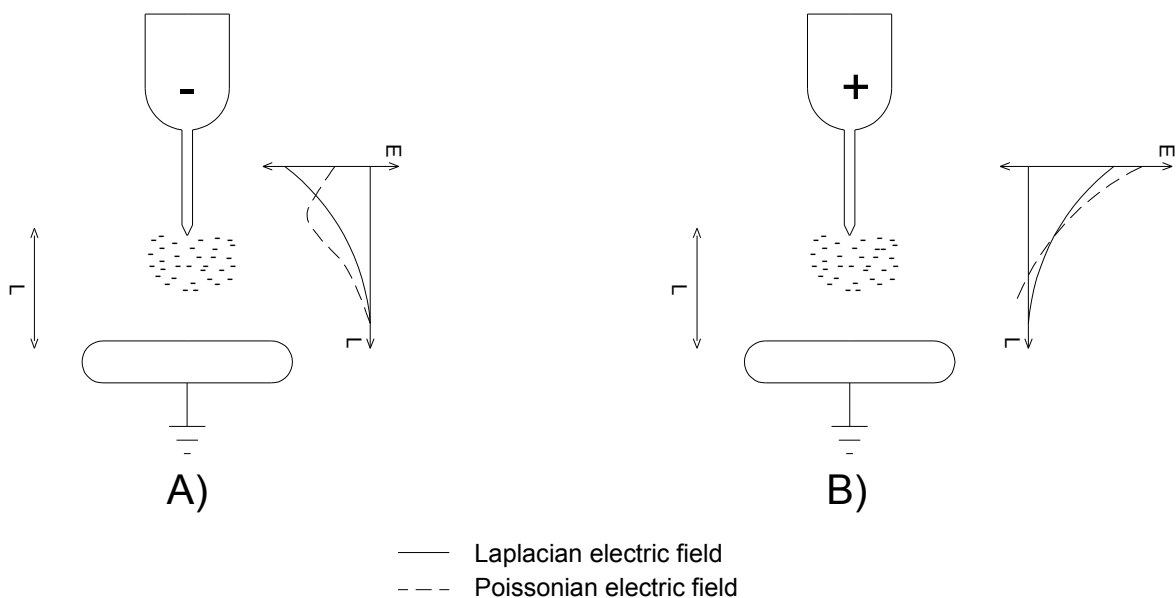


Fig. 8.1 Influence of space charge on the electric field distribution in a point to plane geometry

Since the duration of the applied voltage peak under square waveform is longer than that under sinusoidal voltage, it is expected that more space charge would be injected in the former case and thus the space charge effect is more significant. This fact, along with the faster sign reversal of square voltages could explain why the PDIV values for mineral oil and FR3 are always lower using square waveforms. For low frequencies the effect is still more marked because between each polarity reversal, more time elapses, favoring a bigger injected charge density. Note that this effect can come to a plateau when space charge limits the field, thus increasing the needle/fluid potential barrier up to a point where injection becomes negligible.

Increasing the frequency, the homocharge build up decreases, contributing in this way to a lower electric field enhancement during the polarity reversal. The electric field reduction due to a lower number of carriers makes necessary to further raise the voltage to produce a streamer, increasing in this way the PDIV. This can explain the PDIV increase for frequencies around 50 Hz for sinusoidal and square voltages.

8.1.2 Ionization waves

Under field enhancement conditions, produced by charge injection in the stressed tip region, ionization processes can take place in different ways depending on tip polarity. Two different carriers are developed during ionization: high mobility electrons (10^{-4} m/s/V/m) and low mobility positive ions. The huge difference between carrier mobility influences remarkably the behavior of the charge distributions induced by ionization processes and, consequently, of the discharge features.

Fig. 8.2A shows qualitatively the Laplacian electric field when the needle is positive biased after the negative charge injection process, but considering a very low negative space charge density. As discussed before, the tip of the needle experiences a higher enhanced electric field, which produces ionization in the oil molecules accelerating free carriers. It is important to notice that field enhancement decays quickly as a function of the distance from the needle tip.

Once that oil ionization takes place, an equal concentration of electrons and positive ions is generated and causes a positive and electric field concentration as shown in Fig. 8.2B. At that moment, the generated species begin to migrate towards the electrodes. The difference of mobility means that, for a given time dt , electrons will move significantly, while the positive ions are almost stationary. As an example, assuming that the charge is injected under a field of 0.5 MV/mm , and that the charge lasts $5 \mu\text{s}$ (positive streamer), the ion can displace themselves $10^{-9} \cdot 0.5 \cdot 10^6 \cdot 10^3 \cdot 5 \cdot 10^{-6} = 2.5 \mu\text{m}$ whereas the electrons will move $10^{-4} \cdot 0.5 \cdot 10^6 \cdot 10^3 \cdot 5 \cdot 10^{-6} = 250 \text{ mm}$. The electrons in this way will be swept out from the oil by the positive biased needle, resulting in the formation of a region of positive charge in front of the needle. This is shown in Fig. 8.2C. If the space charge density is large enough, it will result in a peak of the electric field distribution, moving from the needle tip to a point in space in front of the region of positive space charge. This causes ionization to take place away from the needle tip, hence, in the oil gap. The result of this process is the development of a propagating high electric field region, or an electric field wave which propagates through the dielectric liquid from the high field needle electrode towards the low field plane electrode. Fig. 8.2 [71], shows qualitatively the trend as a function of time of the electric field wave.

Molecular ionization also contributes to the development of negative streamers in transformer oil. Fig. 8.3 illustrates this phenomenon. In a similar way to positive streamers, when a negative excitation of sufficient magnitude is applied to the needle electrode, ionization will occur. The result is the generation of equal concentration of positive ions and electrons as shown in Fig. 8.3B. Unlike in the equivalent positive needle situation, the highly mobile electrons move away from the needle tip into the oil bulk as shown in Fig. 8.3C.

In this time scale, the low mobility positive ions do not move appreciably and this results in the formation of a region of positive charge in front of the needle tip (enhancing local electric field) and a region of negative charge into the oil gap because of electrons propagation, that increases the homocharge field further out the needle tip, favoring oil ionization (Fig. 8.3D).

For both sinusoidal and square waveforms, the positive and negative electric field waves take place depending on the voltage polarity. At each polarity reversal the field enhancement due to gap "reduction" is larger, producing also thermal effects in the oil, that can contribute to further oil vaporization. This gets worst at high frequencies and at steeper applied voltages, explaining why the PDIV decreases at higher frequencies and the decrement is always higher for the square waves.

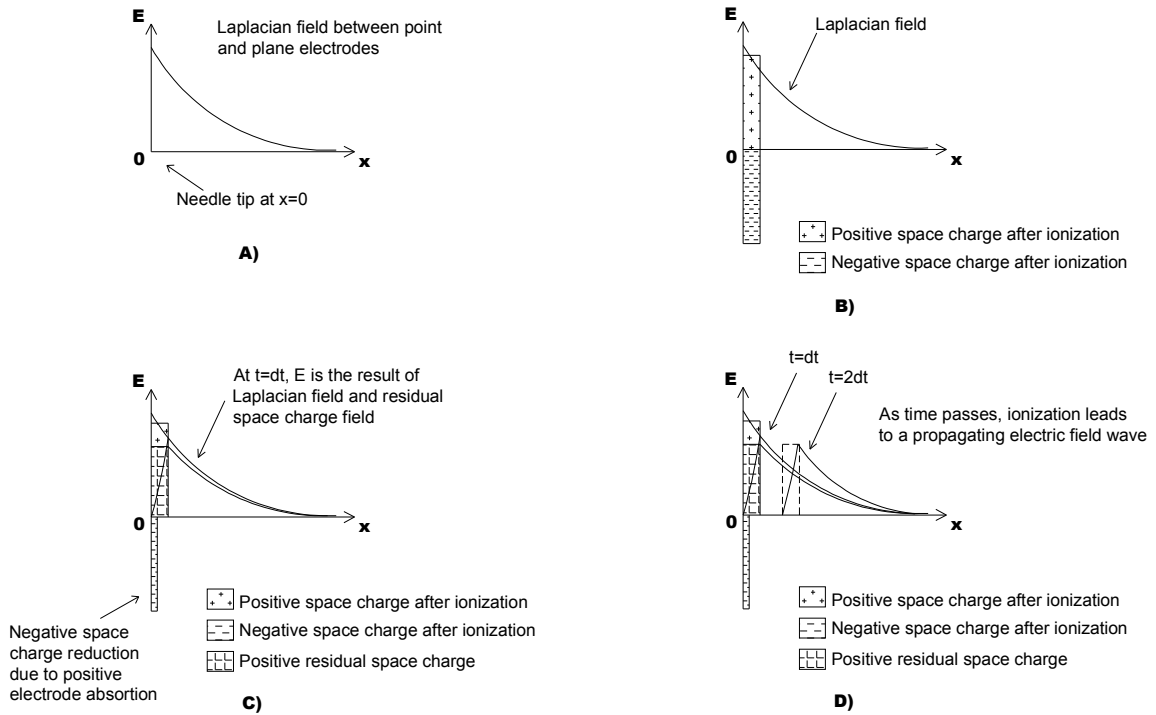


Fig. 8.2 Propagating electric field wave for positive needle electrode

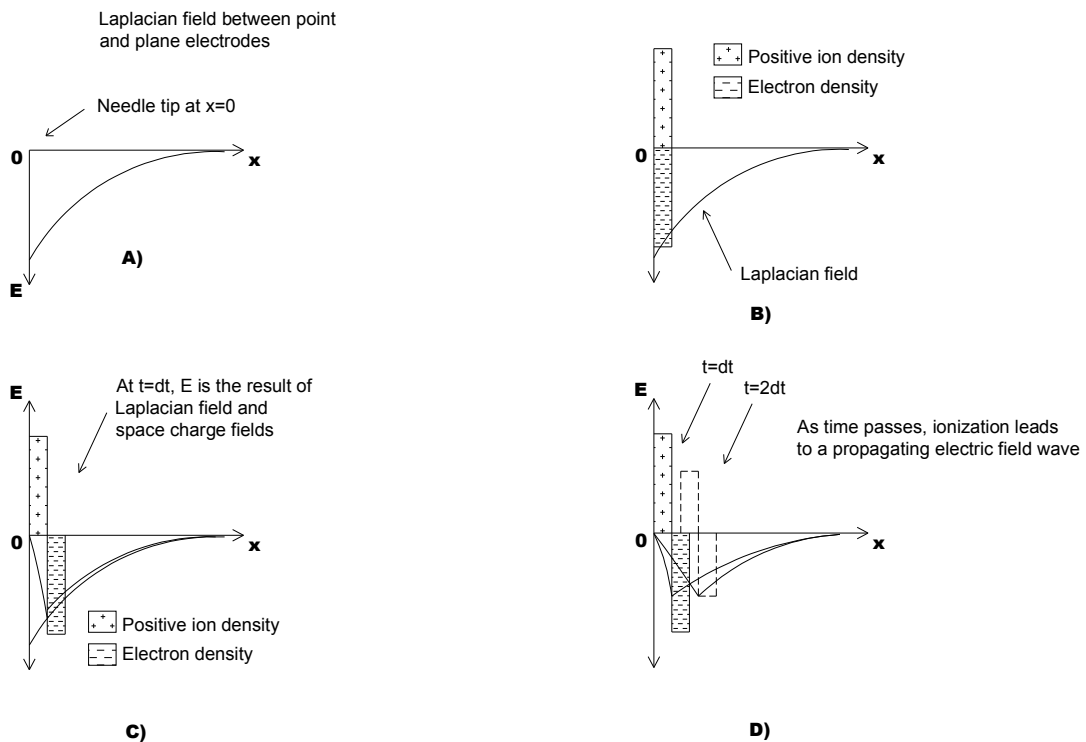


Fig. 8.3 Propagating electric field wave for negative needle electrode

8.2 Partial discharges under HVDC stresses

8.2.1 Behavior of PDIV in pressboard as a function of voltage distribution and space charge

As it can be seen from the results of section 6.3.1, it is clear that the PDIV in Oil-PB-oil and PB-oil geometries depends on the electric field distribution inside the samples. Using the superposition principle, the peak electric field can be calculated as the sum of the peak value of the DC voltage plus the peak value of the AC component.

For the particular case of two oil gaps and one layer of pressboard with the same thickness (1mm), Eq. 35 was used to assess the peak voltage distribution in the pressboard during AC+DC conditions.

$$V_{PB\ Oil-PB-oil} = \left(\frac{2}{5} \left(\frac{\epsilon_{oil}}{2\epsilon_{PB} + \epsilon_{oil}} \right) + \left(\frac{\sigma_{oil}}{2\sigma_{PB} + \sigma_{oil}} \right) \right) V_{DC} \quad \text{Eq. 35}$$

And for oil-PB geometry:

$$V_{PB\ PB-oil} = \left(\frac{2}{5} \left(\frac{\epsilon_{oil}}{\epsilon_{PB} + \epsilon_{oil}} \right) + \left(\frac{\sigma_{oil}}{\sigma_{PB} + \sigma_{oil}} \right) \right) V_{DC} \quad \text{Eq. 36}$$

In these equations, the factor 2/5 represents the AC peak voltage component (40% of the applied DC voltage, a value typical of rectifier transformers).

Due to the PB/oil conductivity ratio, from 4 to 100 times higher in oil, the field lines under DC conditions are concentrated mostly in the pressboard. It is possible to calculate the peak electric field in the pressboard at PDIV under AC+DC voltage in the following way by dividing Eq. 35 and Eq. 36 by the pressboard thickness:

$$E_{PB\ Oil-PB-oil} = \frac{V_{DC}}{d_B} \left[\frac{2}{5} \left(\frac{\epsilon_{oil}}{2\epsilon_{PB} + \epsilon_{oil}} \right) + \left(\frac{\sigma_{oil}}{2\sigma_{PB} + \sigma_{oil}} \right) \right] \quad \text{Eq. 37}$$

And for oil-pressboard (equal thickness of oil and pressboard layers):

$$E_{PB\ PB-oil} = \frac{V_{DC}}{d_B} \left[\frac{2}{5} \left(\frac{\epsilon_{oil}}{\epsilon_{PB} + \epsilon_{oil}} \right) + \left(\frac{\sigma_{oil}}{\sigma_{PB} + \sigma_{oil}} \right) \right] \quad \text{Eq. 38}$$

Where d_b is the thickness of the board.

For the performed tests under DC and AC+DC conditions when the samples contain oil gaps, if one introduces the electric parameters defined in Table 8 in Eq. 35, along with the Weibull scale parameters of the acquired $PDIV_{pk}$ values shown in Fig. 8.4 for each sample geometry, it is possible to calculate the peak partial discharge inception electric field ($PDIE_{pk}$) in the pressboard. Note that high β values (low dispersion) are obtained each time that the DC and AC+DC voltage were used. This observation suggest that a more accurate assessment of PDIV was obtained using DC components. This can be ascribed to the long times

that were used for each voltage stress level to allow a complete polarization of the system and ensure an almost stationary condition within the board.

The calculated values can be compared also with the $PDIE_{pk}$ for pressboard without oil gaps in pure AC and DC conditions. Table 14 shows this comparison.

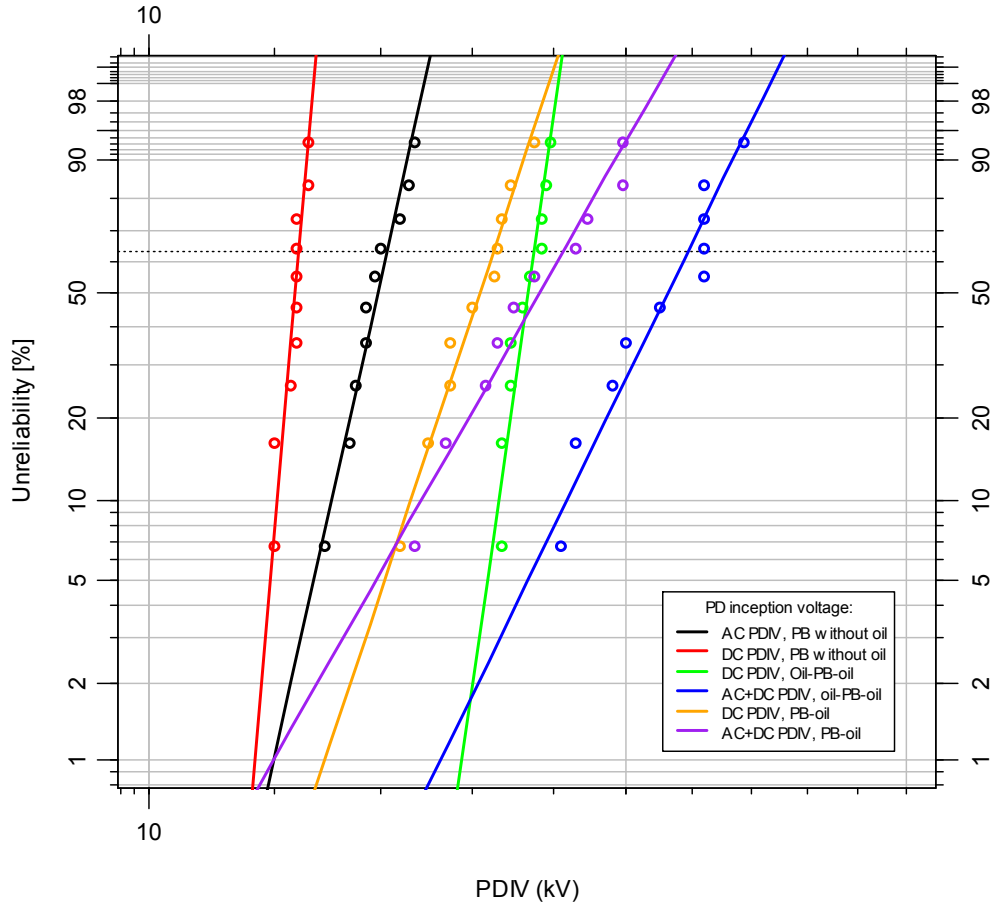
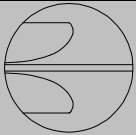
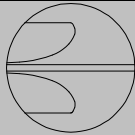
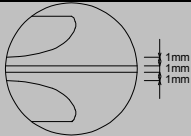
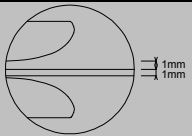
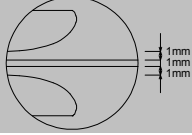
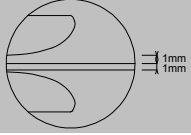
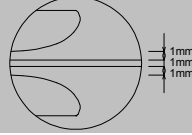
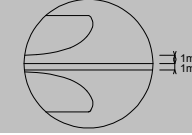


Fig. 8.4 PDIV peak values obtained from different electrodes condition.

Table 14 Comparison of electric field distribution in the pressboard. The values can be measured or calculated, depending on the test conditions

	PDIE at measured AC PDIV (kV/mm)	PDIE α at measured DC PDIV (kV/mm)
Real geometry of the sample		
Voltage condition	AC	DC
Considered geometry	PB	PB
AC	14.1 (PDIV=14.1 kVpk)	12.4 (PDIV=12.4 kVpk)

	PDIE (kV/mm) in the PB (estimated with Eq. 37 and Eq. 38 from measured PDIV)	
Real geometry of the sample		
Voltage condition	DC	
Considered geometry	Oil-PB-oil	PB-Oil
DC	10.5 (PDIV=17.5 kV)	12.4 (PDIV=16.5 kV)

	PDIE (kV/mm) estimated with Eq. 37 and Eq. 38 from measured PDIV		PDIE (kV/mm) estimated with Eq. 37 and Eq. 38, separating AC from DC components	
Real geometry of the sample				
Voltage condition	AC+DC			
Considered geometry	Oil-PB-oil	PB-Oil	Oil-PB-oil	PB-Oil
ACpk	-	-	1.2	1.7
DC	-	-	9.4	9.7
AC _{pk} +DC	10.6 (PDIV=21.9 kV _{pk})	11.4 (PDIV=18.1 kV _{pk})	Σ10.6	Σ11.4

The PDIE_{pk} under AC and DC voltages for a layer of pressboard without oil gaps is easily calculated dividing the PDIV_{pk} by the thickness of the sample (1 mm). Proceeding this way, the PDIE_{pk} for AC and DC are 14.1 kV and 12.4 kV/mm respectively. As it can be seen, under AC voltage, the PDIE_{pk} is almost 2 kV/mm higher than that obtained for DC. This difference seems to be too large to assume that it is caused by chance. If RMS value is calculated for the AC PDIV_{pk}, it comes out that the PDIE_{RMS} (10 kV_{RMS}/mm) is lower than the PDIE_{pk} obtained for DC. Again, this variation does not seem to be correlated to physical processes (for example, dielectric heating) and some considerations regarding the measuring process arise:

The voltage impressed in a cavity inside the pressboard must exceed the minimum breakdown voltage V_{min} to produce a PD. The voltage in excess of V_{min} is indicated as overvoltage ΔV . Thus, the more plausible explanation for the PDIE_{pk} difference mentioned above, is to consider that the DC PDIV_{pk} is the voltage level at which PD really incepts, even in the case when AC is applied (i.e. DC PDIV_{pk} = V_{min}). Under those conditions, Fig. 8.5 shows the time intervals (I to IV) in which the applied sinusoidal voltage exceeds V_{min} i.e. the time intervals where PD inception is possible. The total time length can be evaluated through Eq. 39.

$$T_{PD} = 4 \cdot \arccos\left(\frac{PDIV_{DC}}{AC_{pk}}\right) \cdot \frac{180}{\pi} \quad \text{Eq. 39}$$

A plot of Eq. 39, is shown in Fig. 8.6.

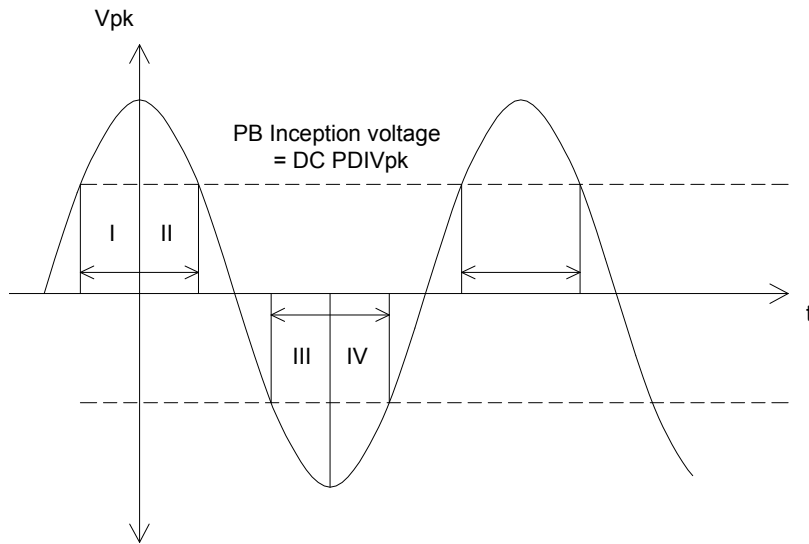


Fig. 8.5 Times for PD inception in AC above DC PDIV_{pk}

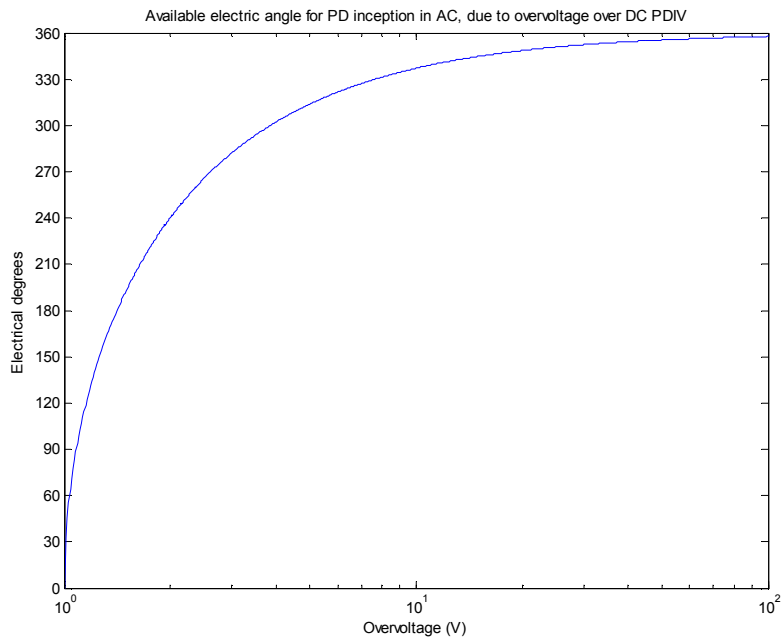


Fig. 8.6 Available time for PD inception due to AC overvoltages over DC PDIV

From Fig. 8.6, it is worth to note that, if AC peak is set at the same voltage level than the DC PDIV_{pk} (overvoltage=0), the probability to incept a discharge is zero for practical measuring periods. In fact, the probability of inception over one cycle of the applied voltage is defined by the interval of the PD hazard rate over [0,1] (Eq. 40). Since $h=0$ when $E(t) \ll E_i$, it comes out that the probability of PD inception can be extremely low when E does not exceed E_i for a sufficiently long time.

$$\int_0^T h(E(t) - E_i) dt \quad \text{Eq. 40}$$

The ΔV at which a PD are first observed has also a direct effect on the PD magnitude: once that the first discharge is produced under AC conditions (after satisfy $V_{\min} + \Delta V$), it is possible to have at least one

discharge per half-cycle. The obtained magnitude of those discharges during the measurements was greater than those obtained under DC (see Table 15).

In order to explain why PD magnitudes under AC voltages are higher, it is convenient to recall the basic conditions to produce a partial discharge event in a hypothetical cavity inside the pressboard. The first one is that the electric field must be sufficiently large to trigger an electron avalanche. The second one is the existence of starting electrons. The starting electrons can be generated by gas photo-ionization inside the cavity, barrier reduction effect caused by the electric field, extraction from interfaces and external agents like radiation. The availability of starting electrons is a stochastic process governed by a statistical time lag.

When a discharge (electron avalanche) occurs, positive ions and electrons are deposited in the cavity surfaces acting as cathode and anode, respectively. This charge is not removed from the cavity surface immediately, thus forming a space charge. The space charge produced by the charge carriers left on the cavity surface by the discharge, produces an internal electric field that quenches the avalanche itself.

It is important to remember that the space charge inside the cavity drifts or recombines following a relaxation process having a time constant τ . When $\tau \ll T$, being T the period of the applied voltage, the space charge effect vanishes rapidly, and the conditions for a new discharge are met soon after the PD event. When τ becomes comparable or larger than T , the space charge prevents PD with the same polarity to occur for a long time. When the voltage polarity reverses, the space charge field and the external field have the same polarity. This tends to generate strong discharges. Theoretically, PD ignited in the presence of space charge having opposite polarity to the external field, can have magnitude double, compared with the maximum PD magnitude obtained in the absence of space charge. i.e., the maximum one obtained under DC conditions.

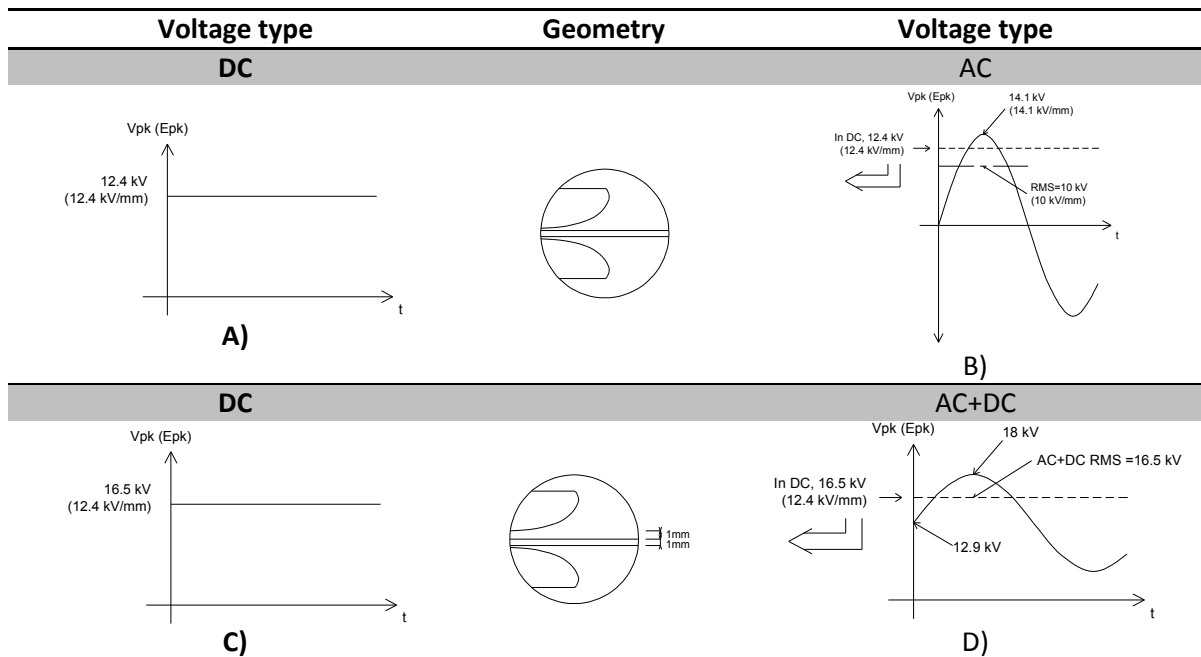
Table 15 PD magnitudes at PDIV for different types of voltage and sample geometries

PD magnitudes at PDIV (pC)			
Voltage type	Sample geometry		
	PB	Oil-PB-oil	PB-oil
AC	900	-	-
DC	300	360	480
AC+DC	-	420	640

Under AC+DC stress, it can be observed that the $PDIE_{pk}$, calculated from the $PDIV_{pk}$ of the combined AC and DC voltages ($AC_{pk}+DC = 1.4 DC$) for oil-PB-oil and PB-oil samples are in the same order of magnitude of the $PDIE_{pk}$ obtained for DC in the same sample geometries. The same reasoning previously used for PB samples can be recalled to explain the necessity of higher AC peaks (higher ΔV). Under AC+DC conditions for oil-PB-oil and PB-oil samples, the PD magnitudes are higher than those obtained in DC in a similar way that when only PB was tested. This fact evidences that when AC components are present (pure AC or AC+DC), the effect of the test voltages is more dangerous at similar electric field levels inside the pressboard, because they produce higher PD magnitudes and repetition frequencies.

Table 16 PDIV comparison for AC, DC and HVDC voltages in PB and PB-oil samples summarizes the PDIV for two different sample configurations: PB and PB-oil. Three different voltage types are displayed: AC, DC and AC+DC. A) and B) shows the different PDIV for an impregnated PB sample stressed with DC and AC voltages respectively. C) and D) show the comparison for DC and AC+DC.

Table 16 PDIV comparison for AC, DC and HVDC voltages in PB and PB-oil samples



The role of space charge at the oil-pressboard interface could also have some influence. In fact, when the pressboard surface is not perfectly smooth, this change can create localized field enhancement. Indeed, this effect could play a secondary role.

In AC conditions, no space charge develops on the board surface and for this reason, it might be necessary a higher voltage and hence a higher electric field to produce partial discharges. A crucial question for testing is how long should the experiments last to be sure that a DC condition has been reached and the pressboard is fully stressed? Both simulations and tests were performed to answer this question.

Fig. 8.7 shows the different trends to reach DC steady conditions estimated using Comsol Multiphysics®. It is possible to observe that for Oil-PB-oil geometry, the time constant is higher than that for PB-oil.

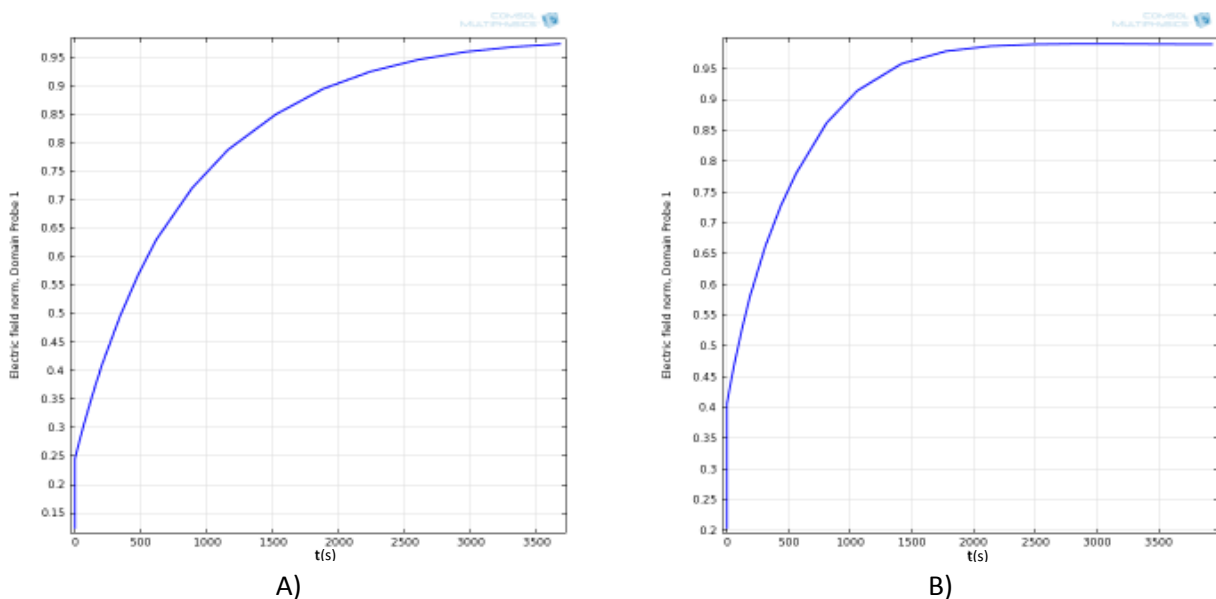


Fig. 8.7 Time to achieve steady state conditions under DC voltage for a) Oil-PB-oil and b) PB-Oil geometries

To obtain a simplified analytic solution for times constants, the following approach based on the Maxwell capacitor theory can also be used:

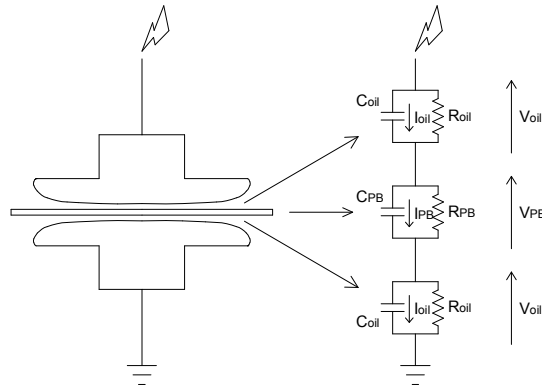


Fig. 8.8 Equivalent circuit for Oil-PB-oil geometry

Applying KVL and KCL for Fig. 8.8, it is possible to obtain:

$$2V_{oil} + V_{PB} = V \quad \text{Eq. 41}$$

$$I_{oil} + \frac{V_{oil}}{R_{oil}} = I_{PB} + \frac{V_{PB}}{R_{PB}} \quad \text{Eq. 42}$$

Currents 1 and 2 can be written in terms of capacitance as shown in Eq. 43

$$I_{oil} = C_{oil} \frac{dV_{oil}}{dt}, I_{PB} = C_{PB} \frac{dV_{PB}}{dt} \quad \text{Eq. 43}$$

Substituting Eq. 43 in Eq. 42, it follows:

$$C_{oil} \frac{dV_{oil}}{dt} + \frac{V_{oil}}{R_{oil}} = C_{PB} \frac{dV_{PB}}{dt} + \frac{V_{PB}}{R_{PB}} \quad \text{Eq. 44}$$

Then, solving Eq. 41 for V_{PB} , and substituting it in Eq. 44, we can obtain

$$C_{oil} \frac{dV_{oil}}{dt} + \frac{V_{oil}}{R_{oil}} = C_{PB} \frac{dV}{dt} - 2C_{PB} \frac{dV_{oil}}{dt} + \frac{V - 2V_{oil}}{R_{PB}} \quad \text{Eq. 45}$$

Re-writing and re-grouping Eq. 45, it follows:

$$(C_{oil} + 2C_{PB}) \frac{dV_{oil}}{dt} + V_{oil} \left(\frac{1}{R_{oil}} + \frac{2}{R_{PB}} \right) = C_{PB} \frac{dV}{dt} + \frac{V}{R_{PB}} \quad \text{Eq. 46}$$

This equation has the form of a non-homogeneous, constant coefficients differential equation. In order to calculate the time constant and assuming null initial conditions, it is only necessary to solve the homogeneous equation:

$$a \frac{dV_{oil}}{dt} + bV_{oil} = 0 \quad \text{Eq. 47}$$

The solution has the form of Eq. 48

$$V_{oil} = \gamma e^{-\frac{b}{a}t} \quad \text{Eq. 48}$$

Where:

$$a = C_{oil} + 2C_{PB} \quad \& \quad b = \frac{1}{R_{oil}} + \frac{2}{R_{PB}} \quad \text{Eq. 49}$$

From this solution, it comes that the time constant for a Oil-PB-oil sample geometry is:

$$\tau = \frac{a}{b} = \frac{C_{oil} + 2C_{PB}}{\frac{1}{R_{oil}} + \frac{2}{R_{PB}}} = \frac{\varepsilon_{oil} + 2\varepsilon_{PB}}{\sigma_{oil} + 2\sigma_{PB}} \quad \text{Eq. 50}$$

Using a similar procedure, it is possible to calculate also the time constant for a PB-oil geometry using Eq. 51

$$\tau = \frac{\varepsilon_{oil} + \varepsilon_{PB}}{\sigma_{oil} + \sigma_{PB}} \quad \text{Eq. 51}$$

And in general, for different thicknesses of both dielectrics:

$$\tau = \frac{b\varepsilon_{oil} + a\varepsilon_{PB}}{b\sigma_{oil} + a\sigma_{PB}} \quad \text{Eq. 52}$$

Where a is the total thickness of oil layers and b the total thickness of the pressboard.

Using these equations, it is possible to obtain a similar response to that obtained with FEM. The analytical values are 799 s for oil-PB-oil geometry and 500 s for PB-oil. Due to the fact that 5τ are required to reach to steady state, each value must be multiplied by 5. So the saturation levels of curves in Fig. 8.7, using analytical solutions are 4000 s for oil-PB-oil geometry and 2500 s for PB-oil.

In order to verify these values, a test of polarization and depolarization currents was carried up in two PB-oil geometries. One of these samples was formed by previously dried and conditioned oil (5 ppm) and pressboard. The other sample was formed by a dry pressboard sheet impregnated with mineral oil with moisture of 35 ppm. 4000 V were applied to both samples using the test cell described in section 4.1.8. Fig. 8.9 and Fig. 8.10 show the trend of charge and discharge currents for the two tested samples.

From both figures, it is evident that, as expected, water content increases the magnitude of both polarization and depolarization currents. For very short times, the value of the current is very high and it decays exponentially due to the finite resistance value of the measuring circuit and mainly due to the higher conductivity of the oil. For long times, the dominant behavior depends on the conduction current, due to the sample conductivity. Between these two different trends, it can be observed the most important current contribution, called absorption current. These current components in the discharge plots show in our case a non linear behavior (from 10 to 4000 seconds) for the wet sample and a linear trend for the dry sample. The duration of this linear trend, which corresponds to the formation of most of the interfacial

charge accumulated at the PB surface, is around 3000 s. So, the theoretical time constant of 500 s seems to be acceptable.

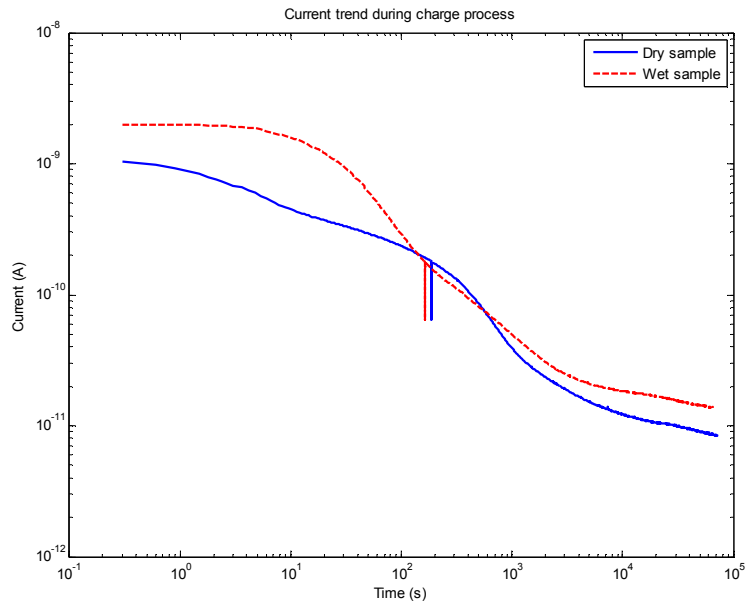


Fig. 8.9 Polarization currents of dry and wet samples (PB-oil geometry)

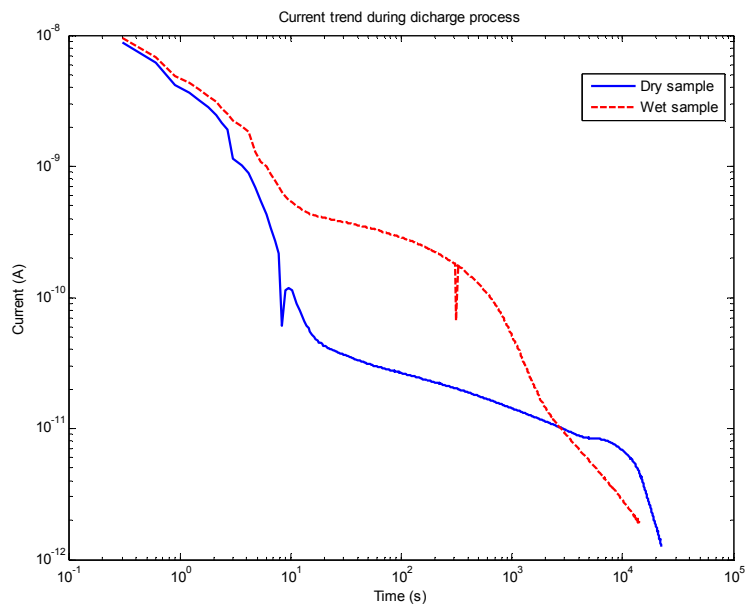


Fig. 8.10 Depolarization currents of dry and wet samples (PB-oil geometry)

In order to analyze how long should be the test in order to ensure that PD are accepted, measurements were carried out, changing the pre-charging times of the samples. In this case, the PDIV values were measured under AC and AC+DC voltage conditions. In both cases, the voltage was raised in steps of about 60 V/s. Under AC+DC voltage, the sinusoidal and DC voltages were raised simultaneously. Measurements were repeated after pre-charging the specimen with DC using 50% of the Weibull scale parameter of AC+DC PDIV values. Pre-charging times were 30, 60, 90, and 120 min.

The measured PDIVs and the conditioning procedure are listed in Table 17 which reports the peak values of the applied voltages. The Weibull scale parameter for PDIV at AC+DC voltages was 16.4 kV, thus a DC voltage with amplitude 8.2 kV was used to pre-charge the specimen.

The Weibull plots for PDIV values are reported in Fig. 8.11. In addition, Fig. 8.12 shows the box plots that summarize the statistical properties of the PDIV as a function of pre-charge times.

The reduction in PDIV becomes less marked when pre-charge exceeds 60 minutes, in comparison with the high reduction between AC+DC without pre-charge and a pre-charge of 30 minutes. For the system considered for this analysis, following the previous analysis, after 60 minutes (3600 s) the transient is practically completed and the DC field in the pressboard has reached its maximum value. This is an indirect confirmation of the analysis performed using Comsol® and the Maxwell capacitor theory.

Table 17 PDIV at different pre-charge times

Waveform	PDIV (kV)				
AC	13.6	12.5	13.9	14.7	13.2
AC+DC	16.4	15.6	15.8	15.4	17.2
Once obtained the Weibull scale parameter η , for AC+DC. The sample pre-charge in DC was $0.5 \cdot \eta$					
Pre-charge 30 min					
	14.2	15.0	14.4	15.6	15.8
Pre-charge 60 min					
	13.8	12.6	13.6	14.3	14.7
Pre-charge 90 min					
	12.6	13.4	14.2	13.6	14.6
Pre-charge 120 min					
	12.3	13.7	13.2	14.4	13.9

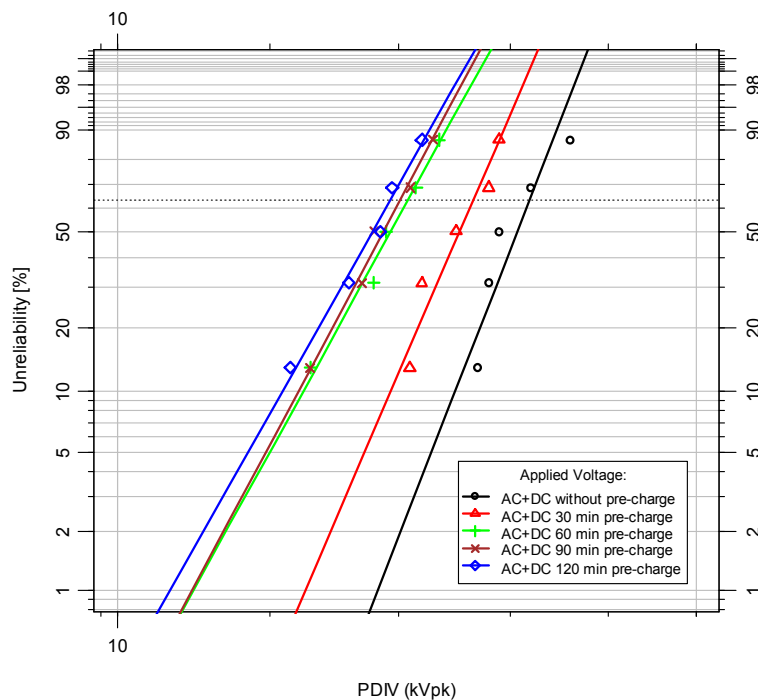


Fig. 8.11 Weibull chart for PDIV values obtained using different pre-charge times for Oil-PB geometry

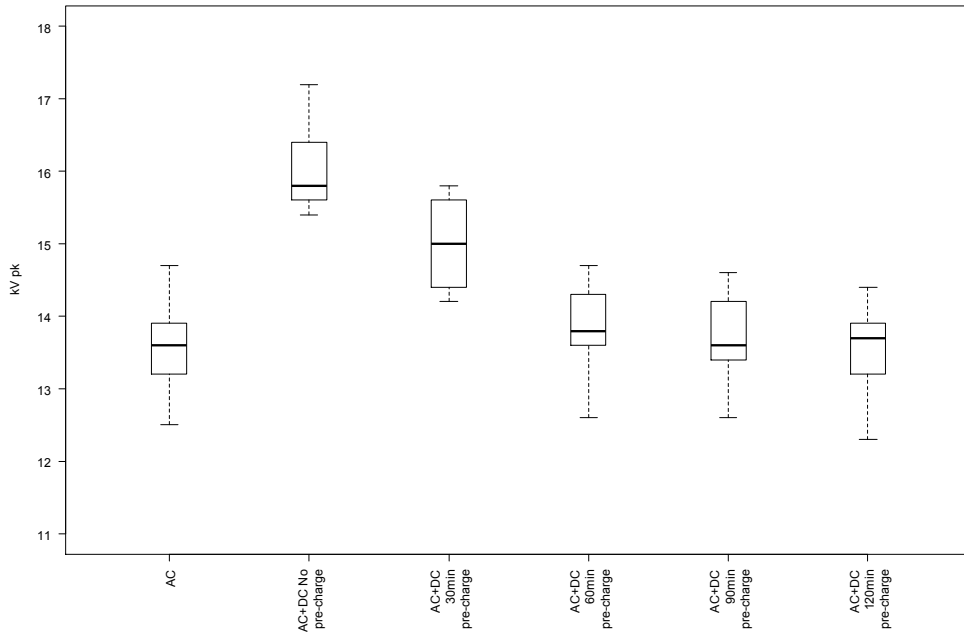


Fig. 8.12 Box plots of the PDIV values obtained using different pre-charge times for Oil-PB geometry

8.2.2 Behavior of PD activity in insulating paper for notched voltage waveforms

Due to the fact that PDIV values seems to follow a trend that depends of notch depths, it is interesting to study if PDIV values are influenced by the RMS values of the notched voltages. After calculating the RMS values with Eq. 53 , the RMS values of the notched voltage waveforms were normalized to the RMS value of a pure sinusoidal voltage waveform. Fig. 8.13 displays the normalized RMS values for different firing and overlap angles. Fig. 8.14 displays the PDIV Weibull scale parameters (α, μ) as a function of the normalized V_{rms} . The results show that the Weibull scales parameters are inversely proportional to the V_{rms} to a certain extent.

$$V_{RMS} = \sqrt{\frac{1}{T} \int_0^T V^2 dt} = \sqrt{\frac{1}{n} \sum_{i=0}^n V_i^2}$$

Eq. 53

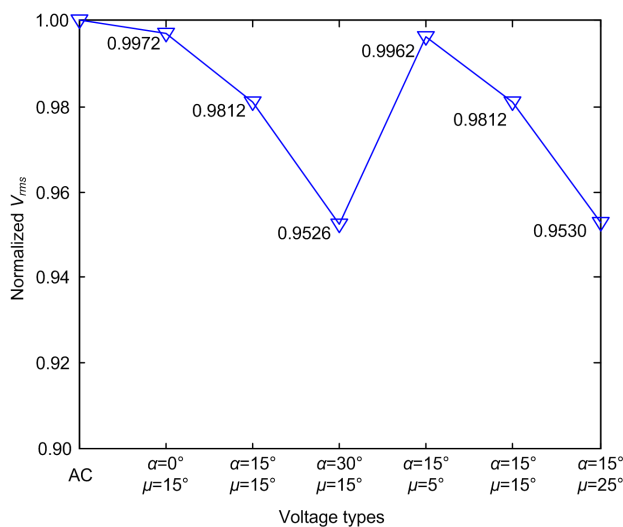


Fig. 8.13 Normalized RMS values for notched waveforms as a function of α and μ

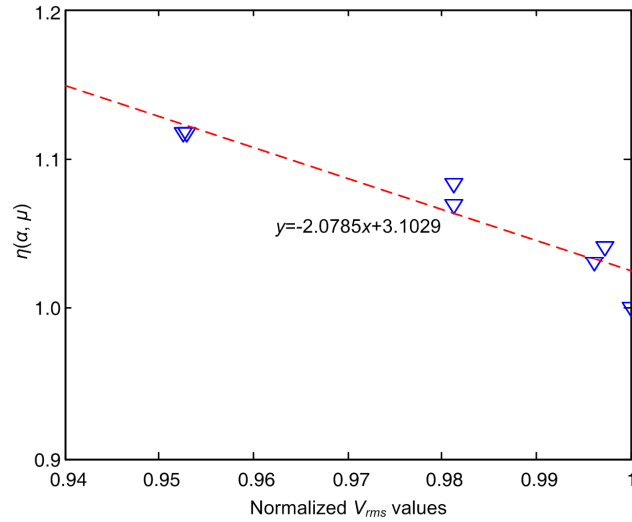


Fig. 8.14 Weibull scale parameter as a function of normalized RMS values

The experimental results show that PDIV values increases slightly as a function of notches width and depth and that the largest PD mostly occur at the rising front of the notches, i.e., where the voltage derivative is maximum (200 V/ μ s as for thyristor switches). Table 18 shows the values of notch depth (ΔV shown in Fig. 4.9) at different firing and overlap angles for 1, 5, 6 and 7 kV. Fig. 8.15 highlights that these discharges become larger increasing the firing and overlap angles, i.e., as the notch depth increases. A complete analysis of the conditions can be observed in Table 19.

Table 18 ΔV of different AC voltage with notches. (unit: kV)

Voltage	1 kV	5 kV	6 kV	7 kV
$\alpha=0^\circ, \mu=15^\circ$	0.2234	1.1170	1.3404	1.5638
$\alpha=15^\circ, \mu=15^\circ$	0.4320	2.1600	2.5920	3.0240
$\alpha=30^\circ, \mu=15^\circ$	0.6113	3.0565	3.6678	4.2791
$\alpha=15^\circ, \mu=5^\circ$	0.2954	1.4770	1.7724	2.0678
$\alpha=15^\circ, \mu=15^\circ$	0.4320	2.1600	2.5920	3.0240
$\alpha=15^\circ, \mu=25^\circ$	0.5556	2.7780	3.3336	3.8892

The Table shows the maximum PD values (q_{max}), occurrence phase angle and indicates if the discharges happen in the notch edge and maximum PD values.

Fig. 8.16 displays the PD amplitudes obtained at these conditions. The plot highlights that PD amplitude is linearly dependent on ΔV . Indeed, the null hypothesis $H_0 := 0$ (R is the population correlation coefficient) was tested by verifying that the statistic test of Eq. 54 is lower than the critical value $t(1-\alpha/2, n/2) = 1.75$ (confidence $\alpha = 0.05$, $n = 15$), being n the number of data points and r the sample correlation factor.

$$t = \left| r \cdot \sqrt{\frac{n-2}{1-r^2}} \right| \quad \text{Eq. 54}$$

As t is much larger in this case (10.37), the null hypothesis can be rejected, which means that a linear fitting is appropriate to describe the dependence of PD magnitude on ΔV .

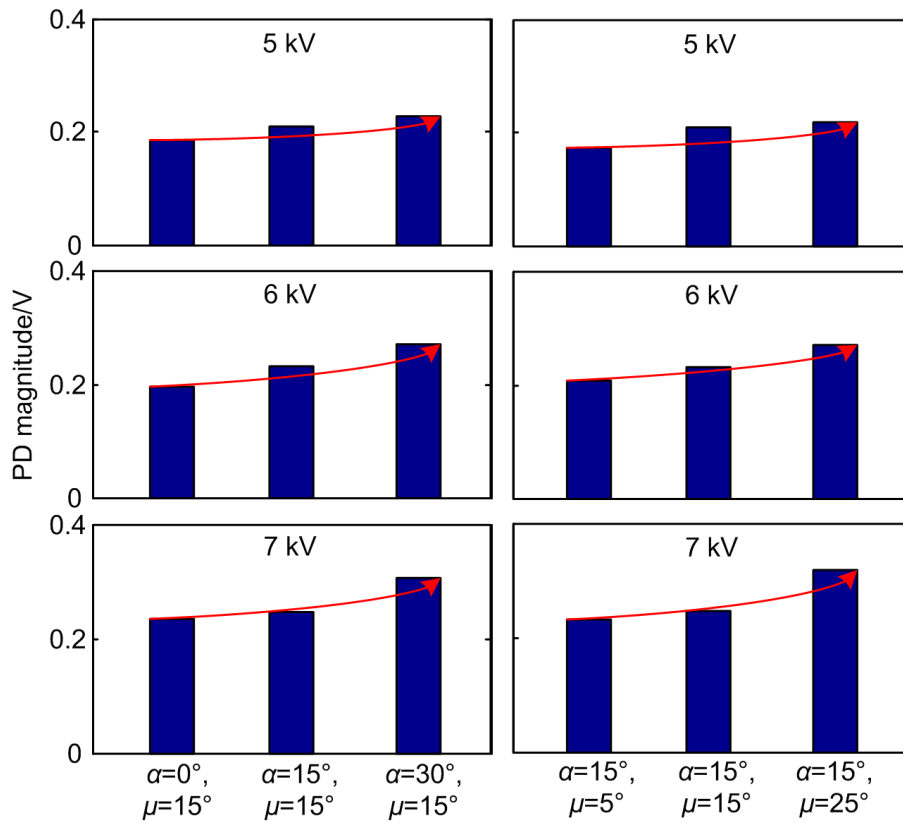


Fig. 8.15 PD amplitude at the notched edges under voltages at different firing and overlap angles

Table 19 Analysis of the maximum PD values under different voltages

Voltage		5 kV	6 kV	7 kV
AC	q_{max}/phase	0.3353/236.34°	0.2601/203.15°	0.3902/9.90°
	q_{max}/phase	0.3060/58.71°	0.3168/45.06°	0.2915/23.75°
	At the notches edge phase?	x	x	x
$\alpha=0^\circ, \mu=15^\circ$	q_{max} at the notch edge	0.1842	0.1964	0.2333
	q_{max}/phase	0.2091/58.50°	0.2327/58.25°	0.2467/238.18°
	In the notches edge phase?	√	√	√
$\alpha=15^\circ, \mu=15^\circ$	q_{max} at the notch edge	0.2091	0.2327	0.2467
	q_{max}/phase	0.2282/15.38°	0.2709/195.23°	0.3054/255.10°
	In the notches edge phase?	√	√	√
$\alpha=30^\circ, \mu=15^\circ$	q_{max} at the notch edge	0.2282	0.2709	0.3054
	q_{max}/phase	0.2831/50.16°	0.3213/215.41°	0.3474/17.45°
	In the notches edge phase?	x	x	x
$\alpha=15^\circ, \mu=5^\circ$	q_{max} at the notch edge	0.1734	0.2085	0.2321
	q_{max}/phase	0.2091/58.50°	0.2327/58.25°	0.2467/238.18°
	In the notches edge phase?	√	√	√
$\alpha=15^\circ, \mu=15^\circ$	q_{max} at the notch edge	0.2091	0.2327	0.2467
	q_{max}/phase	0.2187/250.32°	0.2703/70.33°	0.3194/250.28°
	In the notches edge phase?	√	√	√
$\alpha=15^\circ, \mu=25^\circ$	q_{max} at the notch edge	0.2187	0.2703	0.3194

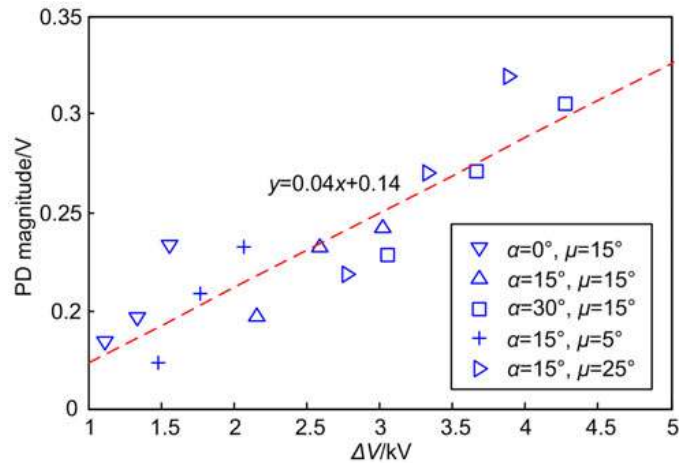


Fig. 8.16 PD amplitude at the rising front of notches as a function of ΔV

In order to observe in a better way the influence of α and μ in notch geometry and hence in PD magnitude, Fig. 8.17 shows the ΔV of different AC with notches voltages. The experimental results show that PDs have larger magnitude in correspondence of the notches edges when ΔV is larger than 1.8 kV (i.e. $\alpha=15^\circ, \mu=5^\circ$, and voltage amplitude equals 6 kV).

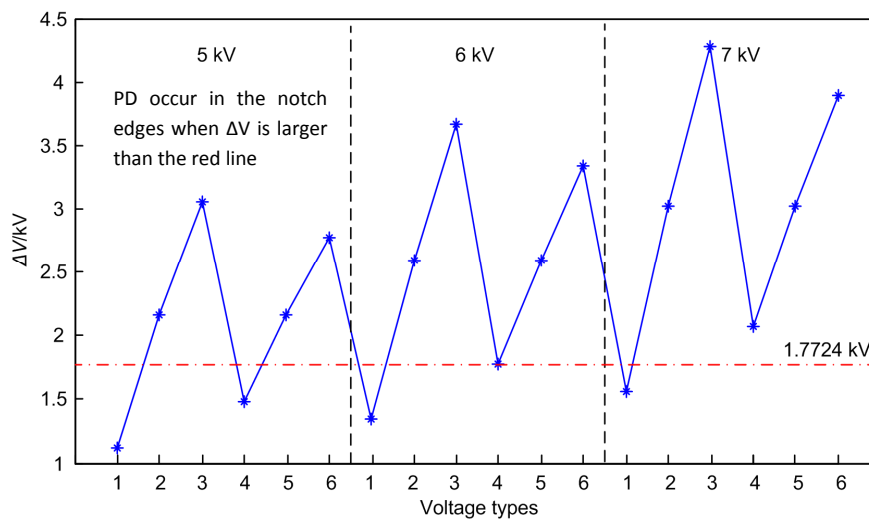


Fig. 8.17 ΔV of different AC with notches voltages: voltage 1: $\alpha=0^\circ, \mu=15^\circ$; voltage 2: $\alpha=15^\circ, \mu=15^\circ$; voltage 3: $\alpha=30^\circ, \mu=15^\circ$; voltage 4: $\alpha=15^\circ, \mu=5^\circ$; voltage 5: $\alpha=15^\circ, \mu=15^\circ$; voltage 6: $\alpha=15^\circ, \mu=25^\circ$

Fig. 8.18 and Fig. 8.19 show the variation of repetition rate N_w under different waveforms at the three selected voltage levels. Obviously, the results indicate that the N_w will be larger increasing the applied voltage. It is however interesting to observe that, despite PD extinguish during the notches, N_w under notched voltages is always larger than that under sinusoidal voltages and, moreover, it increases with increasing firing and overlap angles.

Regarding repetition rate, N_w , the experimental results show that under notched voltages, this parameter is generally larger than that obtained using sinusoidal voltages (despite PD extinguish during notches). Fig. 8.20 highlights that also N_w varies linearly on ΔV . Also in this case, the null hypothesis $H_0: = 0$ was discarded ($t=16.74$), supporting a linear relationship between N_w and ΔV .

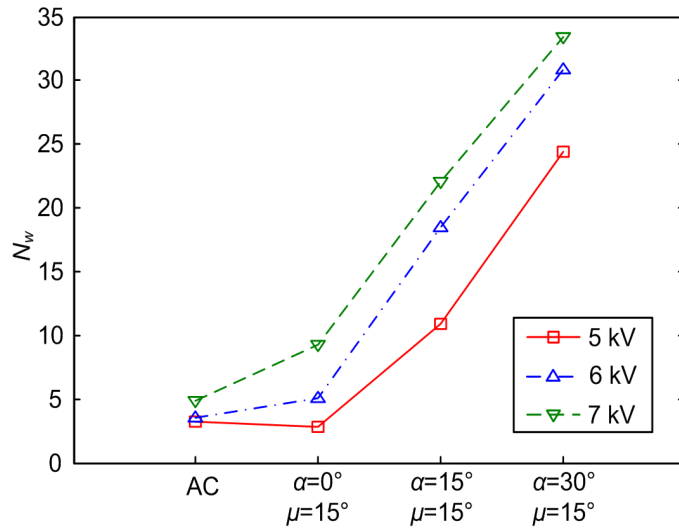


Fig. 8.18 Variation of N_w under voltages at different firing angles when the overlap angle $\mu=15^\circ$

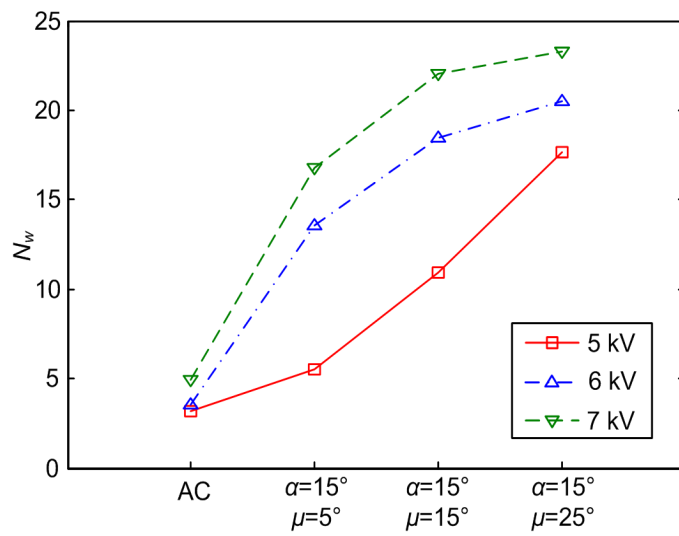


Fig. 8.19 Variation of N_w under voltages at different overlap angles when the firing angle $\alpha=15^\circ$

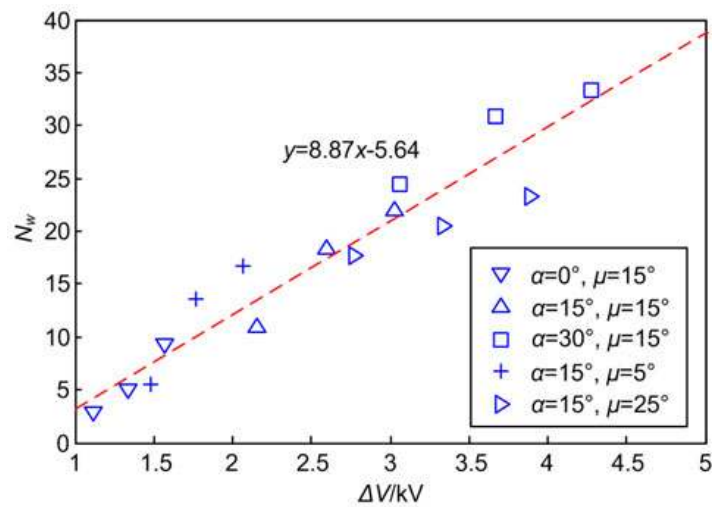


Fig. 8.20 Repetition rate as a function of ΔV

From all the obtained results, it is clear that the deeper the notches the higher the PDIV level increment. However, this result must be accepted in a conservative way during transformer operation and project, due to the fact that, once PD are incepted in the insulation, the magnitude and repetition rate of the discharges are higher than those that take place under a pure sinusoidal voltage. In this way, It is expected that paper-oil insulation lifetime under AC notched voltage could be shorter than that under pure AC voltage. As PD activity progresses under these conditions, discharges cause permanent chemical changes within the affected paper layers and impregnating dielectric fluid. Over time, partially conducting carbonized trees are formed. This impresses greater stress on the remaining healthy insulation, leading to further growth of the damaged region and resistive heating along the tree.

It is also important to notice that the tests were carried out at environment temperature (20°C). In the case of real transformer insulation system, where the temperature trend is load-dependent, the PD repetition rate can be even more dangerous for insulating paper integrity.

8.3 Partial discharges dependence on oil flow speed

Inception of discharges in oil under divergent fields is controlled mostly by (a) pollution at relative low fields, (b) injection of space charge from electrodes. Indeed, according to Lesaint and Top [72], space charge starts to be the most important factor for fields at the needle tip in the order of 1 MV/cm. This value contrasts with the one obtained using the Fowler-Nordheim equation, where 10 MV/cm is the critical electric field as it can be observed in the plot (Fig. 8.21)

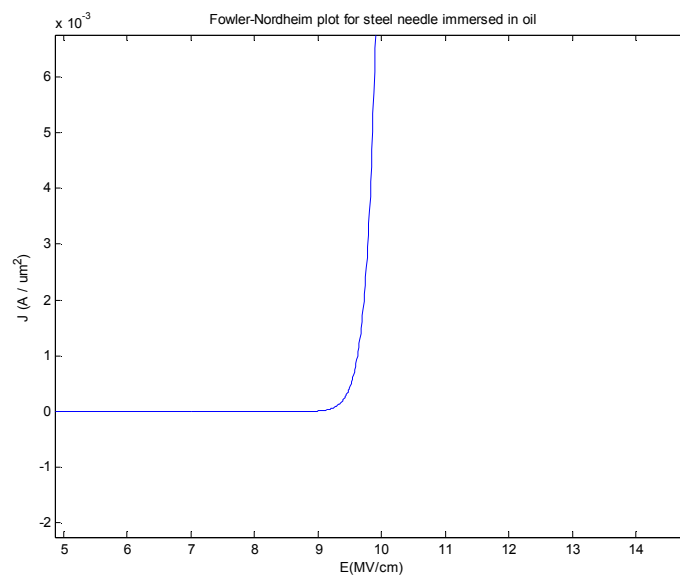


Fig. 8.21 Fowler-Nordheim plot for a steel needle immersed in mineral oil

The field at the needle tip can be estimated using Eq. 27. For the system considered here (tip radius $r=0.4\text{mm}$, gap $d=30\text{mm}$) and for voltages varying in the range 25-35 kVrms, peak field values of 0.1-0.14 MV/cm are obtained. Thus, accordingly to [72] and to Fowler-Nordheim result, these values seem too low to support a major effect of space charge in the phenomena observed during the experiments.

Also, despite the high oil speeds used in the experiments, streaming electrification should not be a major concern. In fact, the oil flow 1) after leaving the pipe tends to expand, losing speed 2) is not parallel to the board surface (hence, its tangential speed is much less than that calculated theoretically. The effects observed seem to be attributed mostly on the dynamics of particles in the oil and at the pressboard/oil

interface. Indeed, due to dielectrophoretic forces, particles in the oil (particularly those with high water content) tend to concentrate in proximity of the needle tip, favoring PD inception. Since the oil flow sweeps the area in front of the needle tip, it prevents the accumulation of particles in high field regions, thus decreasing the probability of partial discharge inception. Also, PD propagation is always associated with oil vaporization, with the consequent formation of a region where the PD itself can develop: at the inception of a PD avalanche, high oil speeds could sweep away gas bubbles from the discharge site, quenching the PD below the sensitivity of the detection system. Eventually, even if space charge seems not to play a major role, the oil flow could sweep away charge, thus increasing the PDIV.

The difference of values of PDIV observed at 50 and 70°C is also interesting. With still oil, the scale parameter increases from 25.8 to 26 kV when increasing temperature from 50 to 70°C, a factor that could be associated also to random fluctuations as shown by the confidence intervals reported in Fig. 6.14. If any difference exists, it could be explained by observing that Brownian motion due to thermal energy (favored also by lower oil viscosity) disrupts particle accumulation at high field regions. At higher oil speeds, however, Brownian motion alone does not seem a plausible explanation for the sharp rise of PDIV. More likely, this phenomenon should be addressed to different oil velocity (and, possibly, pressure) associated with different temperatures (and oil viscosities).

Eventually, it is interesting to compare the patterns obtained with different oil speeds at a temperature of 50°C (see Fig. 6.15). The pattern obtained with still oil shows striking similarities with those that can be obtained with a needle/plane configuration without pressboard [73]. As the pump frequency increases, these features become less and less evident, while PD magnitude decreases and repetition rate increases.

An explanation for these features can be devised looking at the sketch of the test setup (Fig. 6.12) and recalling what observed by Mitchinson et alia [59], who reported that PD from a needle in contact with a pressboard sheet can develop either at the pressboard/oil transition zone or in the liquid phase. It is possible that, with still oil, PD avalanches from the needle tip develop in free oil. When the avalanche reaches the region where self-sustained discharge is no longer possible, the charge carriers diffuse getting trapped at the solid/liquid interface. This space charge, spread somewhere away from the needle, could enable (although with low probability: the repetition rate with still oil is only 0.33 PD per cycle) a positive PD to be incepted from the pressboard back to the needle.

With increasing oil speeds, the velocity component orthogonal to the pressboard could force the discharge at the pressboard/oil transition zone. As a consequence: (a) space charge builds in proximity of the needle tip, and quenches fast the discharge, (b) the space charge itself, being closer to the needle tip, is likely to trigger a positive PD when the voltage reverses its polarity. Both hypotheses seem to be confirmed by the lower magnitudes and higher repetition rates observed with increasing pump frequencies (Fig. 6.16).

9 Conclusions and future work

Following, the main conclusions of the obtained results and some future work is presented for traction and converter transformers.

9.1 Test cell for PDIV determination under divergent field

Test cell and test procedure for PDIV assessment in point to plane geometries were developed and validated. This was done with the scope of overcoming the problems that arise from current standards and recommendations that require a well defined PD pattern or repetitive PD activity for PDIV determination. The use of these concepts makes the determination process more or less arbitrary, depending on the laboratory noise level and other factors. The procedure for increasing the voltage is also very important. Following the procedures described in this Thesis, the variance of recorded data is almost negligible. This finding support the evidence that when the PDIV is reached, the time under this voltage is long enough to ensure that PD are incepted. Therefore, it is possible to avoid the overestimation of PDIV that commonly happens with the standard procedure. The PDIV level obtained using this test technique is thus closer to the true physical PDIV.

In a similar way, a test cell and procedures were developed for surface creeping discharges at oil-cellulose interfaces. The high voltage electrode is a tungsten needle that lays over the pressboard surface. In order to obtain similar contact forces between the needle and the pressboard, the complete body of the HV electrode runs freely by gravity. In this way, the weight of the electrode becomes the contact force that remains uniform for all the tested pressboard samples. The test procedure used for the point to plane geometry in oil was also adopted in this setup in order to assess the true PDIV level. Also in this case, the very low variance of measurement data suggest that the test cell and procedures are able to provide a credible indication of the discharge physics.

After completing this work, enough evidence is available to suggest the use of the proposed creeping discharge test cell for standardization of PD measurements under creeping conditions. The execution of this kind of test is not currently standardized, despite the usefulness of the results.

9.2 Traction transformers (comparison of dielectric fluid behavior)

Ester oils have proved to be a feasible substitute for mineral oils. Their performance is always comparable and in most cases superior to that of mineral oils, at least when new, dried and purified fluids are investigated. Regarding PDIV, it was observed that esters perform better than mineral oil for both corona and creeping discharges.

In order to compare breakdown (BD) behavior of esters, additional resting time must be considered at the beginning of each test set and after a BD event. The number of shots to condition the electrodes when FR3 is used must be twice the recommended number of shots for mineral oil, that is, 12 conditioning shots. These considerations are based on the effect of the higher viscosity of FR3, that prevents the extraction of gas bubbles and BD byproducts from the electrically stressed zone.

During breakdown voltage tests at long gaps, it was observed that mineral oil shows always a better behavior than esters. At long gaps, the better capacity of mineral oil to stop streamers propagation,

contributes to produce higher BDV values. The problem is that when the energy of the BD discharge is not limited, this superior behavior last until the first breakdown discharge occurs. After this event, the breakdown voltage of mineral oil decays dramatically at each flashover, whereas esters breakdown voltage also decreases, but remains constant after some BD discharges. This fact could be explained recalling the superior thermal properties of esters that prevents thermal aging.

Another favorable property of FR3 is that it contributes to a further drying of pressboard after impregnation process. This phenomenon can be noticed analyzing the moisture transfer between PB and mineral oil and between PB and FR3 after a set of PDIV measurements. It was found that, at room temperature, FR3 continues taking water from the PB, thus improving the overall behavior of the insulation system. In fact, the lower the moisture in the pressboard, the longer its useful life. It was also demonstrated, according to the other results obtained during this work, that the additional moisture extracted from the PB does not affect the dielectric behavior of FR3.

The work carried out in PDIV detection for creeping discharges has highlighted some limits in our understanding of the oil/board interface. It seems that besides the barrier effect for discharge propagation caused by protruding PB fibers, the interface could also be strengthened by Van Der Waals forces. These forces may prevent oil molecules directly in contact with PB to drift freely, forming a hydraulic no-slip layer in which a gradual transition from bounded to free oil molecules exists. This transition zone affects the creeping discharge physics depending on many factors, i.e. electrodes geometry, permittivity mismatch, etc. In the case of creeping discharges, the geometry of the test cell and the type of insulating fluid affect the behavior of the interface: for gap distances below 10 mm, with the electrode shapes used in this research, the electric field in FR3 fluid volume tends to be parallel to or directed into the board sheet. On the other hand, at the same gap distance for mineral oil, a greater fraction of field lines are directed from the needle into the oil. This behavior is correlated to the dielectric permittivity mismatch between the fluids and the pressboard. For longer gaps, the electric field tends to be parallel to or directed into the board sheet for both fluids, making the creeping discharges to be directed parallel to the PB surface. These results were confirmed by the PD pattern obtained during the measurements. At short gaps, and mainly for mineral oil, the PD patterns corresponds to PD burst (discharges in oil). At longer gaps, mainly in FR3, the patterns correspond to surface discharges.

As a final remark, it is possible to say that for creeping discharges, it is better to test relatively long gaps. Short gaps, in fact, will provide discharges that can be more likely in the bulk oil instead of at the oil-PB interface, due to the proximity of the ground electrode.

The behavior of different fluids subjected to waveforms having different shape and frequency was also investigated to achieve basic information on the discharge physics.

The behavior of dielectric fluids under square voltages can be explained as follows: for alternating voltage applied to the test cell, when the point electrode has a negative polarity, negative space charge will build up in the neighborhood of the electrode (homocharge). This homocharge will reduce the local field around the electrode increasing the streamer inception voltage. When the voltage polarity becomes positive, this charge will enhance the field at the needle tip, reducing PDIV.

Since the duration of the applied voltage peak under square waveform is longer than that under sinusoidal voltage, it is expected that more space charge would be injected in this case, making more significant the space charge effect under square waveform voltage. This fact could explain why the PDIV (positive streamer inception voltage) for mineral oil and FR3 are always lower for square voltage. For low

frequencies the effect is still more marked because between each polarity reversal, more time elapses, favoring a higher injected charge density.

Increasing the frequency, the homocharge build up decreases (compared with that at lower frequencies), giving rise to lower electric fields at polarity reversal (thus higher PDIV values).

Increasing further the frequency, despite the fact that space charge is further reduced, thermal effect associated with higher dielectric losses increase the temperature of the oil, reducing its density. In these conditions, PD can occur inside low density regions explaining the PDIV decrement for both sinusoidal and square waveforms at higher frequencies. However, this is a speculation and more research is needed to prove it.

It is important to note, that the PDIE for all the test conditions when mineral oil and FR3 were compared is close to the critical emission field calculated from the Fowler-Nordheim equation. This fact confirms indirectly the importance of the role of space charge in the PD processes.

9.3 Converter transformers

It can be concluded from the performed measurements in AC, DC and AC+DC the following behavior:

The peak value of the partial discharge inception fields for pressboard under AC_{pk} , DC and $AC_{pk}+DC$ can be considered similar for all the tested conditions, independently of the sample geometry (PB without oil gaps, Oil-PB-oil and PB-oil). The $PDIE_{pk}$ difference between AC and DC for pressboard sample, and between AC+DC and DC for samples with oil gaps can be explained recalling the need of reaching an overvoltage ΔV over V_{min} . if AC peak is set at the same voltage level than the DC $PDIV_{pk}$, the probability to incept a discharge is zero for practical measuring periods. So, an additional overvoltage is required in AC and AC+DC to produce PD, thus explaining the higher AC PDIV peak. Once that PD have incepted in AC and AC+DC, their magnitude and repetition rate are higher due to the effect of polarity reversal over the space charge inside micro-cavities in the pressboard.

PDIV is reduced when the specimen is pre-charged at AC+DC conditions. This is because the DC field inside the pressboard increases exponentially with time under voltage, reaching a maximum after about one hour. The test results show that PD testing should be performed after an appropriate pre-charge of the samples in order to have the more conservative test conditions.

Regarding AC notched voltages, the following conclusions were obtained:

PDIV values under notched voltages are generally larger than those under sinusoidal voltages. Apparently, PDIV increases when the RMS voltage value decreases. This happens even in the case that the reduction of the RMS values is not significant. The reasons for this behavior are not fully understood.

Once that PD have incepted, their amplitudes at the rising front of notches become larger increasing the notch depth, i.e. firing and overlap angles. A similar behavior can be noticed for PD repetition rate as well.

The combination of this results indicate that voltage notches can produce a positive effect on reliability because PDIV is raised. However, as soon as the applied voltage exceeds the PDIV, insulating paper degradation under notched voltage waveforms can be much faster than that under sinusoidal waveforms due to the increase of PD magnitudes and repetitions rates.

9.4 Oil flow speed influence

The experiments performed in this Thesis were carried out at field levels where injection of space charge from the needle electrode should be negligible. Yet, the effect of oil flow could hardly be ascribed to particles using a point to plane electrode configuration. A possible explanation is that free charges in the oil are attracted towards the needle by dielectrophoretic forces. When the oil flow is sufficiently strong to sweep away these charges, the PDIV must increase.

PD phenomena in oils, as discussed during this Thesis, is always associated with oil vaporization. In these vapor regions PD can develop easily due to gas ionization. High oil speeds could also sweep away this ionized regions, quenching the PD below the sensitivity of the detection system.

10 References

- [1] IEC 60296 (Ed. 3) - 2003, "Fluids for Electrotechnical Applications - Unused Mineral Insulating Oils for Transformers and Switchgear".
- [2] IEC 60422 (Ed.3) - 2005, "Mineral Insulating Oils in Electrical Equipment - Supervision and Maintenance Guidance".
- [3] IEC 61203 (Ed.1) - 1992, "Synthetic Organic Esters for Electrical Purposes - Guide for Maintenance of Transformer Esters in Equipment".
- [4] F. M. Clark, "Factors Affecting the Mechanical Deterioration of Cellulose Insulation," *Transactions of the American Institute of Electrical Engineers*, vol. 61, no. 10, pp. 742-749, 1942.
- [5] Y. Du, M. Zahn, B. C. Lesieutre, A. V. Mamishev, and S.R. Lindgren, "Moisture Equilibrium in Transformer Paper-Oil Systems," *Electrical Insulation Magazine, IEEE*, vol. 15, no. 1, pp. 11-20, Jan-Feb 1999.
- [6] A. J. Kachler Hohlein, "Aging of Cellulose at Transformer Service Temperatures. Part 2. Influence of Moisture and Temperature on Degree of Polymerization and Formation of Furanic Compounds in Free-Breathing Systems," *Electrical Insulation Magazine, IEEE*, vol. 21, no. 5, pp. 20-24, 2005.
- [7] IEEE Std C57.91-1995, *Guide for Loading Mineral-Oil Immersed Transformers*.
- [8] W. Hansen, D. Linhjell, T. J. Painter L. E. Lundgaard, "Aging of Oil-Impregnated Paper in Power Transformers," *IEEE Transactions on Power Delivery*, vol. 19, no. 1, pp. 230-239, 2004.
- [9] A. Bandyopadhyay, "Moisture Sorption Response of Paper Subjected to Ramp Humidity Changes: Modeling and Experiments," *Industrial Engineering Chemistry Research*, vol. 39, no. 1, p. 244, 2000.
- [10] A. Massoquete, S. Lavrykov, S. Ramaswamy B. Ramarao, "Moisture Diffusion Inside Paper Materials in the Hygroscopic Range and Characteristics of Diffusivity Parameters," *Drying Technology*, vol. 21, no. 10, pp. 2007-2056, 2003.
- [11] S. Staykov, G. Cholakov E. Mladenov, "Water Saturation Limit of Transformer Oils," *Electrical Insulation Magazine, IEEE*, vol. 25, no. 1, pp. 23-30, 2009.
- [12] T. V. Oommen, "Moisture Equilibrium in Paper-Oil Systems," , Chicago, 1983, p. Conference of the Electrical/Electronics Insulation.
- [13] A. A. Zaky and R. Hawley, *Conduction and Breakdown in Mineral Oil*. London, UK: Peter Peregrinus Ltd., 1973.

- [14] R. Hancox and H. Tropper, "The Breakdown of Transformer Oil under Impulse Voltages," *IEE Proceedings Part A: Power Engineering*, vol. 105, pp. 250-262, 1958.
- [15] A. A. Zaky and A. Nosseir, "Electrical Breakdown of Mineral Oil under Uniform Field," *Journal of Physics D: Applied Physics*, vol. 10, pp. 1761-1767, 1977.
- [16] I. Y. Megahed and A. A. Zaky, "Effect of Electrode Material, Oxygen and Organic Additive on the Breakdown Strength of Mineral Oil under Non-uniform Fields," *Journal of Electrostatics*, vol. 12, pp. 345-351, 1982.
- [17] H. S. Endicott and K. H. Weber, "Electrode Area Effect for the Impulse Breakdown of Transformer Oil," *Power Apparatus and Systems, Part III Transactions of the American Institute of Electrical Engineers*, vol. 76, pp. 393-397, 1957.
- [18] K. H. Weber and H. S. Endicott, "Area Effect and Its Extremal Basis for the Electric Breakdown of Transformer Oil," *Power Apparatus and Systems, Part III. Transactions of the American Institute of Electrical Engineers*, vol. 75, pp. 371-381, 1956.
- [19] K. H. Weber and H. S. Endicott, "Extremal Area Effect for Large Area Electrodes for the Electric Breakdown of Transformer Oil," *Power Apparatus and Systems, Part III. Transactions of the American Institute of Electrical Engineers*, vol. 76, pp. 1091-1096, 1957.
- [20] M. G. Danikas, "Study of Some Factors Affecting the Breakdown Strength of Transformer Oil," in *International Conference on Dielectric Materials, Measurements and Applications*, 1988, pp. 9-12.
- [21] U. Gafvert, T. Schutte, and U. W. Gedde S. J. Laihonon, "Influence of Electrode Area on Dielectric Breakdown Strength of Thin Polyethylene terephthalate) Films," in *Conference on Electrical Insulation and Dielectric Phenomena*, 2004, pp. 563-567.
- [22] H. Murata, and M. Ikeda Y. Kawaguchi, "Breakdown of Transformer Oil," *IEEE Transactions on Power Apparatus and Systems*, vol. PAS-91, pp. 9-23, 1972.
- [23] T. V. Top and A. Lesaint, "Streamer Initiation in Mineral Oil. Part II: Influence of a Metallic Protrusion on a Flat Electrode," *IEEE Transactions on Dielectrics and Electrical Insulation*, vol. 9, pp. 92-96, 2002.
- [24] O. Lesaint, "Streamers in liquids: Relation with Practical High Voltage Insulation and Testing of Liquids," in *2008 IEEE International Conference on Dielectric Liquids*, 2008, pp. 1-6.
- [25] Y. Torshin, "The Universal Discharge Mechanism in Mineral Oil and Possible Estimation of its Breakdown Voltage," in *2002 International Conference on Dielectric Liquids*, 2002, pp. 107-110.
- [26] H. Borsi, B. Dolata E. Gockenbach, "Research Project on the Comparison of Electric and Dielectric Properties of Natural Ester Fluid with a Synthetic Ester and a Mineral Based Transformer Oil," Institute of Electric Power Systems, Division of High Voltage Engineering, Schering-Institute. University of Hanover, Hanover, Germany, Report No. 2 (Partial discharge behaviour, permittivity and dissipation factor $\tan \delta$) Sept.- Nov. 2005.

- [27] Siemens, High Voltage Direct Current Transmission – Proven Technology for Power Exchange. Answers for energy, 2011.
- [28] ABB, HVDC and HVDC Light. An Alternative Power Transmission System. Symposium on Control and Modeling of Alternative Energy Systems , April 2, 2009.
- [29] Siemens, The Smart Way HVDC PLUS – One Step Ahead. Answers for energy, 2011.
- [30] A. Carlson, "Specific Requirements on HVDC Converter Transformers," in *Proceedings of the International Conference on Electrical Engineering*, 1996, pp. 611-614.
- [31] U. Piovan, HVDC Tutorial at IEEE Transformer Committee Fall Meeting, Las Vegas, 2004.
- [32] F. H. Kreuger, *Industrial High DC Voltage*. Delft, Netherlands: Delft University Press, 1995.
- [33] M. Jeroense, *Charges and discharges in HVDC cables*. Delft, The Netherlands: Delft University Press, 1997.
- [34] ASTM D2413 - 99(2009), "Standard Practice for Preparation of Insulating Paper and Board Impregnated with a Liquid Dielectric".
- [35] Mettler-Toledo International, GTP® - Good Titration Practice in Karl Fischer Titration, 2011.
- [36] IEC 60156 (Ed.1) - 1963, "Method for the Determination of the Electric Strength of Insulating Oils".
- [37] Inc. Agilent Technologies, Agilent 33120A, 15 MHz Function / Arbitrary Waveform Generator User's Manual, 2002.
- [38] M. Bauta M. Grotzbach, "Significance of Working Point Determining Line Current Harmonics in Controlled AC/DC Converter," in *Industrial and Commercial Power Systems Technical Conference, IEEE*, New Orleans, LA , USA, 6-9 May 1996, pp. 131-140.
- [39] E. A. Cherney and J. Cross, "Electric-Field Distortions at Solid-Liquid Dielectric Interfaces," *IEEE Transactions on Electrical Insulation*, vol. EI-9, pp. 37-42, 1974.
- [40] M. Conti, A. Contin, and G. C. Montanari A. Cavallini, "Advanced PD Inference in On-field Measurements. II. Identification of Defects in Solid Insulation Systems," *IEEE Transactions on Dielectrics and Electrical Insulation*, vol. 10, pp. 528-538, 2003.
- [41] H. C. Hall and R. M. Russek, "Discharge Inception and Extinction in Dielectric Voids," *Proceedings of the IEE, Part II: Power Engineering*, vol. 101, pp. 47-55, 1954.
- [42] J. Dai and Z. D. Wang, "A Comparison of the Impregnation of Cellulose Insulation by Ester and Mineral oil," *IEEE Transactions on Dielectrics and Electrical Insulation*, vol. 15, pp. 374-381, 2008.
- [43] D. A. Nattrass, "Partial Discharge Measurement and Interpretation," *IEEE Electrical Insulation Magazine*, vol. 4, pp. 10-23, 1988.

- [44] E. O. Forster, "Partial Discharges and Streamers in Liquid Dielectrics - The Significance of the Inception Voltage," *IEEE Transactions on Electrical Insulation*, vol. 28, pp. 941 - 946, December 1993.
- [45] IEC 61294 (Ed.1) - 1993, "Insulating Liquids - Determination of the Partial Discharge Inception Voltage (PDIV) - Test Procedure".
- [46] H. Yamashita, "Partial Discharge Measurements in Dielectric Liquids under Impulse Voltage," *IEEE Transactions on Electrical Insulation*, vol. 28, pp. 947-955, 1993.
- [47] M. Pompili, and R. Schifani C. Mazzetti, "A Comparative Evaluation of Partial Discharge Inception Voltage of Power Transformer Liquids," in *1988 IEEE International Symposium on Electrical Insulation*, Boston, MA., 1988, pp. 31 - 34.
- [48] C. Mazzetti, M. Libotte, and E. O. Forster M. Pompili, "The Effect of the Definition Used in Measuring Partial Discharge Inception Voltages," *IEEE Transactions on Electrical Insulation*, vol. 28, pp. 1002-1006, 1993.
- [49] IEC 60270 - 2000, "High-voltage test techniques - Partial discharge measurements".
- [50] M. Pompili, H. Yamashita, and E. O. Forster C. Mazzetti, "A Comparison of Streamer and Partial Discharge Inception Voltages in Liquid Dielectrics," in *1992 International Conference on Dielectric Materials, Measurements and Applications*, 1992, pp. 93-95.
- [51] C. Mazzetti, and R. Bartnikas M. Pompili, "PD Pulse Burst Characteristics of Transformer Oils," *IEEE Transactions on Power Delivery*, vol. 21, pp. 689-698, 2006.
- [52] J.H. Mason, "Breakdown of Solid Dielectrics in Divergent Fields," *Proceedings of the IEE - Part C: Monographs*, vol. 102, no. 2, pp. 254-263, September 1955.
- [53] E. Takahashi, Y. Tsutsumi, K. Okuyama, and F. Ogata, "Partial discharge characteristics of oil-immersed insulation systems under DC, combined AC-DC and DC reversed polarity voltage," *Power Apparatus and Systems, IEEE Transactions on*, vol. 95, no. 1, p. 411, January 1976.
- [54] IEC 62539 (Ed.1) - 2007, "Guide for the statistical analysis of electrical".
- [55] G.C., Mazzanti, G., Cacciari, J. and Fothergill, J.C. Montanari, "In search of convenient techniques for reducing bias in the estimation of Weibull parameters for uncensored tests," *IEEE Transactions on Dielectrics and Electrical Insulation*, vol. 4, no. 3, pp. 306-313, 1997.
- [56] G.C., Mazzanti, G., Cacciari, J. and Fothergill, J.C. Montanari, "Optimum estimator for the Weibull distribution of censored data: singly-censored tests," *IEEE Transactions on Dielectrics and Electrical Insulation*, vol. 4, no. 4, pp. 462-469, 1997.
- [57] G.C., Mazzanti, G., Cacciari, J. and Fothergill, J.C. Montanari, "Optimum estimator for the Weibull distribution of censored data: progressively-censored tests," *IEEE Transactions on Dielectrics and Electrical Insulation*, vol. 5, no. 2, pp. 157-164, 1998.

- [58] E. W. Kimbark, *Direct Current Transmission*, 1st ed. New York, USA: John Wiley & Sons , September 10, 1971.
- [59] P. M. Mitchinson, P.L. Lewin, B. D. Strawbridge, and P. Jarman, "Tracking and Surface Discharge at the Oil-Pressboard Interface," *IEEE Electrical Insulation Magazine*, vol. 26, no. 2, pp. 35-41, March-April 2010.
- [60] EPE Centre. (2008) Guide to Transformer Specification Issues. [Online]. <http://www.epecentre.ac.nz/txspec.htm>
- [61] Cooper Industries, *Envirotemp FR3 fluid.*, June 2003.
- [62] Cooper Industries, "Envirotemp FR3 Fluid. Testing Guide," April 2008.
- [63] Schultz K., K uchler A. Dahinden V., "Function of Solid Insulation in Transformers," *Transform 98 - Germany*, pp. 41-54, April 1998.
- [64] M., Mazzetti, C., Bartnikas, R Pompili, "Comparative PD Pulse Burst Characteristics of Transformer Type Natural and Synthetic Ester Fluids and Mineral Oils," *IEEE Trans. Dielectr. Electr. Insul.*, vol. 16, no. 6, pp. 1511–1518, 2009.
- [65] M., Mazzetti, C., Bartnikas, R. Pompili, "PD Pulse Burst Behavior of a Transformer Type Synthetic Organic Ester Fluid," *IEEE Trans. Dielectr. Electr. Insul.*, vol. 15, no. 6, pp. 1498-1506, 2008.
- [66] J. Dai, Z.D. Wang, and P. Jarman, "Creepage Discharge on Insulation Barriers in Aged Power Transformers," *IEEE Transactions on Dielectrics and Electrical Insulation*, vol. 17, no. 4, pp. 1327-1335, August 2010.
- [67] H. Zainuddin, P.L. Lewin, and P. M. Mitchinson, "Characteristics of Leakage Current During Surface Discharge at the Oil-Pressboard Interface," in *Annual Report Conference on Electrical Insulation and Dielectric Phenomena (CEIDP)*, Montreal, CA., 2012, pp. 483-486.
- [68] F. O'Sullivan et al., "A Model for the Initiation and Propagation of Positive Streamers in Transformer Oil ," in *Electrical Insulation, 2008. ISEI 2008. Conference Record of the 2008 IEEE In*, Vancouver, CA, June 2008, pp. 210-214.
- [69] J. Adidian, M. Zahn, N. Lavesson, O. Widlund, and K. Borg, "Effects of Impulse Voltage Polarity, Peak Amplitude, and Rise Time on Streamers Initiated From a Needle Electrode in Transformer Oil," *Plasma Science, IEEE Transactions on*, vol. 40, no. 3, pp. 909-918.
- [70] R. P. Joshi, E. Schamiloglu, J. Gaudet, J. R. Woodworth, J. Qian, "Analysis of polarity effects in the electrical breakdown of liquids," *J. Phys. D: Appl. Phys.*, vol. 39, pp. 359-369, 2006.
- [71] Francis O'Sullivan, *A Model for the Initiation and Propagation of Electrical Streamers in Transformer Oil and Transformer Oil Based Nanofluids*. Cambridge Mss, U.S.A.: Massachusetts Institute of Technology, 2007.

- [72] T. V. Top O. Lesaint, "Streamer Inception in Mineral Oil Under AC Voltage," in *Int. Conf. on Liquid Dielectrics*, June 2011, pp. 1-5.
- [73] G. C. Montanari, F. Ciani A. Cavallini, "Analysis of Partial Discharge Phenomena in Paper-Oil Insulation Systems as a Basis for Risk Assessment Evaluation," in *IEEE Int. Conf. on Dielect. Liquids (ICDL)*, June 2005, pp. 241-244.
- [74] Q. Liu, X.Wang, P.Jarman, G. Wilson Z.D. Wang, "Discussion on Possible Additions to IEC 60897 and IEC 61294 for Insulating Liquid Tests," *IET Electric Power Applications*, vol. 5, no. 6, pp. 486-493, 2011.
- [75] Wang Xin, "Partial Discharge Behaviour And Breakdown Mechanisms Of Ester Transformer Liquids Under AC Stress," PhD Dissertation, The University of Manchester, 2011.
- [76] CIGRE WG A2-35, "Experiences in Service with New Insulating Liquids," *Final Report; Brochure 436*, 2010.
- [77] P. H F Morshuis and J.J. Smit, "Partial discharges at DC voltage: their mechanism, detection and analysis," *Dielectrics and Electrical Insulation, IEEE Transactions on*, vol. 12, no. 2, pp. 328-340, April April.

Publications

- Cavallini, A.; Ramos, C.G.A.; Montanari, G.C.; Saad, H.; Tozzi, M., "UHF detection of PD in power transformers: The influence of disturbances," Electrical Insulation and Dielectric Phenomena (CEIDP), 2011 Annual Report Conference on , vol., no., pp.436,439, 16-19 Oct. 2011.
- Cavallini, A.; Ramos, C.G.A.; Montanari, G.C.; Rubio-Serrano, J.; Garcia-Souto, J.A., "Comparison of ultrasonic, electrical and UHF characteristics of partial discharge emission in oil/paper insulation systems," Electrical Insulation and Dielectric Phenomena (CEIDP), 2011 Annual Report Conference on , vol., no., pp.440,443, 16-19 Oct. 2011.
- Azcarraga, C. G.; Cavallini, A.; Montanari, G.C., "The influence of oil speed and temperature on PD phenomena in transformer insulation," Electrical Insulation (ISEI), Conference Record of the 2012 IEEE International Symposium on , vol., no., pp.494,497, 10-13 June 2012.
- Cavallini, A, Azcarraga C.G.; Final Report "Testing Breakdown voltage and partial discharge inception voltage of new insulating fluids" UNIBO/DUPONT
- Cavallini A. Azcarraga C.G., "Comparison of Partial Discharge Inception Voltages for Ester and Mineral Oils Under Divergent Fields," in 2013 Annual Report Conference on Electrical Insulation and Dielectric Phenomena Vol. II, Shenzhen, China, 2013, pp. 1254-1257
- Azcarraga C.G., Cavallini A., "A Comparison of Withstand Properties of Ester and Mineral Oils", submitted to IEEE Electrical Insulation Magazine
- Garcia-Souto J.A. , Bua I., Azcarraga C.G. "Optical Fiber Sensor of Partial Discharges in High Voltage DC Experiments", submitted to 23rd International Conference on Optical Fiber Sensors